# MASS AND MOMENTUM TRANSPORT IN A TURBULENT BUOYANT VERTICAL AXISYMMETRIC JET

Thesis by

Panayiotis Nikolas Papanicolaou

In Partial Fulfillment of the Requirements

for the Degree of

Doctor of Philosophy

California Institute of Technology

Pasadena, California

1984

(Submitted May 23, 1984)

# ABSTRACT

The entrainment and mixing processes in an axisymmetric vertical turbulent buoyant jet and its transition from a jet to a plume have been studied. The ambient fluid is of uniform density and calm except for the flow induced by the jet, and the density variations are assumed small.

A systematic set of experiments was carried out to examine turbulent buoyant jet behavior over a wide range of initial jet Richardson numbers. All experiments were performed in a glass wall tank with dimensions 1.15m x 1.15m x 3.30m deep, equipped with a jet flow source and an instrument carriage to enable velocity and concentration measurements in the entire jet flow field.

The axial and radial velocity components and the concentration of a Rhodamine 6G dye were measured simultaneously at the same point of the jet flow field using a two - reference beam laser - Doppler velocimeter combined with a laser induced fluorescence measuring device. From the time signals of the axial and radial velocity components (w) and (u) and the concentration (c) of a Rhodamine 6G dye, information was obtained concerning the mean values, turbulent fluctuations and correlations between w, u and c, up to 100 jet and 80 plume diameters downstream of the jet exit.

More specifically, the mean flow (including the spreading rate of the mean velocity and tracer concentration profiles and distribution along the jet axis) and the turbulent structure (including the profile of turbulence intensity, turbulent mass flux of a tracer and turbulent

momentum flux) were investigated as a function of distance from jet origin made dimensionless by a characteristic length scale based on jet buoyancy and momentum fluxes. The results from a detailed dimensional analysis were verified experimentally. It was determined that the turbulent flux of a tracer (or buoyancy) varied from 6-10% for jets and was 15-20% of the total for plumes. The turbulent momentum flux was found to be 15% of the local momentum flux transported by the mean flow.

While the profiles of w and c and the turbulent velocity profiles are found to be much the same for both jets and plumes, the turbulence intensity profiles of the concentration take higher values in plumes than in jets. More rapid dilutions were obtained in buoyancy driven plumes than in momentum driven jets.

Useful information concerning engineering applications is provided from the experimental constants derived.

## AKNOWLEDGMENTS

This work has resulted from a collaboration of a number of people. To thank all of the contributors adequately is not possible. I am sincerely grateful for all the time, tolerance, assistance and friendship of those named and unnamed upon whom I have relied.

First and foremost, I would like to express gratitude and appreciation to my advisor, Professor Ericson John List for his inspired guidance, encouragement, friendship and enthusiasm during this study. He suggested the topic and the technique to be developed and applied in this investigation.

I am also indebted to Professors Norman H. Brooks and Anatol Roshko whose advice and interest in this research, stimulated and inspired me continuously. Their outstanding teaching and enthusiasm have stimulated my interest in turbulent shear flows. I am grateful to Dr. Robert C.Y. Koh for numerous discussions and help in programming; his "MAGIC" language made computer work easier. Special thanks to Professor Vito A. Vanoni for his personal interest, advice, encouragement and help in the design of the tank. I am also grateful to Professor Nikolas E. Kotsovinos for the discussions, encouragement and friendly advise in the summers of 1981 and 1983.

The experimental equipment and instrumentation used in this work, could not have been built without the unique ideas, advise and friendship of the "Cribbage Club". I am indebted to Mr. Elton F. Daly whose creative ability helped in the design of the most complicated parts of the experimental apparatus, to Mr. Joseph Fontana, a magician

in a machine shop, and to Mr. Richard Eastvedt for all his help. I also want to thank Mr. Leonard Montenegro for providing great assistance and ideas in the design and construction of the electronic components of the signal processor.

The continuing friendship and help of Mrs. Joan Mathews and Mrs. Melinda Hendrix-Werts is greatly valued. This thesis and other previous manuscripts could not have been prepared without their help and patience. I am truly thankful. The assistance, love and concern of Mrs. Gunilla Hastrup and Mrs. Rayma Harrison are greatly appreciated.

Discussions with fellow students have provided much needed support and camaradrie. In this regard I would like to thank Costas Synolakis, Gregory Gartrell and James Skjelbreia.

The completion of this thesis required the special support given only by close friends. I would especially like to thank Nick Vasilakos, Yiannis Psycharis, Costas Chazapis and family, Basile Dendrou and family, Panos Georgopoulos, Michael Karyeaclis, Costas Synolakis, Martha Conklin, Agni Storey, Mary King and Diane Austin. Their continuous support, love, help, understanding and all the fun we had together will be unforgettable.

I would like to thank my parents Nikolas and Barbara, the rest of my family and friends from Greece for their continuous love, support and patience over the past six years.

I would like to thank the California Institute of Technology for providing the facilities which made this study possible, and the National Science Foundation for providing the financial support.

TABLE OF CONTENTS

TABLE OF CONTENTS (continued)

TABLE OF CONTENTS (continued)

# LIST OF FIGURES

LIST OF FIGURES (continued)

LIST OF FIGURES (continued)

LIST OF FIGURES (continued)

LIST OF FIGURES (continued)

LIST OF FIGURES (continued)

LIST OF FIGURES (Continued)

# LIST OF TABLES

# NOMENCLATURE

## English Symbols

$a_e$ = universal entrainment coefficient.

$a_j$ = entrainment coefficient for a pure jet.

$a_p$ = entrainment coefficient for a pure plume.

$a_i$, $a_i'$ = constants of proportionality in equations (1.3.2) to (1.3.10), (page 17).

a = distance shown in Figure 2.4.5, (page 46).

A = constant in 5th-order polynomial for the laser-Doppler calibration, (page 62).

b = visual width of the jet, (page 67).

$b_w$ = $b_w(z)$, 1/e-width of the time-averaged mean velocity profile, (e = 2.718...).

$b_c$ = $b_c(z)$, 1/e-width of the time-averaged mean concentration profile, (e = 2.718...).

$b_i$, $b_i'$ = constants of proportionality in equations (1.3.2) to (1.3.10), (page 17).

b = distance in Figure 2.4.5, (page 46).

B = $\left((\Delta\rho)_o/\rho_a\right)g$, specific buoyancy flux at the jet orifice.

B = constant in 5th-order polynomial for the laser-Doppler calibration, (page 62).

c = speed of light in vacuum, (page 38).

c = specific heat of water, (page 17).

c = $c(r,z,t)$, instantaneous concentration excess (above the ambient) at point (r,z) at time t.

$\overline{c}$ = $\overline{c}(r,z)$, time-averaged mean concentration excess (above the ambient) at point (r,z).

$\overline{c}_c$ = $\overline{c}_c(z)$, time-averaged mean concentration excess (above the ambient) at the jet axis.

$c'$ = $c'(x,y,t)$, turbulent component of the concentration, $c' = c - \overline{c}$.

$\overline{c'^2}$ = intensity of turbulent fluctuations of concentration.

NOMENCLATURE (continued)

$c_a$ = ambient fluid concentration of Rhodamine 6G dye.

$c_p$ = $\sqrt{2\pi}b_w/z = C$, plume width parameter (growth coefficient) in equation (1.3.11), (page 16).

$c_j$ = C, jet width parameter (growth coefficient) in equation (1.3.4), (page 17).

C = $\mu/zm^{\frac{1}{2}}$, jet/plume width parameter, (page 14).

$C_o$ = excess (above the ambient) concentration of Rhodamine 6G dye at the jet orifice.

$C_{1w}$, $C_{2w}$ = coefficients for the distribution of the mean velocity along the jet axis.

$C_{1c}$, $C_{2c}$ = coefficients for the distribution of the mean concentration along the jet axis.

C = constant in 5th-order polynomial for the laser-Doppler calibration, (page 62).

D = jet diameter.

D = constant in 5th-order polynomial for the laser-Doppler calibration, (page 62).

e = 2.718..., base of the Napierian logarithms.

$\vec{e}$ = directional unit vector.

E = constant in 5th-order polynomial for the laser-Doppler calibration, (page 62).

E = $w^2$/frequency, $u^2$/frequency, $c^2$/frequency, power of the energy spectrum (frequency distribution) of w, u, c.

$f_p$ = frequency of light scattered by a moving particle.

$f_o$ = frequency of laser light in the direction of the laser beam.

$f_s$ = frequency of the scattered light in the direction of an observer on a photodetector.

$f_R$ = frequency of the reference laser beam of the laser-Doppler velocimeter.

$f_D$ = Doppler frequency.

F = $f_R - f_s$, frequency shift between reference and scattering beams.

NOMENCLATURE (continued)

$F$ = distance, (page 45).

$f_1$ = $f_D - F$.

$f_2$ = $2f_o + 2f_D$.

$f_3$ = $2f_o + F + f_D$.

$f_4$ = $2f_R = 2f_o + 2F$.

$f_{D1}$ = $f_w - F$, Doppler frequency that corresponds to the axial velocity component, w.

$f_{D2}$ = $f_u - F$, Doppler frequency that corresponds to the radial velocity component, u.

$f_{w,u}$ = frequency outputs from the photodetectors that correspond to axial and radial velocity components recorded on diskettes in digital form.

$F_d$ = $\left[W^2/g_o' D\right]^{\frac{1}{2}}$, densimetric jet froude number.

$F_o$ = specific buoyancy flux at a jet exit, (page 25).

$g$ = gravitational acceleration (981 cm/sec$^2$).

$g_o'$ = $\left((\Delta\rho)_o/\rho_a\right)g$, buoyancy force at the jet exit.

$G$ = calibration constant for the induced fluorescence concentration measurement technique.

$h$ = h(R,G), buoyant force function, (page 14).

$H$ = calibration constant for the induced fluorescence concentration measurement technique.

$H_o$ = $QC_o$, Rhodamine 6G dye flux at the jet exit.

$H_M$ = transport of a tracer (Rhodamine 6G dye) by mean flow.

$H_T$ = turbulent tracer (Rhodamine 6G dye) flux.

$k$ = coefficient in the exponent for the exponential weak velocity and concentration profiles, (page 20, page 99).

$K_{1w}$ = spreading rate of the mean velocity profile.

$K_{2w}$ = non-dimensional virtual origin of the mean velocity profile.

$K_{1c}$ = spreading rate of the mean concentration profile.

NOMENCLATURE (continued)

$K_{2c}$ = non-dimensional virtual origin of the mean concentration profile.

$\ell_M$, $l_M$ = $M^{3/4}/B^{1/2}$, characteristic momentum (or buoyancy) length scale.

$\ell_Q$, $l_Q$ = $Q/M^{1/2}$, characteristic length scale proportional to the orifice size.

m = m(z), kinematic momentum flux.

M = QW, specific momentum flux at jet origin.

n = index of refraction.

$\overline{p}$ = mean deviation from the hydrostatic pressure.

q = q(R,C), entrainment function, (page 14).

Q = $(\pi D^2/4)W$, volume flux at the jet orifice.

Q = input heat flux at the jet orifice, (page 26).

r = coordinate axis in the radial direction, normal to the gravity force.

R = (%), indication of the flowmeter, (page 61).

$R_o$ = $\ell_Q/\ell_M$, initial jet Richardson number.

R(z) = $R(z) = \mu\beta^{1/2}/m^{5/4}$, jet Richardson number at a distance z from jet orifice.

$R_p$ = plume Richardson number.

$R_e$ = Reynolds number.

S = $C_o/\overline{c}$, mean dilution.

S' = $C_o/\sqrt{\overline{c'^2}}$, "rms dilution".

t = time.

T = temperature (pages 25-27 and 50).

T' = $T - \overline{T}$, turbulent component of the temperature (pages 25-27).

$\overline{T}$ = time-averaged mean temperature (pages 25-27 and 50).

u = u(r,z,t), instantaneous radial velocity at a point (r,z).

NOMENCLATURE (continued)

$\bar{u}$ = $\bar{u}(r,z)$, time-averaged mean radial velocity.

$u'$ = $u - \bar{u}$, turbulent component of the radial velocity.

$\overline{u'^2}$ = turbulence intensity of the radial velocity component.

$\vec{U}$ = particle velocity, (pages 38,39).

$v$ = $v(r,z,\theta,t)$, instantaneous tangential velocity component at a point $(r,z,\theta)$.

$\bar{v}$ = $\bar{v}(r,z,\theta) = \bar{v}(r,z)$, mean tangential velocity.

$V$ = digital output from the photodiode to the computer.

$w$ = $w(r,z,t)$, instantaneous longitudinal (axial) velocity component at a point $(r,z)$.

$\bar{w}$ = time-averaged mean longitudinal (axial) velocity.

$w'$ = $w - \bar{w}$, turbulent component of the longitudinal (axial) velocity.

$\overline{w'^2}$ = turbulence intensity of the axial velocity component.

$\overline{w_c}$ = $\overline{w_c}(z)$, time-averaged mean axial velocity at the jet axis.

$W$ = velocity at the orifice of the jet.

$\underline{x}$ = position vector of a point in a flow field.

$y$ = $y(\underline{x},t)$, flow parameter at location $\underline{x}$ and time $t$.

$Y$ = $QC_o$, tracer flux at the jet exit.

$z$ = coordinate axis in the vertical direction, same direction as gravity force.

$z_o$ = locus of the virtual origin of a jet.

Greek Symbols

$\alpha$ = $\alpha(z)$, thermal expansion coefficient of the water.

$\alpha$ = constant exponent to be defined, (page 12).

$\beta$ = constant exponent to be defined, (page 12).

$\beta$ = $\beta(z)$, kinematic buoyancy flux.

NOMENCLATURE (continued)

| | | |
|---|---|---|
| $\gamma$ | = | constant exponent to be defined, (page 12). |
| $\delta$ | = | constant of proportionality in equation (1.2.5), (page 5). |
| $\zeta$ | = | $(c_p/R_p)(z/\ell_M)$, dimensionless elevation. |
| $\eta$ | = | $\eta(z) = d\mu/dz = m^{\frac{1}{2}}q(R,C)$, entrainment function. |
| $\theta$ | = | angle. |
| $\lambda$ | = | $b_w/b_c$, width ratio. |
| $\lambda$ | = | wavelength of laser light in a vacuum. |
| $\lambda_{in}$ | = | wavelength of the incident laser light. |
| $\lambda_{em}$ | = | wavelength of the fluorescent (emitted) light. |
| $\overline{\mu}$ | = | $(\mu/Q)(R_o/R_p)$, dimensionless dilution. |
| $\mu$ | = | $\mu(z)$, kinematic volume flux at a distance z from the jet orifice. |
| $\nu$ | = | kinematic viscosity. |
| $\xi$ | = | $\xi(z) = dm/dz = (\mu\beta/m)h(R,C)$, buoyancy function. |
| $\pi$ | = | 3.14159... |
| $\rho_o$ | = | fluid density at the jet orifice. |
| $\rho_a$ | = | ambient fluid density. |
| $\overline{\rho}$ | = | $\overline{\rho}(r,z)$, time-averaged mean fluid density at a point $(r,z)$. |
| $\sigma$ | = | $\sigma$ unit, 1 gr/cc. |
| $\tau$ | = | time. |
| $\phi$ | = | angle. |

Subscripts

| | | |
|---|---|---|
| a | = | quantities of the ambient fluid. |
| c | = | quantities of the jet axis (centerline). |
| $_o$ | = | quantities at the jet orifice. |

NOMENCLATURE (continued)

| | | |
|---|---|---|
| p | = | quantities corresponding to plumes. |
| j | = | quantities corresponding to jets. |

Superscripts

| | | |
|---|---|---|
| $\overline{\ }$ | = | time-averaged mean value. |
| ' | = | fluctuating component. |

Mathematical Symbols

| | | |
|---|---|---|
| $\Delta$ | = | deficiency or difference symbol. |
| expA | = | $e^A$, exponential function. |
| $\pi$ | = | 3.14159... |
| $\Sigma$ | = | summation symbol. |
| $\propto$ | = | is proportional to. |

# 1. INTRODUCTION

## 1.1 Introductory note

The subject of the present experimental work is the study of a round vertical turbulent buoyant jet discharging into a body of water of uniform density. Our purpose is the description of the velocity and concentration distributions in the jet, especially in the region where buoyancy is the driving force rather than the initial momentum flux. Buoyant jets are observed in nature above fires, active volcanos or underwater springs. Man-made jets can be seen at ocean outfalls for wastewater disposal, factory stacks, cooling towers, rocket propelled missiles after launch and airplane jet engines. The continuously growing demand for nuclear electric power and the growth of cities by ocean sites, increase the demands for wastewater disposal into the ocean by ocean outfalls. Design of outfalls that can obtain fast dilution will minimize the disruption of the ecological balance due to thermal or biological pollution. Understanding of the mechanics of buoyant jets, and especially the entrainment and the mixing that occurs at round jets will help in optimal design of ocean outfalls.

Apart from environmental applications, the present investigation will help in understanding some fundamental turbulence characteristics of turbulent free shear flows. It will also contribute to the knowledge of the mechanics of the round plumes, since they have been investigated here in a systematic way, especially in the far field where the flow is fully developed.

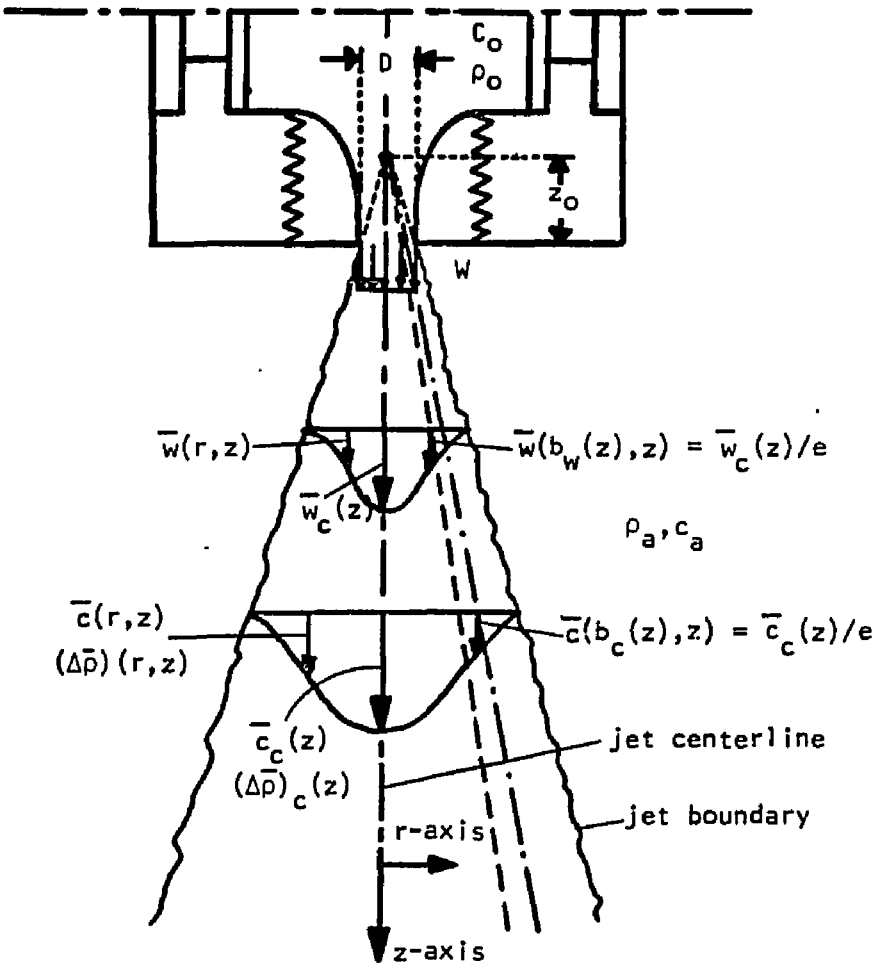


——·——·—— 1/e concentration width

— — — — — — 1/e velocity width

~~~~~~~~~~ jet boundary

$\rho_o$ jet fluid density

$C_o$ jet fluid concentration of Rhodamine 6G dye

W jet exit velocity

$\rho_a$ ambient fluid density

$c_a$ ambient fluid concentration

$z_o$ virtual origin

D jet diameter

Figure 1.2.1. Geometry of a buoyant jet - definition sketch.
~~~~~~~~~~

## 1.2 Definition of the problem - a review of previous theories

Previous investigations of round vertical jets, buoyant jets and plumes will be examined in this chapter. The flow configuration and geometry are shown diagrammatically in Figure 1.2.1 . The basic assumptions to be considered are: (i) The ambient fluid is of uniform density $\rho_a$ and motionless, except for the flow induced by the jet. (ii) The difference between the time - averaged fluid density $\overline{\rho}(r,z)$ at any point and the ambient fluid density will be small, so that

$$(\overline{\rho}(r,z)-\rho_a)/\rho_a \ll 1$$

in the case of buoyant jets and plumes. Thus, there will be little error if the local density $\rho(r,z)$ is replaced by the ambient fluid density $\rho_a$ in the equations of motion in the description of the inertia forces (Boussinesq approximation). (iii) That the flow is fully turbulent and that the viscous and molecular transport of heat, or some other tracer, can be neglected relative to its turbulent transport. (iv) There is no swirl introduced to the jet, so that the mean tangential velocity $\overline{v}(r,z,\theta) = \overline{v}(r,z) = 0$. (v) Within the range of the problem the density of the fluid is assumed to be linear function of tracer concentration above the reference level as shown in Figure 1.2.2. (vi) Pressure is assumed to be hydrostatic throughout the ambient fluid and (vii) The fluids are supposed to be incompressible. Under these assumptions the time - averaged Boussinesq equations for the three-dimensional incompressible motion of a turbulent axisymmetric non-swirling jet with density variations in cylindrical polar coordinates are:

(a) Conservation of volume flux

$$\frac{1}{r}\frac{\partial}{\partial r}(r\overline{u}) + \frac{\partial \overline{w}}{\partial z} = 0 \qquad (1.2.1)$$

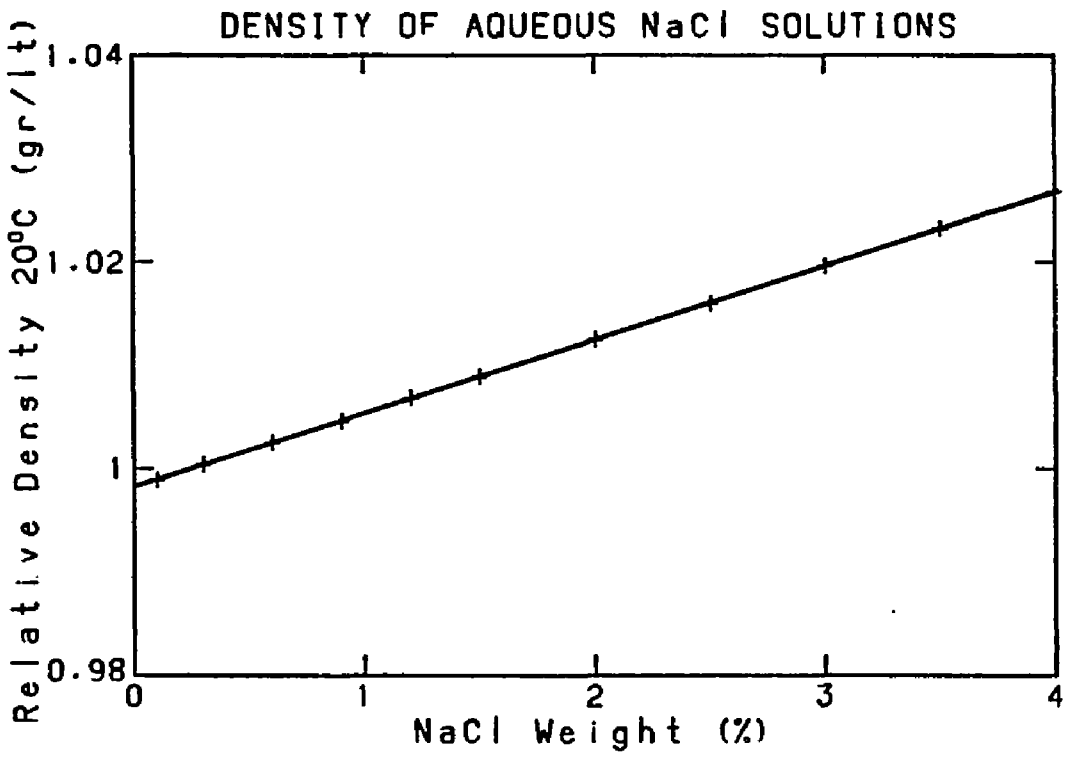


Figure 1.2.2. Relative density of aqueous NaCl solutions as a function of the NaCl weight (%) at 20°C.

(b) Momentum conservation

(i) Axial momentum

$$\frac{1}{r}\frac{\partial}{\partial r}\left[r\left(\bar{w}\bar{u} + \overline{w'u'}\right)\right] + \frac{\partial}{\partial z}\left(\bar{w}^2 + \overline{w'^2} + \frac{\bar{p}}{\rho_a}\right) = \left(\frac{\bar{\rho}-\rho_a}{\rho_a}\right) g \qquad (1.2.2)$$

(ii) Radial momentum

$$-\frac{1}{r}\frac{\partial}{\partial r}\left[r\left(\left(\bar{u}^2 + \overline{u'^2}\right) + \frac{\bar{p}}{\rho_a}\right)\right] + \frac{\partial}{\partial z}\left(\bar{w}\bar{u} + \overline{w'u'}\right) = 0 \qquad (1.2.3)$$

where $w'$ and $u'$ are the deviations in velocity from the time-averaged mean values $\bar{w}$ and $\bar{u}$ respectively, and $\bar{p}$ is the mean deviation from the hydrostatic pressure.

(c) Energy equation (tracer conservation)

$$\frac{1}{r}\frac{\partial}{\partial r}\left(r\bar{c}\bar{u} + r\overline{c'u'}\right) + \frac{\partial}{\partial z}\left(\bar{w}\bar{c} + \overline{w'c'}\right) = 0 \qquad (1.2.4)$$

where $\bar{c}$ is the time-averaged concentration and $c'$ the deviation from this mean value. The linear form

$$\frac{\bar{\rho}(r,z) - \rho_a}{\rho_a} = \delta(\bar{c}(r,z) - c_a) \qquad (1.2.5)$$

is assumed, where $\delta$ is taken to be constant.

The above system of five (5) equations (1.2.1) to (1.2.5) has eleven (11) unknowns $\bar{w}$, $\bar{u}$, $\bar{c}$, $\overline{w'^2}$, $\overline{u'^2}$, $\overline{c'^2}$, $\bar{p}$, $\overline{w'u'}$, $\overline{w'c'}$, $\overline{u'c'}$, $\bar{\rho}$, and therefore cannot be solved even if the appropriate boundary conditions were provided. This is the fundamental problem of turbulent fluid mechanics.

A large number of methods of dealing with this general problem have been proposed but the existing work on axisymmetric free shear flows can be classified into two schools of thought. The first school tries to

derive a constitutive equation between the Reynolds stress tensor and the deformation tensor of the fluid. The early workers in this school in addition assumed self preservation for the mean and fluctuating quantities (see for example, Tollmien (1945), G. I. Taylor (1932), Schlichting (1968) and Rajaratnam (1976)). More recent workers use more complex constitutive equations and solve the appropriate system of equations numerically (see, for example, Saffman (1970), Rodi (1980), Ooms and Wicks (1975), Launder and Spalding (1972).

A second group of investigators integrates the equations of motion across the jet and derives conservation integrals for the mass, momentum and buoyancy fluxes (see Corrsin and Uberoi (1950),Morton et al (1956), Brooks and Koh (1965) and List and Imberger (1973)). For a round vertical buoyant jet this approach leads to equations (see Fischer et al (1979)) of the form

(1) Conservation of volume flux

$$\frac{d}{dz}\int_0^\infty \bar{w}(r,z)\, 2\pi r dr = -\lim_{r\to\infty}(2\pi r\bar{u})$$

or

$$\frac{d\mu}{dz} = -\lim_{r\to\infty}(2\pi r\bar{u}) \;; \quad \mu = \int_0^\infty \bar{w}(r,z)\, 2\pi r dr \tag{1.2.6}$$

(2) Conservation of momentum flux

$$\frac{d}{dz}\int_0^\infty \bar{w}^2(r,z)\, 2\pi r dr = \int_0^\infty \left(\frac{\bar{\rho}(r,z)-\rho_a}{\rho_a}\right) g\, 2\pi r dr$$

or

$$\frac{dm}{dz} = \int_0^\infty \left(\frac{\bar{\rho}(r,z)-\rho_a}{\rho_a}\right) g\, 2\pi r dr \;; \quad m = \int_0^\infty \bar{w}^2(r,z)\, 2\pi r dr \tag{1.2.7}$$

(3) Conservation of buoyancy flux

$$\frac{d}{dz}\int_o^\infty \bar{w}(r,z)\left(\frac{\bar{\rho}(r,z)-\rho_a}{\rho_a}\right) g\ 2\pi r dr = 0$$

or

$$\frac{d\beta}{dz} = 0\ ;\quad \beta = \int_o^\infty \bar{w}(r,z)\left(\frac{\bar{\rho}(r,z)-\rho_a}{\rho_a}\right) g\ 2\pi r dr \qquad (1.2.8)$$

For the derivation of the above three equations the following assumptions were made

(i) The integration is extended to infinity, hence it is argued that

$$\lim_{r\to\infty}\left[\bar{w}\,\bar{u} + \overline{w'u'}\right] = 0$$

$$\lim_{r\to\infty}\left[\bar{w}\,\bar{c} + \overline{w'c'}\right] = 0$$

$$\lim_{r\to\infty}\left[\bar{u}\,\bar{c} + \overline{u'c'}\right] = 0$$

(ii) It is assumed that the turbulent tracer transport $\overline{w'c'}$ is negligible in comparison to $\bar{w}\,\bar{c}$.

(iii) It is assumed that $\overline{w'^2} + \bar{p}/\rho_a \ll \bar{w}^2$. This has been justified by Miller and Comings (1957).

The above three equations have provided the conceptual framework for almost all of the previous investigations of jets, plumes and buoyant jets. From this point on, two approaches have been used to

obtain the basic jet behavior: the entrainment coefficient approach, and dimensional analysis.

(a) Entrainment coefficient approach

The entrainment coefficient approach used by Brooks and Koh (1965), Morton et al. (1956), Morton (1959), Fan (1967) and Fan and Brooks (1969) is based on the hypothesis made by G. I. Taylor (1956) that the entrainment should be proportional to some characteristic velocity of the jet, i.e.

$$\lim_{r\to\infty} (2\pi r\bar{u}) = 2\pi a_e b_w \bar{w}_c \tag{1.2.9}$$

where Morton (1959) assumed the entrainment coefficient $a_e$ to be constant with the same value for jets and plumes. The velocity and concentration profiles are assumed to be similar, based on the experimental results, following Gaussian distributions

$$\bar{w}(r,z) = \bar{w}_c(z) \exp[-(r/b_w)^2] \tag{1.2.10}$$

$$\bar{c}(r,z) = \bar{c}_c(z) \exp[-(r/b_c)^2] \tag{1.2.11a}$$

or

$$\rho(r,z) - \rho_a = (\bar{\rho}_c(z) - \rho_a) \exp[-(r/b_c)^2] \tag{1.2.11b}$$

where the characteristic lengths of the velocity profile, $b_w(z)$, and the concentration profile (density difference), $b_c(z)$, are defined by the relations

$$\bar{w}(b_w(z),z) = \bar{w}_c(z)/e \tag{1.2.12}$$

$$\bar{c}(b_c(z),z) = \bar{c}_c(z)/e \tag{1.2.13a}$$

$$(\Delta\bar{\rho})(b_c(z),z) = (\Delta\bar{\rho})_c(z)/e \tag{1.2.13b}$$

where e is the base of the Napierian logarithms. (Many authors define the b(z)'s as the half-velocity and half-concentration characteristic lengths. This multiplies the exponent of the Gaussian profile by a factor of ln(2)). One further assumption has been that

$$\frac{b_c(z)}{b_w(z)} = \lambda \tag{1.2.14}$$

where $\lambda$ is supposed to be a universal constant.

Under these assumptions the equations (1.2.6), (1.2.7) and (1.2.8) can be written as

$$\frac{d}{dz}(\pi\bar{w}_c b_w^2) = 2\pi a_e b_w \bar{w}_c \tag{1.2.15}$$

$$\frac{d}{dz}\left(\frac{\pi}{2}\bar{w}_c^2 b_w^2\right) = \pi\frac{(\Delta\bar{\rho})_c}{\rho_a}\lambda^2 b_w^2 g \tag{1.2.16}$$

$$\frac{d}{dz}\left(\bar{w}_c\frac{(\Delta\bar{\rho})_c}{\rho_a}g\pi\frac{b_w^2\lambda^2}{1+\lambda^2}\right) = 0 \tag{1.2.17}$$

where $(\Delta\bar{\rho})_c(z) = \bar{\rho}_c(z)-\rho_a$. Fan and Brooks (1969) solved the above system of equations numerically to find the evolution of $b_w(z)$, $\bar{w}_c(z)$,

$(\Delta\bar{\rho})_c(z)$.

At this point it will be useful to try to solve the above system of equations for the two limiting cases, jets and plumes. We define:

(i) Pure momentum jet as the flow driven by continuous injection of momentum at the source

(ii) Pure plume as the flow driven by continuous addition of buoyancy at the source, and

(iii) Buoyant jet as the flow which is driven by both, buoyancy and momentum.

(a) For the limiting case of the pure momentum jet $(\Delta\bar{\rho})_o=0$) system of the above equations (1.2.15), (1.2.16) and (1.2.17) becomes

$$\frac{d}{dz}(\bar{w}_c b_w^2) = 2a_j b_w \bar{w}_c \tag{1.2.18}$$

and

$$\frac{\pi}{2}\bar{w}_c^2 b_w^2 = \pi(D^2/4)W^2 = M \tag{1.2.19}$$

Also the tracer transported by the jet is conserved, therefore

$$\int_o^\infty \bar{w}(r,z)\,\bar{c}(r,z)\,2\pi r dr = \frac{\pi D^2}{4} WC_o \tag{1.2.20a}$$

or

$$\frac{\bar{w}_c \bar{c}_c \lambda^2 b_w^2}{1+\lambda^2} = \frac{D^2}{4} WC_o \tag{1.2.20b}$$

where W and $C_o$ are the velocity and concentration at the jet exit. By substituting equation (1.2.19) into (1.2.18) one can get explicitly

$$\frac{db_w}{dz} = K_{1w} = 2a_j \tag{1.2.21}$$

where $K_{1w}$ is a constant and $a_j$ is the entrainment coefficient for a pure jet. Equation (1.2.21) can be written as

$$\frac{b_w}{D} = K_{1w}\left(\frac{z}{D} + K_{2w}\right) \tag{1.2.22}$$

From the equations (1.2.19) and (1.2.22) the derived centerline mean velocity is

$$\frac{W}{\bar{w}_c} = \sqrt{2}\, K_{1w}\left(\frac{z}{D} + K_{2w}\right) \tag{1.2.23}$$

From equations (1.2.20b) and (1.2.23) the centerline concentration is determined as

$$\frac{C_o}{\bar{c}_c} = \frac{2\sqrt{2}\,\lambda^2}{1+\lambda^2} K_{1w}\left(\frac{z}{D} + K_{2w}\right) \tag{1.2.24}$$

(b) For the limiting case of a pure plume the equations (1.2.15), (1.2.16) and (1.2.17) become

$$\frac{d}{dz}\left(\bar{w}_c b_w^2\right) = 2a_p b_w \bar{w}_c \tag{1.2.25}$$

$$\frac{d}{dz}\left(\bar{w}_c^2 b_w^2\right) = \frac{2B(1+\lambda^2)}{\pi \bar{w}_c} \tag{1.2.26}$$

$$\frac{dB}{dz} = \frac{d}{dz}\left(\bar{w}_c \frac{(\Delta\bar{\rho})_c}{\rho_a}\, g\pi b_w^2 \frac{\lambda^2}{1+\lambda^2}\right) = 0 \tag{1.2.27}$$

where B is the specific plume buoyancy flux. Following Morton et al (1956), we assume that $b_w = bz^{\alpha}$, $\bar{w}_c = wz^{\beta}$, $(\Delta\bar{\rho})_c/\rho_a = \rho z^{\gamma}$, and substituting into (1.2.25), (1.2.26) and (1.2.27) we obtain for a point source

$$\alpha = 1$$

$$\beta = -1/3$$

$$\gamma = -5/3.$$

Substituting for $b_w$, $w_c$ and $(\Delta\bar{\rho})_c$ in equations (1.2.25), (1,2,26) and (1.2.27) leads to

$$b_w = \frac{6}{5} a_p z \tag{1.2.28}$$

$$\bar{w}_c = \frac{5}{6a_p}\left[\frac{9}{5} a_p \frac{1+\lambda^2}{\pi} B\right]^{1/3} z^{-1/3} \tag{1.2.29}$$

or

$$\bar{w}_c \sim \left(\frac{B}{z}\right)^{1/3}$$

and

$$\frac{(\Delta\bar{\rho})_c}{\rho_a} = \frac{B(1+\lambda^2)}{\lambda^2 \pi g}\left[\frac{9}{5} a_p \frac{1+\lambda^2}{\pi} B\right]^{-1/3} \frac{5}{6a_p} z^{-5/3} \tag{1.2.30}$$

or

$$\frac{(\Delta\bar{\rho})_c}{\rho_a} \sim \frac{B^{2/3}}{g} z^{-5/3}$$

From the equations (1.2.21) and (1.2.28) and for a constant entrainment coefficient (i.e. $a_j = a_p$) it is concluded that the width of the jet is

5/3 times the plume width. Experimental evidence shows that they are approximately equal and therefore the assumption of a universal entrainment coefficient is incorrect. Alternatively if $b_w \cong b_c$ then

$$a_p = \frac{5}{3} a_j$$

(b) Dimensional analysis

The results above agree with those deduced from dimensional analysis: For a pure jet in uniform environment, equation (1.2.16) implies that the kinematic momentum flux is conserved i.e.

$$\bar{w}_c^2 b_w^2 = \text{constant}$$

Dimensional analysis then gives for a pure jet

$$b_w(z) \sim z$$

$$\bar{w}_c(z) \sim 1/z$$

(see Schlichting (1968), Landau and Lifshitz (1975) and Rajaratnam (1976)). For a plume, Batchelor (1954) showed that

$\therefore$

$$\bar{w}_c(z) \sim (B/z)^{1/3}$$

$$b_w(z) \sim z$$

$$(\Delta\bar{\rho})_c(z) \sim \frac{B^{2/3}}{g} z^{-5/3}$$

List and Imberger (1973) used dimensional analysis to write the equations of motion in the form

$$\frac{d\mu}{dz} = \xi(z) = m^{1/2}\, q(R,C)$$

$$\frac{dm}{dz} = \eta(z) = \frac{\mu\beta}{m}\, h(R,C)$$

$$\frac{d\beta}{dz} = 0$$

where

$$R = \frac{\mu^2\beta}{m^{5/2}}, \qquad C = \frac{\mu}{zm^{1/2}}$$

and

$$\mu = \int_0^\infty \bar{w}(r,z)\, 2\pi r dr, \qquad m = \int_0^\infty \bar{w}^2(r,z)\, 2\pi r dr$$

$$\beta = \int_0^\infty \frac{\left(\bar{\rho}(r,z) - \rho_a\right)}{\rho_a}\, g\, \bar{w}(r,z)\, 2\pi r dr$$

Their objective was to find the leading terms of the functions q(R,C) and h(R,C).

In the next section we discuss the dimensional analysis approach systematically.

## 1.3 Dimensional analysis

In this section the problem of jets, plumes and buoyant jets is presented using characteristic dimensionless quantities. There are two main reasons this is done here. (i) Both in nature and in the laboratory it is difficult to obtain an ideal pure jet or pure plume. The reason is that there is almost always initial momentum injected to the flow and a temperature difference between the jet and the ambient fluid. (ii) A jet with even very small initial buoyancy will eventually become a plume in a uniform environment. Given these results an understanding of the transition from jets to plumes becomes of significance and in practical applications the following jet parameters with their dimensions are defined

Q...($L^3/T$) initial jet discharge

W...($L/T$) initial jet exit velocity

M...($L^4/T^2$) specific momentum flux at the jet origin

B...($L^4/T^3$) specific buoyancy flux at jet exit

where $W=4Q/\pi D^2$ and $B=(\Delta\rho)_o/\rho_a gQ$. Following Fischer et al. (1979) it is possible to define two characteristic length scales of a jet as follows

$$\ell_Q = \frac{Q}{M^{1/2}}, \qquad \ell_M = \frac{M^{3/4}}{B^{1/2}} \tag{1.3.1}$$

The basic properties of a pure momentum jet and a simple plume based on dimensional arguments as in Chapter 9 by Fischer et al. (1979), are

summarized in Table 1.3.1 The parameters $a_i$, $a_i'$, $b_i$, $b_i'$, and $c_j$ are the constants of proportionality for equations (1.3.2) to (1.3.10); Y and S are defined as

$$Y = QC_o \qquad S = \frac{C_o}{\bar{c}_c} \quad .$$

From equations (1.3.8a) and (1.3.9a) by eliminating z one finds

$$R_p = \mu B^{1/2}/m^{5/4}$$

where $R_p = b_3 b_2^{-5/4}$=constant, and it is called the plume Richardson number. Also by eliminating B from the above equations and by evaluating m(z) and $\mu(z)$ from the Gaussian velocity profile equation (1.3.9) becomes

$$\sqrt{2\pi}\, b_w = c_p z \; ; \quad c_p = b_3/b_2^{\frac{1}{2}} \tag{1.3.11}$$

$c_p$ and $c_j$ are therefore the growth coefficients for plumes and jets.

The jet has initially both momentum M and buoyancy flux B. At a distance z from the orifice the velocity on the axis of the jet will be

$$\frac{\sqrt{M}}{\bar{w}_c z} = f\left(\frac{z}{\ell_M}\right)$$

The two limiting cases for $z/l_M \ll 1$ (momentum driven flow) and $z/l_M \gg 1$ (buoyancy driven flow) lead us to the equations (1.3.2) and (1.3.7) respectively. The same is observed for the concentrations.

The ratio $l_Q/l_M$ is called initial jet Richardson number and for a round jet we define

Momentum Jet

$$\frac{\bar{w}_c Q}{M} = a_1 \frac{\ell_Q}{z} \qquad (1.3.2a) \qquad \text{or} \qquad \frac{\sqrt{M}}{\bar{w}_c z} = a_1' \qquad (1.3.2b)$$

$$\frac{b(z)}{\ell_Q} = a_2 \frac{z}{\ell_Q} \qquad (1.3.3)$$

$$\frac{\mu}{Q} = c_j \frac{z}{\ell_Q} \qquad (1.3.4)$$

$$\frac{m}{M} = \text{constant} \qquad (1.3.5)$$

$$\frac{\bar{c}_c}{C_o} = a_4 \left(\frac{\ell_Q}{z}\right) \qquad (1.3.6a) \qquad \text{or} \qquad \frac{SQ}{z\sqrt{M}} = a_4' \qquad (1.3.6b)$$

Simple Plume

$$\bar{w}_c = b_1 \left(\frac{B}{z}\right)^{1/3} \qquad (1.3.7a) \qquad \text{or} \qquad \frac{\sqrt{M}}{\bar{w}_c z} = b_1' \left(\frac{z}{\ell_M}\right)^{-2/3} \qquad (1.3.7b)$$

$$m(z) = b_2 B^{2/3} z^{4/3} \qquad (1.3.8a) \qquad \text{or} \qquad \frac{m(z)}{M} = b_2' \left(\frac{z}{\ell_M}\right)^{4/3} \qquad (1.3.8b)$$

$$\mu(z) = b_3 B^{1/3} z^{5/3} \qquad (1.3.9a) \qquad \text{or} \qquad \frac{\mu(z) B^{1/2}}{M^{5/4}} = b_3' \left(\frac{z}{\ell_M}\right)^{5/3} \qquad (1.3.9b)$$

$$\frac{\bar{c}_c}{Y} = \frac{b_4}{B^{1/3} z^{5/3}} \qquad (1.3.10a) \qquad \text{or} \qquad \frac{SQ}{z\sqrt{M}} = b_4' \left(\frac{z}{\ell_M}\right)^{2/3} \qquad (1.3.10b)$$

Table 1.3.1. Summary of properties of turbulent jets and plumes.

$$R_o = \frac{\ell_Q}{\ell_M} = \frac{QB^{1/2}}{M^{5/4}} = \left(\frac{\pi}{4}\right)^{1/4}\left[\frac{(\Delta\rho)_o}{\rho_a}\ gD/W^2\right]^{1/2} = \left(\frac{\pi}{4}\right)^{1/4}\frac{1}{F_d}$$

$F_d$ is commonly called the densimetric Froude number. Making use of the previously defined plume coefficients $c_p$ and $R_p$ we write for round jets according to Kotsovinos and List (1976)

$$\bar{\mu} = \frac{\mu B^{1/2}}{R_p M^{5/4}} = \frac{\mu}{Q}\left(\frac{R_o}{R_p}\right)$$

and

$$\zeta = \frac{c_p}{R_p}\frac{z}{\ell_M} = c_p\left(\frac{z}{\ell_Q}\right)\frac{R_o}{R_p}$$

Then equation (1.3.4) for the jet volume flux becomes

$$\bar{\mu} = \zeta, \quad \zeta<<1 \ ; \ R_o/R_p \text{ small.}$$

Similarly equation (1.3.9) becomes

$$\bar{\mu} = \frac{b_3 R_p^{2/3}}{c_p^{5/3}}\zeta^{5/3} = \zeta^{5/3}; \quad \zeta>>1$$

for the volume flux in a plume.

## 1.4 Review of previous experiments

There is a large number of experimental investigations on turbulent jets while the published work for plumes is very limited. Our interest is centered on the investigations that deal with the jet characteristics away from the jet orifice i.e. for $z/l_Q > 7$. Experimenters have determined the flow field of the jet by measuring velocities, concentrations (or temperatures), and pressures, one at a time or simultaneously. Instrumentation and techniques vary for the different investigators and have become more advanced every year. In the following paragraph previous work will be reviewed briefly.

(a) Momentum jet: Experimenters usually measure velocities and concentrations at various locations of the jet field, and plot the growth widths, radial and axial distributions of the mean velocities and concentrations and determine the relations

$$\frac{b_w}{D} = K_{1w}\left(\frac{z}{D} + K_{2w}\right)$$

$$\frac{b_c}{D} = K_{1c}\left(\frac{z}{D} + K_{2c}\right)$$

$$\frac{W}{\bar{w}_c} = C_{1w}\left(\frac{z}{D} + C_{2w}\right)$$

$$\frac{C_o}{\bar{c}_c} = C_{1c}\left(\frac{z}{D} + C_{2c}\right)$$

The coefficients $K_{1w}$, $K_{2w}$, $K_{1c}$, $K_{2c}$, $C_{1w}$, $C_{2w}$, $C_{1c}$, $C_{2c}$, are determined empirically from the experimental data. Some authors report their mean velocity and concentration results in the form

$$\frac{\bar{w}(r,z)}{\bar{w}_c(z)}\ ,\ \frac{\bar{c}(r,z)}{\bar{c}_c(z)} = \exp\left[-k\left(\frac{r}{z}\right)\right]^2$$

without ever determining the location of a virtual origin. The coefficient $K_{1w}$ and $K_{1c}$ then are calculated by

$$K_{1w}, K_{1c} = \frac{1}{\sqrt{k}} \quad .$$

Tables (1.4.1) and (1.4.2) summarize the principal parameters and results (K's and C's) and the turbulence parameters respectively. Abbis, Bradbury and Wright (1975) measured the turbulence characteristics of an air jet up to 25 jet diameters by using laser-Doppler anemometry. The width of the jet was calculated from the mean velocity profile. Albertson et al. (1950) used a Pitot tube to measure the mean velocity of an air jet up to 250 diameters downstream. They reported the mean velocity decay constant $C_{1w}$, but the half velocity width was determined from the mean velocity profile. Antonia et al. (1975) measured velocities and temperatures conditionally in a heated jet with a co-flowing stream using X-wire anemometers for three initial velocity ratios, 59 diameters from the jet origin. The values of the various turbulent parameters (except the axial turbulent velocities) are higher than those reported by other investigators, which implies that the co-flowing stream has some effect on the jet turbulence. Antonia et al. (1980) discuss the accuracy of temperature fluctuation measurements in heated turbulent air jets by using hot wires. They give the mean velocity and temperature profiles at 20 and 60 diameters downstream and conditional probability density functions of the velocity, along with the moments up to the 6th order. Becker et al. (1967) used a light scattering technique to measure concentrations in an air jet traced by oil smoke; their results are of high quality. Mean and turbulence profiles are presented up to 85 jet diameters along with

| AUTHOR (year) | z/D | Re | $b_{0.5}$ $K_{1w}$ | $b_{1/e}$ $K_{1w}$ | $K_{2w}$ | $C_{1w}$ | $C_{2w}$ | $b_{0.5}$ $K_{1c}$ | $b_{1/e}$ $K_{1c}$ | $K_{2c}$ | $C_{1c}$ | $C_{2c}$ |
|---|---|---|---|---|---|---|---|---|---|---|---|---|
| Abbiss et al. (1975) | 0 - 25 | | 0.090 | 0.110 | -0.98 | 0.182 | -0.98 | | | | | |
| Albertson et al. (1950) | 0 - 250 | 22,700 - 90,800 | | 0.110 | | 0.161 | | | | | | |
| Antonia et al. (1975) | 59 | 36,500 | | | | | | | | | | |
| Antonia et al. (1980) | w / 0 20 / 60 | 74,600 - 117,000 | | | | | | | | | | |
| Becker et al. (1967) | 10 - 85 | 54,000 | | | | | | 0.106 | 0.115 | -2.4 | 0.185 | -2.4 |
| Birch et al. (1978) | 7 - 70 | 16,000 | | 0.117 | | 0.20 | -3.7 | | | | 0.250 | -5.8 |
| Chevray & Tutu (1978) | 15 | 332,600 | 0.085 | 0.0995 | | 0.141 | | 0.096 | 0.115 | | 0.177 | |
| Corrsin (1943) | 5 - 50 | 15,800 | 0.083 | 0.100 | | 0.243 | -3.106 | 0.108 | 0.132 | | 0.194 | 1.58 |
| Corrsin & Uberoi (1949) | 0 - 26 | >33,500 | 0.107 | 0.114 | | 0.1241 | -2.76 | 0.107 | 0.140 | | 0.278 | |
| Corrsin & Kistler (1955) | 20 - 52 | 79,000 | 0.098 | 0.122 | 2.50 | | | | | | | |
| Forstall & Gaylord (1955) | 0 - 50 | | 0.085 - 0.113 | | | 0.161 | | 0.096 - 0.115 | | | 0.192 | |
| Gibson (1963) | 50 | | | | | | | | | | | |
| Grandmaison et al. (1977) | 20 - 80 | 21,000 - 270,000 | | | | | | 0.105 | | -2.4 | 0.185 | -2.4 |
| Hinze & Zijnen (1949) | 0 - 40 | 67,000 | 0.083 | 0.102 | | 0.1565 | 3.84 | 0.96 | 0.115 | | 0.319 | -4.17 |
| Kiser (1963) | 0 - 40 | 30,000 - 50,000 | 0.0815 | | 1.15 | 0.164 | 1.15 | 0.104 | | 1.15 | 0.20 | 1.15 |
| Rosenzweig et al. (1961) | 8 - 44 | 26,200 | | 0.100 | | | | | 0.118 | | | |
| Rosler & Rankoff (1963) | 5 - 30 | 48,000 | | | | air/water 0.19/0.186 | air/water 0.8 / 0.9 | | | | | |
| Sforza & Mons (1978) | 0 - 26 | | 0.089 | 4.7 | | 0.16 | 1.8 | 0.108 | | 0.7 | 0.215 | 1.5 |
| Sunavala et al. (1957) | 15 - 85 | 28,700 - 56,900 | 0.117 | 0.141 | | | | | | | 0.215 | -1.5 |
| White (1967) | 10 - 25 | 24,000 - 63,000 | | | | 0.146 | 0.00 | | | | | |
| Wilson & Dankwerts (1964) | 5 - 100 | 38,000 | | 0.120 | | 0.200 | | | 0.156 | | 0.175 | |
| Wygnanski & Fiedler (1969) | 5 - 97.5 | $\approx 10^5$ | 0.085 | 0.104 | | 0.198 | -7.0 | | | | | |

Table 1.4.1. Review of previous experiments for an axisymmetric jet. Mean values - widths.

| AUTHOR (year) | $\sqrt{w'^2}/\bar{w}_c$ | $\sqrt{u'^2}/\bar{w}_c$ | $\overline{w'u'}/\bar{w}_c^2$ | $\ell$ $\sqrt{c'^2}/\bar{c}_c$ | peak $\sqrt{c'^2}/\bar{c}_c$ | $\ell$ $\overline{w'c'}/\bar{w}_c\bar{c}_c$ | peak $\overline{w'c'}/\bar{w}_c\bar{c}_c$ | $\overline{u'c'}/\bar{w}_c\bar{c}_c$ |
|---|---|---|---|---|---|---|---|---|
| Abbiss et al. (1975) | 0.28 | 0.22 | 0.20 | | | | | |
| Albertson et al. (1950) | | | | | | | | |
| Antonia et al. (1975) | 0.30/0.32 | 0.30/0.32 | 0.035 | 0.255 | 0.330 | 0.030 | 0.038 | 0.041 |
| Antonia et al. (1980) | 0.228 - 0.250 | | | 0.210 | 0.260 | | | |
| Becker et al. (1967) | | | | 0.20 | 0.23 | | | |
| Birch et al. (1978) | 0.18 - 0.28 | | | 0.20 - 0.28 | 0.24 - 0.336 | | | |
| Chevray & Tutu (1978) | 0.22 / 0.235 | 0.19 | | 0.20 | 0.24 | 0.213 | 0.028 | 0.016 |
| Corrsin (1943) | 0.26 | | | | | | | |
| Corrsin & Uberoi (1949) | 0.22 | 0.175 | 0.011 | 0.15 | 0.170 | | | 0.0125 |
| Corrsin & Kistler (1955) | | | | | | | | |
| Forstall & Gaylord (1955) | | | | | | | | |
| Gibson (1963) | 0.30 | 0.30 | | | | | | |
| Grandmaison et al. (1977) | | | | | 0.219 | 0.263 | | |
| Hinze & Zijnen (1949) | 0.20-0.27 | | | | | | | |
| Kiser (1963) | | | | | | | | |
| Rosenweig et al. (1961) | | | | 0.170 | 0.220 | | | |
| Rosler & Bankoff (1963) | air/water 0.22 / 0.32 | | air/water 0.016/0.017 | | | | | |
| Sforza & Mons (1978) | 0.25 | | | | | | | |
| Sunavala et al. (1957) | | | | | | | | |
| White (1967) | | | | | | | | |
| Wilson & Dankwerts (1964) | | | | 0.18 | 0.216 | | | |
| Wygnanski & Fiedler (1969) | 0.28 | 0.25 | 0.0165 | | | | | |

Table 1.4.2. Review of previous experiments for an axisymmetric jet. Turbulence properties.

intermittencies, spectra, spatial autocorrelation and integral scales of turbulence. Chevray and Tutu (1978) examined the turbulence parameters and the radial and axial turbulent mass transport of heat in a heated air jet using hot wire probes. Their work is first class but limited to 15 diameters, a region where the flow is not fully developed. Corrsin (1943), Corrsin and Uberoi (1949) and Corrsin and Kistler (1955) examined a heated air jet into air at rest very systematically. Forstall and Gaylord (1955) measured velocities and concentrations in a liquid into liquid jet using a transversing impact tube and conductivity cell with 1% salt added as a tracer into the jet water. Gibson (1963) measured the turbulence spectra, for z/D=50 and found all three components of the velocity fluctuations to be the same on the jet axis, which means that the turbulence there is isotropic, a result that does not agree with the data of any other author(see Table 1.4.2). Grandmaison et al (1977) "repeated" Becker's (1967) experiments at higher Reynolds numbers. Hinze and Zijnen (1949) measured the mean velocity, temperature and concentration profiles in a round air jet using foreign gas as tracer. Kiser (1963), using a technique similar to the one by Forstall and Gaylord (1955), derived the mean profiles and the axial decay of velocities and concentrations. Lassiter (1957) measured the axial velocity component at the initial jet region using hot wire anemometry. Rosenweig et al.(1961) measured concentrations in an air jet utilizing smoke scattered light from the jet. Their data are inconsistent. Rosler and Bankoff (1963) measured velocities in both, air and water jets using a hot wire and a hot film anemometer respectively. Both experiments were performed at the same initial Reynolds number. They found that the decay of the mean velocity along

the centerline was the same for both air and water jet. The rms values measured in the water jet were 30% higher than those measured in the air jet. Sforza and Mons (1978) measured the mass and enthalpy transport in isothermal and non isothermal heated air jets. They used a static pressure probe with sampling ability. White (1967), looked at the jet growth rate and mean velocity profile with fluid additives present. Guar gum up to 50 ppm did not affect the flow, while Polyox solution at 50 ppm reduced the mean velocities. Wygnanski and Fiedler (1969) in a careful experiment using hot wire anemometry measured three velocity components in a round jet. Their flow became self similar after the first 40 jet diameters with two virtual origins observed for z/D less or bigger than 40. The profiles for mean values, intensities of turbulence and shear stresses were also presented, along with the intermittency, spectral properties and the turbulent energy balance. Birch et al. (1978) measured concentrations by using laser Raman spectroscopy. In high quality work they measured the mean and turbulent concentrations, and calculated correlations and integral length scales. Sunavala et al. (1957) and Wilson and Danckwerts (1964) measured temperatures in a heated jet. Their data are comparable but Wilson's experimental work is more complete. Ricou and Spalding (1961) directly measured the entrainment rate in jets and buoyant jets of various gases into air with or without combustion. Hill (1972) used a similar technique in order to measure the entrainment rate at the initial region of a round jet. Ribeiro and Whitelaw (1975) used hot wire anemometers to measure probability density functions and autocorrelations of the velocity components at z/D=57. The use of hot wires or hot films for velocimetry turned out to be very limited, in regions where the flow is reversed.

This is shown clearly in the work of Lau et al (1979). They measured higher turbulent intensities and broader probability density functions with the laser-Doppler anemometer than with the hot wires.

(b) Pure plume. Rouse et al (1952) used a copper-constantan thermocouple and a vane anemometer in order to measure temperatures and velocities above a heated air plume. They calculated the input heat flux *a posteriori* without taking into account the turbulent heat transfer (they assumed that $\overline{w'T'} << \bar{w}\bar{T}$). This kind of experiment is very delicate because in the ambient air small convection currents usually exist. Therefore the assumption of a motionless environment is usually violated. The substantial scatter in their data are probably due to either inadequate instrumentation or to existing ambient air currents. From the mean profiles determined from their data, the half velocity and temperature widths were calculated to be $b_w \sim 0.085z$ and $b_c \sim 0.099z$. George et al (1977) measured velocities and temperatures simultaneously using a two-wire probe. They knew the initial heat flux, and the mean profiles for $\bar{w}$, $\bar{T}$ found were

$$\bar{w} = 3.4F_o^{1/3}z^{-1/3} \exp[-55(r/z)^2], \quad \frac{\Delta\bar{\rho}}{\rho} g = 9.1F_o^{2/3}z^{-5/3} \exp[-65(r/z)^2]$$

The half widths were calculated and found $b_w \sim 0.112z$ and $b_c \sim 0.103z$ which means that the half velocity width is wider than the temperature width, opposite to what Rouse et al (1952) found. The relative turbulent intensities were found to be 0.4 and 0.25 at the plume axis for the temperature and axial velocity respectively. They also found that the turbulent heat transport is about 15% of the total. All measurements were made at 8, 12 and 16 diameters and therefore the assumed self-similarity may not be correct (see Wygnanski and Fiedler

(1969)). Nakagome and Hirata (1976) performed plume experiments above a heated disc measuring velocities and temperatures using hot wires. The half widths were found $b_w \sim 0.133z$ and $b_c \sim 0.105z$ for $\bar{w}$ and $\bar{T}$ respectively, results that agree qualitatively with those of George et al. (1977). They present mean profiles for $\bar{w}$, $\bar{T}$ and the relative turbulent intensities are 0.25 and 0.35 for velocity and temperature respectively. Their measurements extended to radial distances r/z=0.15, without reaching the jet boundary. They found $\overline{w'T'}/\bar{w}\,\bar{T} = 0.04$ on the plume axis. There is some question to how well the flow was developed since their experiments were performed at less than 11 disc diameters downstream. Abraham (1960) measured salt concentrations along the jet axis by using conductivity probe techniques. The tank in which the experiments were performed was very small and the ambient density did not remain constant for very long. From the published data $z/l_M$ was calculated to vary from 2 to 8, which implies measurements in the transition region from jets to plumes (see paragraph 1.3). From these data no asymptotic value for either jets or plumes can be deduced. Zimin and Frik (1977) measured the temperature distribution in a heated water jet by looking at the changes of the refractive index of the fluid with temperature variation. They found that the 1/e temperature width of their jet was $b_c/z=0.110$ and that the average temperature profile was given by the relationship

$$\bar{T}(r,z) = 7 \cdot \frac{(Q\rho c)^{2/3}}{(g\alpha)^{1/3}} z^{-5/3} \exp[-80(r/z)^2]$$

where, Q is the input heat flux at the jet, $\alpha$ is the thermal expansion coefficient and c is the specific heat of the water. They measured from 13 up to 38 diameters downstream, and the virtual origin for the

temperatures along the jet axis was determined at -12.5 jet diameters. Pryputniewicz and Bowley (1975) performed experiments in a finite depth tank up to 40 jet diameters. From the way their experimental results are presented, it is impossible to reach to any conclusion for comparison with other authors. Rao and Brzustowski (1969) present raw data for a plume above a fire up to ten disc diameters downstream. The changes in the velocity and temperature turbulent intensities and the turbulent transport term $\overline{w'T'}$ along the plume axis are found to be dramatic.

In summary, the data resulting from previous experimental studies confirm the basic features of the dimensional analysis. However, there is significant variation in the "universal" constants and basically no experimental evaluation of the fundamental hypothesis that the turbulent fluxes of momentum and mass are relatively small. Furthermore, there is no good experimental evidence to confirm the basic hypothesis used in computation that $\lambda = b_c/b_w$ is constant. Evaluations of the other plume parameter (the Richardson number) are equivocal. Also the already existing data for the plumes were obtained in the initial flow region where it is believed that the flow has not become self-similar. Finally there is no evidence that the profiles of $\overline{w'^2}$ and $\overline{c'^2}$ are necessarily different in plumes compared to jets.

The scope of the present experimental work is detailed investigation of the properties of jets plumes and buoyant jets in the far flow field where the flow becomes self-similar. In particular we seek for jet and plume growth laws, velocity and concentration decay laws and turbulence properties. It will be attempted to define basic

flow parameters of great importance in engineering applications such as the plume Richardson number and the mean plume dilution. Finally a novel experimental approach for simultaneous velocity and tracer concentration measurement is presented, that can be used extensively for experimental investigations in turbulent shear flows.

# 2. EXPERIMENTAL EQUIPMENT AND TECHNIQUES

## 2.1 Introduction

The objective of the experimental investigation was the study of round turbulent vertical buoyant jets over a wide range of initial Richardson numbers. The initial Richardson number $R_o$ is estimated to vary from zero (very small) for jet - like flow to about 1.5 for plume - like flow. Experiments were carried out in a glass wall tank with a cross section 1.15 m x 1.15 m and 3.35 m deep, where a jet was injected from an orifice with diameter which varied from .75 cm to 2.0 cm. Fluid velocities (w and u) and Rhodamine 6G dye concentrations (c) were measured simultaneously at the same point of flow by a laser-Doppler velocimeter combined with a laser-induced fluorescence system. For this purpose, a glass wall tank was equipped with an instrument carriage supporting a laser-Doppler velocimeter and a laser-induced fluorescence concentration measuring device. The carriage was able to move both vertically and horizontally with respect to the tank. Thus measurements of velocity and concentration could be obtained at various axial and radial locations in vertical planes containing the jet axis. The jet was located either deep in the tank and pointing vertically upwards (see Figure 2.1.1 (b)), or on top of the tank and pointing down as shown in Figure 3.1.1. In the first case the jet fluid was less dense than the ambient fluid and in the second case vice-versa. Sodium chloride-water solutions were used to obtain the desired initial density difference between the jet and the ambient fluid.

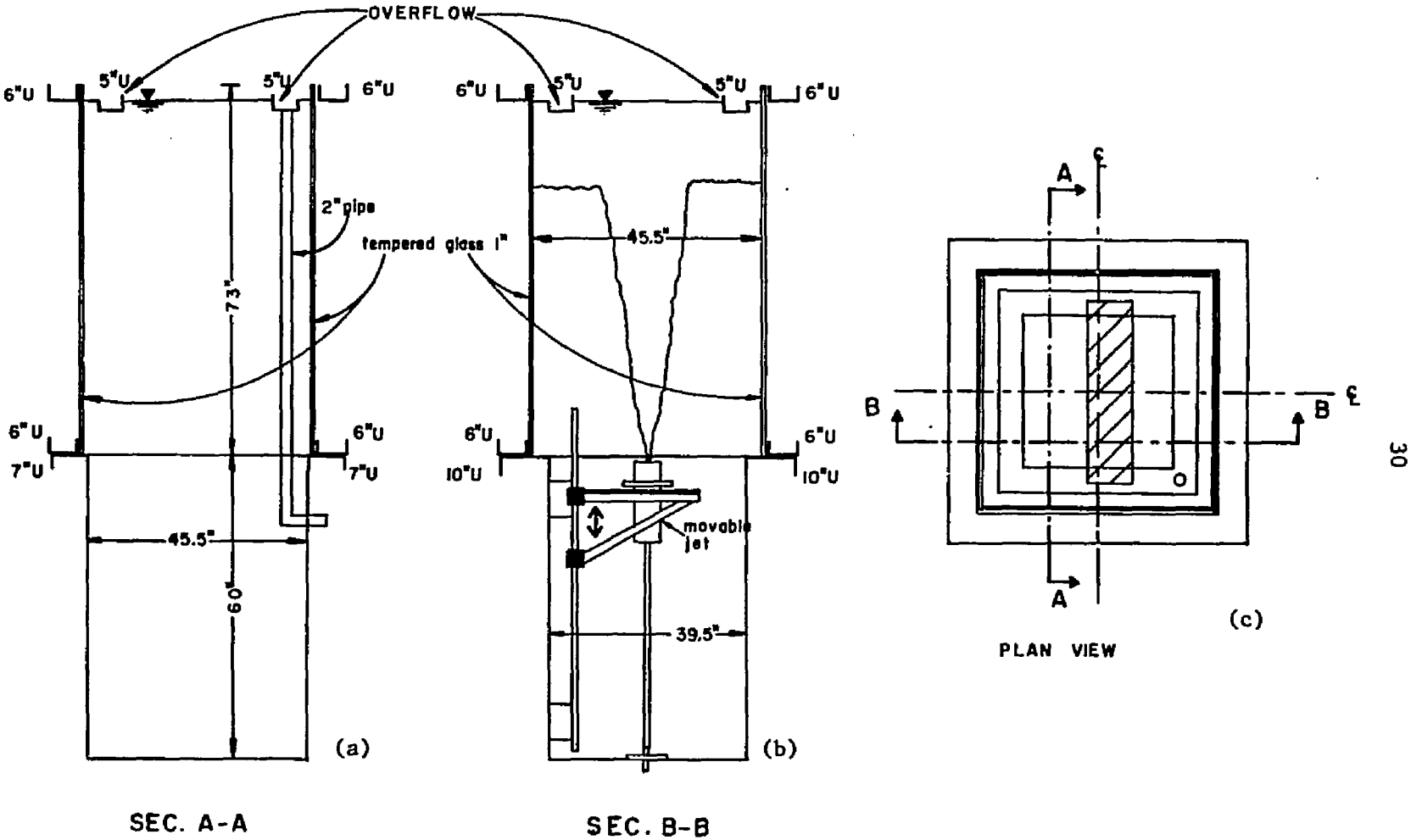


Figure 2.1.1. Glass wall tank - plan view, two vertical sections.

## 2.2 Tank, design and operation

The tank used for the experimental task was designed and constructed in the laboratory. In Figures 2.1.1 (a), (b) and (c) the plan view and two vertical cross sections of the tank are shown. The tank was constructed in two parts:

(a) The upper tank is the part where all the experimental work was carried out. Four corner posts were constructed from rectangular tubing steel cross sections with dimensions 6 in.x3 in.x1/4 in. and 4 in.x2 in.x1/4 in. welded together. They support four 1 in. thick tempered glass panels with dimensions 1.20 m x 1.85 m . The four corner posts, with a 3/8 in. thick plate welded on their upper and lower edge, were held together by two square frames made out of 6 in. wide steel U-section (see Figure 2.2.1 (a)). The glass is located on a 1/2 in. thick rubber inset on the inside edge of the lower tank, as shown in Figures 2.1.1 (a) and (b) and detail in Figure 2.2.2 (a). The glass windows were supported by aluminum clips, screwed to the frame on the top and bottom, and glazed with polyester body putty. Silicon rubber was placed in all four vertical corners and between the glass and the lower frame in order to obtain water tightness, avoiding any possible leakage of water from the tank (see details in Figures 2.2.2 (a), (b) and (c). A square overflow was placed four (4") inches below the top of the tank. It is made out of a 5 in. wide aluminum U-section with a knife-edge towards the glass. Four long screws were used to level the overflow and enable uniform surface drainage of the excess water. A 2 in. hole at one corner was used to drain the excess water out of the tank (see Figures 2.2.3 (a) and (b)). Four precision cylindrical rails 1 in. in diameter manufactured by the Linear

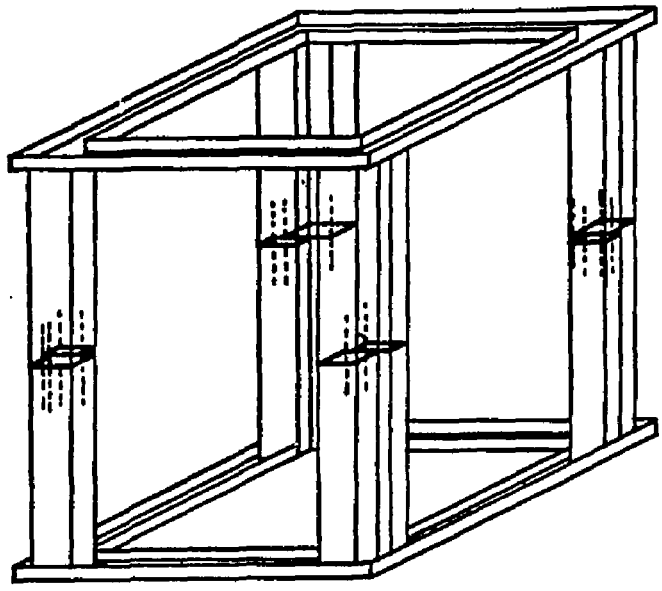

(a)

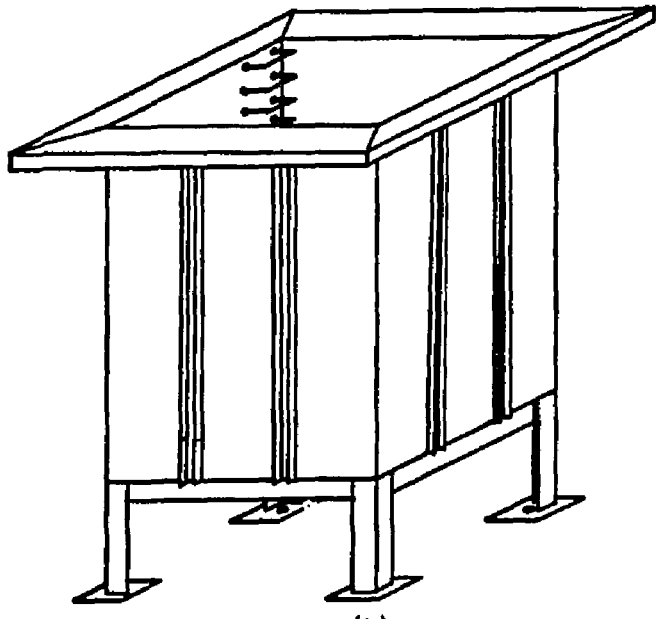

(b)

Figure 2.2.1. Tank: (a) upper frame, (b) lower tank.

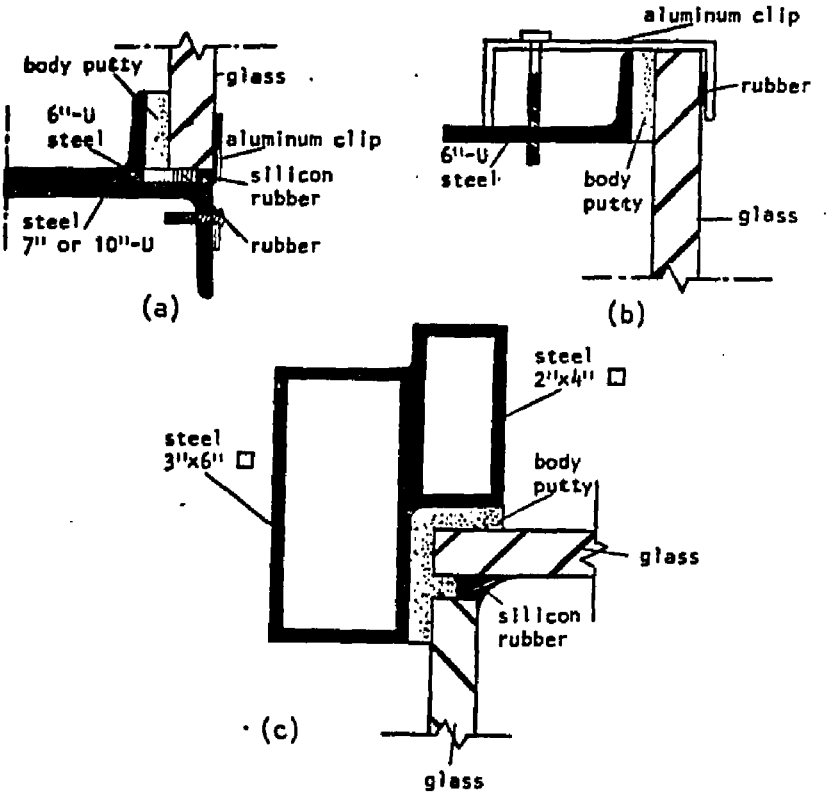


Figure 2.2.2. Details of the layout of the glass panels.
(a) Glass sitting on the lower tank;
(b) glass supported by aluminum clips at the upper square frame;
(c) glass vertical corner posts.

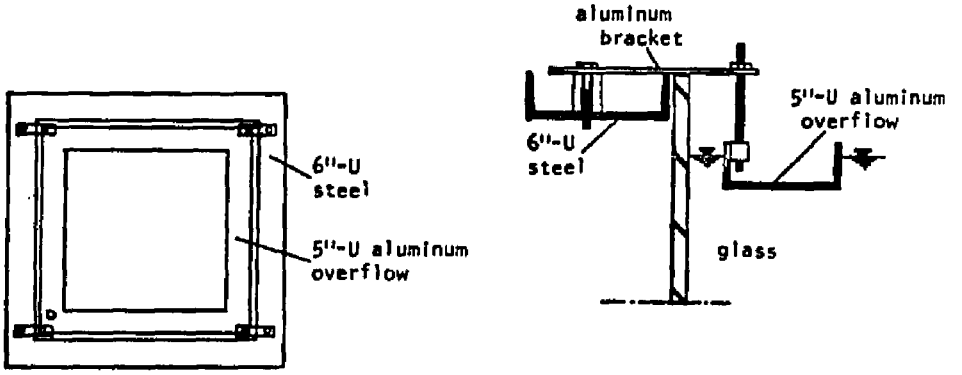


Figure 2.2.3. Overflow. (a) Plan view; (b) set-up detail.

Industries Ltd., were bolted in a vertical position at the four corner posts and used as supports and guides for the instrument carriage.

(b) The upper tank is bolted onto the lower tank. The lower tank (see Figure 2.2.1 (b)) was constructed from five 1/4 in. thick steel plates welded together (four on each side and one on the bottom). A square frame made out of 7 in. and 10 in. wide steel U-sections was welded to the four side plates, and formed a frame to which the upper frame was bolted. Two 3 in. wide steel U-section beams were welded in a vertical direction on each of the four sides and also along the bottom of the tank in order to provide extra support and rigidity. The bottom plate also supported by a steel 4 in.x4 in.x1/2 in. L-section welded around its perimeter. The tank is bolted to the floor with four 22 in. long legs made out of the same L-section as above and welded at each corner. In the center of the free side of the tank a 3 in. pipe section and a valve were attached for drainage. In the top right corner another 3 in. pipe section was welded in order to allow drainage of the excess water of the overflow. A 3 in. pipe connector was welded to the bottom of the tank and used for drainage or filling. Four air injectors, placed at each corner of the bottom and 10 in. from the tank walls were used for mixing to provide homogeneity in the density and concentration of the tank fluid before each experiment. Two 1 in. stainless steel rods were located vertically in one side of the tank to support the jet carriage. All the above details are shown schematically in Figures 2.1.1 and 3.1.1.

## 2.3 Instrumentation carriage

The transmitting and receiving optics of the laser-Doppler

velocimeter and the laser induced fluorescence system, were mounted firmly on a counterweighted instrument carriage. It was attached to the tank so as to provide both, vertical and lateral movement for the instrumentation. The carriage consists of two parts; (a) the main frame (rigid "box") which was attached to the tank and (b) the "platform" on which the instrumentation is mounted. It slides on two shaft assemblies on the main frame. The main frame is a "box" constructed from 4 in.x4 in.x1/4 in. square aluminum tubing and 4 in. wide aluminum U-section in order to provide rigidity (see Figure 2.3.1 (a)). Eight cylindrical bearings, two on each corner of the box, mount the frame to the four 1 in. precision shaft assemblies bolted on the corner posts and allow it to move vertically. Details of the 1 in. shaft assemblies and the pillow blocks containing cylindrical ball bearings (manufactured by the Linear Industries Ltd. ) are shown in Figures 2.3.2 (a) and (b). Four 3/8 in. cables were hooked at the corners of the frame for support. The carriage was counterweighted by four weights at the other edge of the four cables. These allow five (5) feet of vertical motion of the carriage. The counterweights were calculated from the weight distribution of the carriage at the locations of the pillow blocks and allowed the carriage to move easily by hand. The instrumentation platform (see Figure 2.3.1 (b)) was able to slide on two 1" precision shaft assemblies with four cylindrical bushings (pillow blocks). The platform was constructed of three pieces of 4 in. wide aluminum U-section. One side supported the laser-Doppler transmitting optics and the other the receiving optics. The third side supported a 2-watt argon ion laser and the laser-induced fluorescence device transmitting optics.

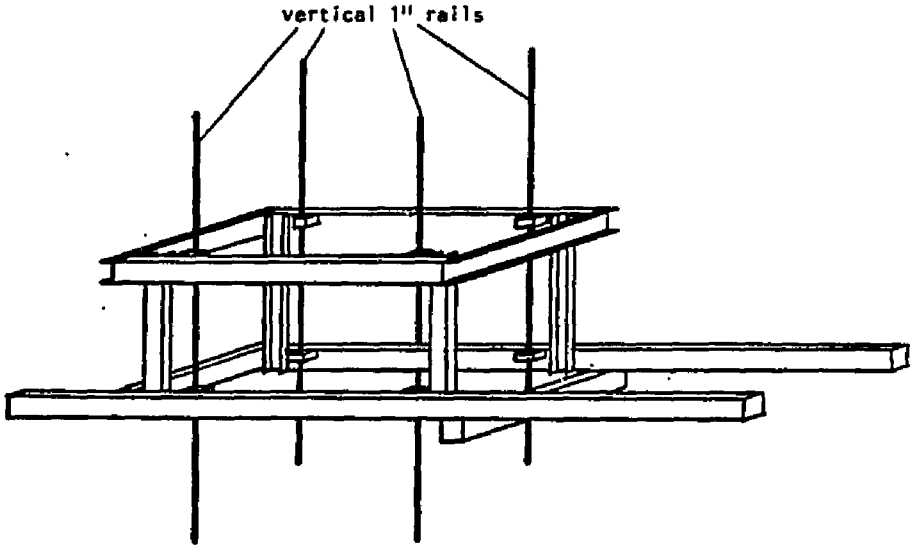


(a)

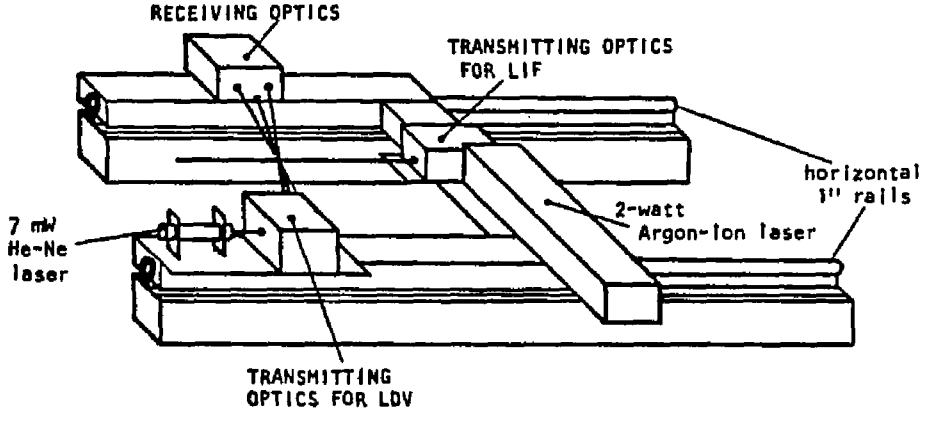


(b)

Figure 2.3.1. Instrumentation carriage:
(a) rigid "box";
(b) instrumentation platform.

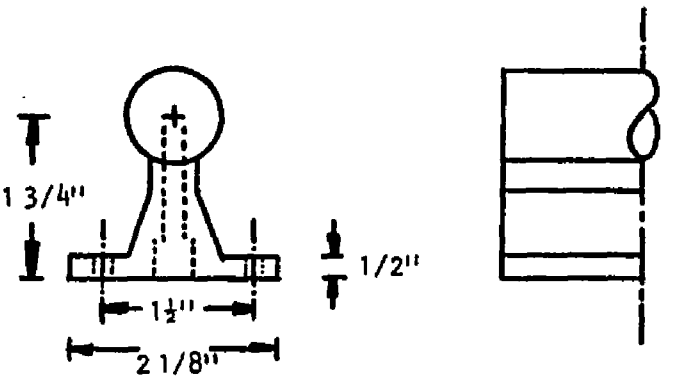


(a) shaft assembly

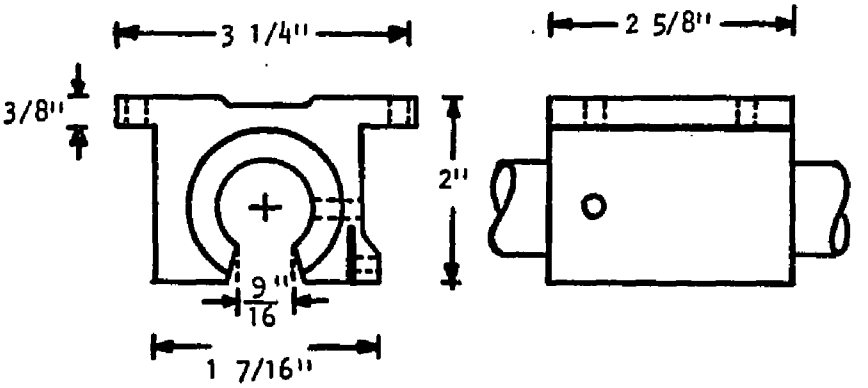


(b) Pillow block

Figure 2.3.2. Precision rail 1":
(a) Shaft assembly;
(b) Pillow block.

## 2.4 The laser-Doppler velocimeter

### 2.4.1 Introduction

The vertical (axial) and horizontal (radial) velocity components w and u were measured simultaneously at the same point of flow using a two reference beam laser-Doppler velocimeter. The basic principles of the laser-Doppler velocimetry will be briefly discussed here. For a more complete description of the technique, see Watrasiewicz and Rudd (1976), Drain (1980) and Durst, Melling and Whitelaw (1976).

Consider a particle moving with velocity $\vec{U}$, irradiated with a beam of polarized laser light of frequency $f_o$ in the direction $\vec{e}_o$ (see Figure 2.4.1). The light scattered by the moving particle will have a frequency $f_p$ given by

$$f_p = f_o\left(1 - n\frac{\vec{e}_o \cdot \vec{U}}{c}\right)$$

where n is the index of refraction of the medium that the particle moves in and c is the speed of light in a vacuum. Light scattered from the same particle towards the direction $\vec{e}_s$ will have frequency $f_s$

$$f_s = f_p\left(1 + n\frac{\vec{e}_s \cdot \vec{U}}{c}\right) = f_o\left(1 - n\frac{\vec{e}_o \cdot \vec{U}}{c}\right)\left(1 + n\frac{\vec{e}_s \cdot \vec{U}}{c}\right)$$

$$= f_o + \frac{nf_o\vec{U}}{c}(\vec{e}_s - \vec{e}_o) + O(1/c^2)$$

$$= f_o + \frac{n\,u\,\sin\theta/2}{\lambda}$$

$$= f_o + f_D$$

where $\theta$ is the angle between $\vec{e}_o$ and $\vec{e}_s$ in the medium of index of

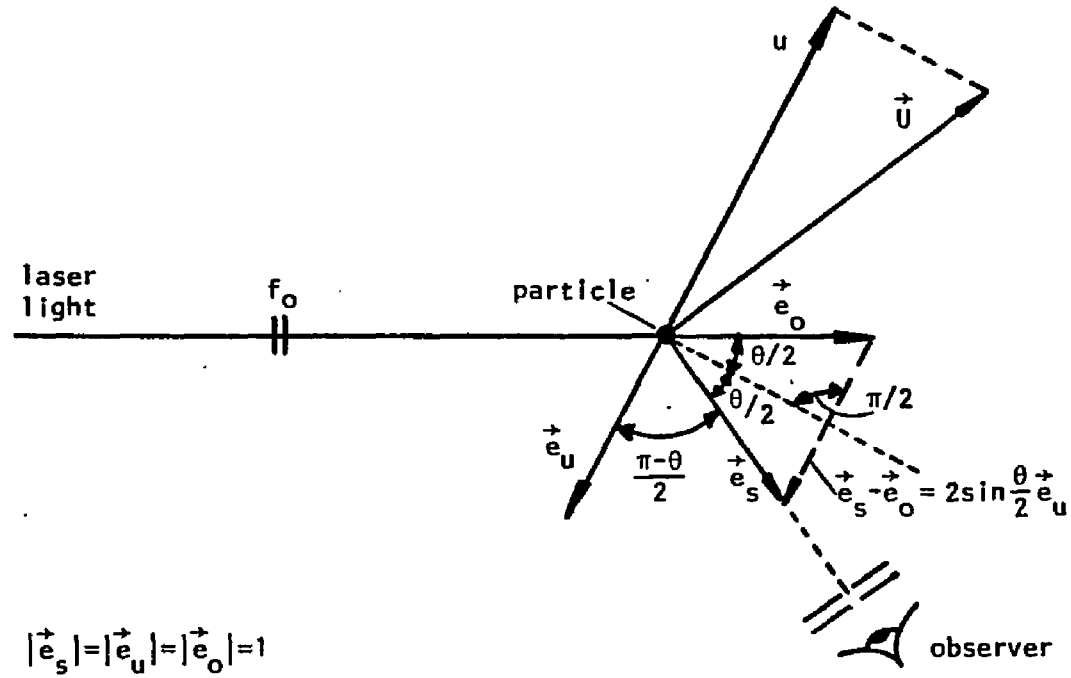


Figure 2.4.1. Scattering light from a moving particle.

refraction n, u is the component of the vector velocity $\vec{U}$ in the plane of $\vec{e}_o$ and $\vec{e}_s$ and perpendicular to their bisectrice and $\lambda$ is the wavelength of the laser light in vacuum. Suppose that a photodetector is placed in the position of an observer and that the scattered light in this direction is mixed with light of frequency $f_R$ from a reference beam with the same polarization as the scattered light. The intensity of the output current of the photodetector will be a waveform

$$i(t) \sim [A_s(t)\sin 2\pi f_s t + A_R \sin 2\pi f_R t]^2$$

$$= 2A_R A_s(t)\sin 2\pi f_s t \sin 2\pi f_R t + A_s^2(t)\sin^2 2\pi f_s t + A_R \sin^2 2\pi f_R t$$

$$= A_R A_s(t)[\cos 2\pi (f_s - f_R)t - \cos 2\pi (f_s + f_R)t]$$
$$+ A_s^2(t)\left(1 - \frac{1}{2}\cos 2\pi (2f_s)t\right) + A_R^2\left(1 - \frac{1}{2}\cos 2\pi (2f_R)t\right)$$

Let the frequency $f_R$ be $f_o + F$ then

$$i(t) \sim A_R A_s(t)\left(\cos 2\pi (f_D - F)t - \cos 2\pi (2f_o + F + f_o)t\right)$$
$$+ A_s^2(t)\left(1 - \frac{1}{2}\cos 2\pi (2f_s)t\right) + A_R^2\left(1 - \frac{1}{2}\cos 2\pi (2f_R)t\right)$$

and the energy spectrum of i(t) will be as shown in Figure 2.4.2 . In order to be able to measure $f_D$ we can band-pass the signal in the frequency band $F+\Delta F$ to $F-\Delta F$ where the frequency $\Delta F$ is a function of u for fixed n, $\theta$ and $\lambda$ . This way we can avoid totally the higher frequencies of the signal and the very low ones due to the fluctuation of the DC component of the current i(t).

2.4.2 The velocimeter, optical layout - operation.

The optical layout of the laser-Doppler velocimeter is shown in

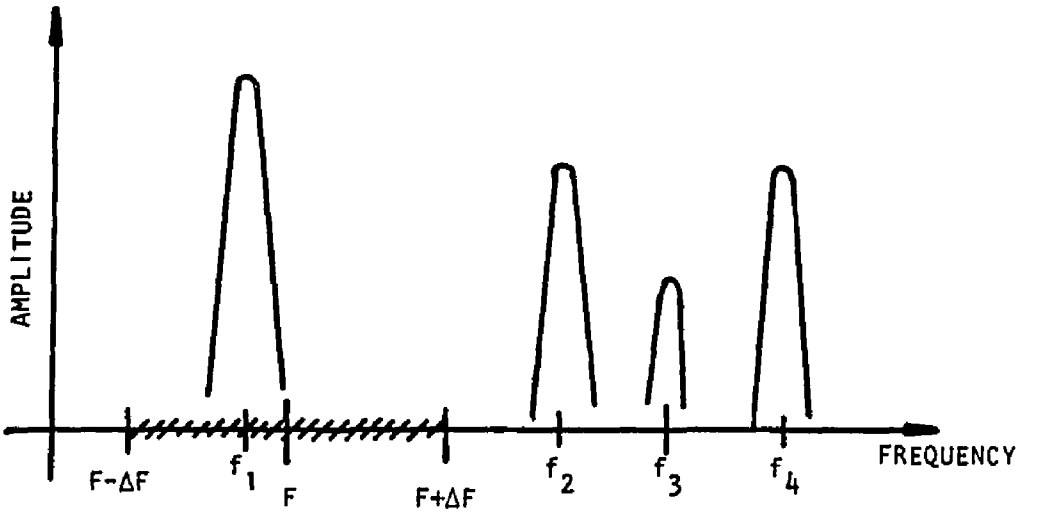


$f_1 = F - f_D$

$f_2 = 2f_o + 2f_D$

$f_3 = 2f_o + F + f_D$

$f_4 = 2F_R = 2f_o + 2F$

expected frequencies from estimated velocities

Figure 2.4.2. Spectrum analysis of the output current signal of the photodetector used in laser-Doppler velocimetry.

Figure 2.4.3. A Model 3027H-P polarized 7 mW helium - neon laser manufactured by Hughes, is operated by a Model 4040 power supply of the same make. The light of the laser beam has a Gaussian magnitude distribution normal to the beam axis and the diameter of the beam defined as where the intensity is $1/e^2$ (e = 2.718...) of the centerline intensity, is 0.80 mm. A 90% - 10% beam splitter is used to split the original laser beam into two beams, the reference beam and the scattering beam with an intensity ratio 1 to 9. Both beams are shifted optically, at frequencies 42.23 MHz and 42.30 MHz for the scattering and the reference beam respectively. Optical shifting is obtained by two 40 MHz Model 305 Bragg cells manufactured by Coherent. The Bragg cells were excited by using oscillating crystals with frequencies 42.23 and 43.00 MHz. The amplifiers used to drive the Bragg cells were Model 300L RF Broadband Power Amplifiers that could cover a frequency range of 250 kHz to 110 MHz, manufactured by the Electronic Navigation Industries Inc.. The electronics for the Bragg cell exciters (oscillating crystals) are shown schematically in Figure 2.4.4 . The shifted scattering beam is splitted into two beams with intensity ratio 55/45 by a cube beam splitter. Two right angle prisms moved the second reference beam approximately to the desired location. Two 1° wedge prisms were used to make the reference beams parallel to the scattering beam, which was set to be horizontal by moving the laser mounting plate. A front surface mirror is set at a 45° angle with the direction of the beams which is parallel to the glass panels of the tank. It deflects the beams in a direction normal to the glass. The parallel beams are focused at the same point inside the tank by a 600 mm focal length converging lens. The lens can be moved

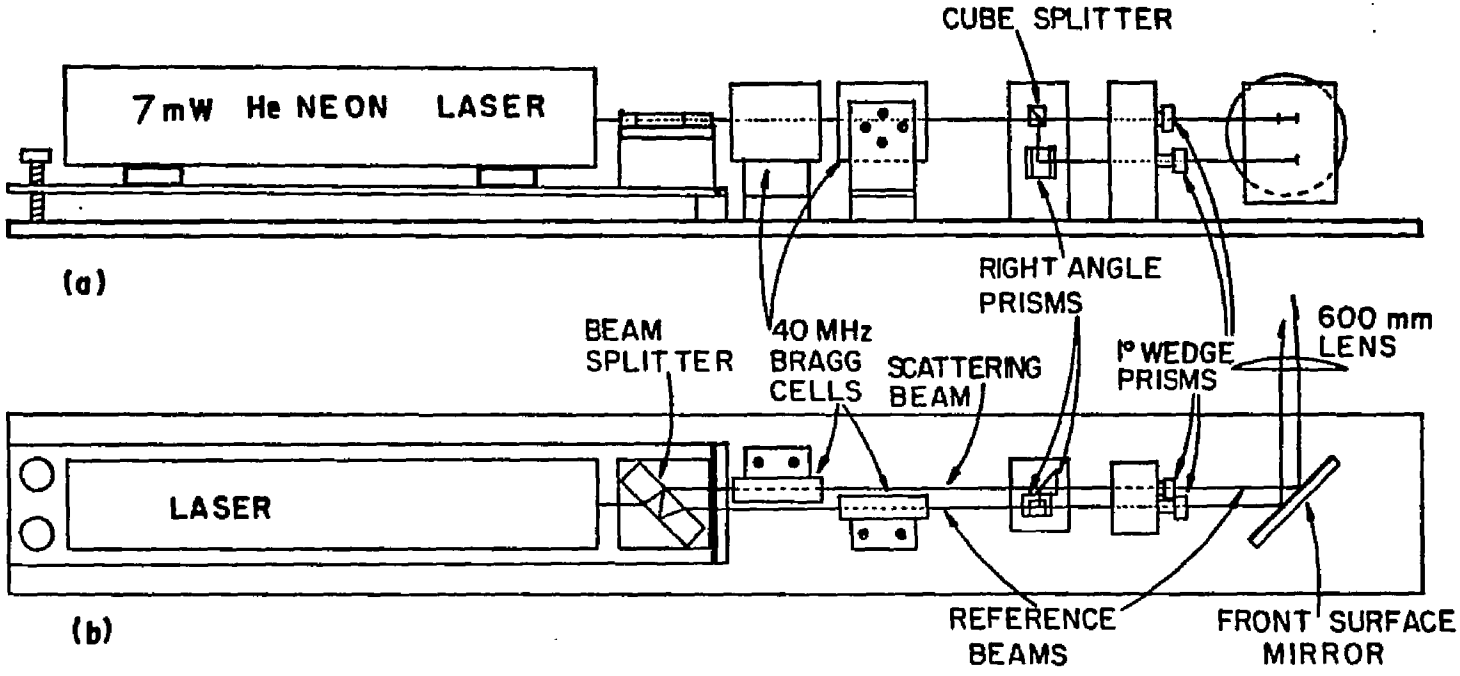


Figure 2.4.3. Optical configuration for laser-Doppler velocimeter. (a) Elevation; (b) plan.

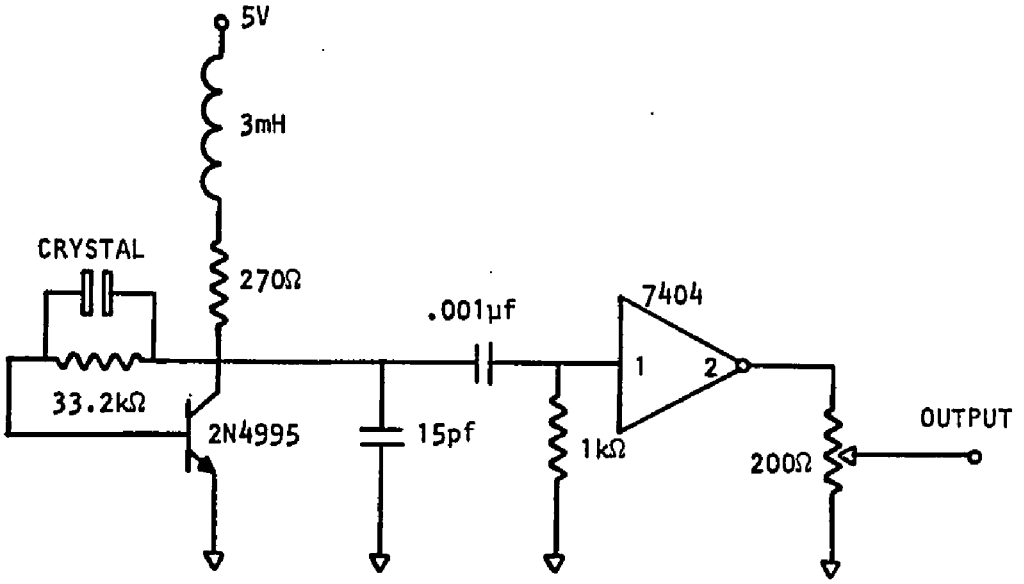


Figure 2.4.4. Electronic circuit for the Bragg cell exciters.

back and forth so that the beam - crossing is obtained close to the center of the tank. All the optics described above and the plate with the mounted laser were firmly attached to a 1/2 in. thick jig plate, which sat bolted on the instrument platform. The beam location in space and the beam crossing point were determined by using a theodolite. In Figure 2.4.5 the location of the beams and other dimensions are shown. The points $R_1$, $R_2$ and S are located on the glass from its wet side, O is the point of the beam intersection at a distance F from the glass, $\theta_1$ and $\theta_2$ are the angles between the scattering and the reference beams $R_1$ and $R_2$ respectively and $\phi_1$ and $\phi_2$ the angles of the sides $R_1S$ and $R_2S$ of the triangle $R_1SR_2$ with the vertical and horizontal directions respectively. From the dimensions given in figure 2.4.5 one can calculate that

(1) vertical velocity component

$$\frac{f_{D1}}{w_1} = \frac{2n \sin(\theta_1/2)}{\lambda} = \frac{2n\theta_1/2}{\lambda} = \frac{2na/2F}{\lambda} = 1129 \text{ Hz/(cm/sec)}$$

$$w = w_1 \cos\phi_1 = 0.9997\ w_1$$

(2) horizontal velocity component

$$\frac{f_{D2}}{u_1} = \frac{2n \sin(\theta_2/2)}{\lambda} = \frac{2n\theta_2/2}{\lambda} = \frac{2nb/2F}{\lambda} = 494.7 \text{ Hz/(cm/sec)}$$

$$u = u_1 \cos\phi_2 = 0.9993\ u_1$$

where n=1.333 for water and $\lambda$=632.8x10 mm. The $1/e^2$ (e=2.718...) diameter of the waist of the beams at the probe volume at their crossing was found to be 0.1mm at a length of 3.55 mm for reference beam $R_1$ and 8.0 mm for reference beam $R_2$ from the formulas given by

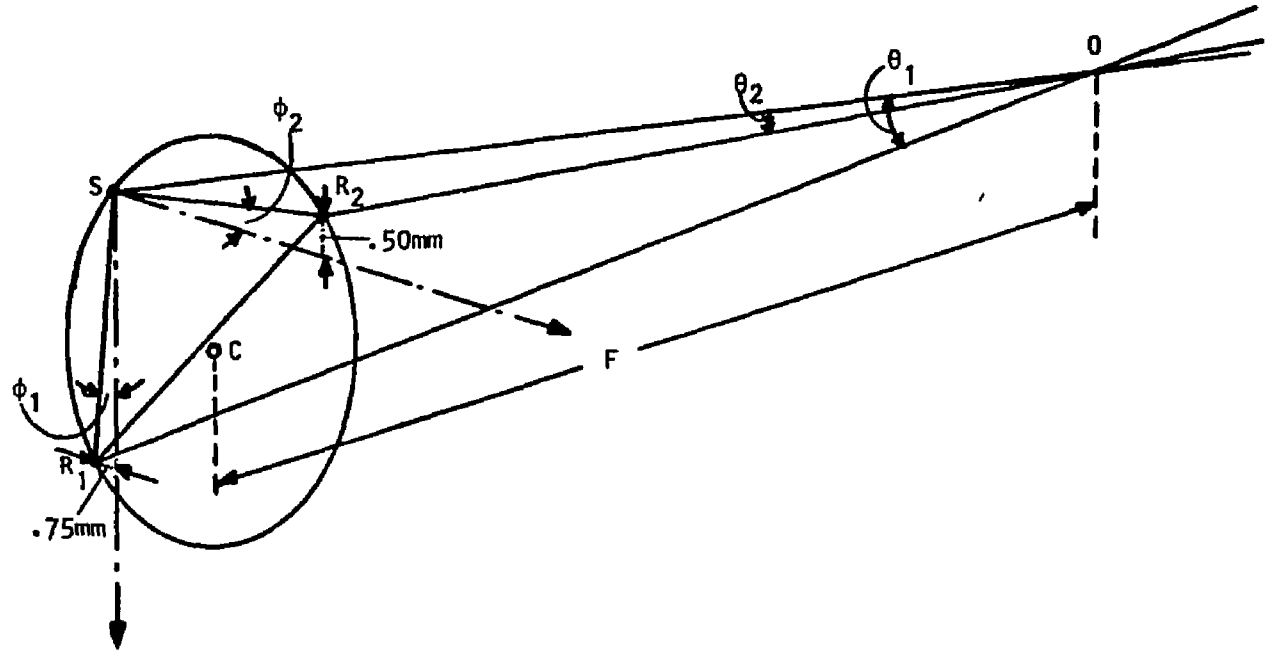


Figure 2.4.5. Three dimensional configuration of the spatial location of the scattering and reference beams; F = 576 mm, $SR_2$ = 13.50 mm, $SR_1$ = 30.87 mm.

Durst et al (1976).

## 2.5 The laser induced fluorescence system

### 2.5.1 Introduction

If a water solution of Rhodamine 6G dye is excited by absorbing monochromatic light of wavelength $\lambda_{in}$, it emits light (fluoresces) at a different wavelength $\lambda_{em}$. Drexhage (1976) gives that if the incident light has a wavelength 514 nm the emitted light will have a wavelength approximately 570 nm. This is the principle that the induced fluorescence technique is based on. The evolution and limitations of this technique and its advantages over the probe based techniques will be discussed in this paragraph. In Figure 2.5.1 a collimated laser beam of intensity I and wavelength $\lambda_{in}$=514 nm excites a Rhodamine 6G dye water solution which flouresces at a wavelength $\lambda_{em}$=570 nm. A photodetector located at the point A' "sees" the point A of the beam through a converging lens L. The light that reaches the photodetector through the aperture P will be a mixture of the fluorescent light at about 570 nm and scattered light at 514 nm from possible existence of other particles in the water. If a high pass light filter is placed in front of the photodetector, which will allow say, only the light of wavelengths longer than 530 nm to go through, then the photodetector will receive only the fluorescent light. This is attenuated a little due to the nature of the optical filter. The output intensity of the photodetector will be "proportional" to the fluorescence from the point A. This is proportional to the concentration of Rhodamine 6G dye in the water, or proportional to the intensity of the laser beam that excites the solution at the point A.

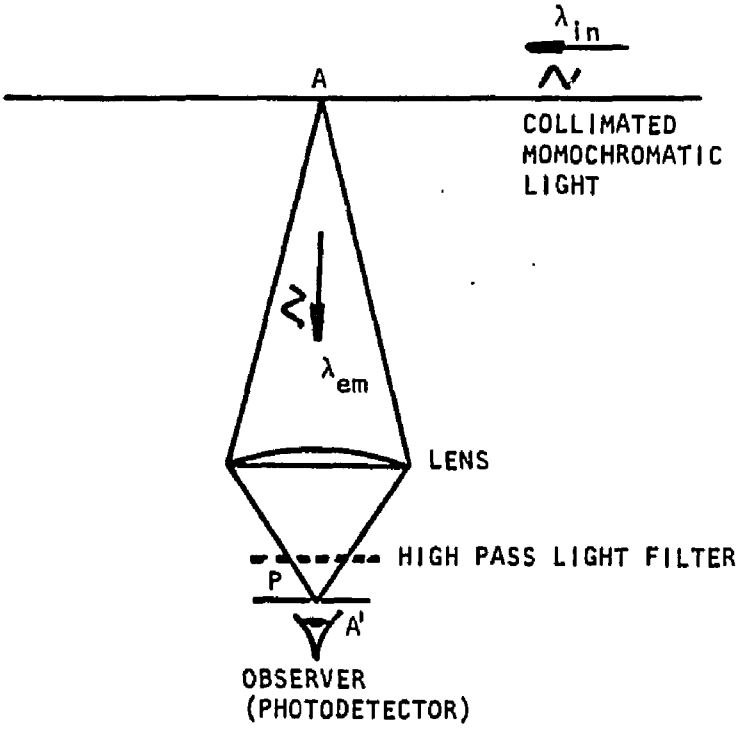


Figure 2.5.1. Principle of the laser induced fluorescence of a Rhodamine 6G dye water solution.

The above observations led to the proper design of an aqueous solution Rhodamine 6G dye concentration measuring device. It was observed that for a given laser light intensity of about 0.8 watts with a collimated beam of 1/e (e=2.718...) diameter 0.4 mm, the current output from the photodetector was linear for Rhodamine 6G dye concentrations varying between 1 and 40 ppb. Also the minimum dye concentration that the photodetector could detect was approximately 0.4 ppb.

2.5.2 The induced fluorescence system

The light source is a 2 - watt Model 164 Spectra Physics argon ion laser operated at a single line of wavelength 514 nm. The laser was operated by a Model 265 Spectra Physics power supply which can provide two modes of operation of the laser; the current mode which is based on stabilizing the current of the input power and the light stabilized mode based on the intensity of the output laser light. The laser in the present experiment was operated at the light stabilized mode. The reason is that the light stabilized mode provides constant light intensity after the laser is warmed up. A fraction of the laser beam ( 1% ) is removed by a beam splitter and input to a photodiode. Possible fluctuations of the laser light intensity are detected by the photodiode and a feedback controlled system readjusts the power supply output, so that the output light intensity does not change from its preset value. It was found that the calibration of the system did not change through the experiment. The light stability was also proved by taking long records of concentration at a point of the tank when the concentration was uniform. The variance was found to be almost 0.05 ppb and it was not due to the light intensity variations but due to electronically induced noise. The noise showed up as a peak at 60 Hz

in the concentration power spectrum. The $1/e^2$ (e=2.718...) diameter of the laser beam is 1.25 mm. A system of optical components (see Figure 2.5.2) such as prisms and front surface mirrors, deflects the beam 90° so that it becomes normal to the tank window. The beam also crosses the intersection of the three beams used for velocimetry and it is focused by a converging lens with focal length 750 mm.

2.5.3 Advantages and limitations of the technique

The main objective of this project was to determine the turbulence characteristics in round jets and plumes by measuring simultaneously two velocity components and the concentration of a tracer. Thus we obtain estimates of the turbulent mass transport of the tracer. Initially we had in mind to use a technique based on laser-Doppler velocimetry combined with a thermistor probe set close to the focal volume of the velocimeter (see Kotsovinos (1975) and Gartrell (1979)). Some preliminary temperature measurements were performed by Papanicolaou and List (1983) by using fast response thermistor probes (characteristic time of the thermistors was 0.014 msec). It was shown that the resolution that we were able to obtain concerning the average and turbulent concentrations, was not good beyond 40 jet or plume diameters. Kotsovinos (1975) was able to measure temperature profiles up to 90 jet diameters and 40 plume diameters downstream. The difference in between the present investigation on the round jets and Kotsovinos' (1975) work on plane jets is that the mean temperature on a round jet axis decays much faster than the temperature along a plane jet axis. The reason is that $T \sim z^{-1/2}$ for a plane jet and $T \sim 1/z$ for a round jet. Also for a plane plume $T \sim 1/z$ while for the round plume $T \sim z^{-5/3}$ (see Chapter 1).

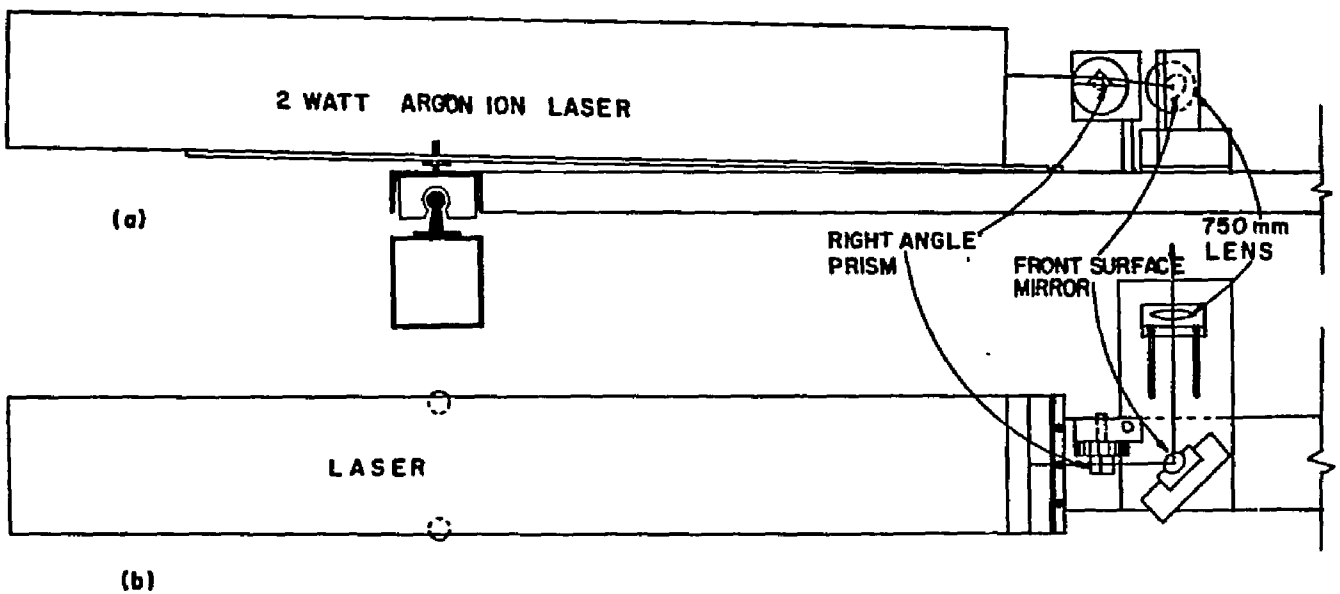


Figure 2.5.2. Optical arrangement for high power laser for laser induced fluorescence system.
(a) Elevation;
(b) Plan.

The reasons that we found important for using an optical technique versus probe-based techniques for tracer concentration measurements are summarized as follows: (i) Probe based techniques, such as thermometry or use of conductivity probes do not give good enough resolution beyond 40 jet or plume diameters in the case of round buoyant jets. Wygnanski and Fiedler (1969) and Birch et al (1978) showed that a jet is fully developed and self similarity is obtained beyond 40 jet diameters. By using high enough initial jet concentrations of Rhodamine 6G, then at 100 diameters we were still able to obtain a mean concentration of 5 to 10 units (ppb). The advantage was that the initial jet concentration up to 200 ppb does not essentially affect the density of the water. Therefore an initially jet-like flow will still behave as a jet for z/D>100.

(ii) The thermistor probes give a certain error at the jet boundaries where reverse flow can appear. The reason is that the fluid attached to the glass bead is not removed properly so that there is bias in the measured temperature. The induced fluorescence technique does not depend upon the direction of the flow.

(iii) Optical techniques do not disturb the flow field like the probe-based techniques. A problem in the present investigation could arise from the heating of the flow field from the dissipated heat from the 2-watt laser beam. Calculations showed that the effects due to the heat dissipation from the laser beam are negligible.

(iv) Kotsovinos had set a thermistor probe 2.5 mm far from the focal volume of his velocimeter. He measured simultaneously both, velocities and temperatures, but not at the same point. Gibson (1963) has found that the Kolmogorov microscale for a round jet around its

axis is 0.8 mm. This may have biased Kotsovinos' data at a certain degree, due to the u - T spatial correlation.

2.6 The receiving optics - data acquisition system

The layout of the receiving optics for both, velocimetry and induced fluorescence measurement, is shown in Figure 2.6.1 . Two fast response silicon photodiodes type DT-25 made by EG & G collected the heterodyning of the two reference beams and the scattering beam. Two converging lenses with focal length 125 mm were set in front the above photodiodes at a distance 125 mm from a 0.5 mm pinhole. The scattering beams were deflected by two front surface mirrors $M_1$ and $M_2$ and directed into pinholes through the center of the lenses $L_1$ and $L_2$. The reason for using the two lenses $L_1$ and $L_2$ at a distance equal to their focal length in front of each photodiode is that small changes in the refractive index (due to density variations) were moving the scattering beams around. Without the lenses the signal was interrupted about 50% of the time. Use of the lenses gave almost uninterrupted signal. In the next chapter the errors in the velocity signals due to the change in the refractive index will be discussed. Another photodiode of the type S1223-01 made by Hamamatsu was used to collect the light emited from point O (intersection of all four beams) in a solid angle $\phi$ through the 250 mm converging lens $L_3$ . A small LED was used in order to excite this photodiode and move its operation in to the linear response region. The light source had no effect on the measurement of the concentration since it was taken into account in the concentration calibration. The S1223-01 photodiode was put on the same side of the tank as the velocimeter transmitting optics, to

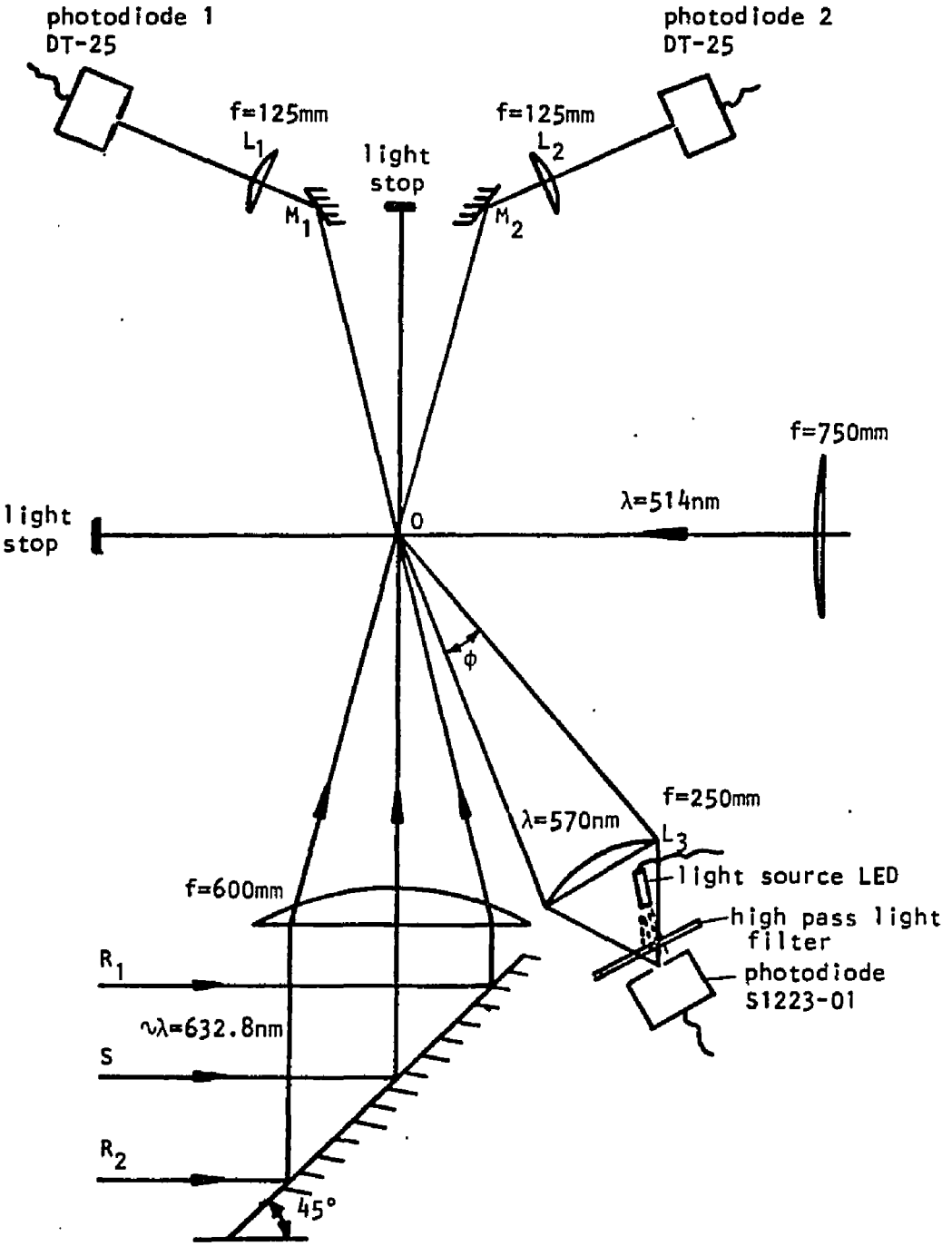


Figure 2.6.1. Plan view - configuration of the receiving optics and photodetectors for the laser-Doppler velocimeter and the laser induced fluorescence measuring system.

avoid any bias to the signal due to the forward scattering of the beams $R_1$, $R_2$ and S. The back scattering was found to have no effect to the signal. Initially the photodiode was put on the opposite side of the tank and an optical band-pass filter was used in order to cut off the unwanted scattered laser light at 632.8 nm. Its transmittance was 45% at $\lambda$ =570 nm and the output signal from the photodiode was very weak. At the present location a low-pass filter is used in order to avoid effects from the scattered light at a wavelength of 514 nm. Due to imperfections of the instrumentation carriage, a pinhole in front of this photodiode did not work accurately enough because the line image of the fluorescent light was moving off center. Thus it was decided to use a vertical slit 0.152mm wide and 1.5 mm long so that the horizontal line image was always detected, especially when there were changes in the refractive index in the flow. The probe volume that the photodiode was seeing was calculated, and found to be a cylinder of diameter 0.4 mm and length 0.4mm. All three photodiodes were mounted properly in aluminum boxes in order to avoid possible bias to their output signals due to electronic noise. A preamplifier was operated by 9 volt batteries enclosed inside the photodiode box. Electronic noise problems due to the 2-watt laser were avoided by insulating the detectors from the carriage using nylon sheet and screws at their contact. Photodiodes, mirrors and lenses could move in three directions.

## 2.7 Signal processing, data acquisition system

The preamplified signal of the photodiodes was processed in order to be brought into a useful form that would allow extraction of all

the desired information. The signal processing for both, laser-Doppler velocimeter and induced fluorescence measuring device, is shown schematically in Figure 2.7.1 . The signal from the photodiode was converted from a current to a voltage and preamplified. The preamplified LDV signal was amplified and filtered with a band pass filter which has a center frequency set near the expected Doppler frequency. The band-pass filters were Krohn-Hite Model 3202 with high-pass and low-pass cutoff frequencies that are continuously adjustable from 20 Hz to 2 MHz in five bands. The signal then passed through a dual processor. One part of the processor detected the level of the Doppler burst and could be externally adjusted so that the burst was continuous. The other part of the processor detected the zero crossings of the Doppler bursts and put out one pulse for each positive going zero crossing. The pulses then were fed into a counter. If the burst detector output was high enough (signal level detector was set low but above the noise level of the photodiode) the zero crossings were counted. The counting of the first pulse started a timer; after counting an externally selected number of pulses the timer stopped and the digital signal was converted to analog output, which was sent and stored in digital form on a diskette of a PDP 11/60 computer for subsequent analysis. For details of the design of the LDV processor see Gartrell (1978). The signal from the photodiode that detected the fluorescence was also converted from a current to a voltage and preamplified, then amplified to a voltage range of ±5.0 volts. The amplified signal was low-pass filtered and the filtered analog output stored in digital form on the same diskette as the velocity signals.

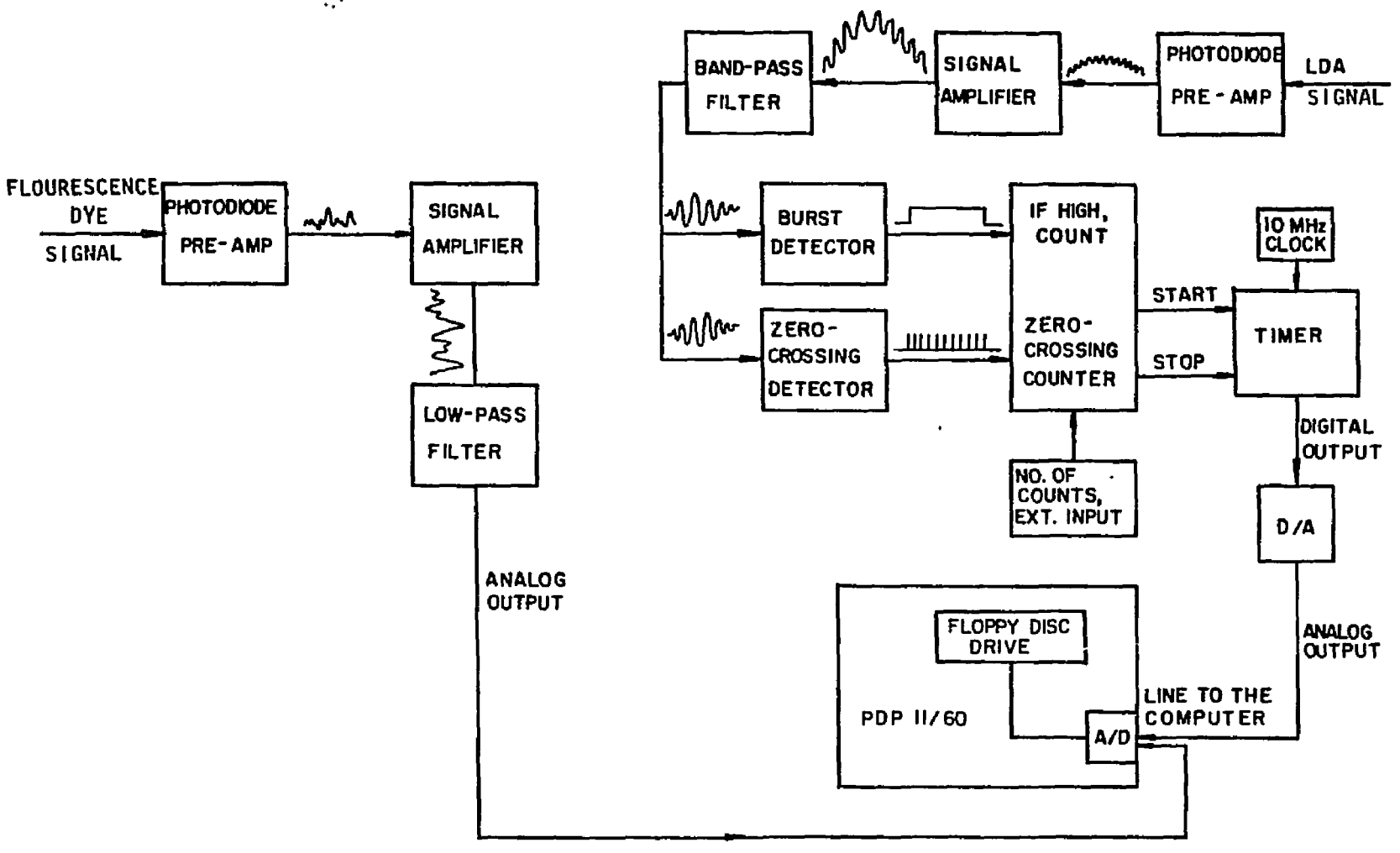


Figure 2.7.1. Schematic for laser-Doppler velocimeter signal processor and data collection system.

# 3. EXPERIMENTAL PROCEDURE

## 3.1 Introduction

In this chapter the details for calibration and usage of the experimental apparatus are given and the experimental procedures are described. In addition, sources of possible errors are discussed. The chapter will be closed with the full description of a typical experiment, the acquisition and subsequent reduction of the sampled data.

## 3.2 Tank, jet, operation and usage

Figure 3.2.1 is a schematic diagram of the plumbing, operation and usage of the tank and jet. A 3/4 in. PVC pipe was used to bring water from the 1 in. laboratory high pressure water supply to the tank. Valves $V_5$ and $V_6$ were used for draining the tank when needed. A 2 in. in diameter spiral hose was used for a tank overflow drain when the jet was running during the experiments, or whenever needed. Four air injectors were located at the bottom of the tank and connected with the laboratory air-supply line. They were activated by valve $V_7$. The resulting air-bubble jets were used for mixing of the tank water in the following cases: (i) To dissolve anhydrous granular sodium sulfite ($Na_2SO_3$) in order to dechlorinate the tank water. Dechlorination of the tank and jet fluid were found to be necessary as the chlorine content of the laboratory water oxidized the Rhodamine 6G dye used in jet concentration measurements. (ii) To mix filtered salt-water solutions with the tank water in order to get a desired

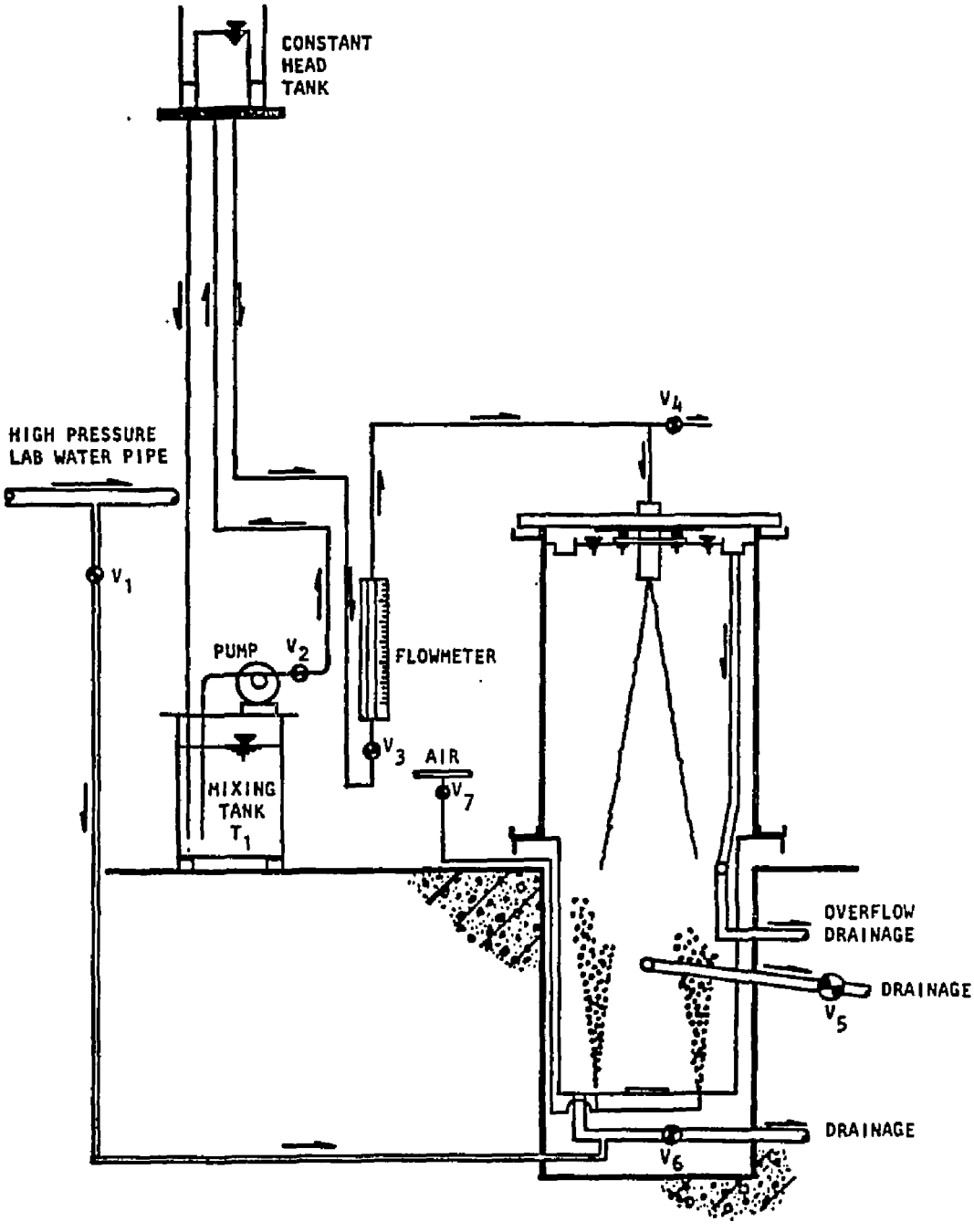


Figure 3.2.1. Overall experimental set-up.

ambient fluid density. (iii) To mix high concentration Rhodamine 6G - water solutions with the water in the tank providing the desired ambient tracer concentration. (iv) To destratify the tank after each experiment and provide an ambient fluid of uniform density and dye concentration for a subsequent experiment.

The jet fluid supply consisted of a 220 liter mixing tank $T_1$ , with constant head tank, pump, flowmeter and 3/4in. connecting hoses. After the water in tank $T_1$ was dechlorinated, it was mixed with the exact quantities of salt (NaCl) and concentrated Rhodamine 6G solution that would provide the desired initial jet density and concentration. The jet was supplied from the constant head tank located approximately 4 meters above the free surface of the tank. A return pipe took the excess water from the constant head tank to the mixing tank $T_1$. The jet supply hose incorporated a valve and a flowmeter. Valve $V_3$ was used to regulate the flowmeter and adjust the flow according to the flowmeter calibration shown in Figure 3.2.2 . Valve $V_4$ was used to bleed any possible air which might be trapped in the jet supply system.

## 3.3 Laser-Doppler velocimeter

### 3.3.1 Calibration

Calibration of the laser-Doppler velocimeter was obtained electronically. A frequency generator fed the counter with sinusoidal waves at known frequencies($f_i$). The analog output of the processor was sent and recorded by the computer in digital (binary) form($V_i$). From the available pairs ($f_i$,$V_i$) a least square fifth order polynomial

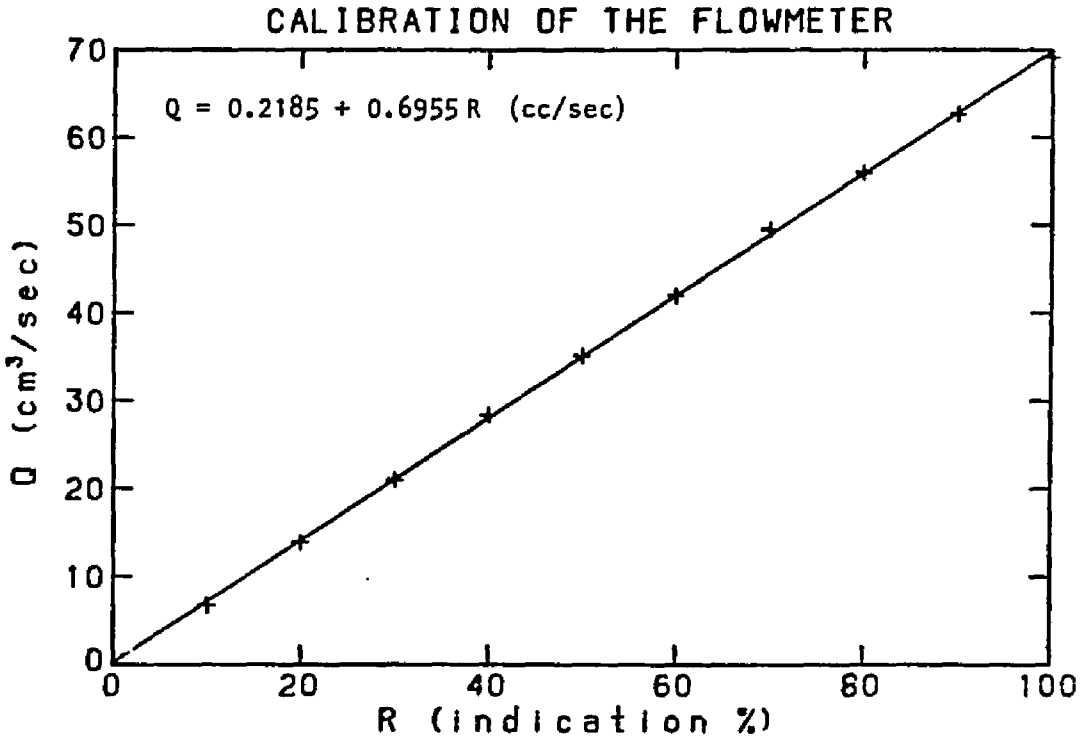


Figure 3.2.2. Flowmeter calibration curve. Discharge as a function of the flowmeter indication (%).

$$f=A/V^2+B/V+C+DV+EV^2 \qquad (3.3.1)$$

was found to be the best fit to the data, and the values of the constants A,B,C,D and E were calculated. Equation 3.3.1 is the calibration curve for the detected frequencies versus the digital output recorded by the computer. In Figures 3.3.1 (a) and (b), typical calibration curves are shown for the frequencies that correspond to the axial and radial velocity components w and u respectively. The Doppler frequency $f_D$ then was calculated from the measured frequencies $f_{w,u}$ as

$$f_D = f_{w,u} - F$$

where F is the frequency shift between the reference and scattering beams. The frequency shift F is the frequency difference between the two Bragg cell exciters and it was measured exactly.

The axial velocity w was estimated to be bigger than -3 cm/sec and the radial varied in the interval ±5 cm/sec. These values correspond to frequencies $f_{w,u}$ less than 70. kHz. Therefore frequencies larger than 75. kHz that could possibly bias the data are totally avoided (see Figures 3.3.1 (a) and (b)). The calibration was checked to be very stable. Drifts in the electronics occurred in about one week period of time. The laser-Doppler processor was always on ON position, and it had to be calibrated once a week. In fact it was calibrated every day that experiments were run.

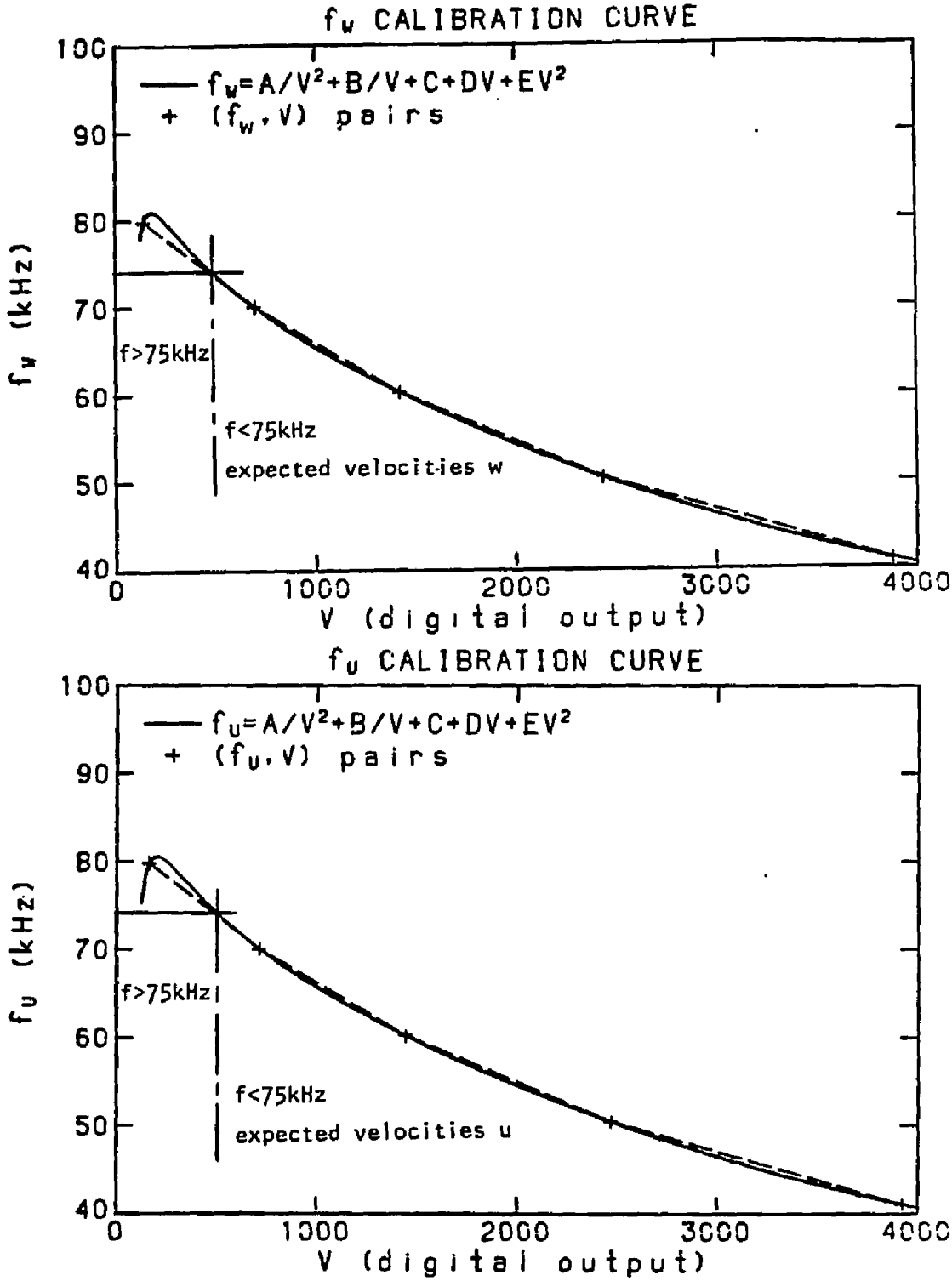


Figure 3.3.1. Typical calibration curves for the detected frequencies by the photodetectros used in laser-Doppler velocimetry versus digital output to the computer.
(a) Axial velocity component.
(b) Radial velocity component.

### 3.3.2 Errors in the velocity measurements

There are various sources of error inherent in the velocimetry used in this study. The estimated relative errors due to the nature of the processor and the data acquisition system will be discussed The absolute error as a result of the proper tests will be described. Thus the accuracy of the measured velocities can be estimated. Error sources and their estimates are discussed in the following paragraphs.

(i) Large scattering particles can cause significant measurement error because they do not follow the fluid trajectories. Hunt (1978) measured the particle distribution of the laboratory water used in this experiment. He found no particles larger than 5 μm (see Gartrell (1979)). According to Durst et al (1976), particles with a diameter smaller than 15 μm are required for measuring turbulence in the water. Hence it is believed that the scattering particles are small enough that they essentially followed the fluid trajectories. Therefore no significant measurement errors resulted from this source.

(ii) Counter, data-digitization errors. One source of error is the inability of the counter system to distinguish two signals of slightly different frequency. The estimated error (see Gartrell (1978), (1979)) was found to be

$$\frac{\Delta f}{f} \simeq 1.6 \times 10^{-6} \frac{f_m}{k-1}$$

where $\Delta f/f$ is the relative error in the frequency measurement, $f_m$ is the measured frequency in Hertz and k-1 is the number of periods timed by the counter. The maximum number of Doppler periods in a signal burst from the laser-Doppler system was about sixty, but the counters were set to time twenty-four to thirty periods. Thus it was ensured

that the particles crossed the beams near the center of their intersection. The number of periods also was not so large as to require such a low threshold setting that the counter system could not distinguish noise from a signal burst. For the range of frequencies measured, $\Delta f/f$ was found to be less than 0.005.

Another source of error is the digitization error while the data were being acquired. The analog output of the processor was amplified and offset before being sampled by the A/D converter in order to utilize as much of the ±5 V range as possible. The range ±5 V was recorded in a digital form and corresponded to 4090 numbers. Therefore the laboratory data acquisition system had a precision of 0.0025V in the ±5V range used in the measurements. From the frequency calibration curves and for a range of frequencies 45 kHz to 70 kHz the digitization error was estimated to be

$$\frac{\Delta f}{f} < 2.00 \times 10^{-7} \, f_m$$

where $f_m$ is the measured frequency in Hertz. Hence the absolute error was calculated to be 0.1mm/sec and 0.2mm/sec for the axial and radial velocity components respectively.

The combined error due to digitization and the counter was measured as follows. A sinusoidal wave of frequency f=69.547 kHz was fed in the processor (counter) and the output was sampled for 10 seconds at a rate of 50 Hz by the A/D converter and recorded by the computer in digital form. The calculated mean and rms values for the two velocity components were calculated to be

$$\bar{w} = -0.245 \text{cm/sec} \qquad \bar{u} = 0.972 \text{cm/sec}$$

$\sqrt{\overline{w'^2}}$ =0.017cm/sec $\sqrt{\overline{u'^2}}$ =0.040 cm/sec

Assuming that the absolute maximum error is twice the standard deviation, it is obvious then that the maximum absolute error was +0.04cm/sec and +0.08cm/sec for w and u velocities respectively.

(iii) It was desired to have continuous velocity signal, therefore the threshhold level for the Doppler bursts was lowered. This means that the threshhold level was moved close to the noise level of the photodiodes and therefore an error was introduced to the system. Furthermore the existence of many particles in the probe volume introduced some noise to the velocimetry. In order to measure the combined effects of all the previously described error sources, the following test was performed. With the threshold level close to the photodetector noise level and with no flow in the tank the processor was fed with the output from the photodiodes. From the recorded digital signal the mean and rms values were calculated to be $\bar{w}=\bar{u}=0$ cm/sec as expected,and

$\sqrt{\overline{w'^2}}$ =0.087cm/sec and $\sqrt{\overline{u'^2}}$ =0.156cm/sec

respectively. Therefore the maximum combined absolute error in the velocities due to the processor, data acquisition system, low threshold level for the Doppler burst detection, and multiparticle scattering from the beam-crossing did not exceed the ±0.15cm/sec and ±0.312cm/sec for the axial and radial velocities respectively. The above measured rms values of w and u are the maximum noise levels of the output signal of the system to the computer. The contribution of this noise

to the velocity signals will be discussed in following paragraphs. It will be shown from the velocity energy spectrum that this noise does not essentially affect the velocimetry.

(iv) The deflection of the glass panels because of the hydrostatic pressure can introduce an error in defining the exact location of the beam-crossing inside the jet flowfield. The location of the beam crossing at the point of measurement, could be read from two scales one vertical and one horizontal, which determined the relative position of the instrument carriage with respect to the tank and the jet origin. Thus the readings on the vertical and horizontal scales could be easily converted to axial and radial distances z and r of the beam-crossing from the jet origin and axis respectively. The maximum deflection that occurred at 2/3 height of the glass distance from the water surface, was calculated and measured to be 1.30mm. The error in the beam crossing location, after laborious calculations was estimated to be ±0.2mm in the radial (r) and ±0.5mm in the axial (z) direction. This location error was also measured as follows: on the side of the tank where the receiving optics are and at a distance 1 meter from the tank, a vertical board covered with millimeter paper was placed parallel to the glass panel. The carriage was moved at various distances $z_i$ from the jet. For each $z_i$ the beam spots were marked for various $r_i$'s. Thus for each pair $(z_i, r_{ij})$ measured on the scales a pair $(z_m, r_{mj})$ was measured on the millimeter paper. From these values the same estimates as above were calculated concerning the location of the beam-crossing. The relative error in the jet region where the flow became self similar (z/D>40) was estimated to be $\Delta z/z, \pm 0.0167$ and $\Delta r/b, \pm 0.0067$ where b is defined to be the visual

width of the jet.

The laser beam used for the induced fluorescence was affected by the glass deflection only in the vertical direction. That is because it was only able to move on a vertical plane through the middle of the tank. Its relative position with respect to the center of the probe volume for velocimetry was zero in the vertical (z) direction and at most +0.2mm in the radial (r) direction.

(v) A very important source of error in the measurement of the velocity is due to the changes of the index of refraction in the buoyant jet and plume flow field. Figure 3.3.2 shows the change of the refractive index of aqueous sodium chloride (NaCl) aqueous solutions as a function of the density. Equation (1.2.5) shows that the density fluctuations in the plume flow field follow the fluctuations of the tracer concentration, resulting in a laser beam wobble. The wobble of the laser beams can introduce noise to the velocity signal as (a) fictitious fluid velocity due to the movement of the beam-crossing volume and (b) discontinuities in the Doppler bursts received by the photodetector when the reference beam does not mix with the scattered light on the pinhole. Mizushina et al (1979) proposed a correction technique for application to laser-Doppler velocimetry in non-isothermal flows. Also in order to avoid the beam wobble because of changes in the refractive index, Mc Dougall (1979) proposed a technique for matching of the refractive indices of the jet and ambient fluid. He used two solutes to produce density differences which would avoid the double-diffusion convection (salt-finger type). Mc Dougall's (1979) technique was applied by the author using commercial salt-water and sugar-water solutions for the ambient and

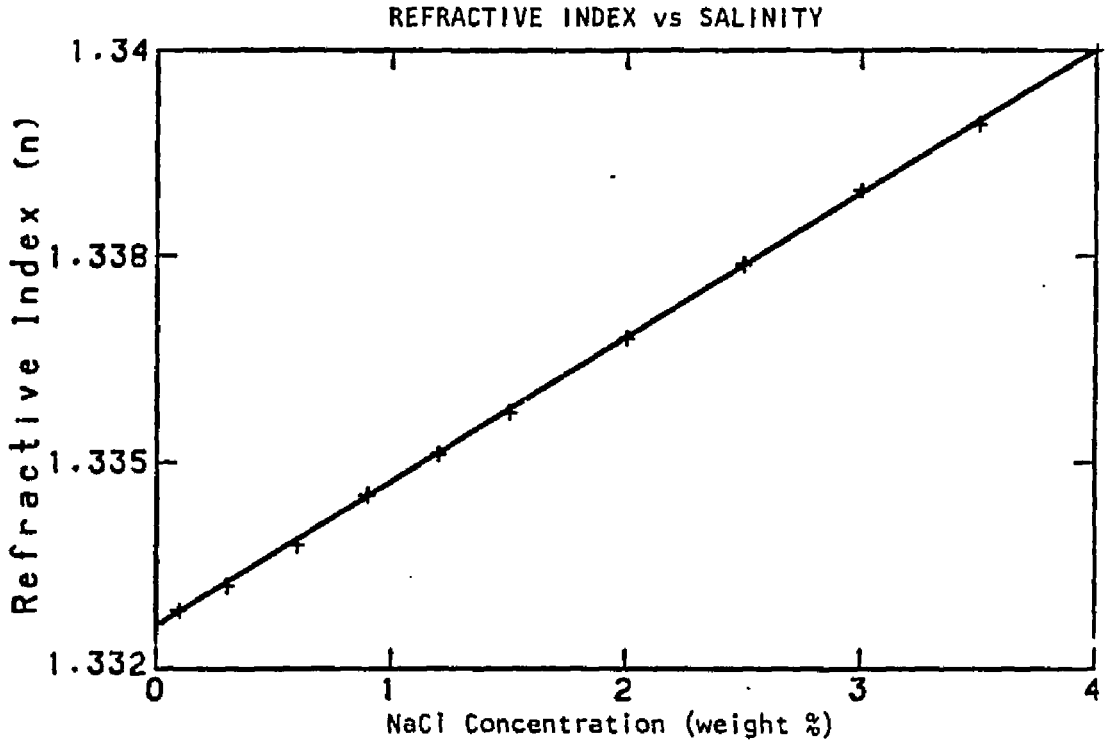


Figure 3.3.2. Variation in the refractive index of water vs NaCl concentration.

the jet respectively and it was succesful. Use of reasonable amounts of salt and sugar resulted an initial density difference of 2 - 3 $\sigma$ units. However in order to perform measurements in the fully developed plume region in this experimental tank, very large concentrations of salt and sugar would be needed to obtain initial density differences of 10 to 20 $\sigma$ units. On the other hand use of salt-water solutions for the jet, and fresh water for the ambient fluid have an initial density difference of about 20 $\sigma$ units, but the salt concentration is not large for $z/l_M > 40$. This is true because of the high dilution of the initial salt concentration at large distances from the jet origin. In the following paragraph, the tests performed to describe the effects of the density gradient in velocimetry, will be summarized.

The velocity measuring system was tested for the highest possible mean local density difference that was expected to be measured. An initial density difference of 25.0 $\sigma$ units was chosen and for a plume diameter D=1.25cm, velocity measurements were performed at $z/l_M \sim 45$. There existed some beam wobble but lenses $L_1$ and $L_2$ shown in Figure 2.6.1, contributed to obtaining a continuous signal from the photodetectors. The maximum beam wobble was marked on the millimeter paper on the vertical board described previously and did not exceed 1mm. This corresponded to a wobble of $\pm$0.4mm at the beam crossing point. A 3.5mm thick plexiglass plate was then introduced into the plume flow field at the beam-crossing point so that the 3mm long probe volume for the axial velocity component (and also the center part of the probe volume for the radial velocity) were enclosed in the plexiglass. Then with the plume running both mean velocities were

measured and were found to be zero. The turbulence intensities also did not exceed the values measured in a calm environment. These results imply that the probe volume did not move out of the plexiglass plate because of the beam wobble.

Another test was performed to measure the noise level of the signal due to the changes of the index of refraction. A square bottle 3cm x 3cm and 15cm high filled with tank water was introduced into the flow, at the point containing the beam crossing. Both longitudinal and transverse velocities were measured with and without the plume running. In the case of a calm ambient fluid it was found that inside the bottle

| $\bar{w}$ | $\bar{u}$ | $\sqrt{\overline{w'^2}}$ | $\sqrt{\overline{u'^2}}$ | $\overline{w'u'}$ | |
|---|---|---|---|---|---|
| -0.063 | -0.084 | 0.069 | 0.099 | -0.001 | (cm/sec) |

For a plume operating with $(\Delta\rho)_o$ =25 gr/lt and at $z/l_M$ =52.8 the measured velocities inside the bottle were

| $\bar{w}$ | $\bar{u}$ | $\sqrt{\overline{w'^2}}$ | $\sqrt{\overline{u'^2}}$ | $\overline{w'u'}$ | |
|---|---|---|---|---|---|
| -0.063 | -0.084 | 0.099 | 0.248 | 0.001 | (cm/sec) |

These measurements indicate the beam wobble noise is almost twice as big as the noise introduced into the system by the various sources that were discussed previously. However, part of this noise attributed to the beam wobble is probably due to the vibration of the plexiglass bottle by the plume flowfield.

In Figures 3.3.3 and 3.3.4 the energy spectra for w and u are

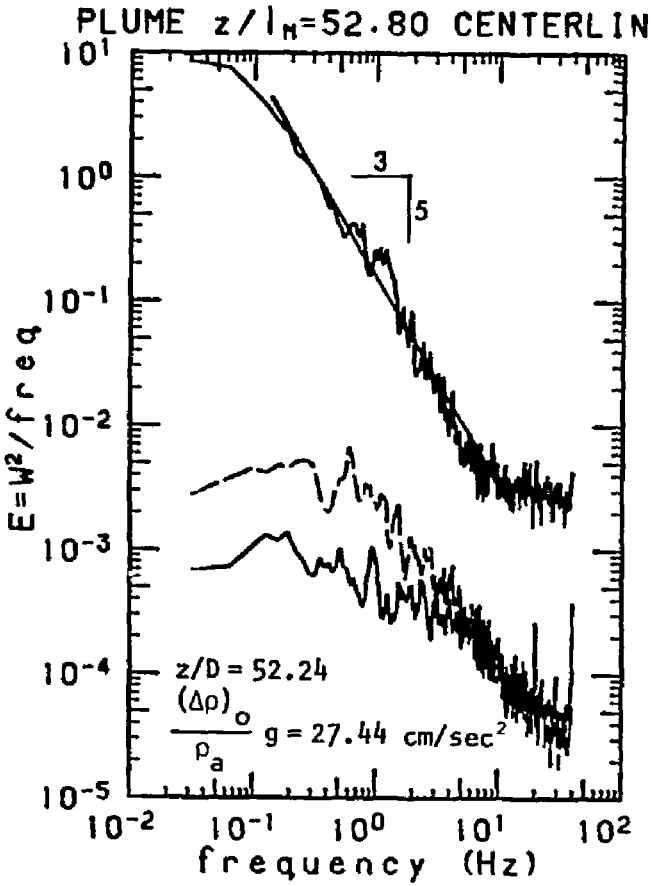


Figure 3.3.3. Power spectral estimate for the axial velocity component w at a plume centerline. Noise levels from the processor (solid line) and from changes in the refractive index (dotted line).

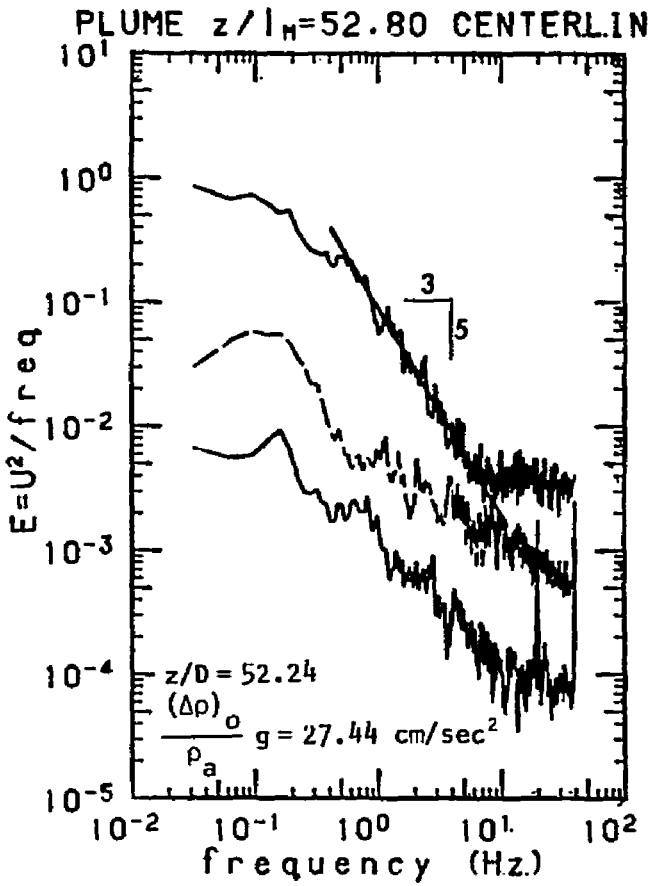


Figure 3.3.4. Power spectral estimate for the radial velocity component u at a plume centerline. Noise levels from the processor (solid line) and from changes in the refractive index (dotted line).

presented at $z/l_M$=52.8 close to the plume centerline with $\bar{w}$=5.48cm/sec, $\bar{u}$=-0.291cm/sec, $\sqrt{\overline{w'^2}}$ =1.287cm/sec, $\sqrt{\overline{u'^2}}$ =0.695cm/sec and $\overline{w'u'}$=0.117($cm^2/sec^2$). In the same figures the spectra obtained from the signals measured inside the bottle are plotted for comparison. It can be seen that the noise sources do not have any essential contribution to the energy spectrum. These spectra are in agreement with the spectral estimates of Mizushina et al (1979). It is also apparent here that for r/z>0.1, the effect of the fluctuations in the index of refraction is diminished as would be expected from the lower density differences and smaller segments of the laser beams that cross the plume flow field.

3.4 Calibration and errors of the laser induced fluorescence technique

As it was mentioned in Chapter 2, the concentration of Rhodamine 6G dye for a laser intensity of 800 mW is a linear function of the amplified voltage output from the photodetector. It can be written as

$$c = G + H\,V \qquad (3.4.1)$$

where V is the digital output to the computer, G and H are calibration constants. c varies from 1 to about 40 ppb. The photodiode could not detect Rhodamine 6G concentrations smaller than 0.4 ppb for an 800 mW power output from the argon ion laser. A typical calibration is shown in Figure 3.4.1. The laser and the electronics were turned on for at least one hour before the experiment started, so that electronic drift was avoided. The initial jet concentration varied from 100 to 200

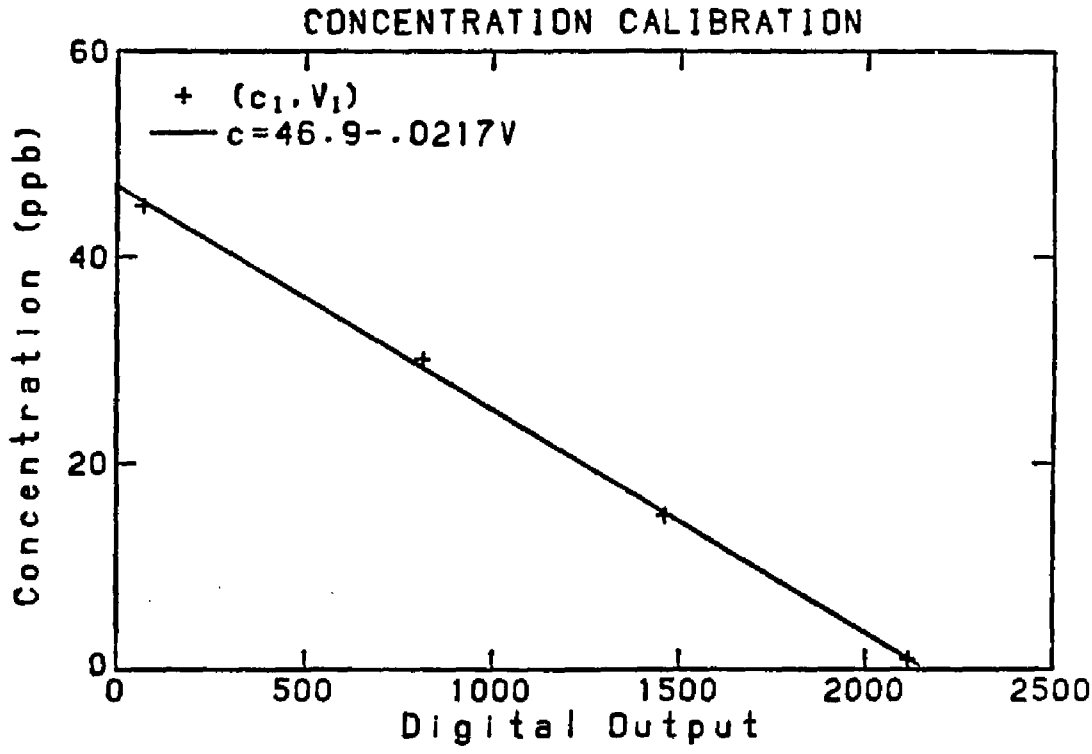


Figure 3.4.1. Typical calibration curve of the laser induced fluorescence concentration measuring system. Concentration (ppb) of Rhodamine 6G dye versus digital output to the computer.

ppb. Jet fluid was diluted and samples were made at various concentrations from 1 to about 40 ppb. The samples were put in square plexiglass bottles with cross-section 3cm x 3cm and placed at the beam-crossing point so that the photodiode was focused on the beam section within the sample concentration. From the known pairs $(c_i, V_i)$ of sample concentrations and digital outputs to the computer, a least square straight line was fitted leading to Equation (3.4.1).

3.4.1 Errors in the laser induced fluorescence technique

Several different tests were performed in order to justify the usefulness, validity and limitations of the technique. The errors resulting from various sources were measured. They will be discussed explicitly in the following paragraphs.

(i) The laser beam is attenuated as it travels through Rhodamine 6G dye solutions. The attenuation is due to the light absorption from the Rhodamine molecules and is proportional to the Rhodamine concentration and is hence minimized by low Rhodamine 6G concentrations. The attenuation of the laser beam was measured in a test performed as shown in figure 3.4.2. The ambient concentration was measured at point A with and without the jet of high Rhodamine concentration flowing. The results found are

| $\bar{V}$ | $\sqrt{\overline{V'^2}}$ | $\bar{c}$(ppb) | $\sqrt{\overline{c'^2}}$ (ppb) | |
|---|---|---|---|---|
| 1622.0 | 2.77 | 0.757 | 0.246 | (jet flowing) |
| 1620.7 | 3.27 | 0.873 | 0.290 | (no jet flowing) |

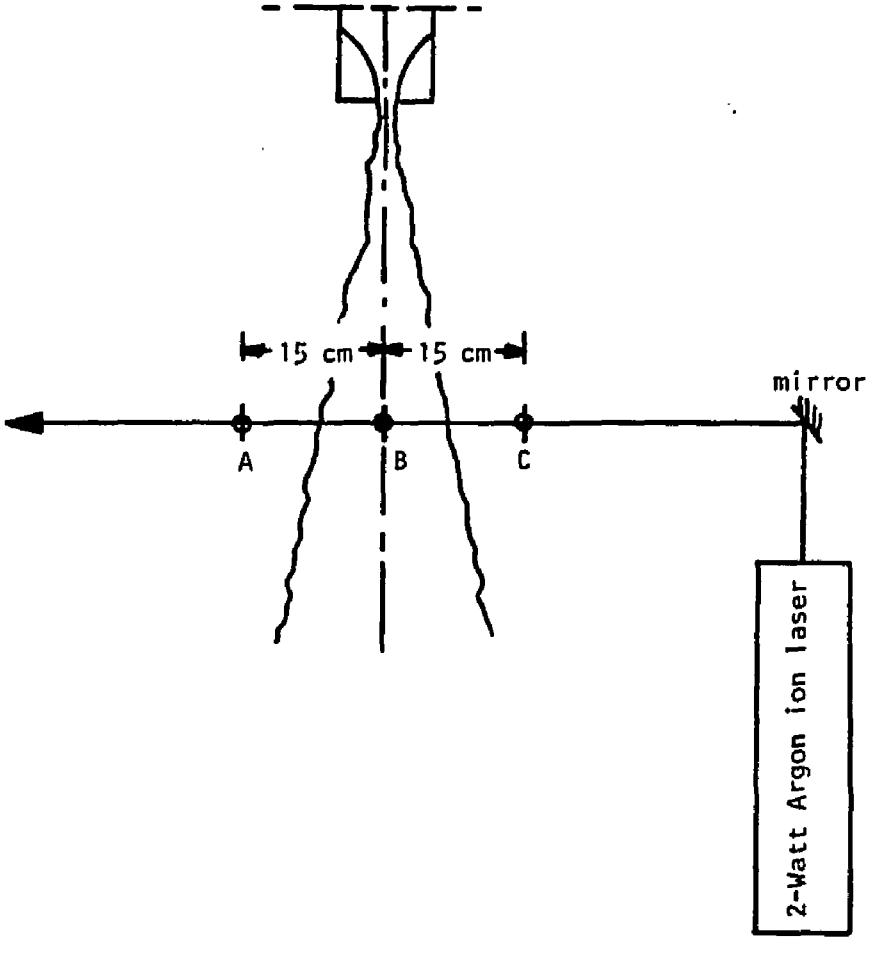


Figure 3.4.2. Schematic for the fluorescence attenutation tests performed at points A, B, and C.

and the difference in concentrations was found to be of the order of 0.1ppb which is of the same order of magnitude as other errors discussed consequently.

(ii) A second source of error is the lateral position of the instrumentation platform. Deflection of the glass and slight changes in the beam diameter can produce errors. At points A, B and C shown in Figure 3.4.2 with AB=BC=15cm the concentrations of two Rhodamine 6G solutions were measured and found

| | $\overline{c_1}$(ppb) | $\overline{c_2}$(ppb) | r(cm) |
|---|---|---|---|
| point A | 3.783 | 8.743 | -15.0 |
| point B | 3.728 | 8.468 | 0.00 |
| point C | 3.599 | 8.457 | +15.0 |

From the data shown in the table above for small and large concentrations the absolute error with respect to the centerline concentration is at most ±0.28ppb for radial distances ±15cm. This error is significant close to the jet boundaries, but absolutely insignificant everywhere else. The fact that the concentrations are higher at point A than those at point B prove the point that the beam waist changed slightly for various radial distances from the jet axis.

(iii) Another noise source is the beam wobble because of the changes in the index of refraction. A bottle containing a known concentration of Rhodamine was placed in the tank and the concentration was measured with and without the plume active. For the flow conditions described in section 3.2 (v) of this chapter, no significant error was determined. For high density differences the

relative error reached values as large as 8% of the measured mean concentration. In Figure 3.4.3 the spectrum of this noise is compared with the energy spectrum of the concentration variation in the plume flow field.

All the above tests give a reasonable estimate of the errors to be expected. Since simultaneous velocity and concentration measurements were made, it is apparent that the beam wobble could possibly introduce large errors in the turbulent mass transport estimates. In order to not to exceed the error estimates made previously for velocity and concentration measurements, the source density was chosen carefully to provide appropriate expected local mean densities at the measurement point. Hence the changes in the refractive index would not introduce error bigger than the previously estimated. Thus all tests that are discussed previously in paragraphs 3.3 and 3.4 were the guidelines for the subsequent experimental procedure.

3.5 Response of the measuring systems, sampling times and sampling rates - spectrum of turbulence

The response (characteristic) time for both, the laser-Doppler velocimeter and induced fluorescence system were very low. With the laser-Doppler system and the processor set to count 24 to 30 periods this time was 0.001sec. The response time for the laser induced fluorescence measurements varied from 0.005sec to 0.001sec. Hence there were no limitations in the sampling rates imposed by the response of the instrumentation. With relatively high sampling rates the sampling time was chosen to be longer than that necessary to give

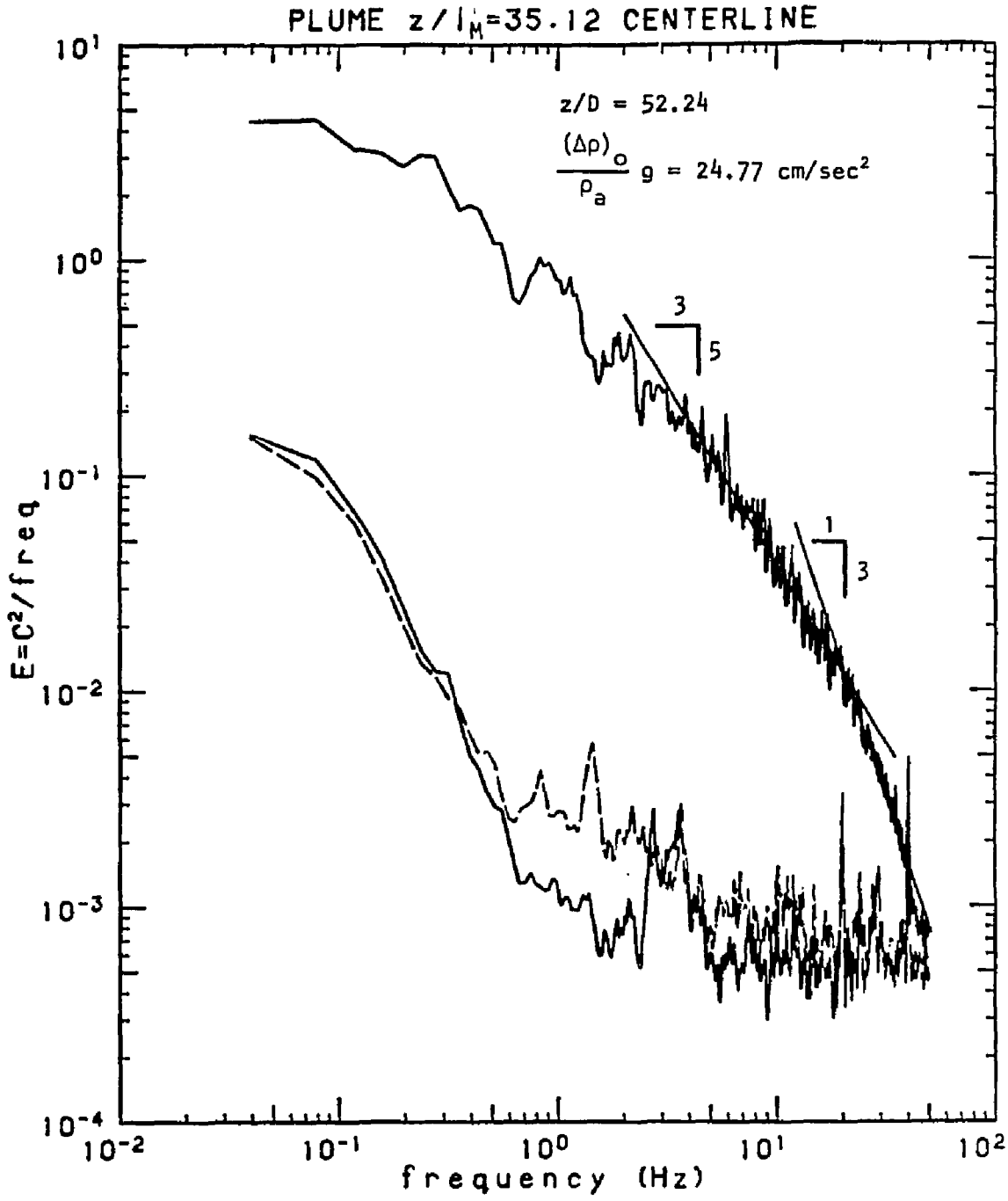


Figure 3.4.3. Power spectral estimate for the Rhodamine 6G concentration C at a plume centerline. Noise levels from the set-up (solid line) and from changes in the refractive index (dotted line) for constant concentration.

constant values of the first three moments of the signal recorded. The values of the three moments plotted versus sampling time were constant for sampling times longer than 80 seconds. The sampling time at a point of the flow was chosen to be larger than 100 seconds. Sampling rates varied from 25 to 50 data per second (except for data acquired in order to examine the spectral properties of the jet). For the momentum driven jets (fast flows) higher sampling rates were required than for the slow (plume-like) flows. The reason is that large velocity fluctuations occur much more frequently for jet-like flows at a point of the jet flow field.

The probe volume resolution for both velocity and concentration measurements was also a regulatory factor for the choice of the sampling rates. Very small probe volumes allow higher sampling rates that provide better information about the measured flow field. In figures (3.5.1), (3.5.2), (3.5.3), (3.3.3), (3.3.4) and (3.4.3) the energy spectra of w, u and c are given for jets and plumes. From the spectral energy distribution it can be seen that the maximum contribution comes from frequencies lower than 10 Hz. The amplitude drops in the frequency range 0.1 to 10 Hz by almost three orders of magnitude. Thus the minimum sampling rate should not be less than 0.05 seconds. Also, for frequencies larger than 10 Hz the noise contribution becomes very significant. This can be seen in all the Figures discussed above above.

In figures (3.3.3), (3.3.4) and (3.4.3) the spectral distributions of w,u and c close to a plume centerline are plotted. Also the noise spectra of a calm environment (bottle) are plotted in both cases, with and without changes in the refractive index in the

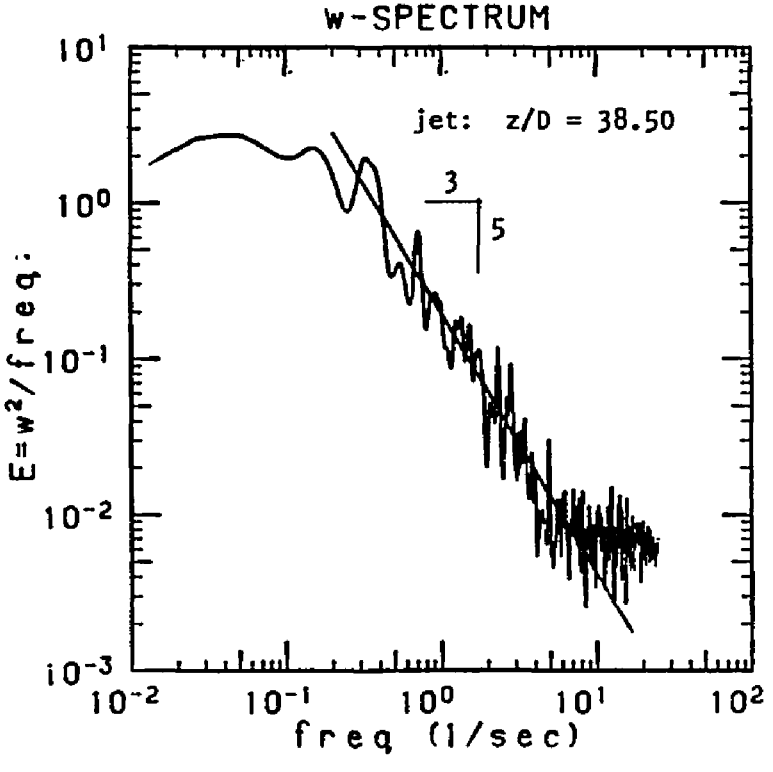


Figure 3.5.1. Power spectral estimate of w at a jet axis with z/D = 38.50, D = 1.25 cm, W = 29.65 cm/sec, $R_e$ = 3700, $C_o$ = 98.2 ppb.

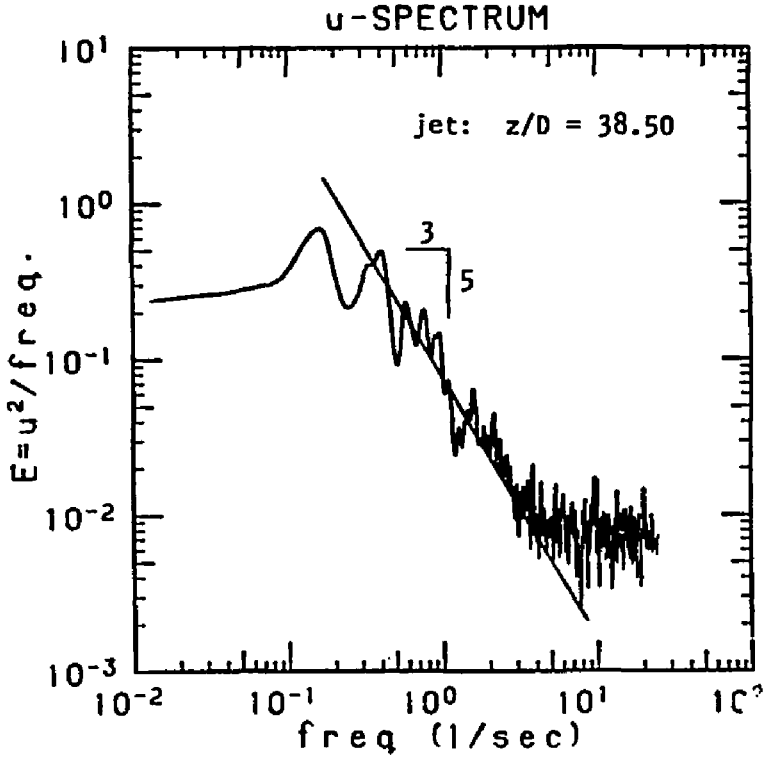


Figure 3.5.2. Power spectral estimate of u at a jet axis with initial conditions as in Figure 3.5.1.

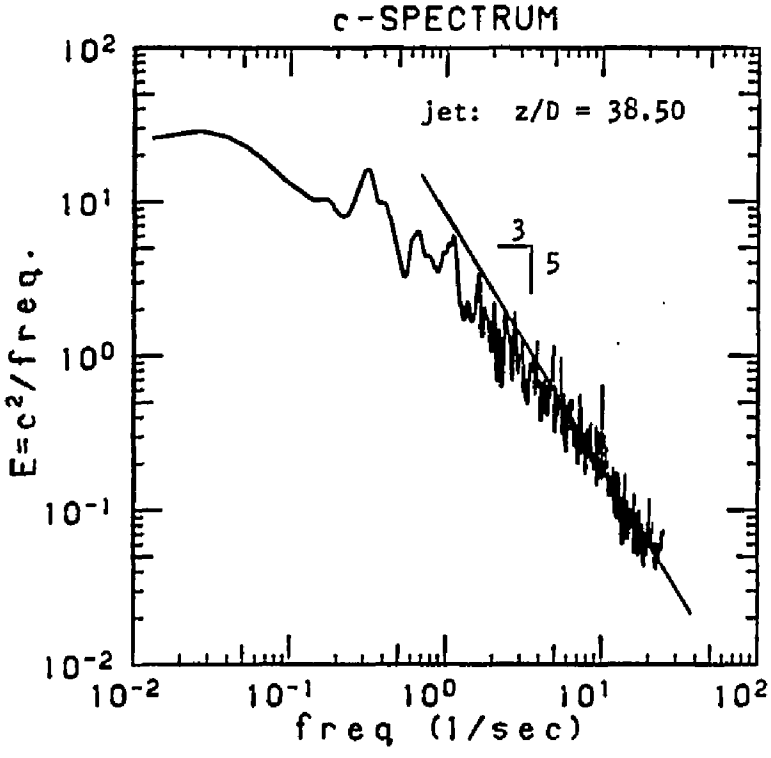


Figure 3.5.3. Power spectral estimate of c at a jet axis with initial conditions as in Figure 3.5.1.

medium around the calm volume of fluid. It can be easily observed that the noise contribution is negligible in the low frequencies, and becomes more significant at higher frequencies. Also the noise level is higher when changes in the refractive index occur (dotted lines in figures). Furthermore the noise level is of great importance near the the jet boundaries where velocities and concentrations are small.

## 3.6 Data acquisition

The two velocity and concentration signals detected by the three photodiodes, were amplified and processed with the analog outputs offset so that the range of the expected values would be within +5V. Data were transmitted to a PDP 11/60 where they were converted into digital form and recorded on diskettes for subsequent analysis. Using the calibrations for w,u and c the digital data were converted into velocities and concentration. Figures 3.6.1 and 3.6.2 represent typical filtered and unfiltered time records respectively, of the two velocity components and the concentration measured simultaneously at the same point. Also the calculated values of $w'^2$ , $u'^2$ , $c'^2$ , $w'u'$, $w'c'$ and $u'c'$ from w,u and c are plotted as functions of time. All the information needed to study the turbulence field of the jet was provided from the discrete signals in time for the two velocity components and concentration. The results of these experiments are presented in detail in the next chapter.

## 3.7 Procedure followed in a typical experiment

The entire procedure of a typical experiment will be presented step by step in this paragraph. That is, for a desired set of jet

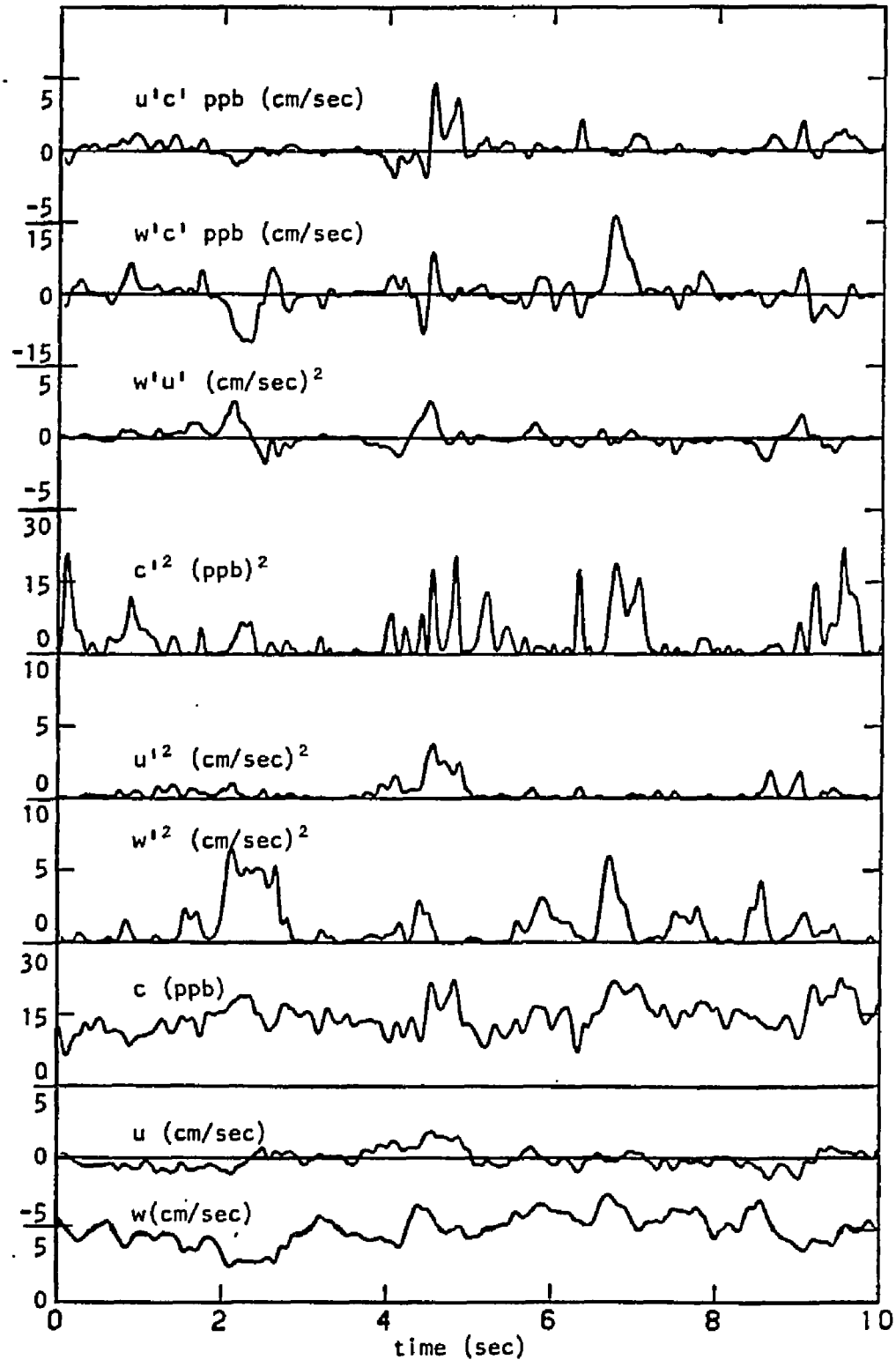


Figure 3.6.1. Filtered time-records of w, u and c (measured) and $w'^2$, $u'^2$, $c'^2$, $w'u'$, $w'c'$, $u'c'$ (calculated). Jet centerline: $z = 48.50$ cm, $D = 1.25$ cm, $W = 29.65$ cm/sec, $\bar{w}_c = 5.134$ cm/sec.

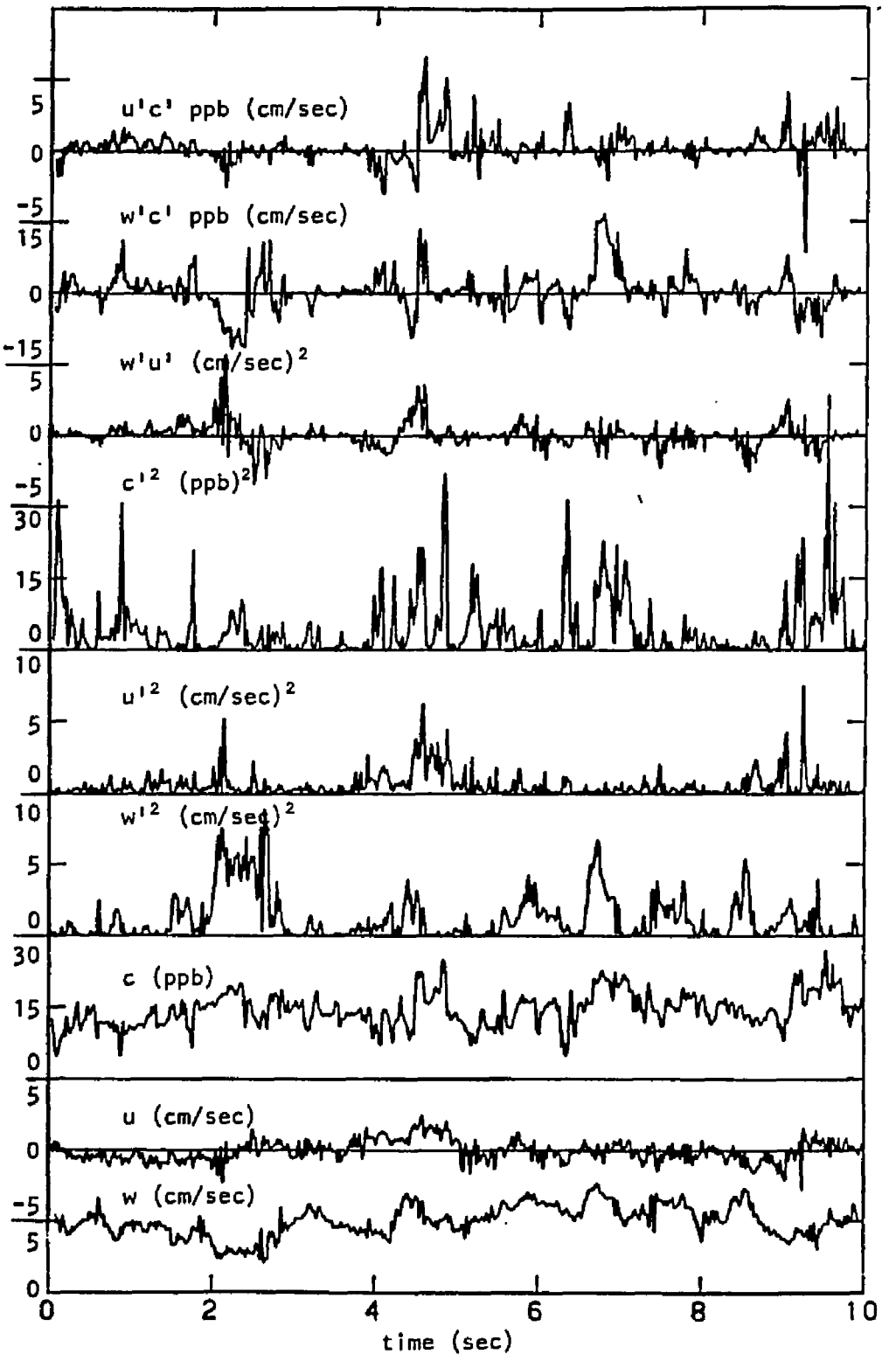


Figure 3.6.2. Unfiltered time-records (labels as in Figure 3.6.1).

initial conditions D, M and B, how the mean and turbulence characteristics of w, u and c were obtained in the entire jet cross-section at a distance z from the origin. The step by step procedure is:

(1) Assume that information is needed for a given $z/l_M$. After some preliminary calculations the jet diameter D, the initial density difference $(\Delta\rho)_o$ and the distance z from the jet origin were estimated. The experimental parameters were chosen in a such way that the error in the measurements does not exceed the maximum estimates made previously.

(2) The tank was filled with fresh lab water, $Na_2SO_3$ was added and mixed with the water in the tank for dechlorination. A proper amount of Rhodamine 6G dye in aqueous solution with known concentration was added and mixed in the tank so that the ambient water concentration was close to 1 ppb.

(3) The water in the small mixing tank $T_1$ was dechlorinated. Then filtered solutes of known high concentrations of NaCl and Rhodamine 6G dye were added accurately so that the jet initial $C_o$ and $(\Delta\rho)_o$ were known. In this case the jet was denser than the ambient fluid and pointed down, as shown in Figure 3.2.1.

(4) Both lasers and all electrical units such as amplifiers, Bragg cell exciters and data processors were turned on at least one hour in advance. The laser-Doppler velocimeter was calibrated. Maximum and minimum velocities and concentrations were estimated so that the analog outputs of the three signals were offset to be always in the $\pm 5$V region.

(5) The battery operated preamplifiers of the photodetectors were turned on. The LED to excite the photodetector used to detect the

induced fluorescence was turned on and the pump was started. The output frequencies from the Bragg cell exciters were measured and their difference F was the frequency shift between the reference and scattering beams.

(6) A 10 second record of the ambient fluid conditions (ambient w, u and c) was sampled.

(7) The jet was turned on and valve V3 (see Figure 3.2.1) adjusted to the prescribed flowmeter indication R (%).

(8) After the jet had reached steady state (2 - 3 minutes later), data sampling for w,u and c was performed at 10 to 15 different radial distances from the known jet centerline, at sampling times and rates previously discussed. It was not possible to perform data sampling at more than 10 to 15 points for the reason that after a while the interface of the density and concentration stratified body of the tank water reached the cross section where measurements were performed.

(9) After the run was completed the laser induced fluorescence system was calibrated.

(10) The tank water was mixed using by air-bubble jets from the four air injectors at the bottom of the tank and a new uniform ambient fluid was created.

The time history of w, u and c for various radial positions was recorded on diskettes in binary form. The data were then converted to velocities and concentration using the previously derived calibration curves. The converted data were properly analyzed to provide the information about the turbulent jets and plumes that is discussed in the following chapter.

The next experimental run for measurements at a new $z/l_M$ with the new ambient conditions followed the steps (5) to (10). No more than three consecutive experiments were performed before the tank water was renewed, so that the ambient Rhodamine 6G concentration would not exceed 5 ppb, thereby avoiding beam attenuation problems.

# 4. EXPERIMENTAL RESULTS

## 4.1 Basic experimental parameters and initial data

Complete information regarding the basic initial parameters of all the experimental work that will be subsequently presented is given in Tables 4.1.1, 4.1.2 and 4.1.3. More specifically, Table 4.1.1 contains the initial data from the combined velocity and Rhodamine 6G dye concentration measurements (EXP series) for all cases, jets, plumes and buoyant jets. Table 4.2.2 contains measured flow parameters such as mean and turbulent velocities and concentrations and the derived widths of the jet for the EXP series. Table 4.1.3 contains the initial jet parameters and measured parameters of velocimetry for the case of a simple jet (VEL and PAP series).

(i) The initial flow parameters mentioned above are

- $z$ the distance from the jet origin at which measurements were performed (cm)
- $D$ the jet diameter (cm)
- $W$ jet exit velocity (cm/sec)
- $C_o$ excess (above the ambient) concentration of Rhodamine 6G dye at the jet orifice (ppb)
- $g_o' = \left((\Delta\rho)_o/\rho_a\right)g$ buoyancy force at the jet exit (cm/sec$^2$)
- $l_M$ jet momentum length scale (cm).

(ii) Measured quantities at a distance z from the jet origin

- $\bar{w}_c$ mean velocity at the jet centerline (cm/sec)

| | z | D | W | $C_o$ | $\frac{(\Delta\rho)_o}{\rho_a} g$ | $\ell_M$ |
|---|---|---|---|---|---|---|
| | cm | cm | cm/sec | ppb | $cm/sec^2$ | cm |
| EXP01 | 48.250 | 1.500 | 7.601 | 98.740 | 7.225 | 3.260 |
| EXP05 | 40.750 | 1.000 | 13.560 | 97.000 | 7.225 | 4.750 |
| EXP08 | 58.050 | 2.000 | 3.390 | 98.000 | 8.850 | 1.510 |
| EXP09 | 57.950 | 2.000 | 6.710 | 97.100 | 8.850 | 3.003 |
| EXP10 | 44.450 | 2.000 | 3.169 | 96.000 | 8.850 | 1.418 |
| EXP11 | 44.450 | 2.000 | 3.390 | 98.000 | 8.850 | 1.520 |
| EXP12 | 83.000 | 2.000 | 4.500 | 97.800 | 15.337 | 1.530 |
| EXP15 | 35.900 | 0.750 | 46.934 | 98.650 | 1.082 | 36.794 |
| EXP16 | 53.600 | 0.750 | 55.590 | 96.800 | 1.082 | 43.582 |
| EXP17 | 24.600 | 0.750 | 35.128 | 95.100 | 1.082 | 27.540 |
| EXP18 | 48.600 | 0.750 | 31.980 | 94.200 | 1.082 | 25.070 |
| EXP19 | 48.600 | 0.750 | 31.980 | 98.400 | 0.688 | 31.428 |
| EXP20 | 63.700 | 0.750 | 47.722 | 97.600 | 0.688 | 46.900 |
| EXP21 | 39.600 | 0.750 | 31.980 | 95.500 | 0.688 | 31.428 |
| EXP22 | 59.500 | 0.750 | 39.850 | 97.000 | 0.688 | 39.163 |
| EXP23 | 59.500 | 0.750 | 31.980 | 97.600 | 5.800 | 10.825 |
| EXP24 | 39.900 | 0.750 | 31.980 | 96.400 | 5.800 | 10.826 |
| EXP25 | 39.900 | 0.750 | 16.237 | 95.750 | 5.800 | 5.497 |
| EXP27 | 50.100 | 0.750 | 47.720 | 97.750 | 0.197 | 87.740 |
| EXP28 | 34.100 | 0.750 | 39.850 | 96.410 | 0.197 | 73.200 |
| EXP29 | 73.600 | 0.750 | 47.720 | 96.600 | 0.197 | 87.740 |
| EXP30 | 58.100 | 0.750 | 39.850 | 94.600 | 0.197 | 73.200 |
| EXP31 | 58.100 | 1.250 | 4.712 | 98.500 | 10.913 | 1.500 |
| EXP32 | 43.600 | 1.250 | 5.845 | 127.900 | 10.710 | 1.879 |
| EXP33 | 43.600 | 1.250 | 11.513 | 127.400 | 10.710 | 3.703 |
| EXP34 | 70.100 | 1.250 | 8.680 | 126.400 | 10.710 | 2.791 |
| EXP35 | 32.000 | 1.250 | 5.845 | 129.000 | 10.710 | 1.880 |
| EXP36 | 32.000 | 1.250 | 11.510 | 98.650 | 3.146 | 6.833 |
| EXP37 | 32.000 | 0.750 | 24.108 | 97.100 | 3.146 | 11.082 |
| EXP38 | 37.700 | 0.750 | 31.979 | 97.150 | 3.146 | 14.700 |
| EXP39 | 62.100 | 2.000 | 2.283 | 208.150 | 15.815 | 0.764 |
| EXP40 | 62.100 | 2.000 | 3.390 | 207.500 | 15.815 | 1.130 |
| EXP41 | 92.400 | 1.500 | 4.925 | 209.250 | 15.815 | 1.428 |
| EXP42 | 77.700 | 1.500 | 5.161 | 207.800 | 15.815 | 1.496 |
| EXP43 | 56.800 | 1.500 | 5.043 | 208.700 | 15.815 | 1.462 |
| EXP44 | 77.600 | 1.500 | 5.200 | 207.400 | 15.815 | 1.508 |
| EXP45 | 77.600 | 1.250 | 5.845 | 199.550 | 24.060 | 1.254 |
| EXP46 | 39.800 | 1.250 | 5.847 | 248.900 | 25.066 | 1.229 |
| EXP47 | 60.100 | 1.250 | 5.959 | 248.000 | 25.066 | 1.253 |

Table 4.1.1. Initial jet parameters of the simultaneous velocity-concentration measurement.

| | $\overline{w}_c$ cm/sec | $\overline{c}_c$ ppb | $\sqrt{\overline{w_c'^2}}$ cm/sec | $\sqrt{\overline{u_c'^2}}$ cm/sec | $\sqrt{\overline{c_c'^2}}$ ppb | $(\overline{w'c'})_c$ $\frac{\text{ppb cm}}{\text{sec}}$ | $b_w$ cm | $b_c$ cm |
|---|---|---|---|---|---|---|---|---|
| EXP01 | 5.180 | 6.350 | 1.091 | 0.741 | 2.264 | 1.159 | 5.635 | 5.800 |
| EXP05 | 4.900 | 7.880 | 1.000 | 0.640 | 2.650 | 1.230 | 4.310 | 4.420 |
| EXP08 | 4.500 | 3.493 | 0.967 | 0.643 | 1.346 | 0.650 | 5.774 | 6.934 |
| EXP09 | 5.880 | 5.900 | 1.210 | 0.868 | 2.114 | 1.345 | 5.808 | 6.967 |
| EXP10 | 4.715 | 5.000 | 1.036 | 0.731 | 1.918 | 1.053 | 4.725 | |
| EXP11 | 4.700 | 4.675 | 1.071 | 0.654 | 2.019 | 1.105 | 5.399 | 5.315 |
| EXP12 | 5.502 | 1.878 | 1.300 | 0.800 | 1.129 | 0.600 | 8.704 | 10.847 |
| EXP15 | 7.110 | 11.500 | 1.400 | 1.023 | 2.325 | 1.371 | 3.669 | 4.940 |
| EXP16 | 5.687 | 8.130 | 1.207 | 0.914 | 1.889 | 1.190 | 5.455 | 6.900 |
| EXP17 | 6.500 | 17.000 | 1.280 | 0.980 | 3.275 | 2.020 | 2.800 | 3.200 |
| EXP18 | 3.570 | 7.539 | 0.705 | 0.528 | 1.898 | 0.745 | 5.490 | 5.630 |
| EXP19 | 3.475 | 10.000 | 0.736 | 0.532 | 2.209 | 0.705 | 5.384 | 5.773 |
| EXP20 | 3.728 | 6.850 | 0.882 | 0.628 | 1.477 | 0.506 | 7.392 | 8.304 |
| EXP21 | 4.012 | 9.569 | 0.834 | 0.638 | 2.352 | 0.858 | 4.635 | 4.810 |
| EXP22 | 3.190 | 7.084 | 0.743 | 0.543 | 1.853 | 0.523 | | |
| EXP23 | 5.023 | 5.250 | 1.048 | 0.734 | 1.595 | 0.879 | 5.670 | 6.324 |
| EXP24 | 6.200 | 8.500 | 1.184 | 0.850 | 2.260 | 1.420 | | |
| EXP25 | 4.200 | 6.030 | 0.850 | 0.640 | 2.181 | 0.838 | 4.375 | 5.000 |
| EXP27 | 4.700 | 9.000 | 0.970 | 0.740 | 2.000 | 0.881 | | |
| EXP28 | 5.650 | 11.600 | 1.200 | 0.810 | 2.611 | 1.676 | 3.907 | 5.064 |
| EXP29 | 3.350 | 7.312 | 0.705 | 0.580 | 1.419 | 0.408 | 8.771 | 10.850 |
| EXP30 | 3.500 | 7.200 | 0.690 | 0.553 | 1.783 | 0.533 | 6.594 | 7.454 |
| EXP31 | 4.000 | 3.300 | 0.806 | 0.635 | 1.433 | 0.737 | 6.450 | 6.820 |
| EXP32 | 4.600 | 4.880 | 1.025 | 0.690 | 2.210 | 1.090 | | |
| EXP33 | 6.500 | 9.800 | 1.209 | 0.967 | 3.051 | 1.860 | 4.472 | 4.767 |
| EXP34 | 4.800 | 3.850 | 1.000 | 0.740 | 1.384 | 0.715 | 6.742 | 7.063 |
| EXP35 | 4.900 | 8.800 | 1.086 | 0.745 | 3.416 | 1.822 | 3.780 | 3.835 |
| EXP36 | 4.500 | 15.500 | 0.960 | 0.685 | 4.920 | 1.900 | 3.410 | 3.770 |
| EXP37 | 5.250 | 10.500 | 0.918 | 0.716 | 3.096 | 1.457 | 3.310 | 3.750 |
| EXP38 | 4.800 | 9.000 | 0.950 | 0.700 | 2.400 | 1.057 | 4.470 | 5.000 |
| EXP39 | 4.200 | 3.300 | 1.137 | 0.724 | 1.680 | 1.192 | 7.905 | 8.300 |
| EXP40 | 5.200 | 4.700 | 1.150 | 0.785 | 1.900 | 1.000 | 6.325 | 7.450 |
| EXP41 | 4.723 | 3.400 | 0.921 | 0.757 | 1.238 | 0.580 | 9.129 | |
| EXP42 | 4.903 | 5.000 | 1.172 | 0.779 | 2.057 | 1.253 | 8.452 | |
| EXP43 | 4.875 | 6.417 | 1.072 | 0.790 | 2.700 | 1.610 | 6.350 | 6.040 |
| EXP44 | 5.326 | 4.300 | 1.121 | 0.711 | 1.792 | 1.126 | 7.274 | 7.590 |
| EXP45 | 5.300 | 2.950 | 1.122 | 0.766 | 1.100 | 0.533 | 7.071 | 7.900 |
| EXP46 | 6.750 | 9.500 | 1.243 | 0.912 | 3.530 | 2.100 | 4.714 | 5.000 |
| EXP47 | 5.500 | 4.750 | 1.274 | 0.868 | 2.012 | 1.191 | 5.774 | 5.980 |

Table 4.1.2. Basic experimental turbulence parameters measured in the simultaneous velocity and concentration measurements.

| | z<br>cm | D<br>cm | W<br>cm/sec | $\overline{w}_c$<br>cm/sec | $\sqrt{\overline{w_c'^2}}$<br>cm/sec | $\sqrt{\overline{u_c'^2}}$<br>cm/sec | $\frac{(\Delta\rho)}{\rho_a} \cdot g$<br>cm/sec$^2$ | $\ell_M$<br>cm | $b_w$<br>cm |
|---|---|---|---|---|---|---|---|---|---|
| VEL05 | 67.100 | 0.750 | 79.210 | 5.800 | 1.517 | 0.929 | 0.085 | 222.130 | 7.440 |
| VEL07 | 50.400 | 0.750 | 66.613 | 7.000 | 1.675 | 1.040 | 0.131 | 150.200 | 5.712 |
| VEL10 | 64.900 | 0.750 | 80.781 | 6.131 | 1.487 | 0.934 | 0.197 | 148.534 | 6.468 |
| VEL11 | 77.300 | 0.750 | 95.736 | 5.612 | 1.487 | 0.963 | 0.287 | 145.690 | 8.006 |
| VEL13 | 33.500 | 0.750 | 55.590 | 7.900 | 1.780 | 1.165 | 0.263 | 88.300 | 3.987 |
| VEL15 | 60.500 | 0.750 | 87.080 | 7.250 | 1.621 | 1.159 | 0.263 | 138.320 | 6.667 |
| VEL17 | 82.500 | 0.750 | 111.085 | 6.750 | 1.768 | 1.141 | 0.281 | 170.820 | 8.607 |
| VEL19 | 63.750 | 0.750 | 94.950 | 7.500 | 1.700 | 1.159 | 0.351 | 130.660 | 6.324 |
| VEL21 | 45.000 | 0.750 | 63.464 | 7.320 | 1.600 | 1.000 | 0.260 | 101.380 | 4.657 |
| VEL23 | 26.250 | 0.750 | 40.638 | 7.100 | 1.597 | 0.843 | 0.306 | 59.920 | 2.820 |
| PAP12 | 48.750 | 0.750 | 61.890 | 6.143 | 1.492 | 0.905 | 0.192 | 115.260 | 4.530 |
| PAP13 | 63.750 | 0.750 | 110.690 | 7.850 | 1.718 | 1.115 | 0.279 | 170.810 | 6.711 |
| PAP16 | 18.250 | 0.750 | 31.980 | 6.900 | 1.762 | 1.021 | 0.110 | 78.570 | 2.370 |
| PAP17 | 37.500 | 0.750 | 70.550 | 8.600 | 2.351 | 1.437 | 0.088 | 194.440 | 4.124 |
| PAP20 | 75.000 | 0.750 | 142.180 | 8.800 | 2.133 | 1.527 | 0.043 | 557.300 | 7.956 |
| PAP21 | 52.500 | 0.750 | 94.950 | 8.200 | 1.913 | 1.421 | 0.043 | 372.220 | 5.774 |
| PAP30 | 66.000 | 0.750 | 140.600 | 11.000 | 2.517 | 1.581 | 0.150 | 296.075 | 6.788 |
| PAP32 | 38.250 | 0.750 | 79.206 | 10.500 | 2.232 | 1.593 | 0.150 | 166.790 | 3.922 |
| PAP31 | 51.600 | 0.750 | 98.880 | 9.147 | 2.275 | 1.521 | | | |
| PAP34 | 79.350 | 0.750 | 140.600 | 8.468 | 1.999 | 1.312 | | | |
| PAP34 | 70.650 | 0.750 | 140.600 | 9.936 | 2.396 | 1.476 | | | |
| PAP34 | 60.950 | 0.750 | 140.600 | 11.321 | 2.820 | 1.733 | | | |
| PAP34 | 49.350 | 0.750 | 63.460 | 5.832 | 1.559 | 0.857 | | | |
| PAP34 | 40.350 | 0.750 | 63.460 | 7.711 | 1.664 | 1.038 | | | |
| PAP34 | 30.850 | 0.750 | 47.720 | 7.273 | 1.525 | 0.958 | | | |
| PAP34 | 26.250 | 0.750 | 31.980 | 5.361 | 1.153 | 0.713 | | | |
| PAP34 | 21.000 | 0.750 | 24.110 | 4.960 | 0.999 | 0.646 | | | |
| PAP34 | 75.000 | 0.750 | 126.430 | 8.169 | 1.878 | 1.288 | | | |
| PAP34 | 54.600 | 0.750 | 94.950 | 8.754 | 1.945 | 1.196 | | | |

Table 4.1.3. Basic experimental parameters and data for the velocity measurements in jets.

$\sqrt{\overline{w'^2_c}}$ axial rms velocity at the jet axis (cm/sec)

$\sqrt{\overline{u'^2_c}}$ radial rms velocity at the jet axis (cm/sec)

$\bar{c}_c$ mean (time-averaged) concentration above the ambient of Rhodamine 6G dye at the jet axis (ppb)

$\sqrt{\overline{c'^2_c}}$ rms concentration at the jet axis (ppb)

$\overline{w'c'}$ turbulent transport term (w, c correlation) at the jet axis (ppb cm/sec)

$b_w$ 1/e mean velocity width of the jet (cm)

$b_c$ 1/e mean concentration width of the jet (cm).

The 1/e-widths were calculated from the least square Gaussian curves fitted to the transverse time-averaged velocity and concentration profiles that are shown in Appendix A. All other jet parameters that will be presented in the following sections are calculated from the data in Tables 4.1.1, 4.1.2 and 4.1.3 and the data presented in Appendix B and are shown in Tables 4.1.4 and 4.1.5.

4.2 Calculation of the turbulence parameters

From the time signal $y(\underline{x},t)$ of a parameter measured in a turbulent steady flow at a point x the time averaged value $\bar{y}(\underline{x})$ of $y(\underline{x},t)$ is

$$\bar{y}(\underline{x})=\lim_{T\to\infty}\frac{1}{T}\int_0^T y(\underline{x},t)dt \qquad (4.2.1)$$

for a continuous time signal or

$$\bar{y}(\underline{x})=1/N\sum_{i=1}^{N} y(\underline{x},t_i)=\overline{y_i(\underline{x})} \quad ; \quad y_i(\underline{x})=y(\underline{x},t_i) \qquad (4.2.2)$$

for a discrete signal where

# LIST OF CALCULATIONS
## FOR TABLES 4.1.4 and 4.1.5

$$Q = \frac{\pi D^2}{4} W$$

$$M = \frac{\pi D^2}{4} W^2$$

$$B = \frac{(\Delta\rho)_o}{\rho_a} g Q$$

$$R_e = \frac{WD}{\nu}$$

$$R_o = \frac{l_Q}{l_M}$$

$$R(z) = \left[ \frac{4\sqrt{2\pi}\ \lambda^2}{1 + \lambda^2} \left( \frac{(\Delta\rho)_o}{\rho_a} g \frac{\bar{c}_c}{C_o} \frac{b_w}{\bar{w}_c^2} \right) \right]^{1/2}$$

$$\mu(z) = \int_o^\infty \bar{w}(z) 2\pi r dr = \pi \bar{w}_c b_w^2$$

$$m(z) = \int_o^\infty \bar{w}^2 2\pi r dr = \frac{\pi \bar{w}_c^2 b_w^2}{2}$$

$$H_M = \int_o^\infty \bar{w}\ \bar{c}\ 2\pi r dr = \frac{\pi \bar{w}_c \bar{c}_c \lambda^2 b_w^2}{1 + \lambda^2}$$

$$H_T = \int_o^{b(z)} \overline{w' c'}\ 2\pi r dr \quad \text{(numerical integration)}$$

$$m_T(z) = \int_o^{b(z)} \overline{w'^2}\ 2\pi r dr \quad \text{(numerical integration)}$$

$b(z)$ = edge of jet

| | $\frac{z}{l_M}$ | Q $\frac{cm^3}{sec}$ | M $\frac{cm^4}{sec^2}$ | B $\frac{cm^4}{sec^3}$ | $QC_o$ $\frac{cm^3 ppb}{sec}$ | $R_e$ | $R_o$ | R(z) | $\mu(z)$ $\frac{cm^3}{sec}$ | $m(z)$ $\frac{cm^4}{sec^2}$ | $H_M$ $\frac{cm^3 ppb}{sec}$ | $H_T$ $\frac{cm^3 ppb}{sec}$ | $m_T(z)$ $\frac{cm^4}{sec^2}$ |
|---|---|---|---|---|---|---|---|---|---|---|---|---|---|
| EXP01 | 14.80 | 13.43 | 102.09 | 97.04 | 1326.28 | 1140.15 | 0.4077 | 0.7094 | 516.73 | 1338.34 | 1687.96 | 232.7 | 180.00 |
| EXP05 | 8.57 | 10.65 | 144.41 | 76.94 | 1033.05 | 1356.00 | 0.1866 | 0.7359 | 285.95 | 700.59 | 1155.05 | 158.9 | 93.44 |
| EXP08 | 38.44 | 10.65 | 36.10 | 94.25 | 1043.70 | 678.00 | 1.1683 | 0.7298 | 471.31 | 1060.46 | 972.19 | 141.3 | 232.90 |
| EXP09 | 19.29 | 21.08 | 141.44 | 186.55 | 2046.88 | 1342.00 | 0.5903 | 0.7310 | 623.13 | 1832.00 | 2169.06 | 375.6 | 550.05 |
| EXP10 | 31.34 | 9.95 | 31.55 | 88.10 | 955.75 | 633.80 | 1.2498 | | 330.70 | 779.62 | | | 125.17 |
| EXP11 | 29.24 | 10.65 | 36.10 | 94.25 | 1043.70 | 678.00 | 1.1683 | 0.7136 | 430.40 | 1011.44 | 990.28 | 125.6 | 223.30 |
| EXP12 | 54.24 | 14.13 | 63.61 | 216.82 | 1382.61 | 900.00 | 1.1586 | 0.7187 | 1309.50 | 3602.45 | 1495.98 | 276.9 | 706.37 |
| EXP15 | 0.97 | 20.73 | 973.17 | 22.43 | 2045.49 | 3520.05 | 0.0181 | 0.2432 | 300.68 | 1068.94 | 2228.57 | 125.0 | 165.04 |
| EXP16 | 1.22 | 24.55 | 1365.23 | 26.57 | 2377.30 | 4169.25 | 0.0153 | 0.3075 | 531.64 | 1511.73 | 2659.83 | 220.8 | 214.02 |
| EXP17 | 0.89 | 15.51 | 545.15 | 16.79 | 1475.86 | 2634.59 | 0.0241 | 0.2698 | 160.09 | 520.31 | 1541.44 | 110.2 | 59.65 |
| EXP18 | 1.93 | 14.12 | 451.82 | 15.28 | 1330.89 | 2398.50 | 0.0265 | 0.4378 | 338.03 | 603.39 | 1306.30 | 145.2 | 83.43 |
| EXP19 | 1.54 | 14.12 | 451.82 | 9.72 | 1390.23 | 2398.50 | 0.0212 | 0.4089 | 316.45 | 549.84 | 1692.48 | 137.3 | 69.74 |
| EXP20 | 1.35 | 21.08 | 1006.12 | 14.50 | 2057.69 | 3579.14 | 0.0142 | 0.3790 | 639.95 | 1192.87 | 2445.69 | 174.0 | 152.98 |
| EXP21 | 1.26 | 14.12 | 451.82 | 9.72 | 1349.25 | 2398.50 | 0.0212 | 0.3185 | 271.00 | 543.64 | 1344.11 | 160.8 | 73.46 |
| EXP22 | 1.51 | 17.60 | 701.56 | 12.11 | 1707.70 | 2988.75 | 0.0170 | | 10.02 | | | 252.0 | |
| EXP23 | 5.49 | 14.12 | 451.82 | 81.94 | 1378.92 | 2398.50 | 0.0614 | 0.6243 | 507.31 | 1274.12 | 1476.50 | 221.1 | 239.90 |
| EXP24 | 3.68 | 14.12 | 451.82 | 81.94 | 1361.97 | 2398.50 | 0.0614 | | 19.47 | | | 126.1 | |
| EXP25 | 7.25 | 7.17 | 116.47 | 41.60 | 686.84 | 1217.77 | 0.1209 | 0.7172 | 252.55 | 530.36 | 862.52 | 78.2 | 68.80 |
| EXP27 | 0.57 | 21.08 | 1006.03 | 4.15 | 2060.77 | 3579.00 | 0.0076 | | 14.76 | | | 190.6 | |
| EXP28 | 0.46 | 17.60 | 701.56 | 3.46 | 1697.32 | 2988.75 | 0.0091 | 0.1350 | 270.94 | 765.42 | 1970.21 | 127.3 | 106.66 |
| EXP29 | 0.83 | 21.08 | 1006.03 | 4.15 | 2036.53 | 3579.00 | 0.0076 | 0.2658 | 809.64 | 1356.14 | 3580.36 | 264.7 | 187.77 |
| EXP30 | 0.79 | 17.60 | 701.56 | 3.46 | 1665.45 | 2988.75 | 0.0091 | 0.2131 | 478.09 | 836.66 | 1931.09 | 177.2 | 108.63 |
| EXP31 | 38.73 | 5.78 | 27.24 | 63.10 | 569.57 | 589.00 | 0.7379 | 0.8832 | 522.79 | 1045.58 | 910.67 | 113.9 | 196.52 |
| EXP32 | 23.20 | 7.17 | 41.92 | 76.82 | 917.41 | 730.62 | 0.5893 | | 14.45 | | | 126.1 | |
| EXP33 | 11.77 | 14.12 | 162.66 | 151.31 | 1799.98 | 1439.12 | 0.2992 | 0.6819 | 408.38 | 1327.24 | 2128.72 | 246.5 | 193.99 |
| EXP34 | 25.11 | 10.65 | 92.45 | 114.08 | 1346.41 | 1085.00 | 0.3968 | 0.7077 | 685.43 | 1685.05 | 1380.79 | 194.5 | 226.86 |
| EXP35 | 17.02 | 7.17 | 41.92 | 76.82 | 925.30 | 730.62 | 0.5893 | 0.7648 | 219.95 | 538.88 | 981.77 | 99.1 | 84.33 |
| EXP36 | 4.68 | 14.12 | 162.57 | 44.43 | 1393.42 | 1438.75 | 0.1622 | 0.6775 | 164.38 | 369.87 | 1401.44 | 112.2 | 84.92 |
| EXP37 | 2.88 | 10.65 | 256.76 | 33.50 | 1034.17 | 1808.10 | 0.0600 | 0.4798 | 180.70 | 474.34 | 1066.48 | 87.2 | 84.43 |
| EXP38 | 2.56 | 14.12 | 451.79 | 84.44 | 1372.52 | 2398.42 | 0.0452 | 0.5613 | 301.30 | 723.13 | 1507.16 | 159.3 | 106.89 |
| EXP39 | 81.28 | 7.17 | 16.37 | 113.42 | 1492.90 | 456.60 | 2.3191 | 0.7686 | 824.52 | 1731.49 | 1426.74 | 230.2 | 419.30 |
| EXP40 | 54.95 | 10.65 | 36.10 | 168.43 | 2209.88 | 678.00 | 1.5618 | 0.6987 | 653.54 | 1699.21 | 1785.02 | 266.5 | 315.64 |
| EXP41 | 64.70 | 8.70 | 42.86 | 137.64 | 1821.14 | 738.75 | 0.9310 | | 1236.55 | 2920.12 | | | 452.53 |
| EXP42 | 51.93 | 9.12 | 47.07 | 144.23 | 1895.19 | 774.15 | 0.8884 | | 1100.34 | 2697.50 | | | 409.42 |
| EXP43 | 38.85 | 8.91 | 44.94 | 140.93 | 1859.87 | 756.45 | 0.9092 | 0.7866 | 617.54 | 1505.27 | 1882.31 | 324.0 | 305.85 |
| EXP44 | 51.45 | 9.18 | 47.78 | 145.32 | 1905.83 | 780.00 | 0.8818 | 0.6629 | 885.31 | 2357.59 | 1984.31 | 299.2 | 317.72 |
| EXP45 | 61.88 | 7.17 | 41.92 | 172.58 | 1431.35 | 730.62 | 0.8833 | 0.7060 | 832.50 | 2206.13 | 1363.52 | 250.5 | 477.77 |
| EXP46 | 32.38 | 7.17 | 41.95 | 179.85 | 1785.94 | 730.87 | 0.9012 | 0.7249 | 471.22 | 1590.39 | 2370.02 | 219.6 | 199.04 |
| EXP47 | 47.96 | 7.31 | 43.57 | 183.30 | 1813.57 | 744.87 | 0.8843 | 0.6896 | 576.05 | 1584.15 | 1416.07 | 219.2 | 300.33 |

Table 4.1.4. Calculated flow parameters from data in Tables 4.1.1 and 4.1.2 and Appendix B for the EXP series of experiments.

| | $\frac{z}{D}$ | $R_e$ | Q $\frac{cm^3}{sec}$ | M $\frac{cm^4}{sec^2}$ | B $\frac{cm^4}{sec^3}$ | $R_o$ | $\mu(z)$ $\frac{cm^3}{sec}$ | m(z) $\frac{cm^4}{sec^2}$ | $\frac{z}{l_M}$ | R(z) | $m_{T(z)}$ $\frac{cm^4}{sec^2}$ |
|---|---|---|---|---|---|---|---|---|---|---|---|
| VEL05 | 89.46 | 6093.0 | 34.99 | 2771.8 | 2.97 | 0.0030 | 1008.6 | 2924.9 | 0.3021 | 0.0868 | 443.9 |
| VEL07 | 67.20 | 5124.0 | 29.42 | 1960.3 | 3.85 | 0.0044 | 717.5 | 2511.2 | 0.3356 | 0.0903 | 355.6 |
| VEL10 | 86.53 | 6213.9 | 35.68 | 2882.9 | 7.03 | 0.0045 | 805.7 | 2470.1 | 0.4369 | 0.1185 | 491.1 |
| VEL11 | 103.06 | 7364.3 | 42.29 | 4049.1 | 12.13 | 0.0046 | 1130.0 | 3170.9 | 0.5306 | 0.1679 | 626.5 |
| VEL13 | 44.66 | 4276.1 | 24.55 | 1365.2 | 6.45 | 0.0075 | 394.5 | 1558.3 | 0.3794 | 0.1161 | 222.2 |
| VEL15 | 80.66 | 6698.4 | 38.47 | 3350.0 | 10.11 | 0.0048 | 1012.3 | 3669.9 | 0.4374 | 0.1218 | 562.3 |
| VEL17 | 110.00 | 8544.9 | 49.07 | 5451.6 | 13.79 | 0.0039 | 1570.9 | 5301.8 | 0.4830 | 0.1315 | 903.2 |
| VEL19 | 85.00 | 7303.8 | 41.94 | 3982.9 | 14.72 | 0.0051 | 942.3 | 3533.6 | 0.4879 | 0.1290 | 748.1 |
| VEL21 | 60.00 | 4881.8 | 28.03 | 1779.3 | 7.29 | 0.0066 | 498.7 | 1825.3 | 0.4439 | 0.1162 | 284.3 |
| VEL23 | 35.00 | 3125.9 | 17.95 | 729.5 | 5.49 | 0.0111 | 177.3 | 629.7 | 0.4381 | 0.1324 | 92.7 |
| PAP12 | 65.00 | 4760.7 | 27.34 | 1692.2 | 5.25 | 0.0058 | 396.0 | 1216.4 | 0.4230 | 0.1128 | 245.6 |
| PAP13 | 85.00 | 8514.6 | 48.90 | 5412.9 | 13.64 | 0.0039 | 1110.6 | 4359.4 | 0.3732 | 0.1132 | 689.8 |
| PAP16 | 24.33 | 2459.9 | 14.12 | 451.8 | 1.55 | 0.0085 | 121.7 | 420.0 | 0.2323 | 0.0898 | 57.5 |
| PAP17 | 50.00 | 5426.9 | 31.16 | 2198.9 | 2.74 | 0.0034 | 459.4 | 1975.8 | 0.1929 | 0.0593 | 312.1 |
| PAP20 | 100.00 | 10936.9 | 62.81 | 8930.7 | 2.70 | 0.0012 | 1749.9 | 7699.7 | 0.1346 | 0.0398 | 1579.8 |
| PAP21 | 70.00 | 7303.8 | 41.94 | 3982.9 | 1.80 | 0.0018 | 858.8 | 3521.2 | 0.1410 | 0.0435 | 655.9 |
| PAP30 | 88.00 | 10815.3 | 62.11 | 8733.4 | 9.31 | 0.0022 | 1592.3 | 8757.6 | 0.2229 | 0.0586 | 1253.8 |
| PAP32 | 51.00 | 6092.7 | 34.99 | 2771.5 | 5.24 | 0.0040 | 507.4 | 2663.8 | 0.2293 | 0.0613 | 425.4 |

Table 4.1.5. Calculated flow parameters from data in Table 4.1.3 and Appendix B for the VEL and PAP series of experiments.

$\tau$ = sampling time in seconds

N = total number of samples during $\tau$ seconds

$N/\tau$ = sampling rate (samples/sec)

$t_i = \frac{\tau}{N} i$, $i = 1,2,3,\ldots N$.

For a discrete signal the variance $\overline{y'^2}(\underline{x})$ of $y(\underline{x},t_i)$ is calculated as

$$\overline{y'^2(\underline{x})} = \overline{[y(\underline{x},t_i)-y(\underline{x})]^2} = \overline{y^2(\underline{x},t_i)} - \bar{y}^2(\underline{x}) \tag{4.2.3}$$

and the correlation $\overline{y_1'(\underline{x})y_2'(\underline{x})}$ of the deviations $y_1'(\underline{x})$ and $y_2'(\underline{x})$ from the mean of two flow parameters $y_1(\underline{x},t_i)$ and $y_2(\underline{x},t_i)$ measured simultaneously at point x

$$\overline{y_1'(\underline{x})y_2'(\underline{x})} = \overline{y_1(\underline{x},t_i)y_2(\underline{x},t_i)} - \bar{y}_1(\underline{x})\bar{y}_2(\underline{x}) \tag{4.2.4}$$

In the present experimental work from the discrete time signals of velocities w and u and concentration c at the point (r,z) of the flow $w_i(r,z)=w(r,z,t_i)$, $u_i(r,z)=w_i(r,z,t_i)$ and $c_i(r,z)=c(r,z,t_i)$, $i=1,2,\ldots N$, one has

$$\left.\begin{aligned}
\bar{w} &= \overline{w_i(r,z)} \\
\bar{u} &= \overline{u_i(r,z)} \\
\bar{c} &= \overline{c_i(r,z)} \\
\overline{w'^2} &= \overline{w_i^2(r,z)} - \bar{w}^2(r,z) \\
\overline{u'^2} &= \overline{u_i^2(r,z)} - \bar{u}^2(r,z) \\
\overline{c'^2} &= \overline{c_i^2(r,z)} \cdot \bar{c}^2(r,z) \\
(\overline{w'u'}) &= \overline{w_i(r,z)u_i(r,z)} - \bar{w}(r,z)\bar{u}(r,z) \\
(\overline{w'c'}) &= \overline{w_i(r,z)c_i(r,z)} - \bar{w}(r,z)\bar{c}(r,z)
\end{aligned}\right\} \tag{4.2.5}$$

and

$$\overline{(u'c')} = \overline{u_i(r,z)c_i(r,z)} - \bar{u}(r,z)\bar{c}(r,z)$$

for the total number of samples N at a point (r,z) of the flow, where w',u' and c' are the deviations from the mean values $\bar{w}$, $\bar{u}$ and $\bar{c}$.

## 4.3 Velocity measurements in jets

### 4.3.1 Centerline velocity decay

The experimental results presented in this section correspond to experiments VEL and PAP-series in Table 4.1.3 and EXP-series from Table 4.1.4 for $z/l_M < 1$. The velocity at the jet exit W normalized by the mean velocity $\bar{w}_c$ at the jet axis has been plotted versus the dimensionless distance from the jet origin z/D in Figure 4.3.1. The turbulence, axial and radial intensities of velocity at the jet axis normalized by $\bar{w}_c$ have been plotted in the same figure versus z/D. Following the dimensional arguments in Chapter 1

$$\frac{W}{\bar{w}_c} = C_{1w}\left(\frac{z}{D} + C_{2w}\right) \qquad (4.3.1)$$

The constants $C_{1w}$ and $C_{2w}$ were calculated from the least square fit to the data and found to be 0.149 and 2.56 respectively. The virtual origin of the jet is located at 2.56 diameters upstream. For z/D<40 data points show the tendency to move the jet virtual origin further upstream as shown in Figure 4.3.1. This agrees with the observation reported by Wygnanski and Fiedler (1969) of the existence of two apparent virtual origins for the mean longitudinal velocities at the jet centerline, for distances smaller or larger than 40 jet diameters. Figure 4.3.1 also shows that the rms values of w and u at the jet axis normalized by $\bar{w}_c$ are

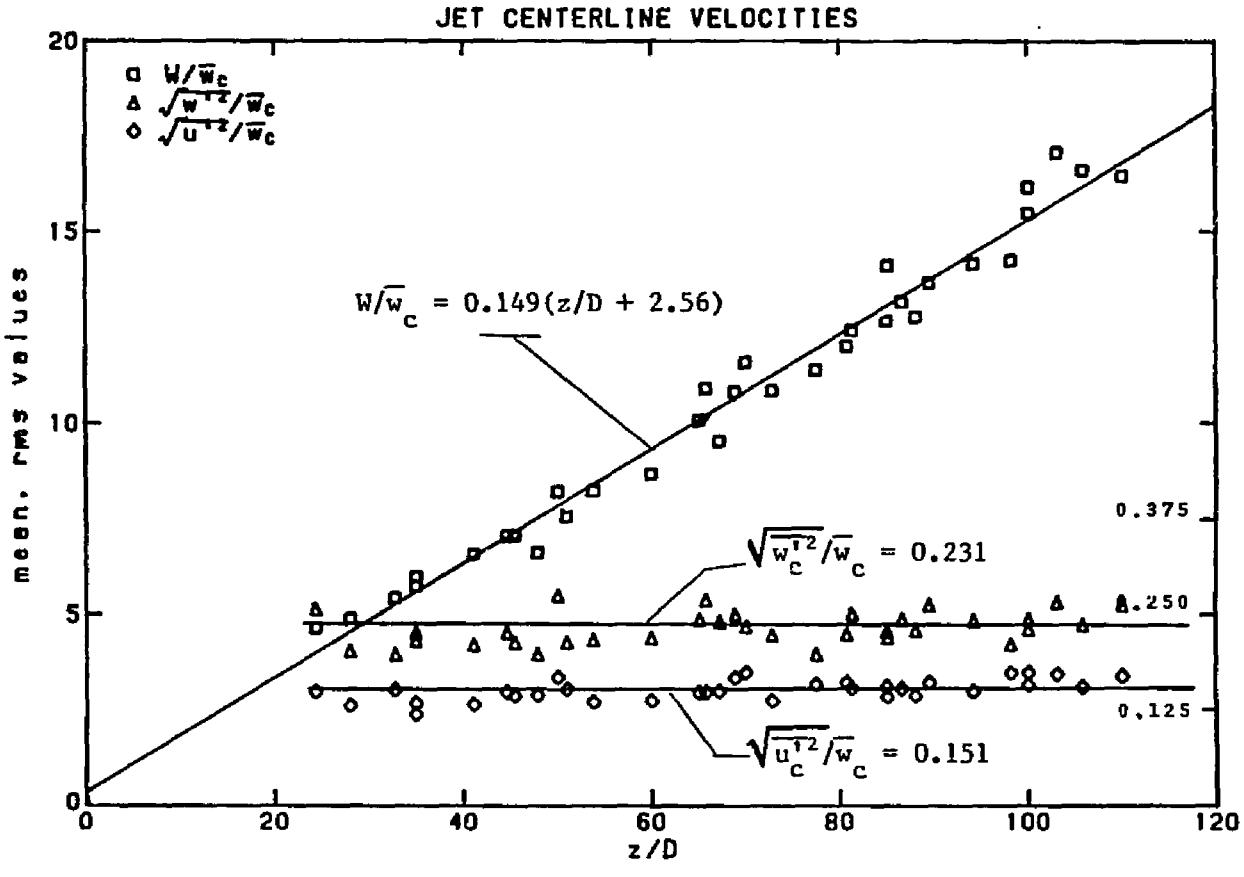


Figure 4.3.1. Non-dimensional velocity distribution along the jet axis plotted against non-dimensional distance from jet origin. Decay of the mean velocity, axial and radial turbulent intensities.

| | mean | st.dev | max | min | |
|---|---|---|---|---|---|
| $\sqrt{\overline{w_c'^2}}/\bar{w}_c$ | 0.231 | 0.0209 | 0.273 | 0.197 | (4.3.2) |
| $\sqrt{\overline{u_c'^2}}/\bar{w}_c$ | 0.151 | 0.0150 | 0.173 | 0.118 | (4.3.3) |

constant along the jet axis. Wygnanski and Fiedler (1969) reported that the axial and radial turbulent velocities become constant after about 40 and 70 jet diameters respectively. The mean velocity at the jet axis is measured to be larger than that reported by various authors (see Table 1.4.1). The Reynolds numbers used in the present investigation varied from 2460 to 10900. These are fairly low compared to ones of other authors; for example Wygnanski and Fiedler (1969) used Reynolds numbers of order of $10^5$ . Therefore the flow in the present investigation probably was not fully developed and higher mean velocities should be expected. The normalized turbulent intensities $\sqrt{\overline{w_c'^2}}/\bar{w}_c$ and $\sqrt{\overline{u_c'^2}}/\bar{w}_c$ by the mean velocity at the centerline of the jet are lower than those measured by other authors (see table 1.4.2). This is attributed to higher mean velocities measured around the jet axis and to the fact that the flow was not fully developed. All authors in Table 1.4.2 reported the radial turbulent velocities to be smaller than the axial ones, except Antonia et al (1979) and Gibson (1963) who measured the axial and radial turbulent velocities to be the same. Rosler and Bankoff (1963) measured higher turbulent velocities in water than in air at the jet axis using the same Reynolds number for both air and water experiments.

The maximum and minimum values of w at the jet axis normalized by $\bar{w}_c$ have been plotted in Figure 4.3.2. They are found

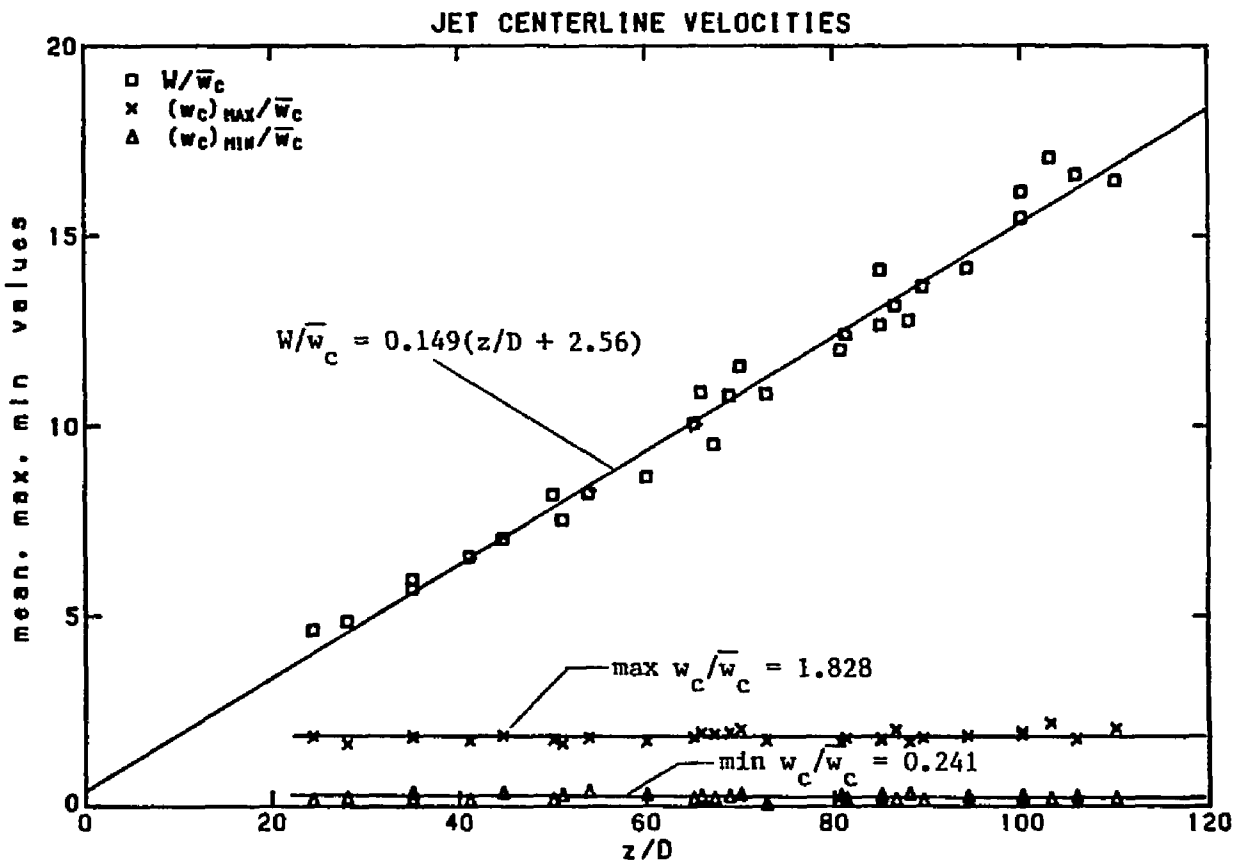


Figure 4.3.2. Mean, maximum and minimum axial velocities along the jet axis.

| | mean | st.dev. | max | min |
|---|---|---|---|---|
| max $w_c/\bar{w}_c$ | 1.828 | 0.1236 | 2.180 | 1.636 |
| min $w_c/\bar{w}_c$ | 0.241 | 0.0700 | 0.384 | 0.056. |

to have constant values for all z/D's. The maximum velocity along the jet axis was measured to be twice $\bar{w}_c$ and the minimum was measured to be small but always positive. Thus reverse flow is not expected to appear around the jet axis.

4.3.2 Width of a momentum jet

The width of a jet at a distance z from the origin was calculated from its Gaussian mean velocity distribution

$$\bar{w} = \bar{w}_c \exp(-kr^2) \qquad (4.3.4)$$

to be

$$\bar{b}_w = 1/\sqrt{k}. \qquad (4.3.5)$$

From all jet experiments the calculated $b_w$'s normalized by the jet diameter D have been plotted in Figure 4.3.3 versus z/D. A straight line least square fit to the data leads to

$$b_w/D = 0.104(z/D + 2.58). \qquad (4.3.6)$$

Equation (4.3.6) predicts a virtual origin at 2.58 diameters upstreams of the jet. The slope of the jet growth $b_w/z$ was calculated to be equal to 0.109 and therefore

$$b_w \sim 0.109z \; ; \; b_w/z = 1/N \sum_{1}^{N} b_i/z_i \quad (i=1...N) \qquad (4.3.7)$$

value in agreement with 0.107, the average value of many authors

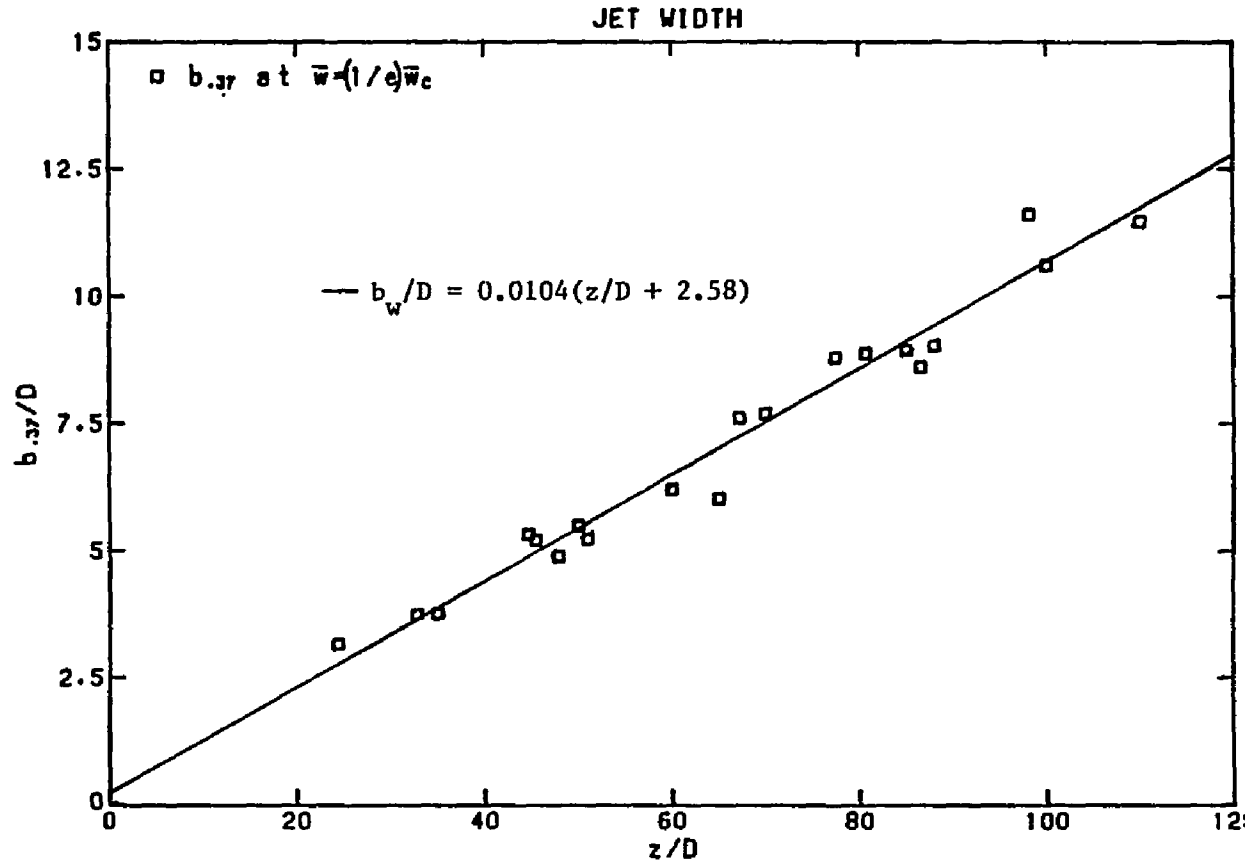


Figure 4.3.3. Non-dimensional velocity 1/e-width of a turbulent jet plotted against non-dimensional distance from jet orifice.

calculated and suggested by Fischer et al (1979). The discrepancy of the data points in Figure 4.3.3 should be attributed to the fact that no measurements were performed with the same initial jet parameters (except for the jet diameter D).

4.3.3 Mean and turbulent velocity profiles in jets

The mean and turbulent velocity characteristics measured in a momentum jet will be presented in this paragraph. Mean velocities, rms values and correlations are normalized by the mean velocity at the jet axis. The radial distances from the jet axis are normalized by the distance z from the jet origin. The dimensionless mean and rms velocities have been plotted separately for $z/D<50$ and $z/D>50$ that correspond to transition and self-similar regions respectively, according to Wygnanski and Fiedler (1969).

The normalized mean velocities have been plotted versus r/z in Figures 4.3.4 and 4.3.5 for $z/D>50$ and $z/D<50$ respectively. The least square Gaussian fit to the data was found slightly different in each case. For $z/D>50$ these data are in good agreement with Wygnanski an Fiedler's (measured values).

The normalized axial and radial turbulent velocities have been plotted in Figures 4.3.6, 4.3.7, 4.3.8 and 4.3.9 for large and small z/D's versus r/z. Most of the investigators (see Table 1.4.2) measured the axial and radial normalized turbulent velocities to be 0.26 - 0.30 and 0.17 - 0.25 respectively. The present investigation shows lower values for the reasons explained in the previous section. The normalized turbulent intensity profiles are found to be 1.8 times wider than the mean velocity profile. The values around the jet centerline

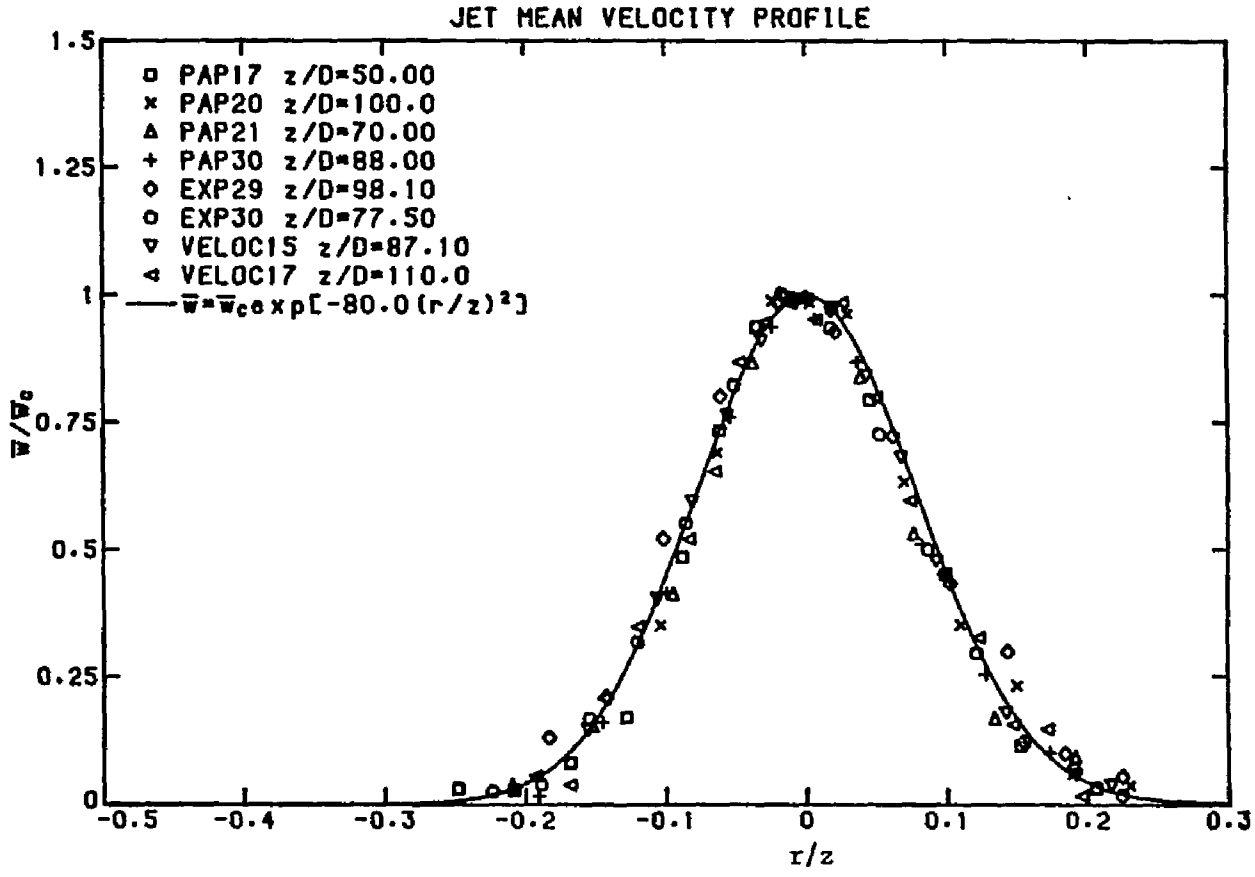


Figure 4.3.4. Non-dimensional mean axial velocity profile for a turbulent jet plotted against non-dimensional distance from jet axis, $z/D \geq 50$.

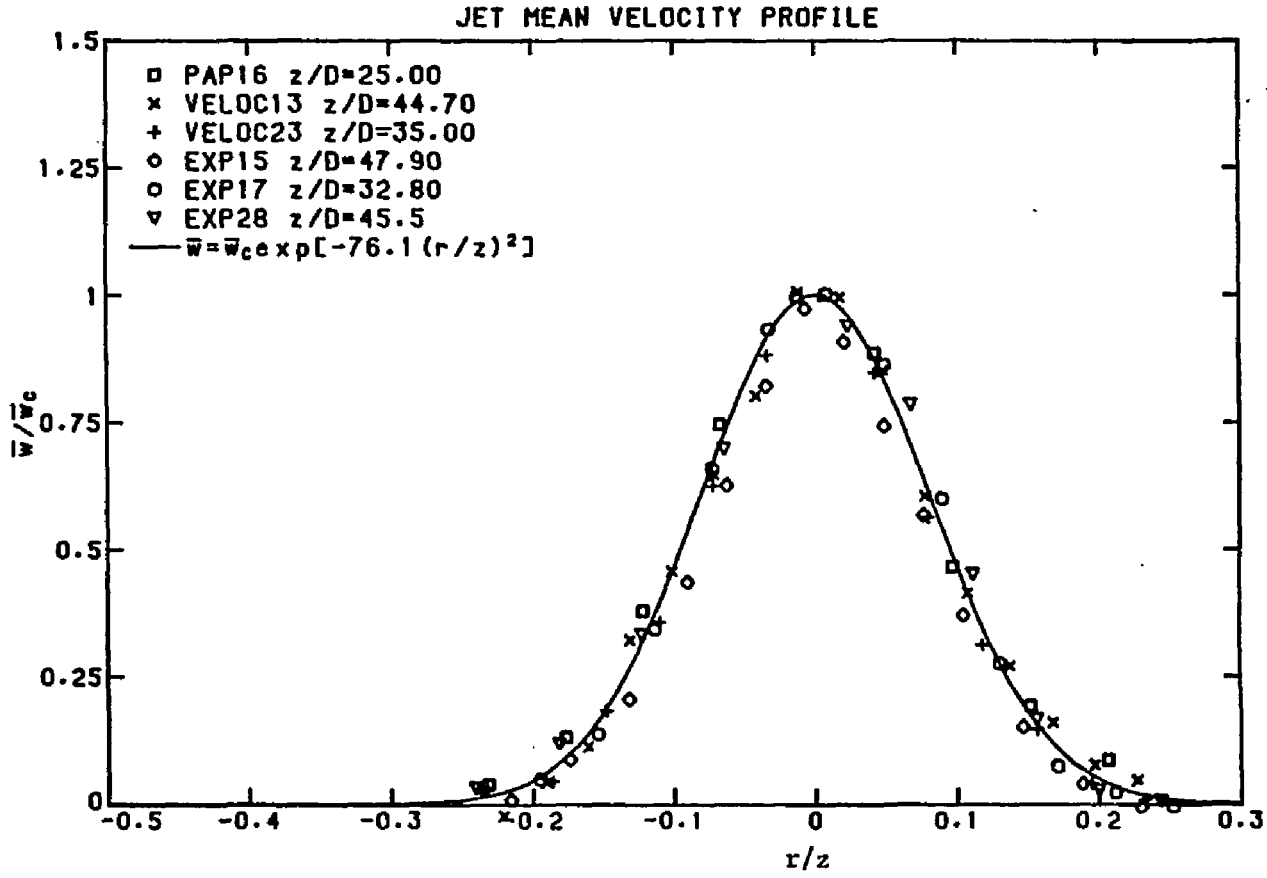


Figure 4.3.5. Non-dimensional mean axial velocity profile for a turbulent jet plotted against non-dimensional distance from jet axis, z/D < 50.

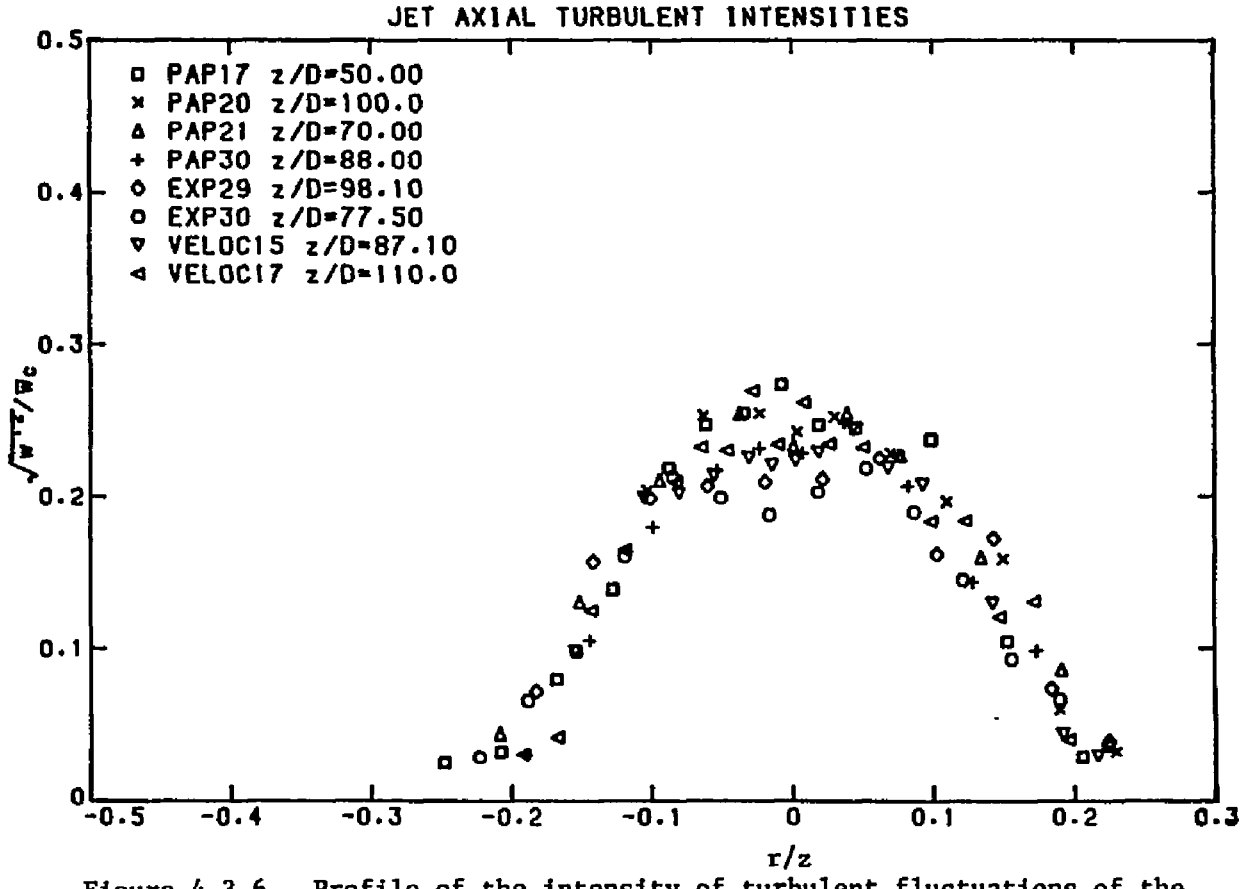


Figure 4.3.6. Profile of the intensity of turbulent fluctuations of the the axial velocity across a turbulent jet, $z/D \geq 50$.

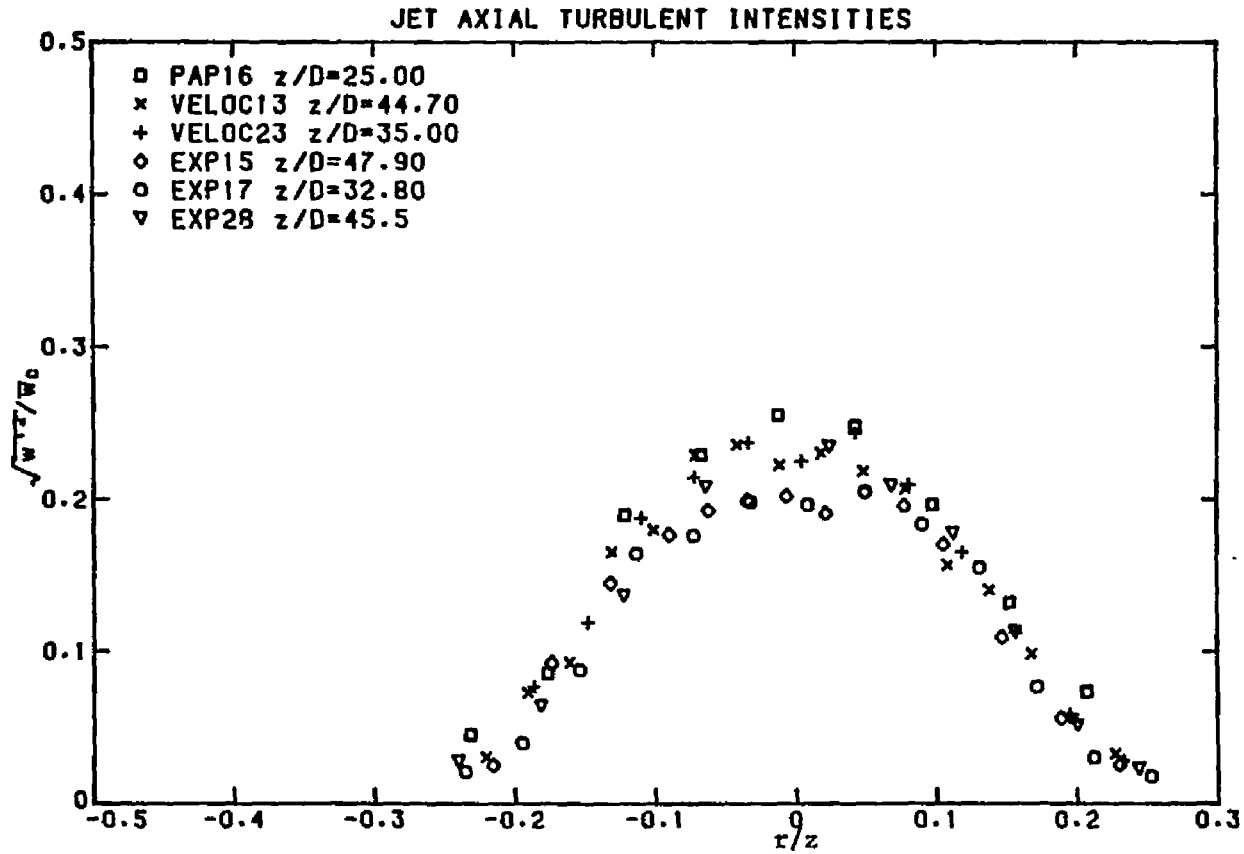


Figure 4.3.7. Profile of the intensity of turbulent fluctuations of the axial velocity across a turbulent jet, z/D < 50.

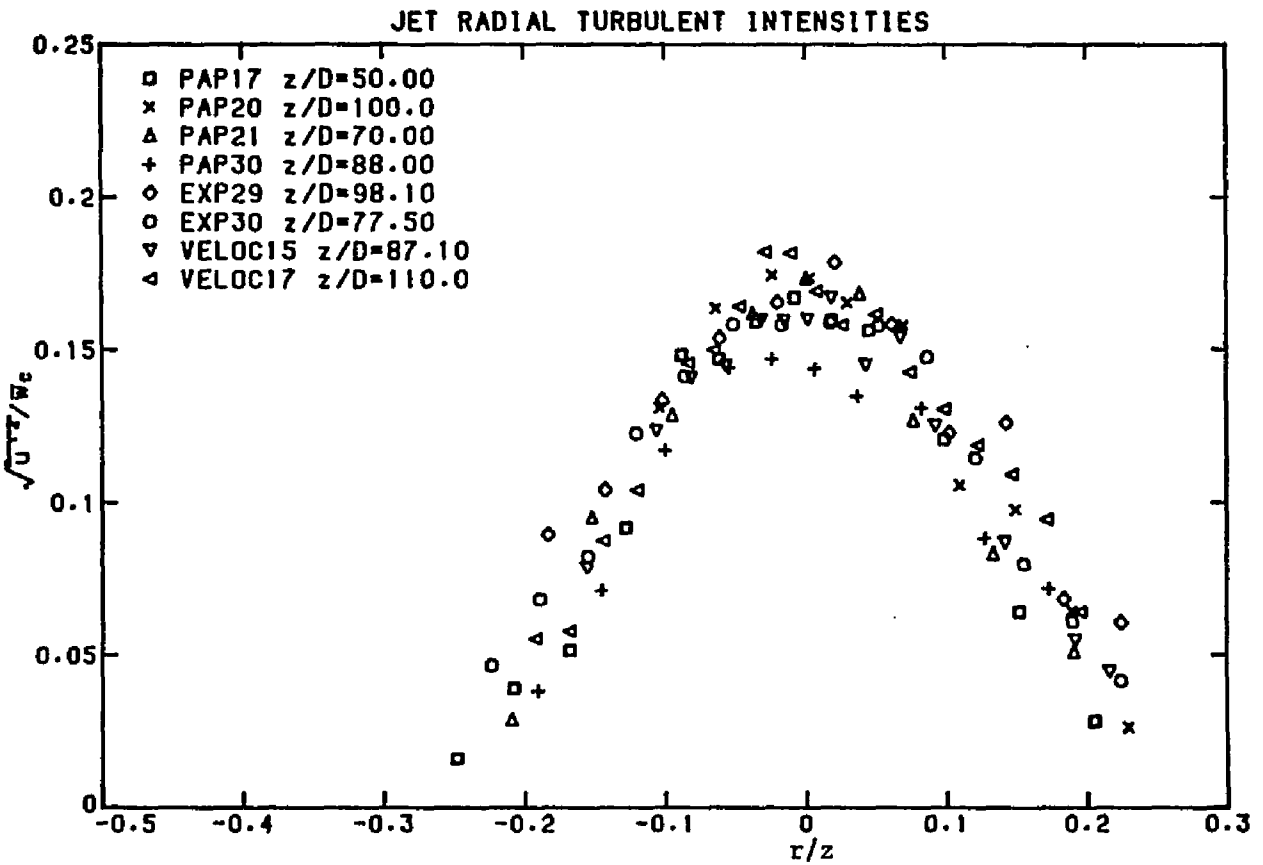


Figure 4.3.8. Profile of the intensity of turbulent fluctuations of the radial velocity across a turbulent jet, $z/D \geq 50$.

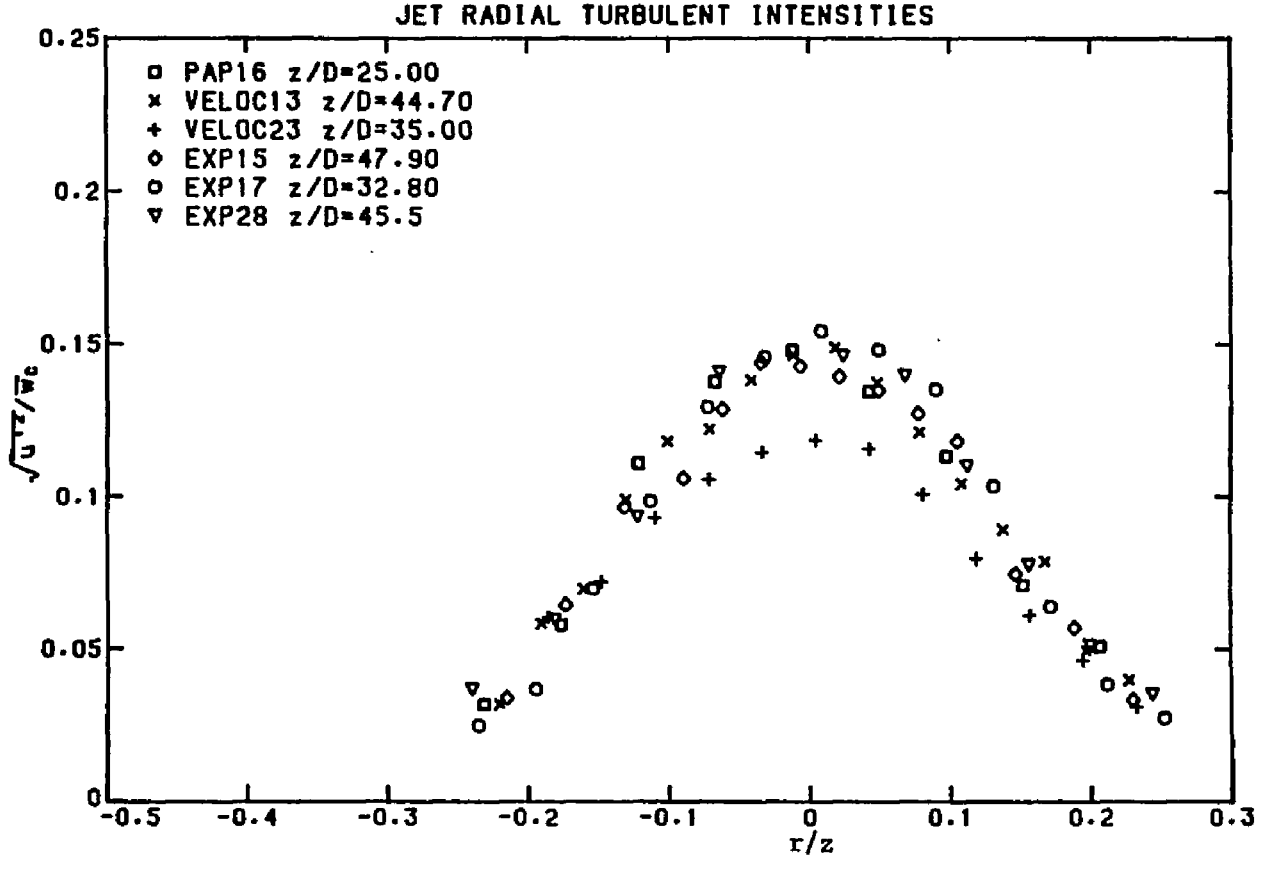


Figure 4.3.9. Profile of the intensity of turbulent fluctuations of the radial velocity across a turbulent jet, z/D < 50.

varied from 0.20 to 0.25 for the axial and from 0.13 to 0.18 for the radial turbulent velocities.

In Figures 4.3.10 and 4.3.11 the normalized turbulent shear stresses have been plotted versus r/z, for z/D>50 and z/D<50 respectively. The discrepancy of the data for z/D<50 and the existence of very low turbulent shear stresses proves that the flow is not self-similar in this region. After 50 jet diameters the maximum normalized shear stesses are found to be approximately 0.012 which is less than that reported by Wygnanski and Fiedler (1969) 0.0165, Rosler and Bankoff (1963) 0.018 for air and 0.0165 for water, Abbiss et al (1975) 0.022 and the very high value 0.035 reported by Antonia et al (1975).

Finally the maximum observed velocity normalized by $\bar{w}_c$ has been plotted versus r/z in Figure (4.3.12). This is the maximum value observed over the sampling period which did not exceed 150 seconds. The maximum value is almost twice the mean centerline velocity for small r/z. No results from other authors exist for comparison in the available literature.

4.3.4 On the mass and momentum conservation in jets

The momentum flux per unit mass (specific momentum flux) at a distance z from the jet origin is

$$m(z) = \int_0^{b(z)} (\bar{w}^2 + \overline{w'^2}) 2\pi r dr. \qquad (4.3.8)$$

Following List (1982), $\sqrt{\overline{w'^2}}$ is assumed to follow a Gaussian distribution with 1/e width 1.6 times the mean velocity width, $b_w$,

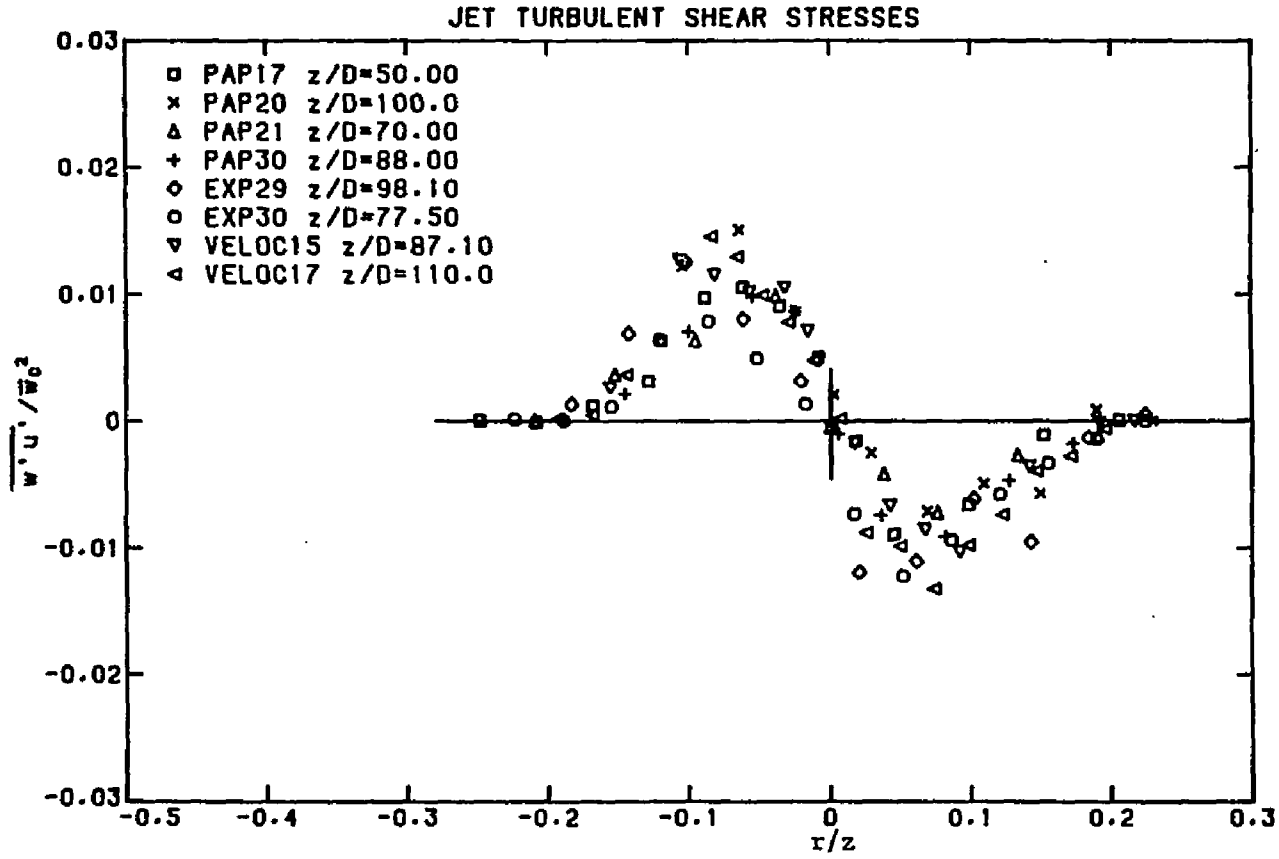


Figure 4.3.10. Shear stress distribution across a turbulent jet, $z/D \geq 50$.

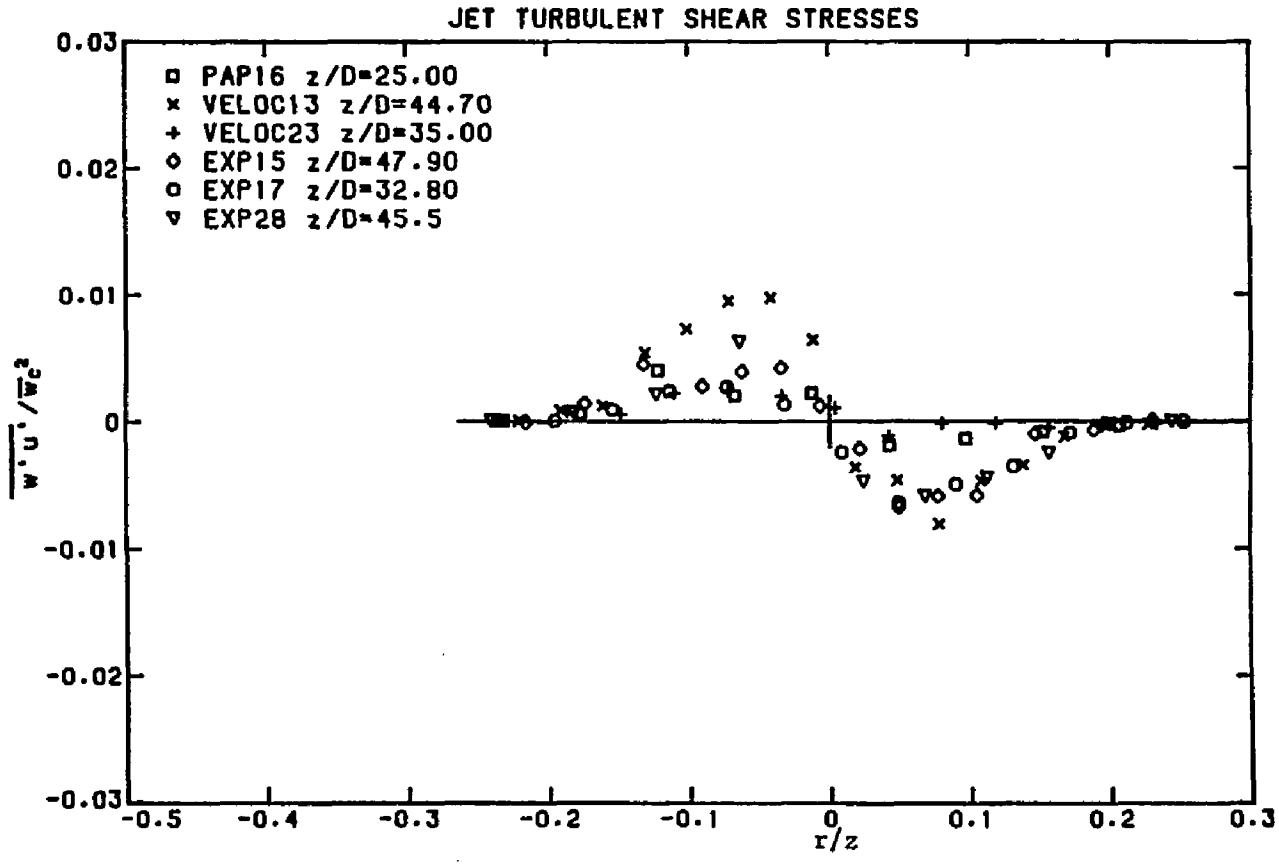


Figure 4.3.11. Shear stress distribution across a trubulent jet, z/D < 50.

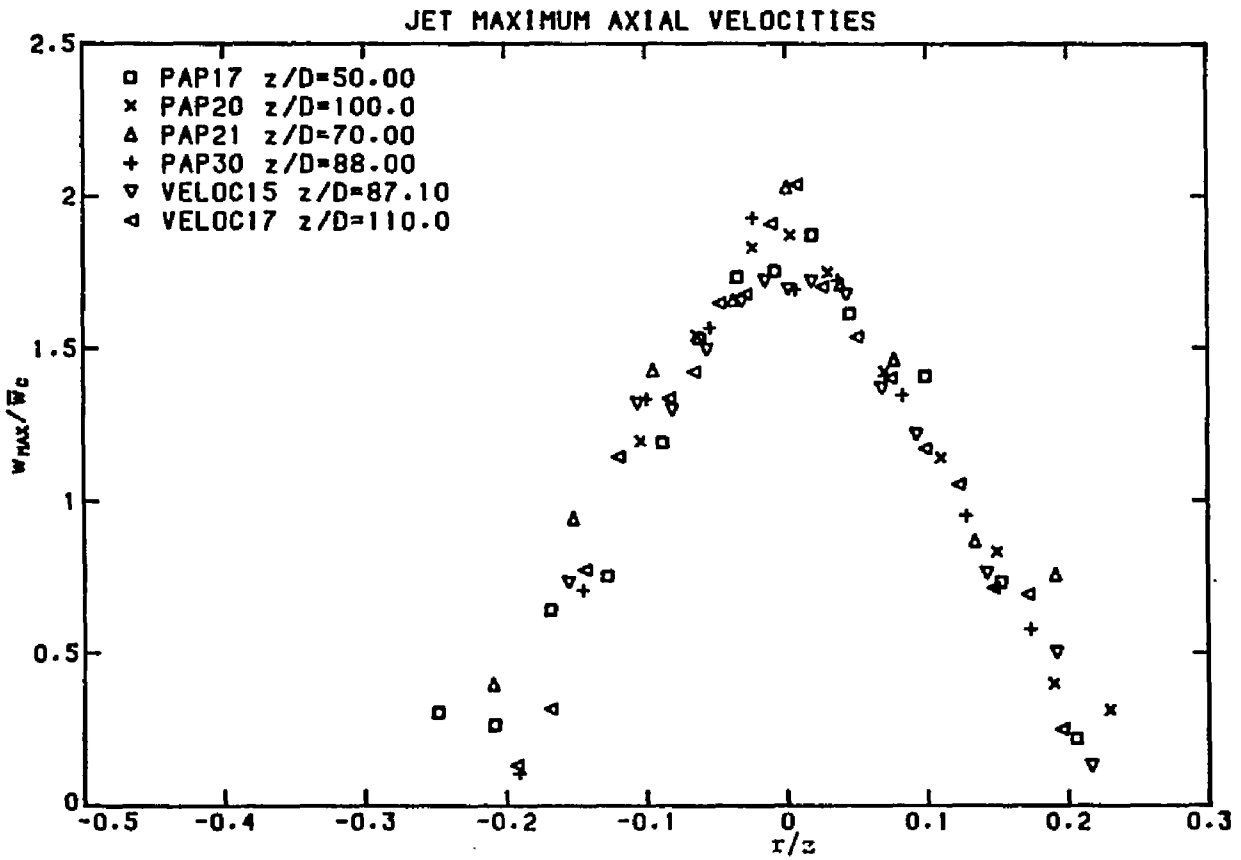


Figure 4.3.12. Profile of the maximum axial velocity across a turbulent jet.

$$\sqrt{\overline{w'^2}} = 0.230\bar{w}_c \exp[-0.386(r/z)^2 ]. \qquad (4.3.9)$$

Therefore

$$m(z) = \frac{\pi}{2} b_w^2 \bar{w}_c^2 \left(1 + \frac{(0.231)^2}{0.386}\right)$$

$$= 1.138 \frac{\pi}{2} b_w^2 \bar{w}_c^2 \qquad (4.3.10)$$

and the contribution of turbulence adds approximately 14% to the specific momentum flux of the jet that is calculated from the mean velocities.

The calculated momentum flux from the mean velocity profile normalized by the initial jet momentum flux M has been plotted versus z/D in Figure 4.3.13. The averaged value was found

| | mean | st.dev. | max | min | |
|---|---|---|---|---|---|
| m(z)/M | 0.96 | 0.131 | 1.281 | 0.72 | (4.3.11) |

and therefore

$$m(z)/M = 0.96 + 0.138 = 1.098 \qquad (4.3.12)$$

which is slightly higher than the initial jet momentum flux. According to Kotsovinos(1978), assuming that the tank behaves as a closed system (no momentum loss from the overflow), the excess momentum flux is balanced by the momentum flux of the induced circulation in the tank. Actually, negative mean velocities were measured at radial distances

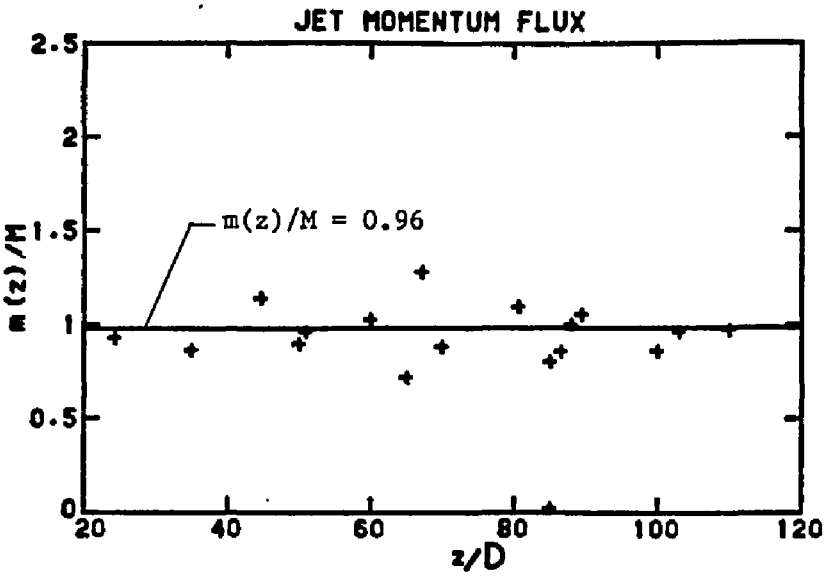


Figure 4.3.13. Experimental values for the kinematic momentum flux m(z) of a turbulent jet as a function of distance from the origin.

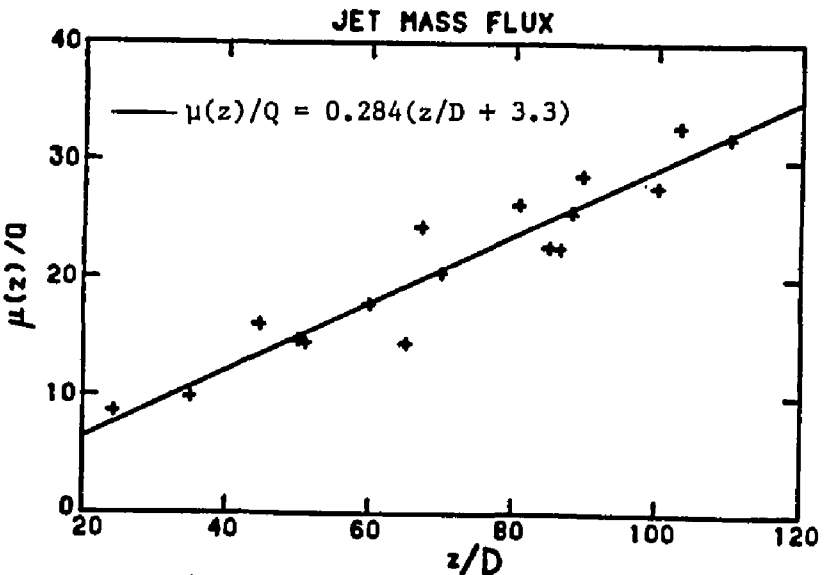


Figure 4.3.14. Experimental values for the kinematic mass flux μ(z) of a turbulent jet as a function of distance from the origin.

r/z>0.30.

The normalized advective mass flux due to the mean flow with the jet initial mass flux Q has been plotted in Figure 4.3.14 versus z/D. Following dimensional arguments made in section 1.3, the least square straight line fit to the data is

$$\frac{\mu(z)}{Q} = 0.284\left(\frac{z}{D} + 3.3\right) \qquad (4.3.13)$$

with the virtual origin located 3.3 jet diameters upstreams. Albertson et al. (1950) and Ricou and Spalding (1961) reported a value of 0.32 Fischer et al (1979) suggest an average value 0.282 which is in agreement with the predicted value above.

## 4.4 Velocity measurements in plumes

### 4.4.1 Velocities along a plume axis

A characteristic length scale $l_M$ was defined by equation (1.3.1)as

$$l_M = \frac{M^{3/4}}{B^{1/2}}$$

for jets driven initially by both, buoyancy and momentum. Following dimensional analysis (Table 1.3.1) and equations (4.3.2) and (4.3.3) the dimensionless groups for the mean and turbulent velocities at the centerline

$$\frac{\sqrt{M}}{\overline{w}_c z}\ ,\quad \frac{\sqrt{M}}{\sqrt{\overline{w_c'^2}}\ z}\ ,\quad \frac{\sqrt{M}}{\sqrt{\overline{w_c'^2}}\ z} \tag{4.4.1}$$

have been plotted in Figure 4.4.1 versus the dimensionless distance from the jet origin $z/l_M$ . For a jet,

$$\frac{\sqrt{M}}{\overline{w}_c z} = a_1' = \text{constant} \tag{4.4.2}$$

following Table 1.3.1. From equations (1.3.2a) and (4.3.1) it can be seen that

$$C_{1w} = (2/\sqrt{\pi})a_1' \tag{4.4.3}$$

and therefore for $C_{1w}$=0.149

$$a_1' = 0.132 \tag{4.4.3a}$$

In the same manner, since the turbulent intensities were found to be constant along the jet axis, equations (4.3.2,), (4.3.3) and (4.4.1) give

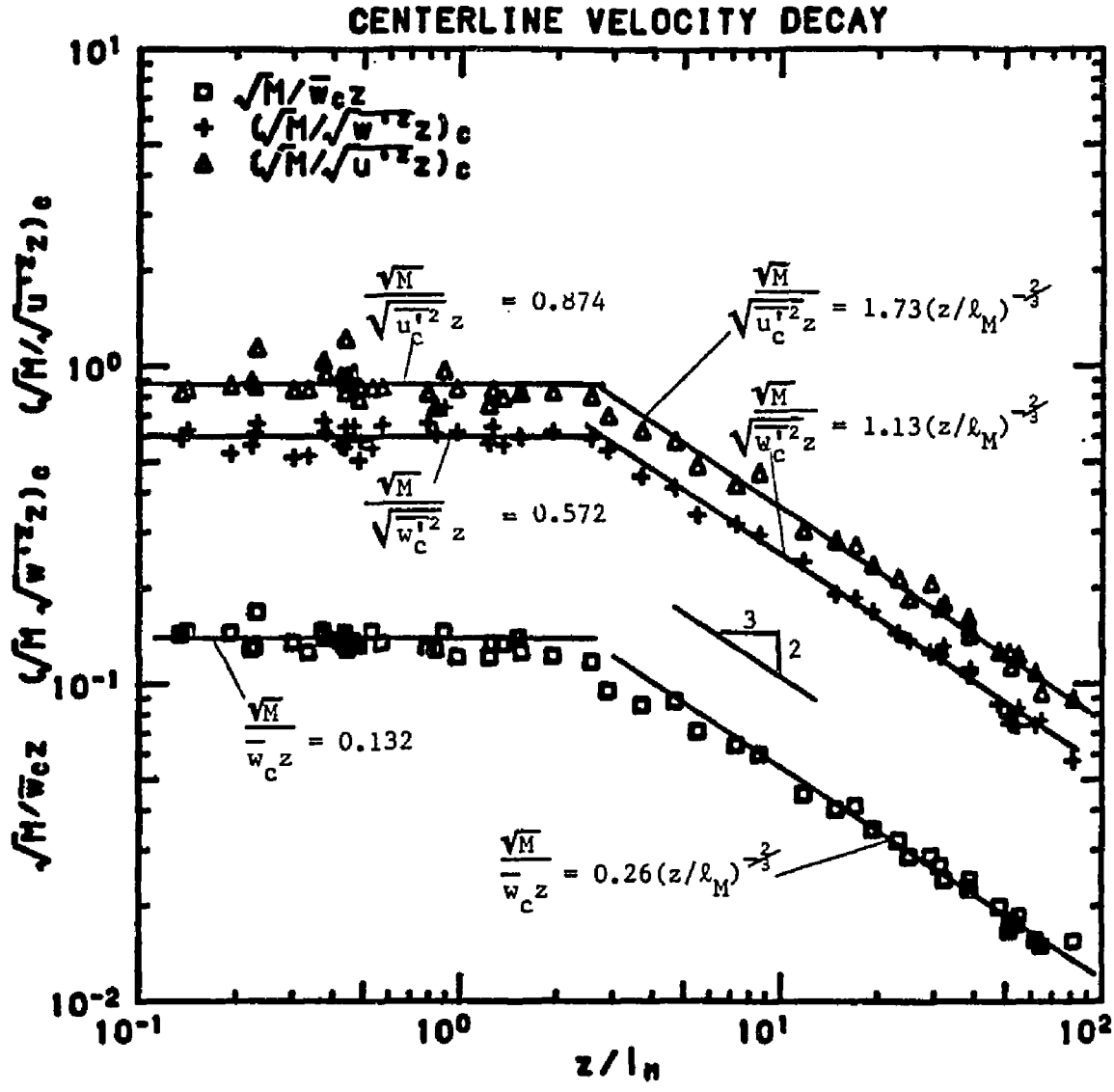


Figure 4.4.1. Non-dimensional velocity distribution along the axis of a buoyant jet plotted against the non-dimensional distance from jet origin. Decay of the mean velocity, axial and radial turbulent intensities.

$$\frac{\sqrt{M}}{\sqrt{w_c'^2}\ z} = 0.572 \ , \quad \frac{\sqrt{M}}{\sqrt{u_c'^2}\ z} = 0.874 \tag{4.4.4}$$

at the axis of a jet, that is also shown in Figure 4.4.1 for $z/l_M < 1$.

For large values of $z/l_M$ , $\sqrt{M}/\bar{w}_c\ z$ is proportional to $(z/l_M)^{-2/3}$ (plume case, equation (1.3.7b)). From Figure 4.4.1 it is obvious that for $z/l_M > 5$

$$\frac{\bar{M}}{\bar{w}_c z} = b_1' \left(\frac{z}{l_M}\right)^{-2/3} \tag{4.4.5}$$

where $b_1'$ was calculated to be 0.26. From this point on it should be noted that an initially momentum driven flow with a small initial buoyancy flux B, will become a plume after about 5 characteristic lengths $l_M$ . It can also be seen from Figure 4.4.1 that the turbulent intensities along the plume axis decay as $(z/l_M)^{-2/3}$. From Figures 4.4.3 and 4.4.4 the turbulent intensities at the plume centerline were found to be

$$\sqrt{w_c'^2} = 0.23\bar{w}_c \quad \text{and} \quad \sqrt{u_c'^2} = 0.15\bar{w}_c \ . \tag{4.4.6}$$

Substitute $\bar{w}_c$ from (4.4.6) into (4.4.5) to obtain

$$\sqrt{M}/(\sqrt{w_c'^2}\ z) = 1.13(z/l_M)^{-2/3} \tag{4.4.7}$$

and

$$\sqrt{M}/(\sqrt{u_c'^2}\ z) = 1.73(z/l_M)^{-2/3} \tag{4.4.8}$$

The mean velocity at the plume centerline can be also written as

$$\bar{w}_c = b_1 B^{1/3} z^{-1/3}, \quad b_1 = 3.85 \tag{4.4.9}$$

from equations (1.3.7a) and (1.3.7b). This value is in agreement with the value $b_1 = 3.4$ reported by George et al (1977). Rouse et al (1952) reported $b_1 = 4.7$ that corresponds to velocities that can be observed in the transition region $1 < z/l_M < 5$.

4.4.2 Profiles of mean velocity, turbulent intensities and $\overline{w'u'}$ correlation in plumes

The mean axial velocity normalized by $\bar{w}_c$ has been plotted in Figure 4.4.2 versus r/z. There is substantial scatter to the data since $z/l_M$ varies from 8 (not fully developed plume) to about 80 where the plume is fully developed. Different size jet diameters and initial density differences were used so that no virtual origin for the plume case could be obtained. A least square Gaussian fit to the data is

$$\bar{w} = \bar{w}_c \exp[-80(r/z)^2] \tag{4.4.10}$$

the same as the one obtained for $z/D > 50$ for the case of a jet.

In Figures 4.4.3, 4.4.4 and 4.4.5 the normalized root mean square turbulent axial and radial velocities and shear stresses have been plotted versus r/z. The normalized profiles of the rms axial and radial velocities are similar to the ones obtained in a jet case shown in Figures 4.3.6 and 4.3.8. The values measured at the plume centerline are found to be 0.23 and 0.15 for the axial and radial turbulent velocities, which are smaller than 0.28 reported by George et al (1977) and Nakagome and Hirata (1976).

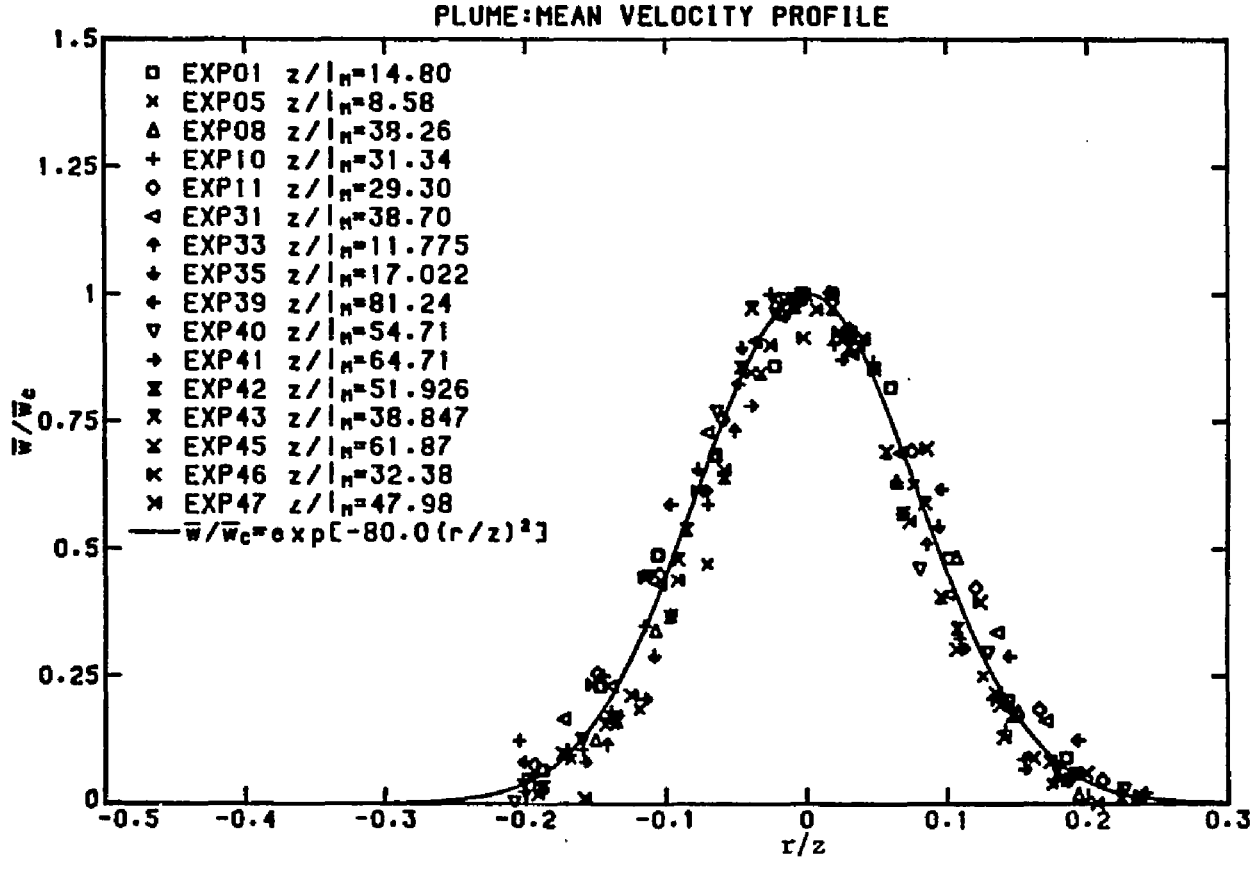


Figure 4.4.2. Non-dimensional mean axial velocity profile across a turbulent plume.

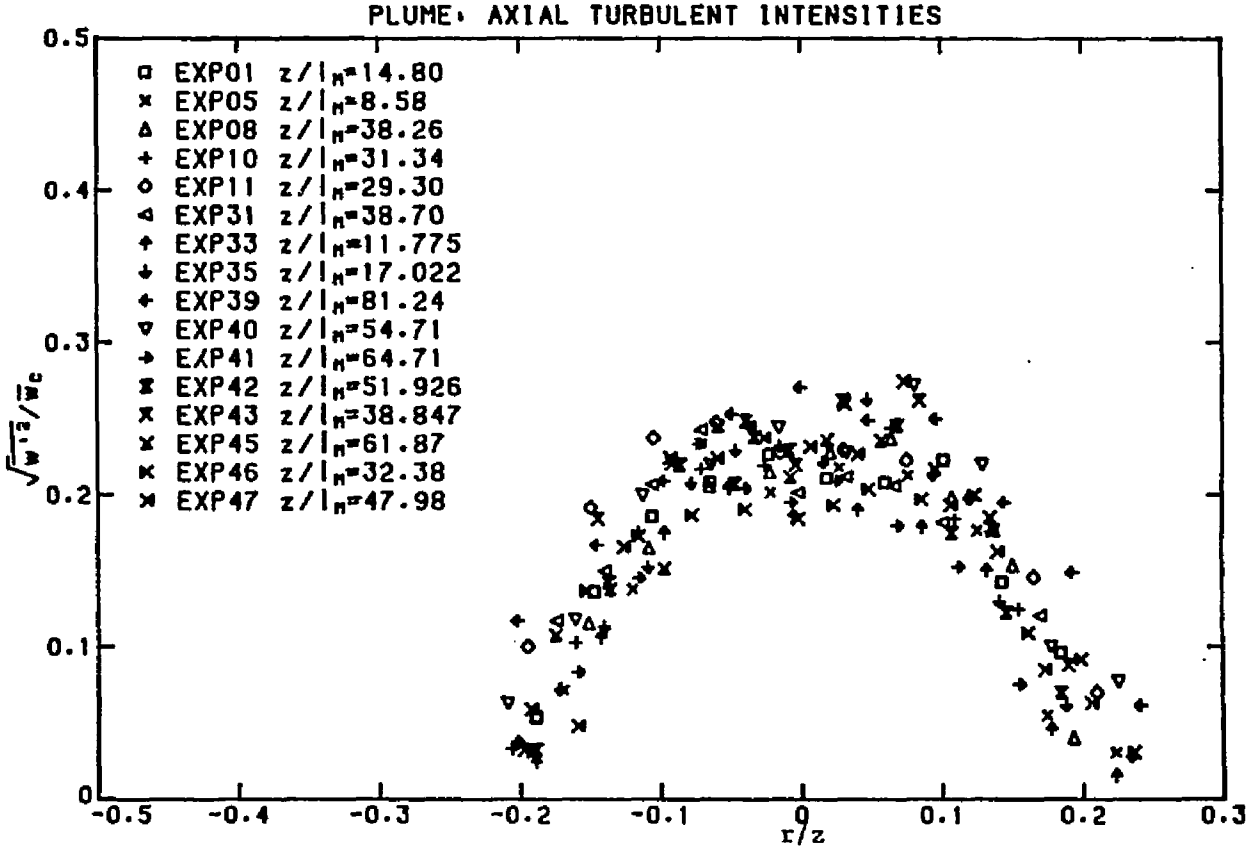


Figure 4.4.3. Profile of the intensity of turbulent fluctuations of the axial velocity across a turbulent plume.

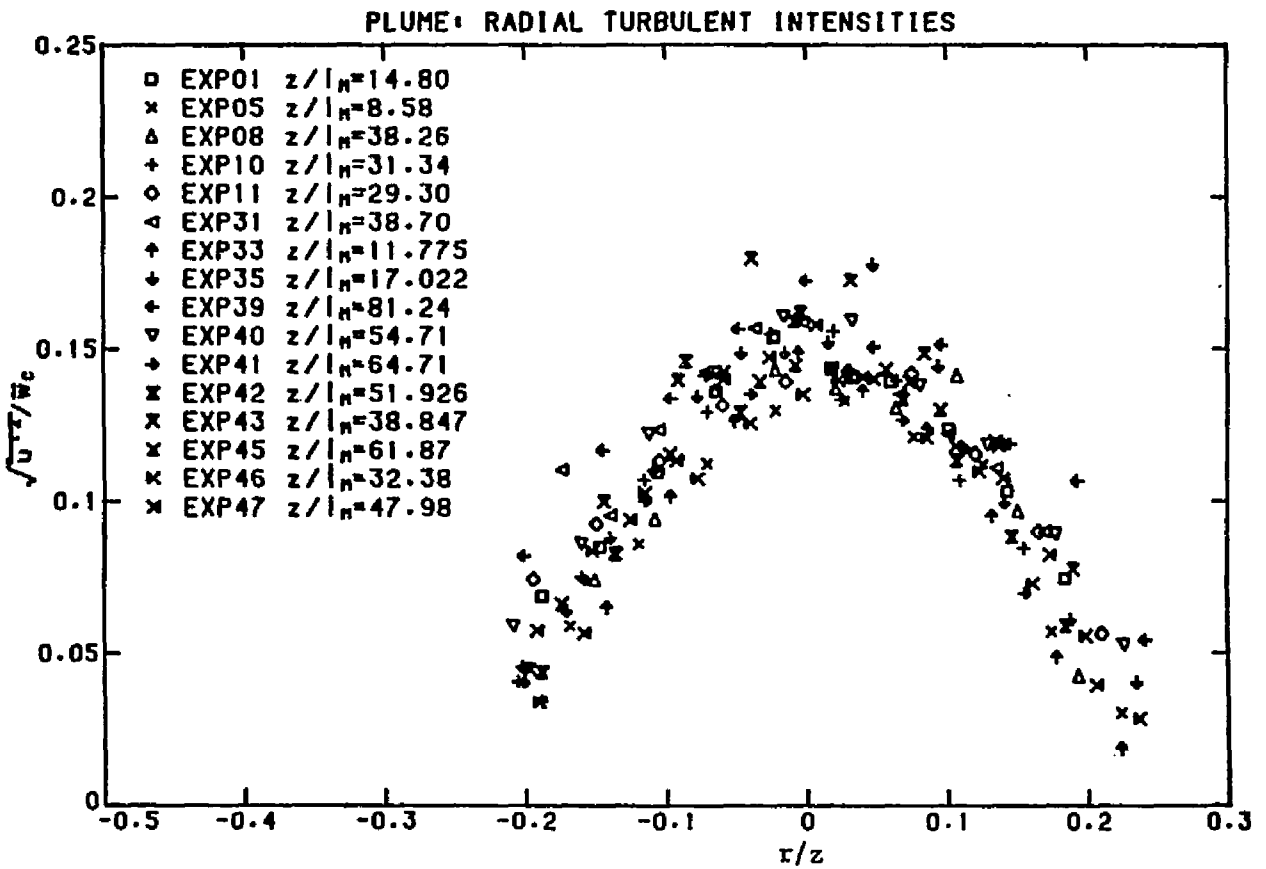


Figure 4.4.4. Profile of the intensity of turbulent fluctuations of the radial velocity across a turbulent plume.

The normalized turbulent shear stresses $\overline{w'u'}/\overline{w_c}^2$ plotted versus r/z in Figure 4.4.5 have maximum values varying from 0.008 to 0.017 with an average value of 0.13. They compare well with those obtained for jets (Figure 4.3.10).

4.4.3 Width of a plume

The 1/e mean velocity plume width $b_w$ normalized by $l_M$ has been plotted versus $z/l_M$ in Figure 4.4.6 for all experiments. The region $z/l_M < 1$ corresponds to momentum driven jets and $z/l_M > 1$ corresponds to buoyancy driven plumes. The reason that the plume width was normalized by $l_M$ rather than by the plume diameter D is that the initial diameter is not the relevant length scale for plumes. A least square fit to the data for all $z/l_M$ implies

$$b_w/l_M = 0.108(z/l_M)^{0.995} \qquad (4.4.11)$$

where the exponent 0.995 is very close to the value of 1.0 predicted by dimensional analysis. Nonlinearity is involved due to the different spreading angles for jets and plumes. For the plume case ($z/l_M > 5$) a least square fit to the data implies

$$b_w/l_M = 0.105(z/l_M)^{1.002} \sim 0.105(z/l_M) \qquad (4.4.12)$$

and it becomes obvious that a jet will grow with a smaller angle for $z/l_M > 5$.

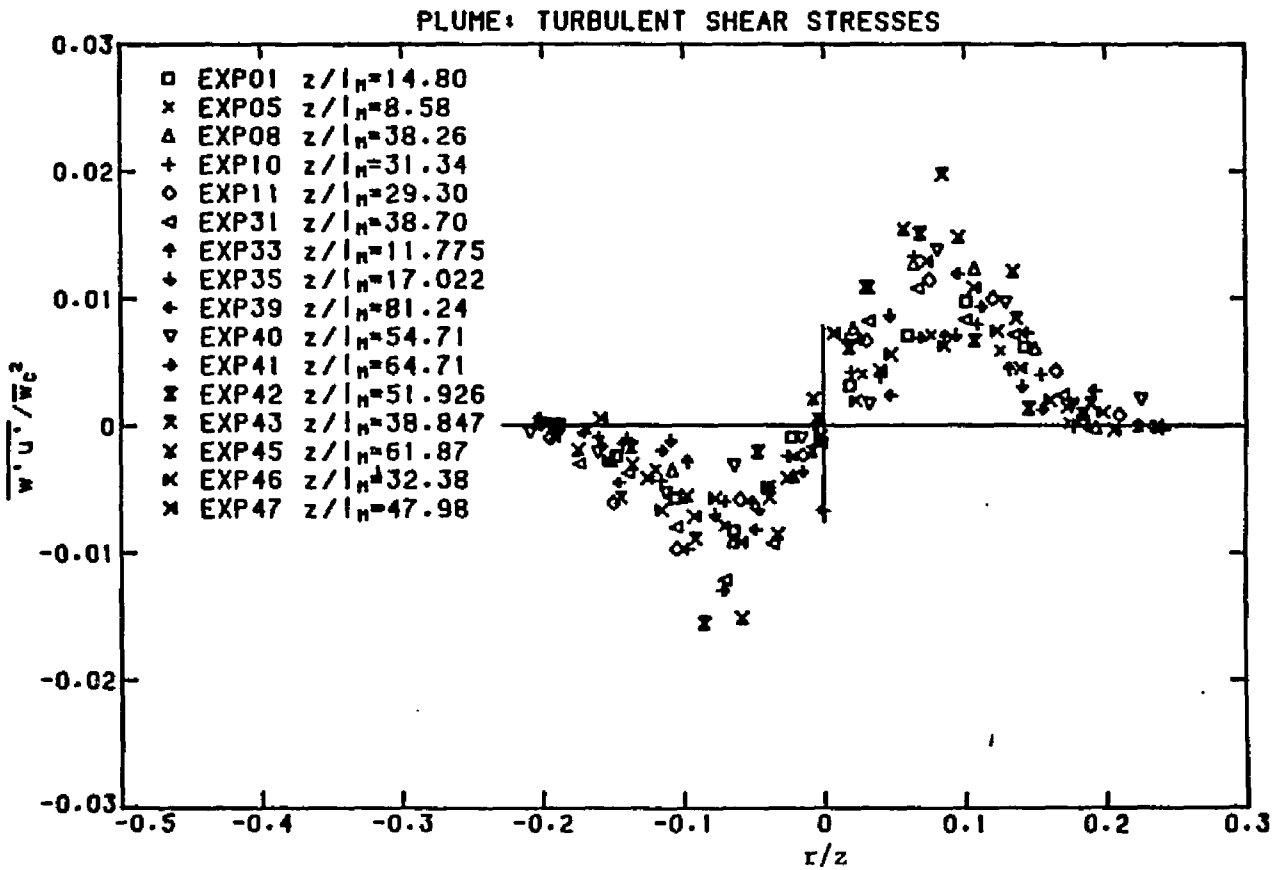


Figure 4.4.5. Shear stress distribution across a turbulent plume.

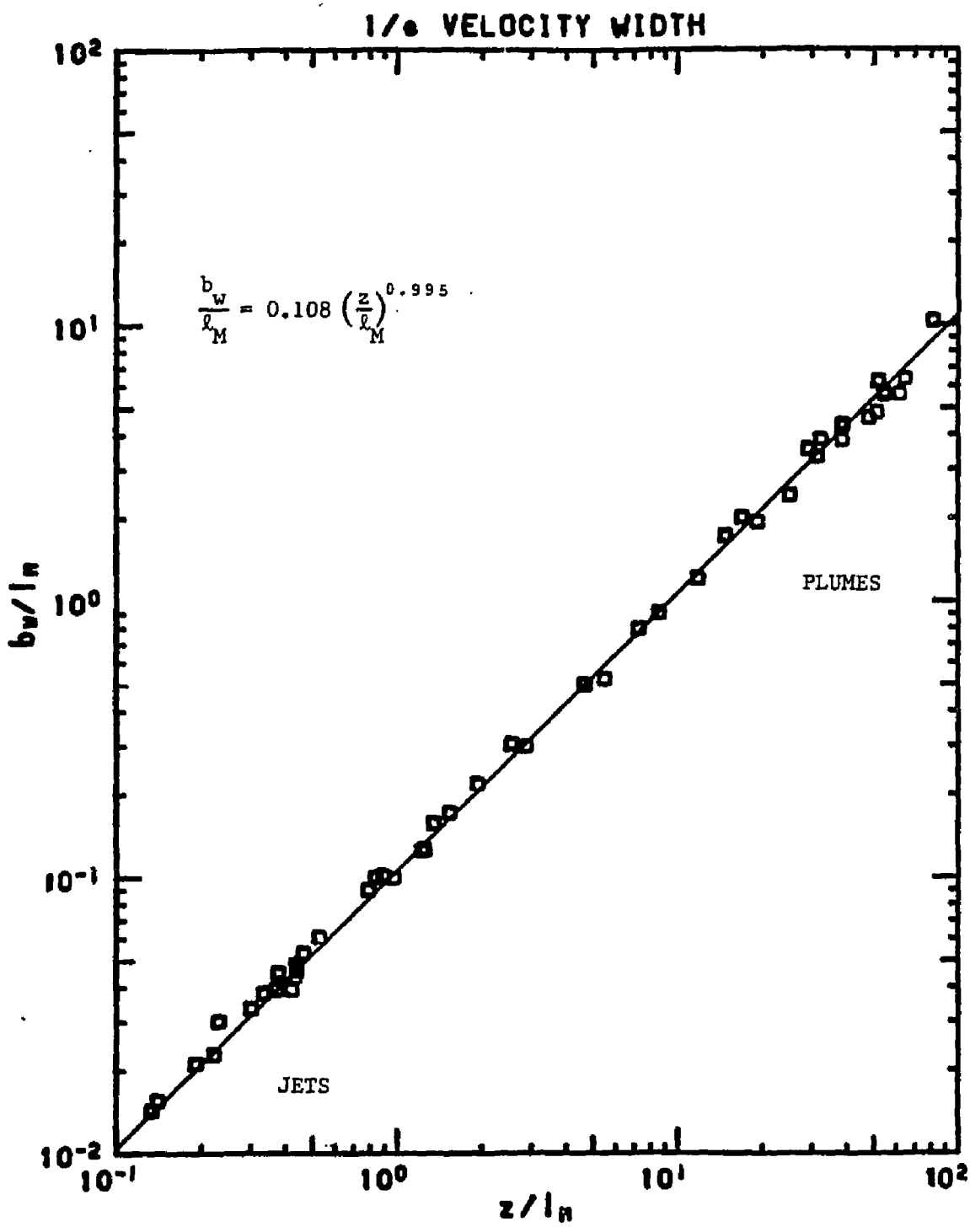


Figure 4.4.6. Non-dimensional velocity 1/e-width of a turbulent buoyant jet plotted against $z/\ell_M$.

## 4.5 Concentration measurements in jets

### 4.5.1 Centerline concentration decay - width of a jet

The reciprocal of the mean concentration on the jet axis, normalized by the initial jet concentration has been plotted versus the dimensionless distance from the jet origin z/D in Figure 4.5.1. A least square linear fit to the data is found to be

$$\frac{C_o}{\bar{c}_c} = 0.157\left(\frac{z}{D} + 4.35\right) \qquad (4.5.1)$$

with a virtual origin at 4.35 diameters upstream. The normalized root mean square turbulent concentration at the jet axis has been plotted versus z/D in the same figure. It shows a constant average value

$$\left(\sqrt{\overline{c'^2}}\right)_c = 0.216\ \bar{c}_c \qquad (4.5.2)$$

for z/D varying from 33 to 98. The mean concentration along the axis of the jet is quite higher than the values reported by other authors shown in Table 1.4.2. More specifically Becker et al.(1967), Forstall and Gaylord (1955), Grandmaison et al.(1977), Kiser (1963) and Birch et al. (1978) report the values of the constant of proportionality $C_{1c}$ in the region between 0.185 and 0.25 for the equation

$$\frac{C_o}{\bar{c}_c} = C_{1c}\left(\frac{z}{D} + C_{2c}\right).$$

The turbulent intensities predicted by the authors mentioned above are

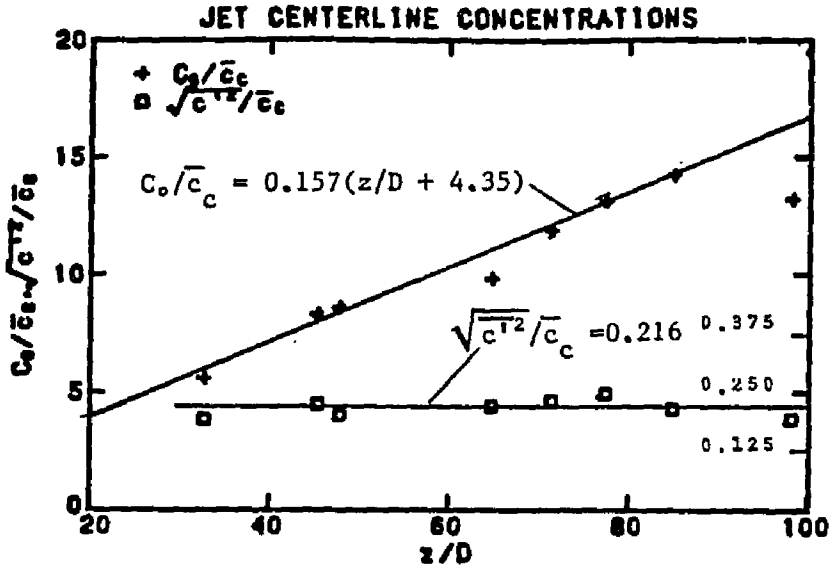


Figure 4.5.1. Non-dimensional concentration distribution along the jet axis plotted against non-dimensional distance from jet origin. Decay of mean and rms concentrations.

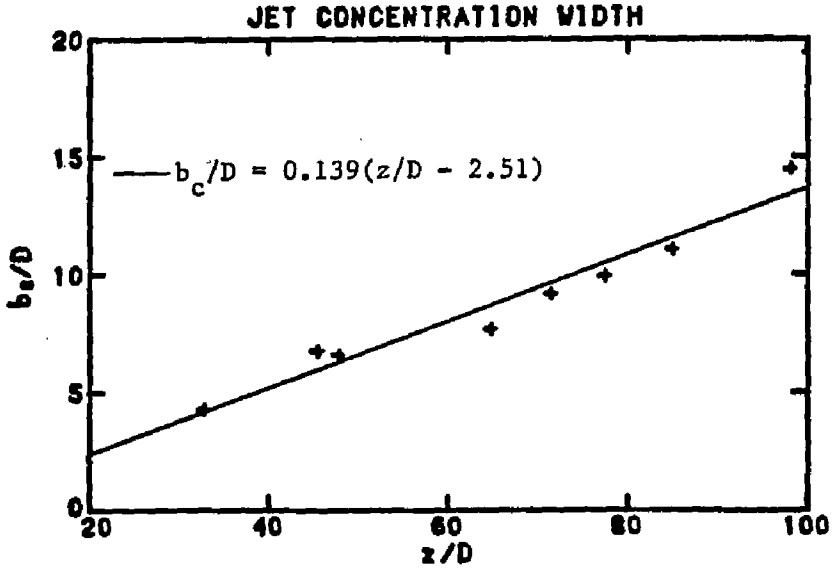


Figure 4.5.2. Non-dimensional concentration 1/e-width of a turbulent jet plotted against non-dimensional distance from jet orifice.

in agreement with the ones measured in the present investigation. The concentration width $b_c$ of the jet normalized by the jet diameter D has been plotted versus z/D in Figure 4.5.2. A least square fit to the data leads to

$$\frac{b_c}{D} = 0.139(\frac{z}{D} - 2.51) \qquad (4.5.3)$$

which predicts a virtual origin at 2.51 jet diameters downstream. The value of the constant of proportionality varies for the different authors mentioned above from 0.101 up to 0.140. Fischer et al (1979) suggest a mean value 0.127 for a jet.

4.5.2 Jet mean and turbulent concentration profiles

The mean and root mean square turbulent concentrations normalized by the mean centerline concentration have been plotted versus r/z in Figures 4.5.3 and 4.5.4 for various dimensionless distances z/D from the jet origin. A least square Gaussian fit to the mean concentration profile gives

$$\bar{c}/\bar{c}_c = \exp[-55(r/z)^2] \qquad (4.5.4)$$

which implies a much wider than the mean velocity profile. The root mean square concentration fluctuation profile has a peak value 0.25 at about r/z=0.08 and a value of 0.22 at the jet axis, results that are in agreement with those predicted by the various authors mentioned previously (see also Table 1.4.2).

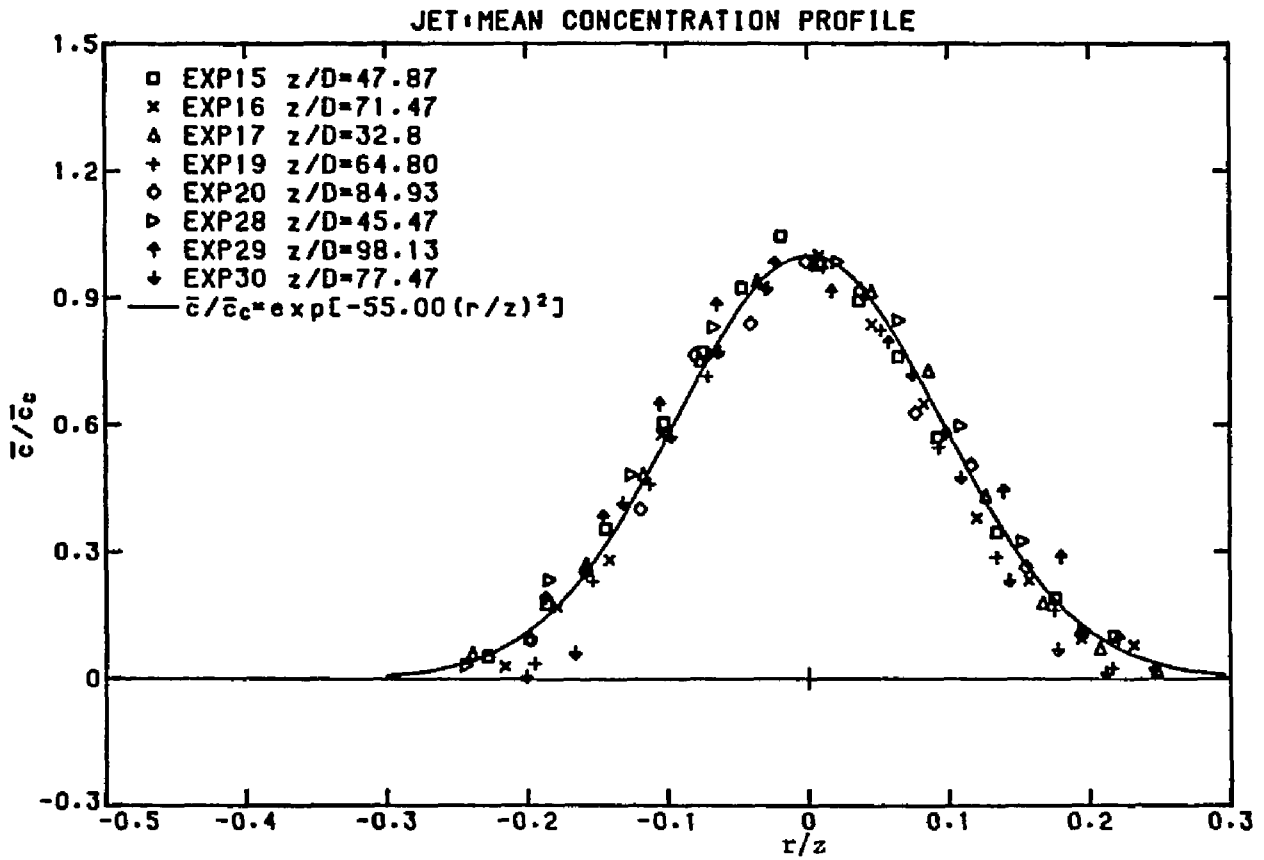


Figure 4.5.3. Non-dimensional mean concentration profile for a turbulent jet plotted against non-dimensional distance from jet axis.

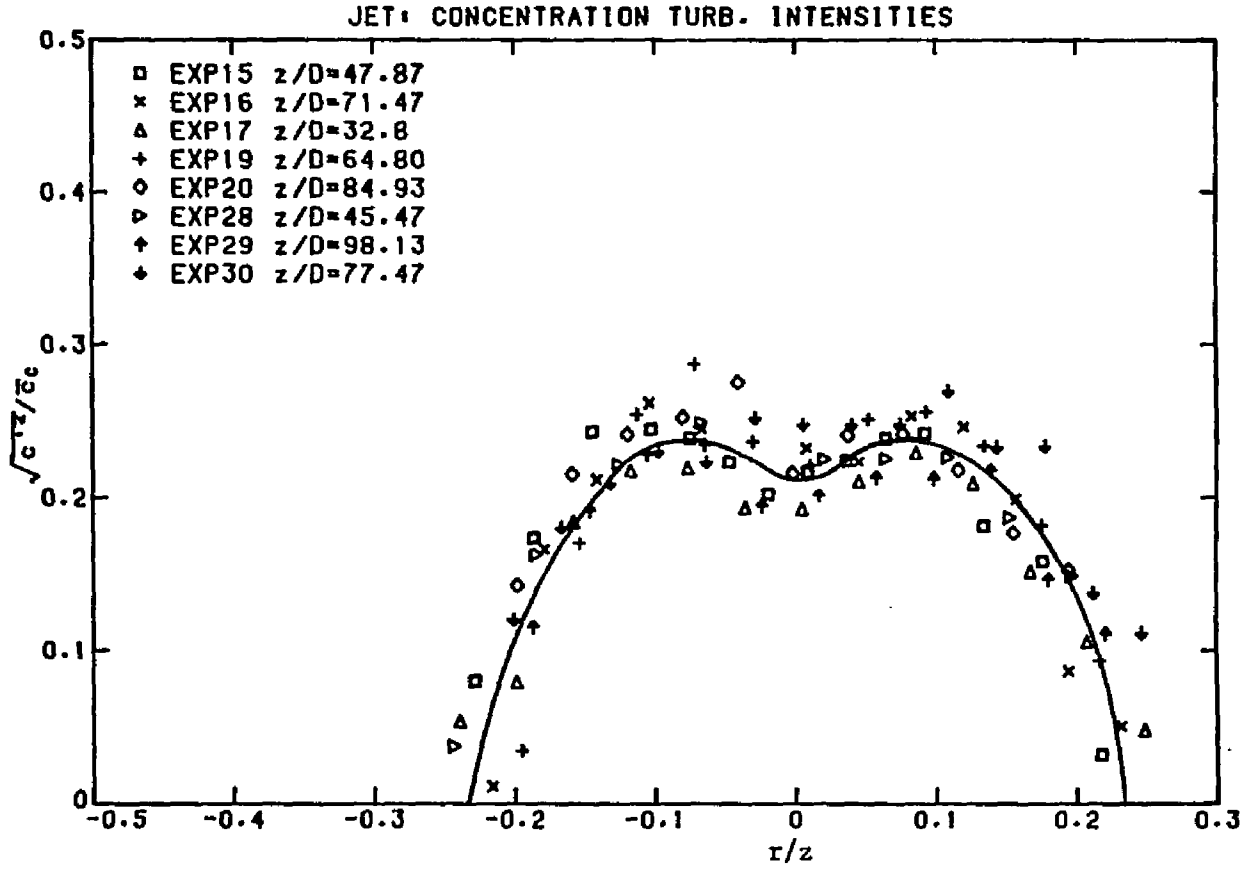


Figure 4.5.4. Profile of the intensity of turbulent fluctuations of the concentration across a turbulent jet.

## 4.6 Concentration measurements in plumes

### 4.6.1 Mean and turbulent concentrations at the plume axis

The normalized mean centerline concentration

$$\frac{SQ}{z\sqrt{M}} \quad \text{with} \quad S = \frac{C_o}{\bar{c}_c} \tag{4.6.1}$$

has been plotted against $z/l_M$ in Figure 4.6.1. Following dimensional arguments, the constants a' and b' from equations (1.3.6b) and (1.3.10b) in Table 1.3.1 are determined to be 0.07 and 0.147 for $z/l_M > 5$ (plumes) and $z/l_M < 1$ (jets). The mean centerline concentration along the jet axis was discussed previously in section 4.5.1. For the mean concentrations at a plume centerline Rouse *et al.* (1952) reported $b_4' = 0.091$, Zimin and Frik (1977) measured $b_4' = 0.142$ and Papanicolaou and List (1983) $b_4' = 0.090$. Fischer *et al.* (1979) suggest $b_4' = 0.11$, a value reported by George *et al.* (1977). The mean concentrations measured along the plume axis in the present work are higher than those reported by all other authors. For the root mean square turbulent concentration fluctuations at the plume axis as normalized

$$\frac{S'Q}{z\sqrt{M}} \quad \text{with} \quad S' = \frac{C_o}{\sqrt{\overline{c'^2}_c}} \tag{4.6.2}$$

have also been plotted in Figure 4.6.1. These data indicate

$$S'Q/z\sqrt{M} = 0.681 \quad \text{for} \quad z/l_M < 1 \tag{4.6.2a}$$

and

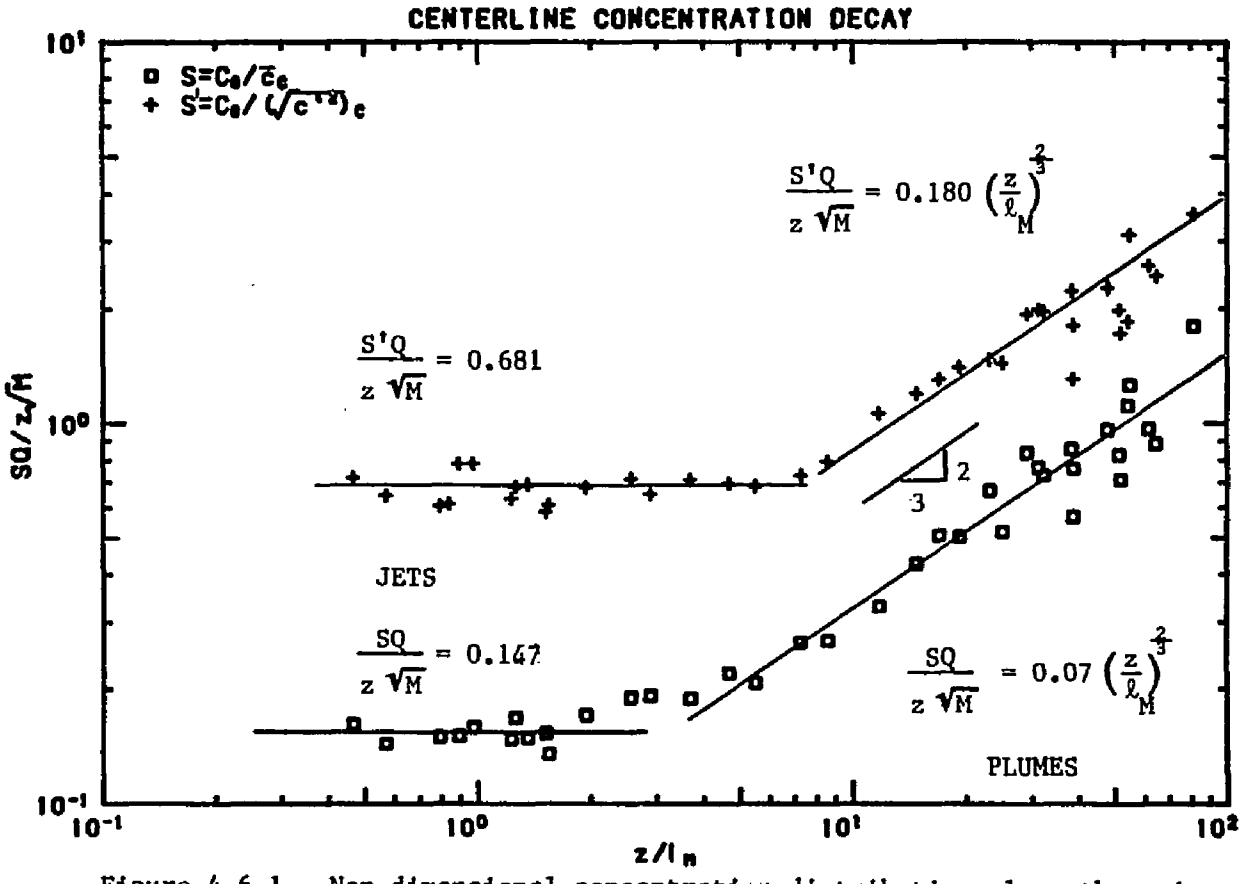


Figure 4.6.1. Non-dimensional concentration distribution along the axis of a buoyant jet plotted against the non-dimensional distance from jet origin. Decay of the mean concentration and turbulence intensities.

$$S'Q/z\sqrt{M}=0.180(z/l_M)^{2/3} \quad \text{for} \quad z/l_M > 5 \qquad (4.6.3)$$

in the plume regime.

4.6.2 Mean and rms concentration profiles

The mean concentration and root mean square turbulent fluctuation profiles normalized by the mean concentration at the plume centerline, have been plotted in Figures 4.6.2 and 4.6.3 respectively. A least square Gaussian fit to the mean concentrations indicates

$$\bar{c} = \bar{c}_c \exp[-80(r/z)^2] \qquad (4.6.4)$$

and the value of the constant in the exponent (80) is in agreement with values reported by Zimin and Frik (1977) and Papanicolaou and List (1983). George et al. (1977), Nakagome and Hirata (1976) and Rouse et al. (1952) reported lower value indicating wider concentration profiles. The rms concentration fluctuations vary from 0.35 to 0.45 with a mean value 0.40. The values also reported by Nakagome and Hirata (1976), George et al. (1977) and Papanicolaou and List (1983) are found to be close to 0.40.The peaks observed in the turbulent concentration profiles for jets appear to coalesce in plumes, result found also by Kotsovinos (1975) in plane plumes.

4.6.3 Plume width

The normalized 1/e concentration width $b_c$ by $l_M$ has been plotted versus $z/l_M$ in Figure 4.6.4 for both, jets and plumes. A least square fit to all data points leads to the relation

$$b_c/l_M = 0.129(z/l_M)^{0.994} \qquad (4.6.5)$$

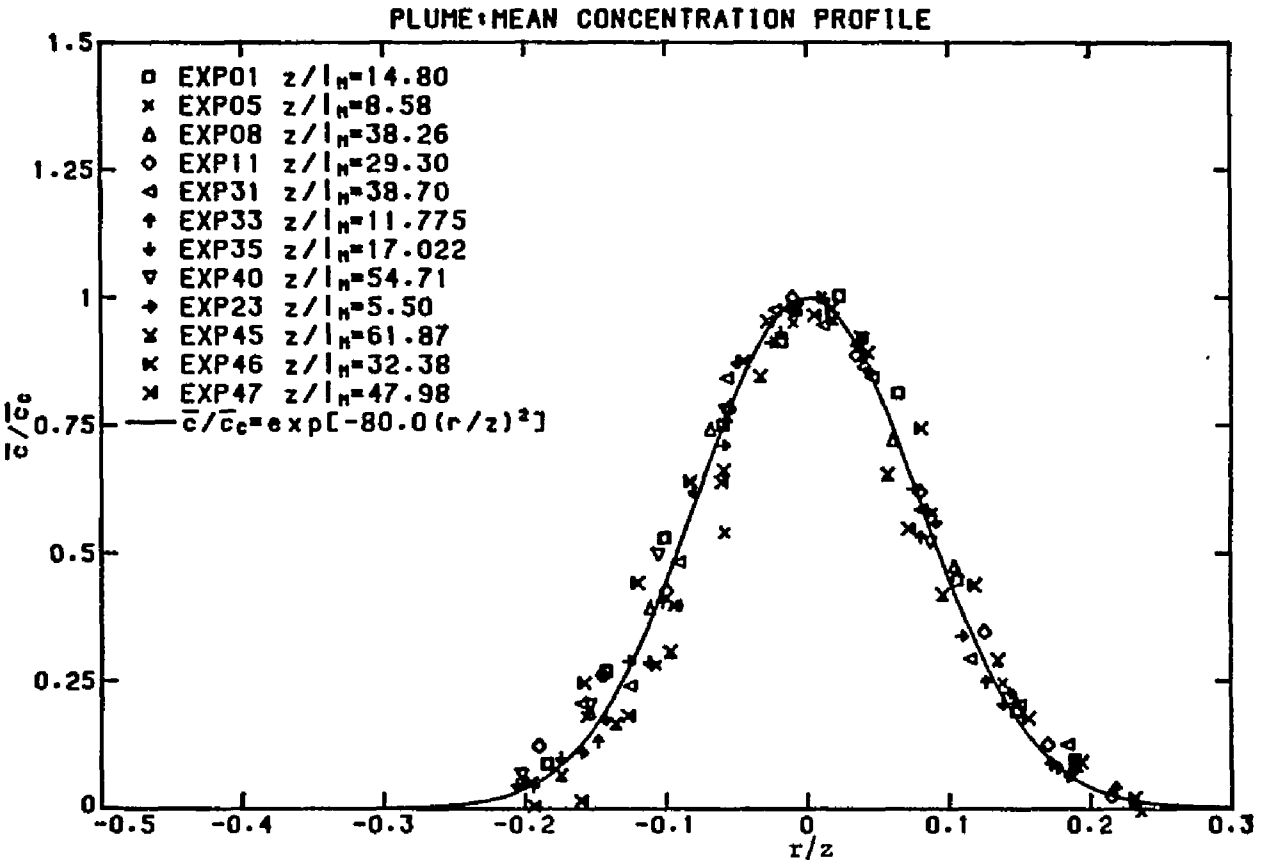


Figure 4.6.2. Non-dimensional mean concentration profile across a turbulent plume.

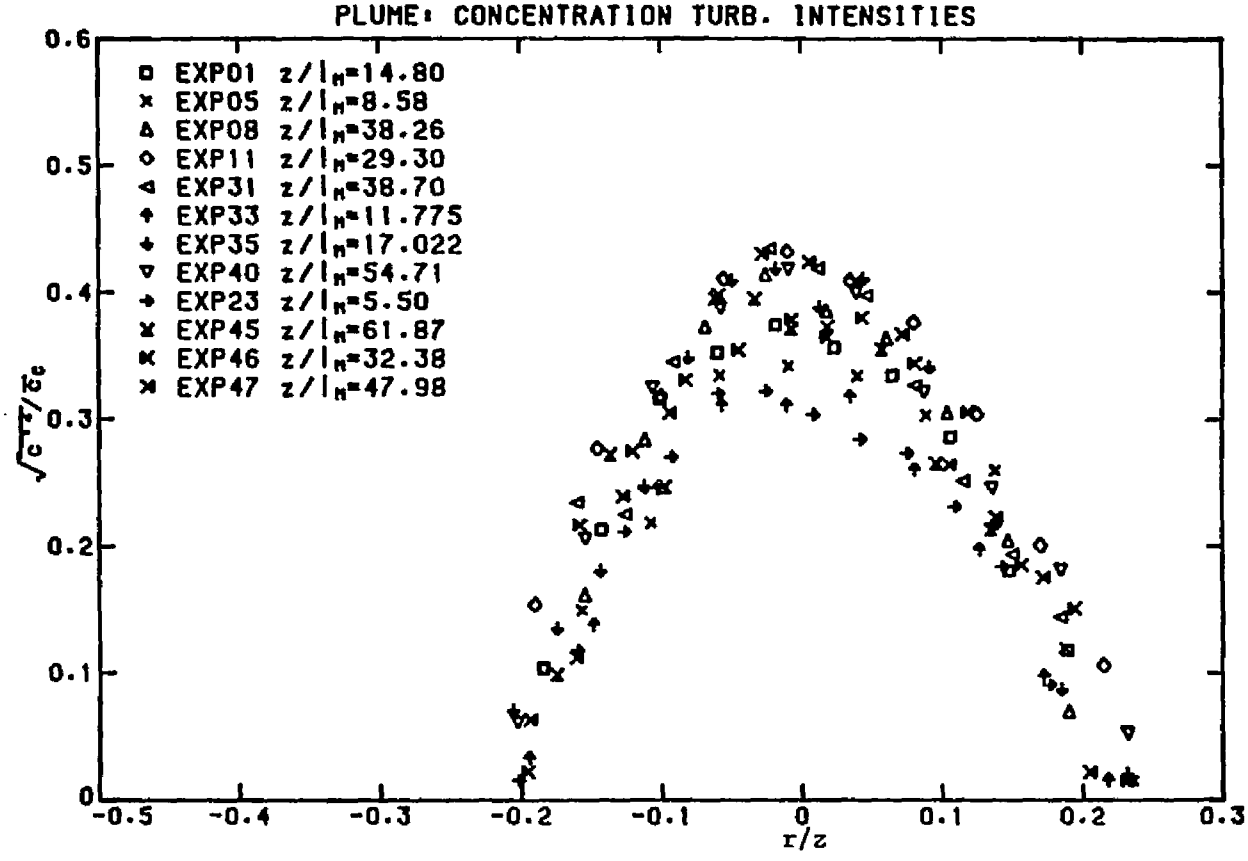


Figure 4.6.3. Profile of the intensity of turbulent fluctuations of the concentration across a turbulent plume.

where the exponent 0.994 is close to the expected value of 1.0. For the plumes ($z/l_M > 5$) the data fit implies

$$b_c / l_M = 0.112 (z/l_M)^{1.007} \qquad (4.6.5a)$$

that a plume growth appears to be slightly slower than for jets. However, the exponent is again very close to unity.

With these data a comparison is possible between the concentration and velocity profile growth rate. Although all the experimenters have observed that for jets the concentration profile is wider than the velocity profile, some plume investigators find $b_c$ less than $b_w$ (see for example George et al. (1977) and Nakagome and Hirata (1976)). The results of the present investigation indicate that $b_c > b_w$ for both jets and plumes. This is shown by the equations (4.3.7), (4.4.12), (4.5.3) and (4.6.5) and also in the comparison plot in Figure 4.6.5 where $b_w / l_M$ and $b_c / l_M$ are plotted versus $z/l_M$. These data appear to give an average value

$$\lambda = b_c / b_w = 1.194$$

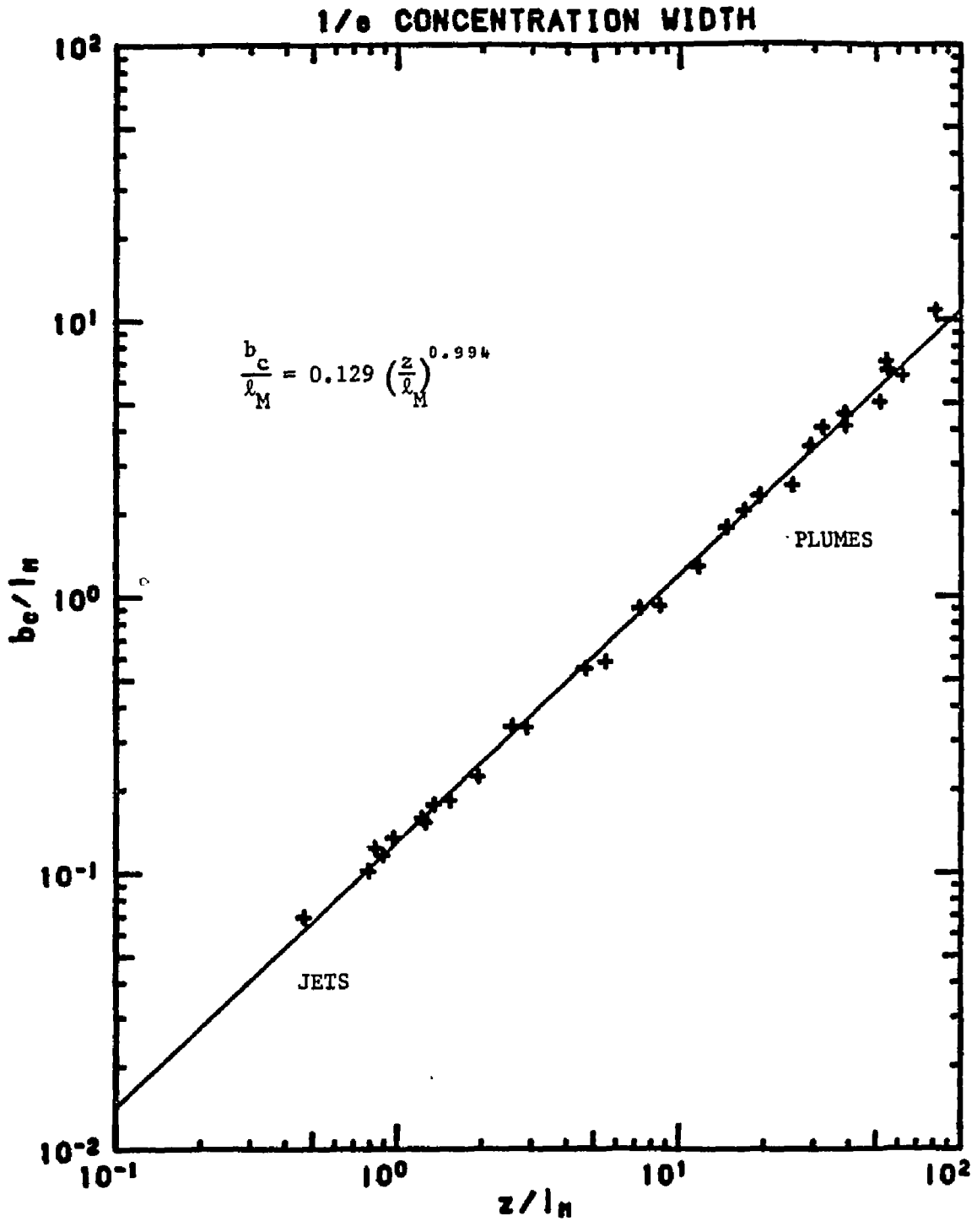


Figure 4.6.4. Non-dimensional concentration 1/e-width of a turbulent buoyant jet plotted against $z/\ell_M$.

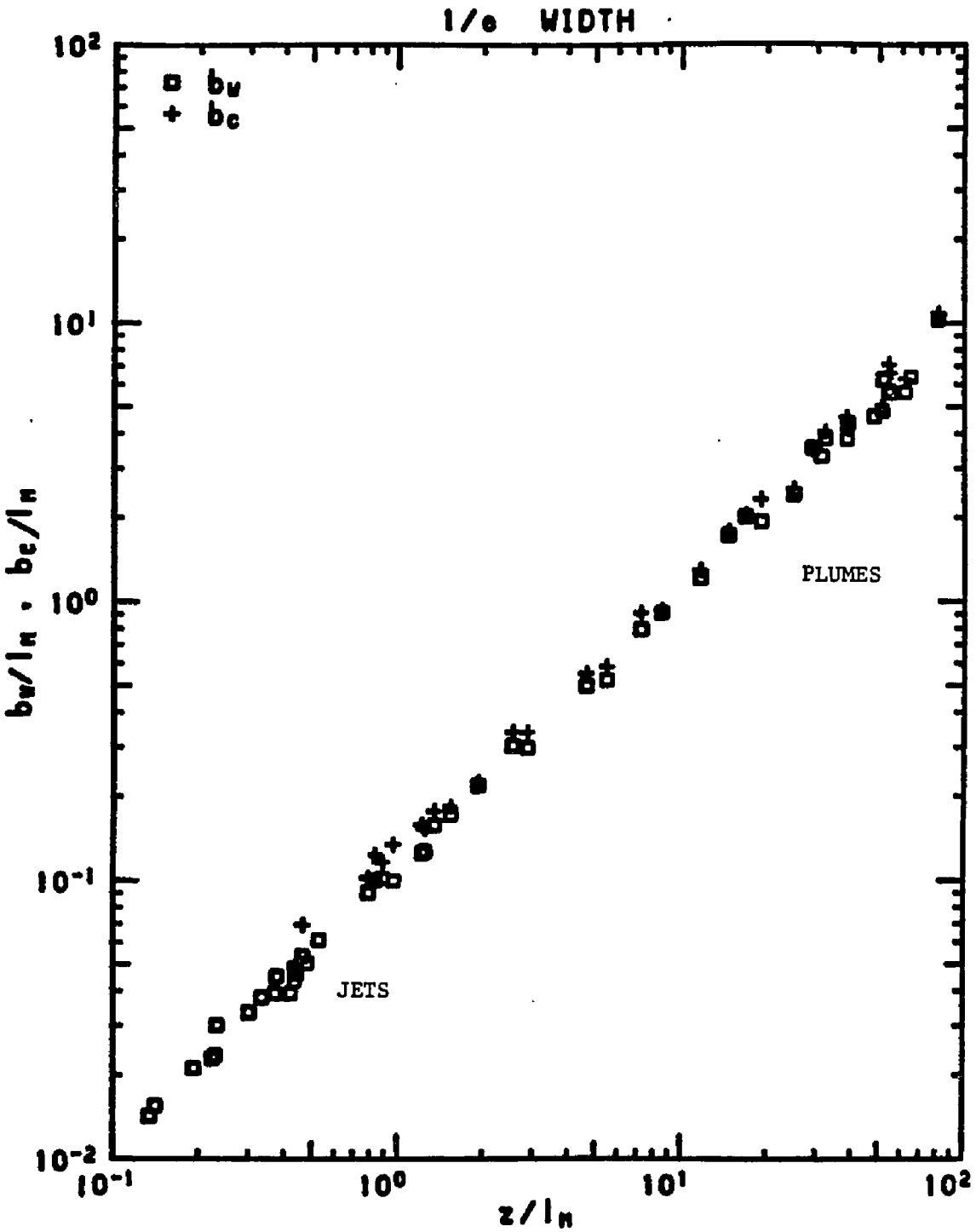


Figure 4.6.5. Non-dimensional velocity and concentration 1/e-width of a turbulent buoyant jet plotted for comparison against $z/\ell_M$.

## 4.7 Turbulent mass flux in jets and plumes

### 4.7.1 Introduction

It was mentioned in section 1.2 of the introductory chapter that the contribution of the turbulent mass flux term to the total mass transport of a tracer by the jet has generally been neglected, on the basis that it was small compared to the mean advective flux i.e.

$$\overline{w'c'} << \bar{w}\,\bar{c}$$

If we define

$$H_o = QC_o$$

to be the initial flux of a tracer carried by the jet fluid at the jet exit then at a transverse section to the jet axis, downstream of the jet origin, continuity implies that

$$H_o = QC_o = \int_o^{b(z)} \overline{w\,c}\; 2\pi r\, dr = \int_o^{b(z)} \bar{w}\,\bar{c}\; 2\pi r\, dr + \int_o^{b(z)} \overline{w'c'}\; 2\pi r\, dr$$

$$= \quad H_M + \quad H_T$$

where $H_M$ and $H_T$ are the contributions to the tracer transport by the mean jet flow and the turbulence. Kotsovinos (1975) reported $H_T / H_o$ to vary from 6% in a jet case to 40% in a plume for the two - dimensional case, a value that is much higher than those reported by George et al

(1977) and Nakagome and Hirata (1976). Kotsovinos (1975)measured $\overline{w'c'}$ and for the 2-D plume case around the centerline he found

$$\overline{w'c'}/\bar{w}_c\,\bar{c}_c = 0.25.$$

Ramaprian and Chandrasekhara (1983) "repeated" Kotsovinos' 2-D buoyant jet experiment and predicted that the maximum normalized $\overline{w'c'}/\bar{w}_c\,\bar{c}_c$ did not exceed the value 0.05. Antonia et al (1975) and Chevray and Tutu (1977)measured the constant in the equation above to be 0.022 to 0.028 at the jet axis and 0.03 to 0.04 at the peaks. George et al (1977) reported the constant to be 0.07 and Nakagome and Hirata (1976) determined a value of 0.04 around the plume axis.

4.7.2 Turbulent mass fluxes in jets and plumes

The turbulent flux of a tracer (Rhodamine 6G in the present case) transported by the jet can be calculated from the radial distribution of $\overline{w'c'}$as

$$H_T = \int_0^{b(z)} \overline{w'c'} 2\pi r\, dr$$

The normalized velocity - concentration correlations $\overline{w'c'}$ and $\overline{u'c'}$ by the mean velocity and concentration at the jet axis, have been plotted versus r/z in Figures 4.7.1, 4.7.2, 4.7.3 and 4.7.4 for both jets and plumes. Figures 4.7.1 and 4.7.2 show the radial distributions of $\overline{w'c'}$ and $\overline{u'c'}$ in a jet, and Figures 4.7.3 and 4.7.4 these distributions in a plume. From Figures 4.7.1 and 4.7.2 the centerline and peak values of the w - c and u - c correlations for a jet were

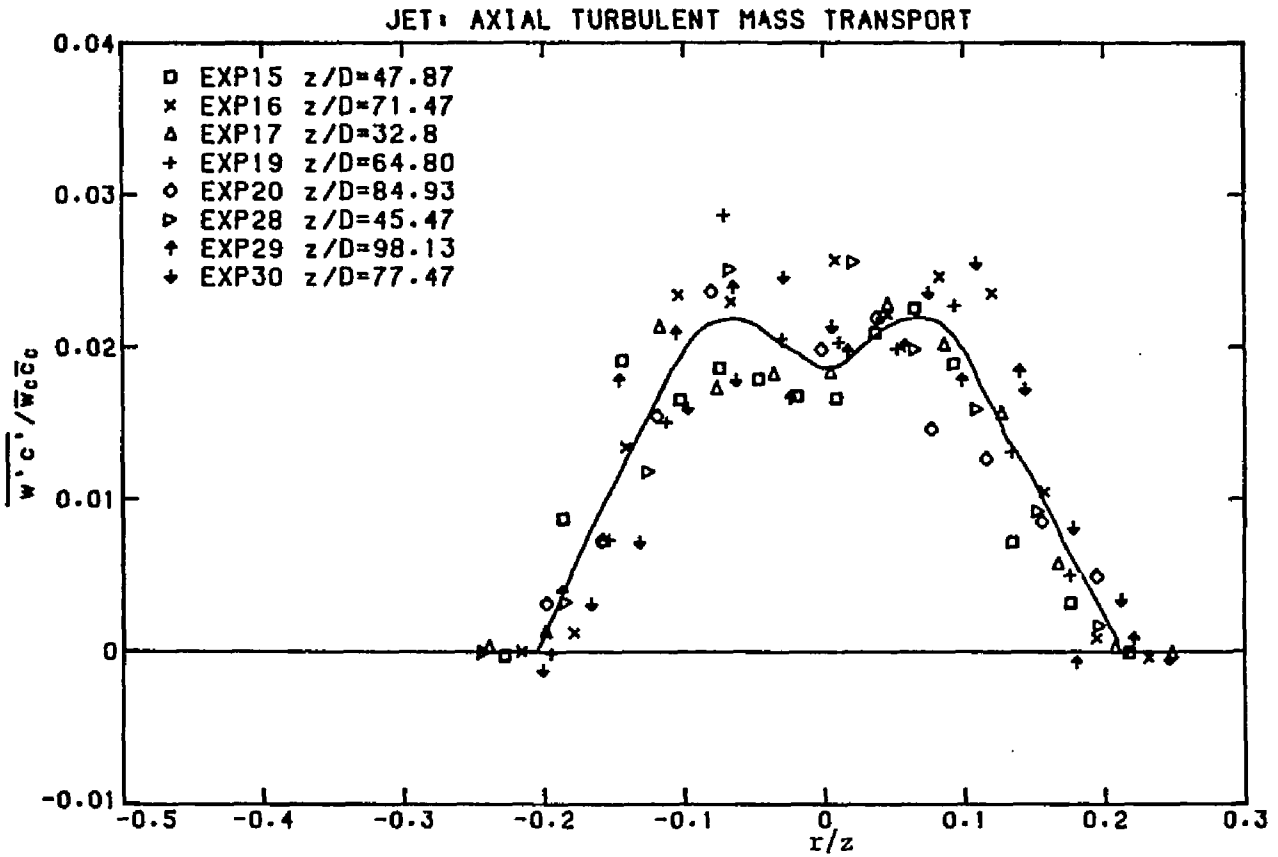


Figure 4.7.1. Non-dimensional profile of axial turbulent tracer (Rhodamine 6G) flux across a turbulent jet.

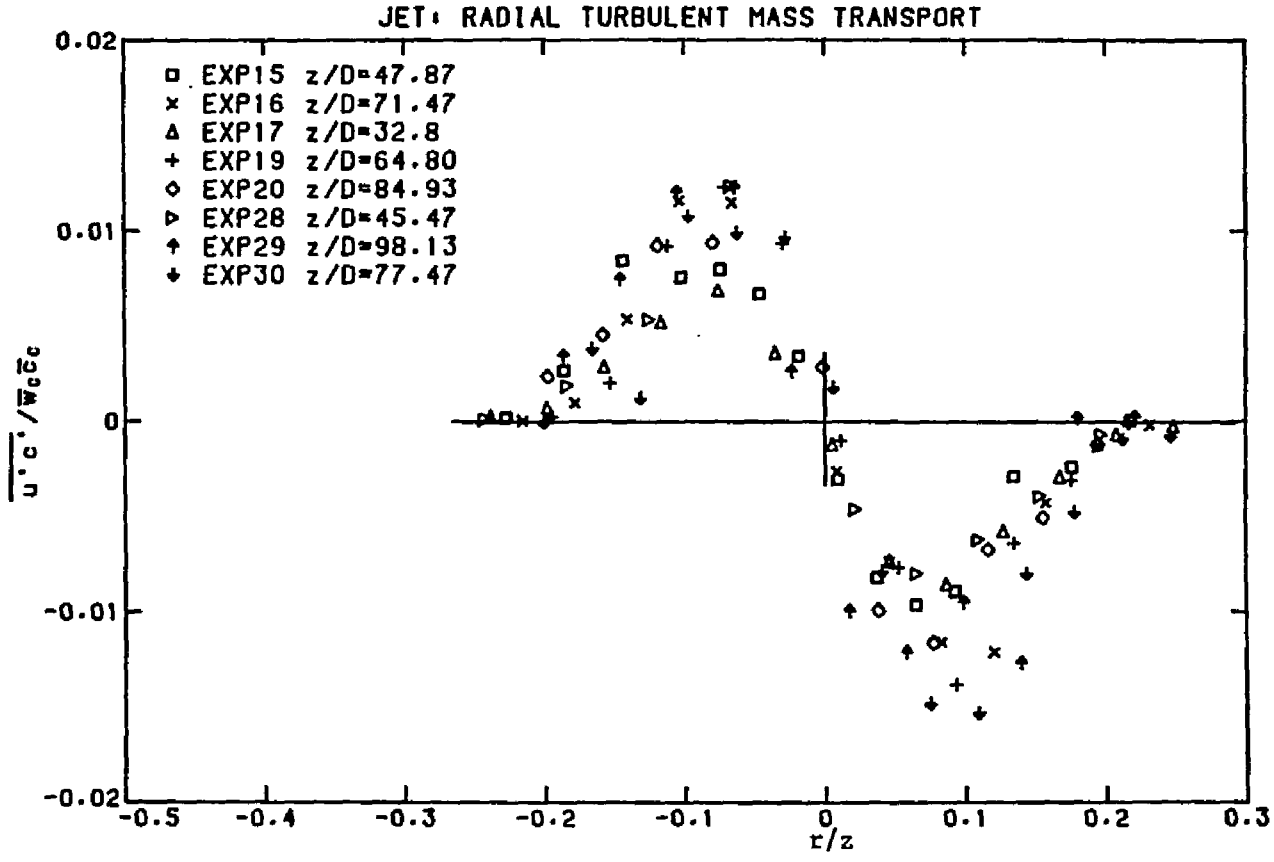


Figure 4.7.2. Non-dimensional profile of radial turbulent tracer flux across a turbulent jet.

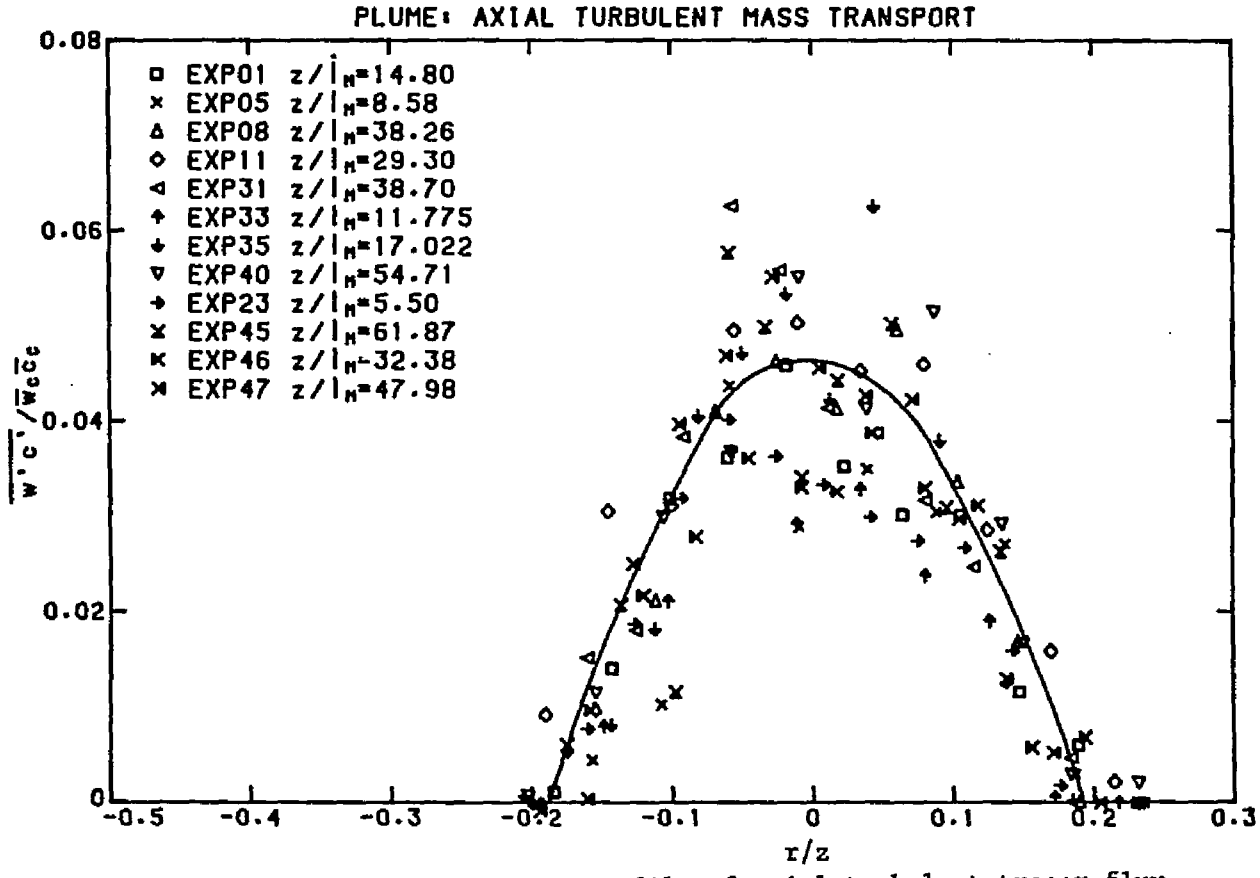


Figure 4.7.3. Non-dimensional profile of axial turbulent tracer flux across a turbulent plume (representative profiles).

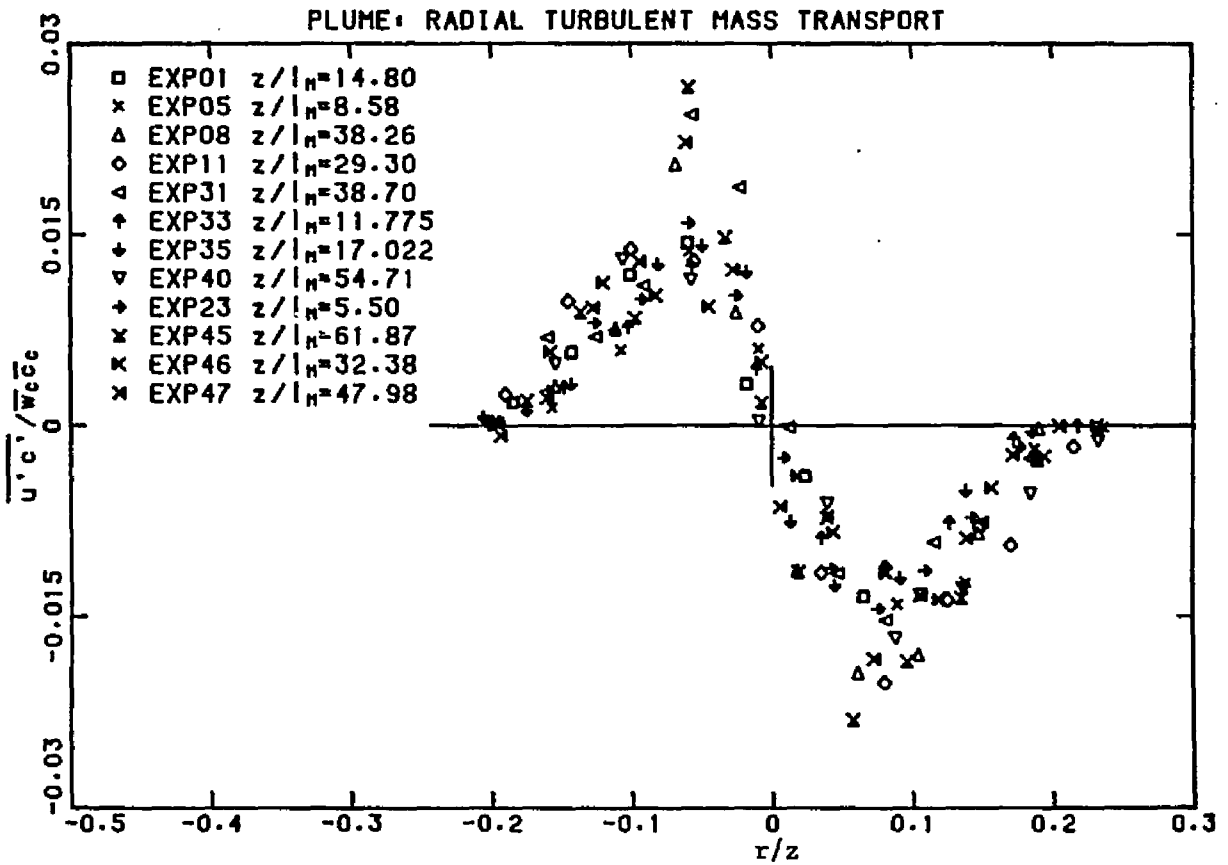


Figure 4.7.4. Non-dimensional profile of radial turbulent tracer flux across a turbulent plume (representative profiles).

measured and found

| | centerline | peak value |
|---|---|---|
| $\overline{w'c'}/\overline{w}_c\ \overline{c}_c$ | 0.020 | 0.024 |
| $\overline{u'c'}/\overline{w}_c\ \overline{c}_c$ | 0.000 | 0.010 |

For a plume the w - c and u - c correlations shown in Figures 4.7.2 and 4.7.3 take peak and centerline values

| | centerline | peak value |
|---|---|---|
| $\overline{w'c'}/\overline{w}_c\ \overline{c}_c$ | 0.030-0.040 | 0.040-0.050 |
| $\overline{u'c'}/\overline{w}_c\ \overline{c}_c$ | 0.000 | 0.015-0.025 |

From the measured values above it is expected that the turbulent tracer mass flux is bigger in a plume than in a jet. For the case of the jet the average values of $\overline{w'c'}$ measured are smaller than those reported by Antonia et al (1975) and Chevray and Tutu (1978). List (1980) used the results reported by the above authors to calculate the total longitudinal tracer mass fux of a tracer by a jet. He assumed Gaussian distribution for the $\overline{w'c'}$ with a maximum 0.03 to 0.04 at the jet axis and width twice the 1/e width of the jet, and found that 14% of the heat flux is carried by the turbulence.

In Figure 4.7.5 the measured $H_T$ normalized by the initial tracer flux is plotted versus $z/l_M$. It is shown clearly in this figure that for a jet the turbulent mass flux of a tracer is 6 - 14 % of the total while for a plume it becomes 15 - 20 % of the total (open symbols). Therefore the calculations in Chapter 1 based on the assumption that

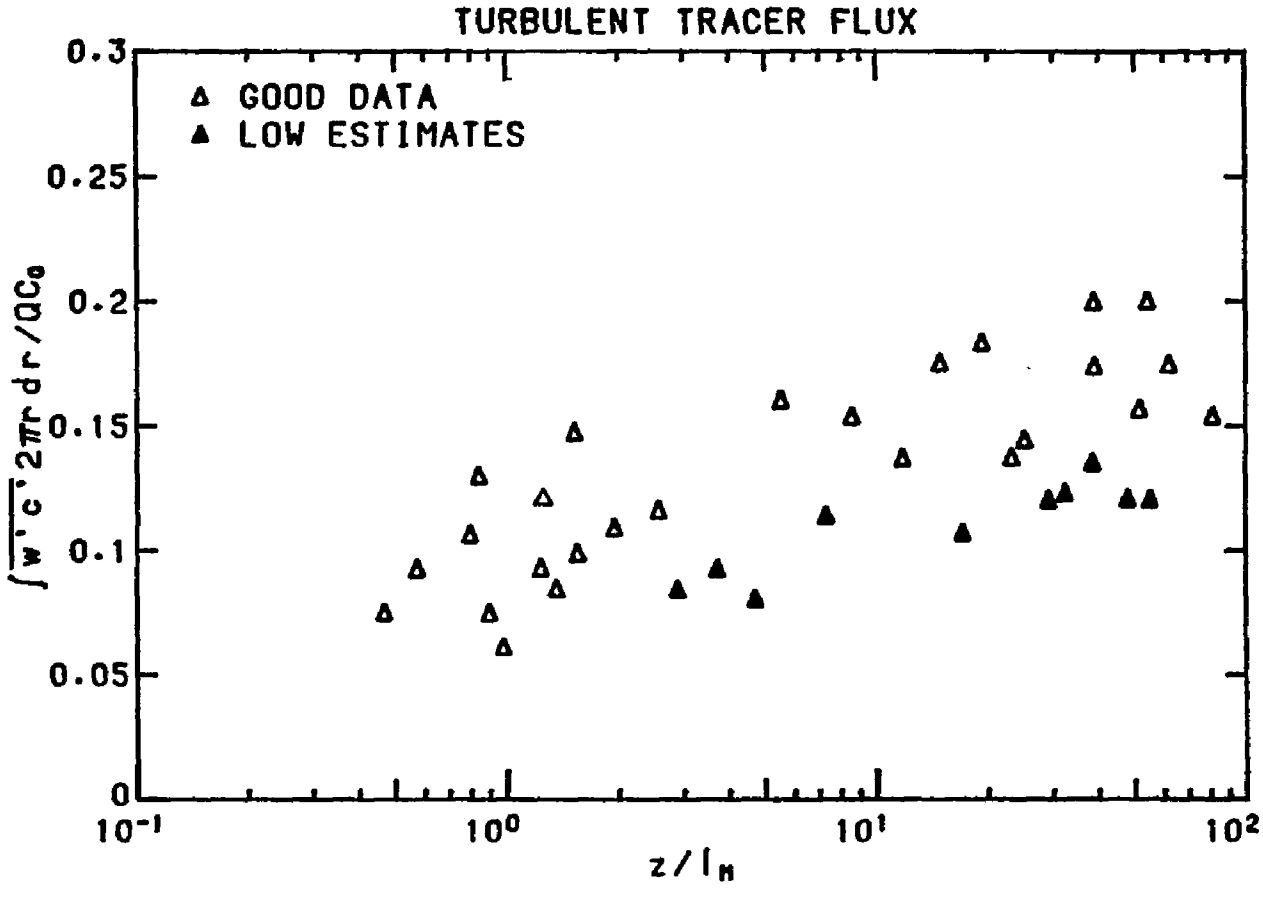


Figure 4.7.5. Turbulent tracer flux in a turbulent buoyant jet, normalized by the tracer flux at the jet orifice as a function of the non-dimensional distance $z/\ell_M$ from the jet origin.

$\overline{w'c'} \ll \bar{w}\ \bar{c}$ need reevaluation. The assumption appears questionable especially in the plume case where the observed values $H_T/H_o$ can be as high as 20%. In consideration of these results it is important to discuss the closure

$$H_o = H_M + H_T$$

In the present experiment both $H_M$ and $H_M + H_T$ were found to exceed $H_o$ for almost all data points except the low estimates as shown in Figure 4.7.6. This means that the mean concentration and probably the turbulent fluxes are overestimated. This may be a systematic error in that a comparison of the mean concentration values measured by other authors and the results of the present investigation showed that the measured concentrations were higher. An investigation of this can be performed using some preliminary results based on temperature measurements by Papanicolaou and List (1983) (see Appendix A), which used the same jet, as follows. The mean centerline dilution is given as

$$\frac{SQ}{z\sqrt{M}} = 0.165 \text{ (Jets)} \quad \text{and} \quad \frac{SQ}{z\sqrt{M}} = 0.090 \left(\frac{z}{l_M}\right)^{2/3} \text{ (Plumes)}$$

Using these concentration decay rates in the computation of

$$H'_M = \int_o^{b(z)} \bar{w}\ \bar{c}_1 2\pi r dr \begin{cases} \bar{c}_1 = \dfrac{0.147}{0.165}\bar{c} = 0.890\bar{c} \text{ ; jets} \\ \bar{c}_1 = \dfrac{0.070}{0.090}\bar{c} = 0.777\bar{c} \text{ ; plumes} \end{cases}$$

and keeping $H_T$ as computed previously the sum

$$H'_o = H'_M + H_T$$

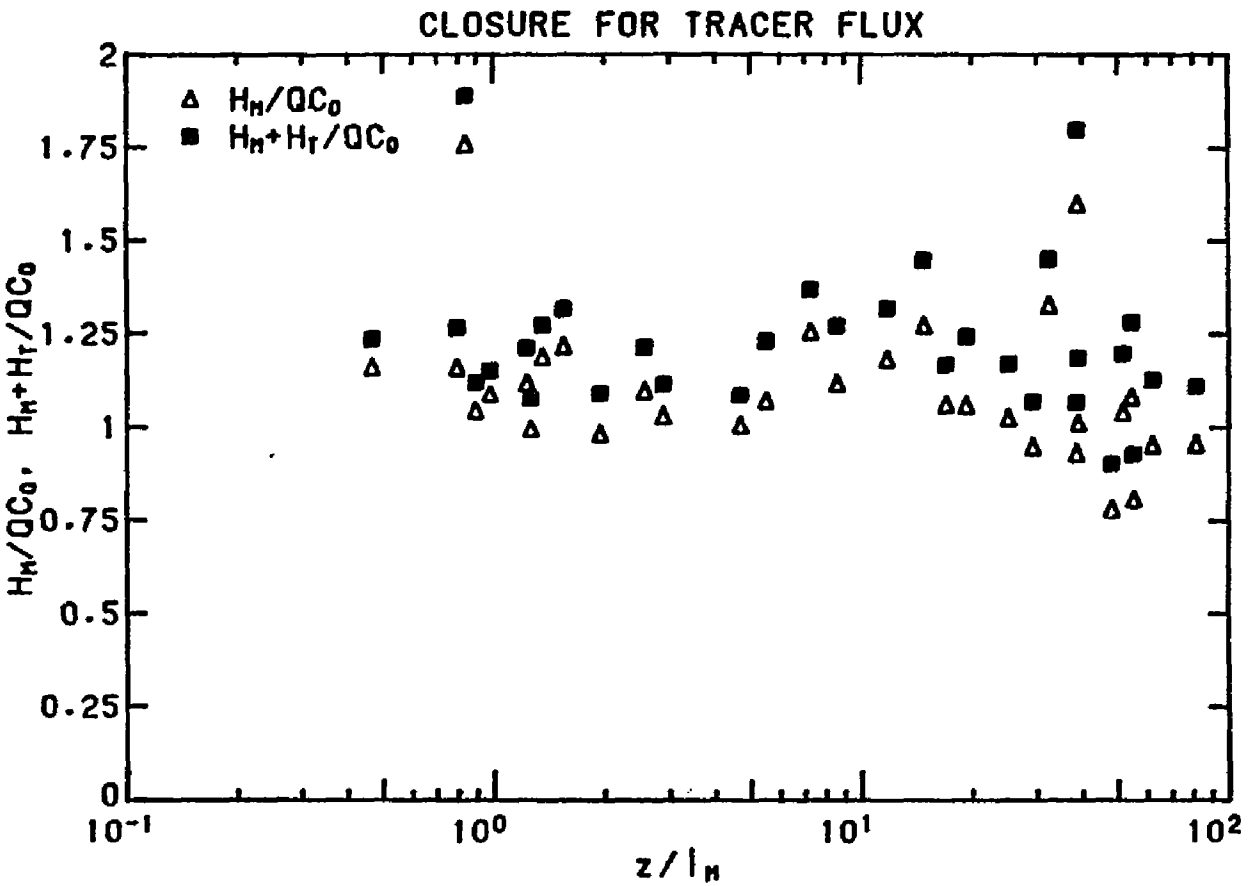


Figure 4.7.6. Normalized calculated mean and total tracer fluxes $H_M$ and $H_M + H_T$, plotted versus $z/\ell_M$.

is found to take values close to $QC_o$. This is shown in Figure 4.7.7 where the sum of the corrected $H'_M$ and uncorrected $H_T$ normalized by $QC_o$ has been plotted versus $z/l_M$. The discrepancy in the data points is due to the discrepancy of the normalized mean velocities and concentrations along the jet axis and the widths $b_w$ and $b_c$ shown in Figures 4.4.1, 4.6.1, 4.4.6 and 4.6.4 respectively and used for the calculation of $H'_M$.

Using the mean velocity profiles in Figures 4.3.4 and 4.4.2 for a jet and a plume respectively and the velocity decay along the axis in Figure 4.4.1, and from Figures 1, 2(a) and 2(b) in Appendix A one has

$$H_M = \int_o^\infty \bar{w}\,\bar{c}\,2\pi r dr = \frac{\pi\, Q\, C_o}{(0.132)(0.165)(80+75)} = 0.93\, Q\, C_o \quad \text{(JET)}$$

and

$$H_M = \int_o^\infty \bar{w}\,\bar{c}\,2\pi r dr = \frac{\pi\, Q\, C_o}{(0.090)(0.260)(80+80)} = 0.839\, QC_o \quad \text{(PLUME)}.$$

Hence it is confirmed that the turbulent tracer flux varies from about 7% in jets to about 16% in plumes which is observed in Figure 4.7.5.

This would suggest that the error is involved in the measurements of the mean concentration. It may well result from an increase in the background light intensity seen by the laser fluorescence system and resulting from internal reflections and scattering of laser light from the intense beam used to induce the fluorescence. The nature of the experimental set-up i.e. existence of particles in both jet and ambient fluid that scatter laser light in all directions can cause fluorescence of Rhodamine 6G dye in the vicinity of the laser beam that is detected by the photodiode biasing the output signal. Absorbtion of Rhodamine 6G

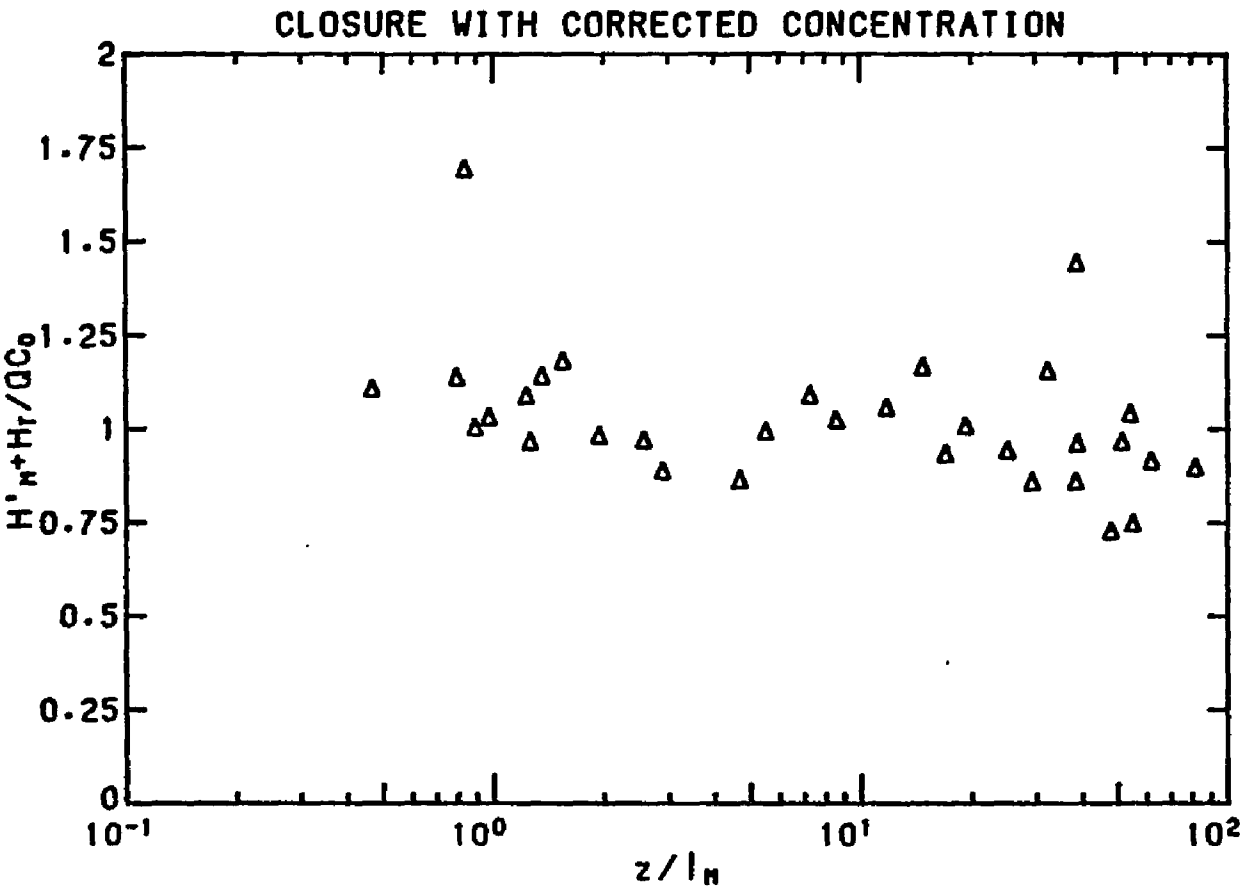


Figure 4.7.7. Total tracer mass transport from the corrected concentration profiles and the measured turbulent tracer transport normalized by the initial tracer transport at the jet origin, plotted versus $z/\ell_M$.

dye by the particles crossing the probe volume may also result an increment in the fluorescence from the dye dissolved in the fluid of the probe volume.

## 4.8 Dilution in vertical round buoyant jets

Fischer et al (1979) defined the constants of proportionality in the dilution formulae in Table 1.3.1 based on existing data of various investigators. For simple plumes they defined the constants of proportionality for velocity and concentration decay from the work of Rouse et al (1952) and George et al(1977). As mentioned in sections 4.3 and 4.5 a plume becomes self similar for $z/l_M > 5$; this is shown clearly in Figures 4.4.1 and 4.6.1. For $z/l_M > 5$ the dimensionless mean velocities and concentrations on the plume axis, as defined by the equations (4.4.2) and (4.6.1), are proportional to $(z/l_M)^{2/3}$ and $(z/l_M)^{2/3}$ respectively, as anticipated by the dimensional arguments. It is believed that Rouse et al.(1952) probably measured in the transition region $1<z/l_M<5$, or may have measured the velocities inaccurately. Furthermore since all plume parameters derived by prior investigations from data up to 20 initial diameters it is likely that the plumes had not become self similar. For these reasons some of the basic parameters discussed in sections 1.2 and 1.3 will be redefined from the data obtained in the present investigation.

### 4.8.1 The plume Richardson number

The local Richardson number for a buoyant jet is defined as

$$R(z) = \frac{\mu\beta^{1/2}}{M^{5/4}} \qquad (4.8.1)$$

where $\mu$, m and $\beta$ are the local estimates of the mass, momentum and buoyancy fluxes respectively. Substituting the local mean velocity and concentration profiles

$$\bar{w} = \bar{w}_c \exp[-(r/b_w)^2] \tag{4.8.2}$$

$$\bar{c} = \bar{c}_c \exp[-(r/b_c)^2] \tag{4.8.3}$$

with

$$\lambda = b_c / b_w \tag{4.8.5}$$

and

$$(\Delta \bar{\rho})_c(z)/(\Delta \rho)_o = \bar{c}_c / C_o \tag{4.8.5}$$

into the equations (1.2.6), (1.2.7) and (1.2.8) equation (4.8.1.) can be rewritten as

$$R(z) = \left[\frac{4\sqrt{2\pi}\,\lambda^2}{1+\lambda^2}\left(g\frac{(\Delta\rho)_o}{\rho_a}\right)\left(\frac{\bar{c}_c}{C_o}\frac{b_w}{\bar{w}_c^2}\right)\right]^{1/2} \tag{4.8.6}$$

The local jet Richardson number R(z) as computed from equation (4.8.6) has been plotted versus $z/l_M$ in Figure 4.8.1. The + symbols correspond to $\lambda = b_c / b_w$ calculated exactly from simultaneous velocity and concentration measurements. The $\Delta$ symbols in the jet region correspond to values of R(z) calculated from velocity measurements only (experiments PAP and VEL series) using $\lambda = 1.2$ and $C/\bar{c}_c = 0.157z/D$ from equation (4.5.1).

For $z/l_M \ll 1$ (jets)

$$m(z) = \text{constant}$$

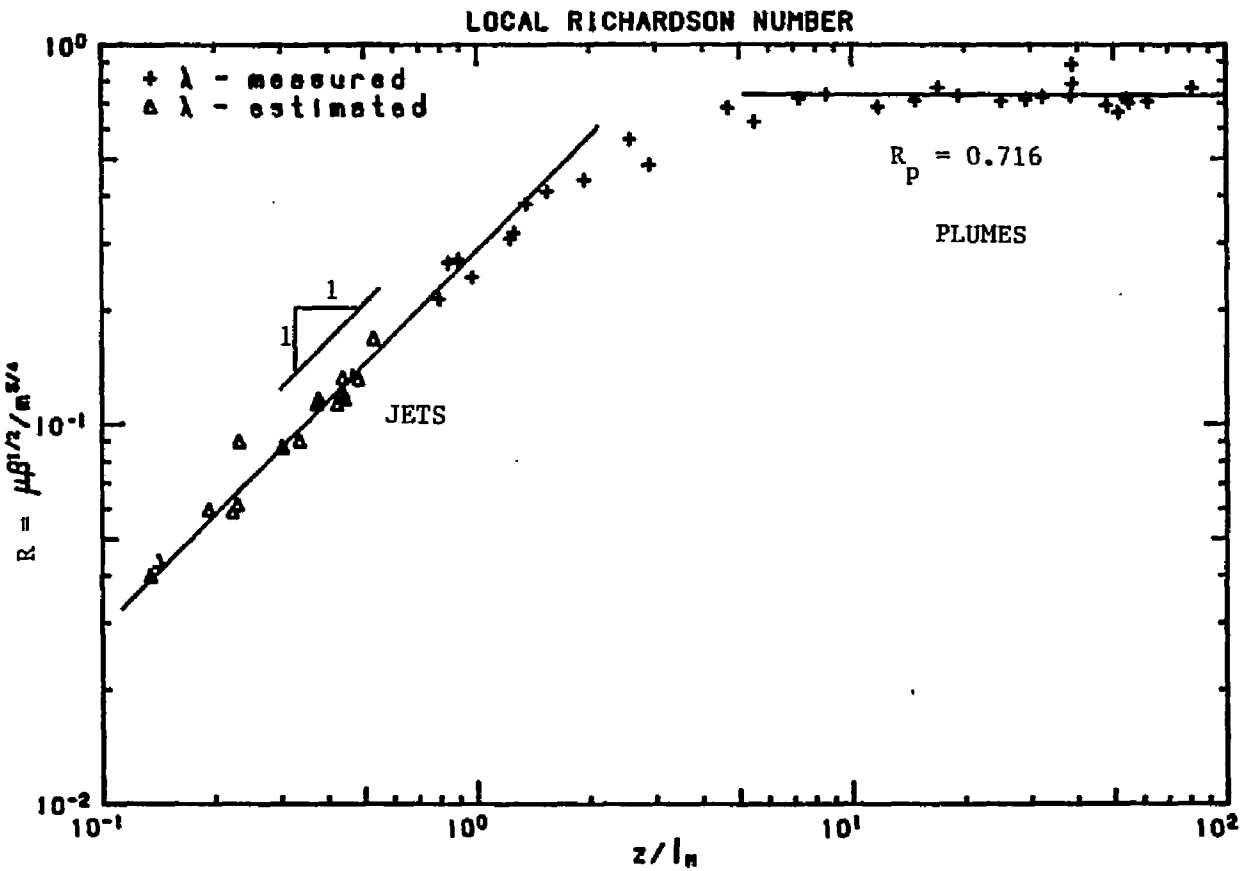


Figure 4.8.1. Richardson number in a turbulent buoyant jet plotted against the dimensionless distance from jet origin.

$$\mu(z) = 0.2842(z/D)$$

$$\beta(z) = \text{constant}$$

and therefore

$$R(z) \sim z/l_M \tag{4.8.7}$$

which is also shown in figure 4.8.1. For $z/l_M >> 1$ (plumes) substituting equations (1.3.8a) and (1.3.9a) into (4.8.1)

$$R(z) = \text{constant} = R_p \tag{4.8.8}$$

where $R_p$ is defined as the plume Richardson number. From Figure 4.8.1 and for $z/l_M > 5$ one can notice that R(z) is invariant with $z/l_M$, and the calculated value was found

$$R_p = 0.716 \tag{4.8.8a}$$

significantly higher than $R_p = 0.557$ proposed by Fischer et al (1979). This experimentally observed constant Richardson number for $z/l_M$ beyond 5, is further evidence that plume - like behavior exists for large $z/l_M$.

4.8.2 Jet/plume width parameter

From equation (1.3.11) the plume width parameter defined as

$$c_p = \sqrt{2\pi} b_w / z \tag{4.8.9}$$

has been plotted versus $z/l_M$ in Figure 4.8.2. Its value is supposed

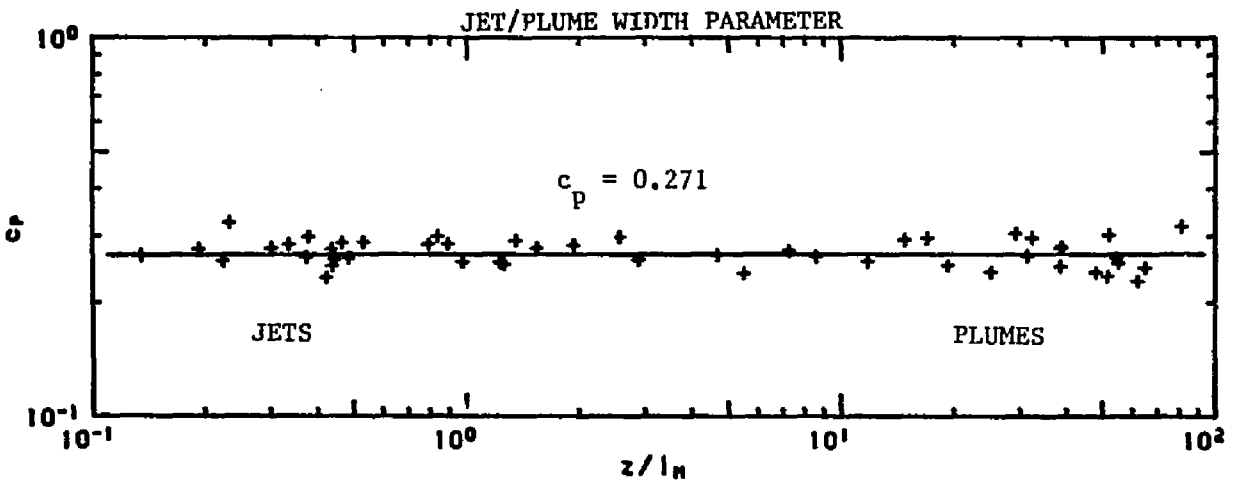


Figure 4.8.2. Round plume width parameter $c_p$ for turbulent buoyant jets showing a constant value of 0.271.

constant, since from equations (4.3.5) and (4.4.12) it is clear that $b/z \simeq$ constant for both jets and plumes. From Figure 4.8.2

| | mean | st.dev. | max | min | |
|---|---|---|---|---|---|
| $c_p$ | 0.271 | 0.022 | 0.326 | 0.233 | (4.8.9a) |

This value of $c_p = 0.271$ is higher than the 0.25 recommended by Fischer et al (1979).

The estimates for $R_p$ and $c_p$ calculated in this section were used to calculate the dimensionless dilution $\bar{\mu}$ and dimensionless elevation $\zeta$ defined in equations (1.3.13) and (1.3.14) as

$$\bar{\mu} = \frac{\mu B^{1/2}}{R_p M^{5/4}} = \frac{\mu}{Q}\left(\frac{R_o}{R_p}\right); \quad \zeta = \frac{c_p}{R_p}\frac{z}{\ell_M} = c_p \frac{z}{\ell_Q}\left(\frac{R_o}{R_p}\right) \tag{4.8.10}$$

In Figure 4.8.3 $\bar{\mu}$ has been plotted versus $\zeta$ and is shown clearly that the theoretical predictions

$$\bar{\mu} = \zeta, \quad \zeta < 1$$
$$\bar{\mu} = \zeta^{5/3}, \quad \zeta > 1$$

are in a remarkably good agreement with the results of the present investigation.

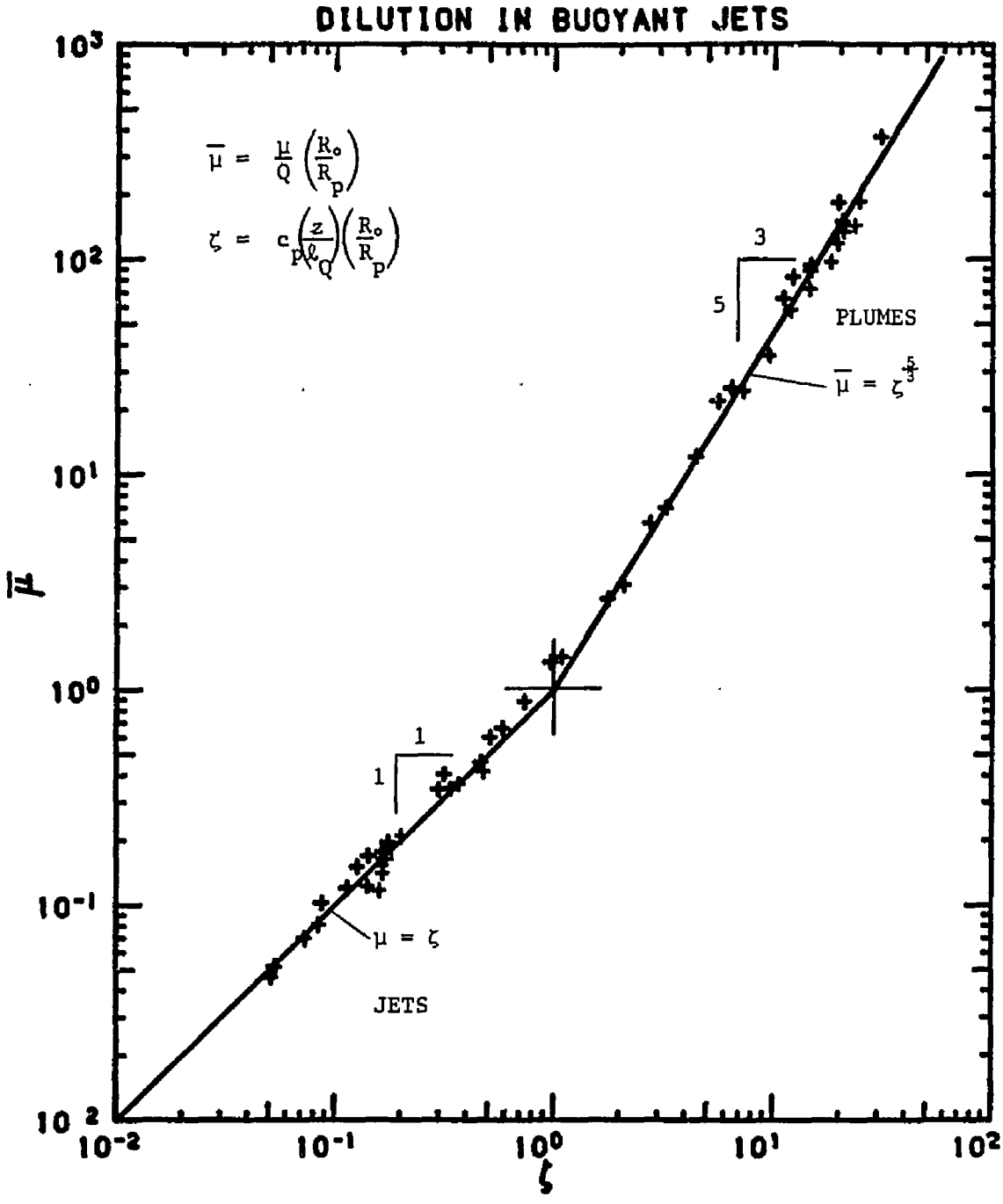


Figure 4.8.3. Mean dilution, $\overline{\mu}$, in turbulent buoyant jets plotted against non-dimensional elevation, $\xi$.

## 4.9 Entrainment, mass and momentum balance in a round vertical turbulent buoyant jet

### 4.9.1 Entrainment coefficients

In this section the entrainment coefficient implied by the present data will be calculated for both jets and plumes. Substituting directly the estimates for the mean velocities at the centerline and the widths $b_w$ for both jets and plumes into the equation

$$d/dz(\bar{w}_c\, b_w^2) = 2a_e\, b_w\, \bar{w}_c \qquad (4.9.1)$$

one has:

(a) For jets $W/\bar{w}_c = 0.149z/D$ and $b_w = 0.109z$ and therefore

$$2a_j = 0.109;\ a_j = 0.0545.$$

(b) For plumes $w_c = 3.85B^{1/3}z^{-1/3}$ and $b_w = 0.105z$ and therefore

$$2a_p = 5/3(0.105);\ a_p = 0.0875.$$

The value $a_p = 0.0545$ is in agreement with the suggested 0.0535 by Fischer *et al.* (1979) for jets but their suggested value 0.0833 for plumes based on the data of Rouse *et al.* (1952) is lower than that obtained here.

### 4.9.2 Mass and momentum balance in round vertical buoyant jets

The local mass flux $\mu(z)$ and momentum flux $m(z)$ at a distance $z$ from the jet origin were calculated from the mean velocity profiles. The normalized $\mu(z)$ has been plotted versus $z/l_M$ in Figure 4.9.1. For

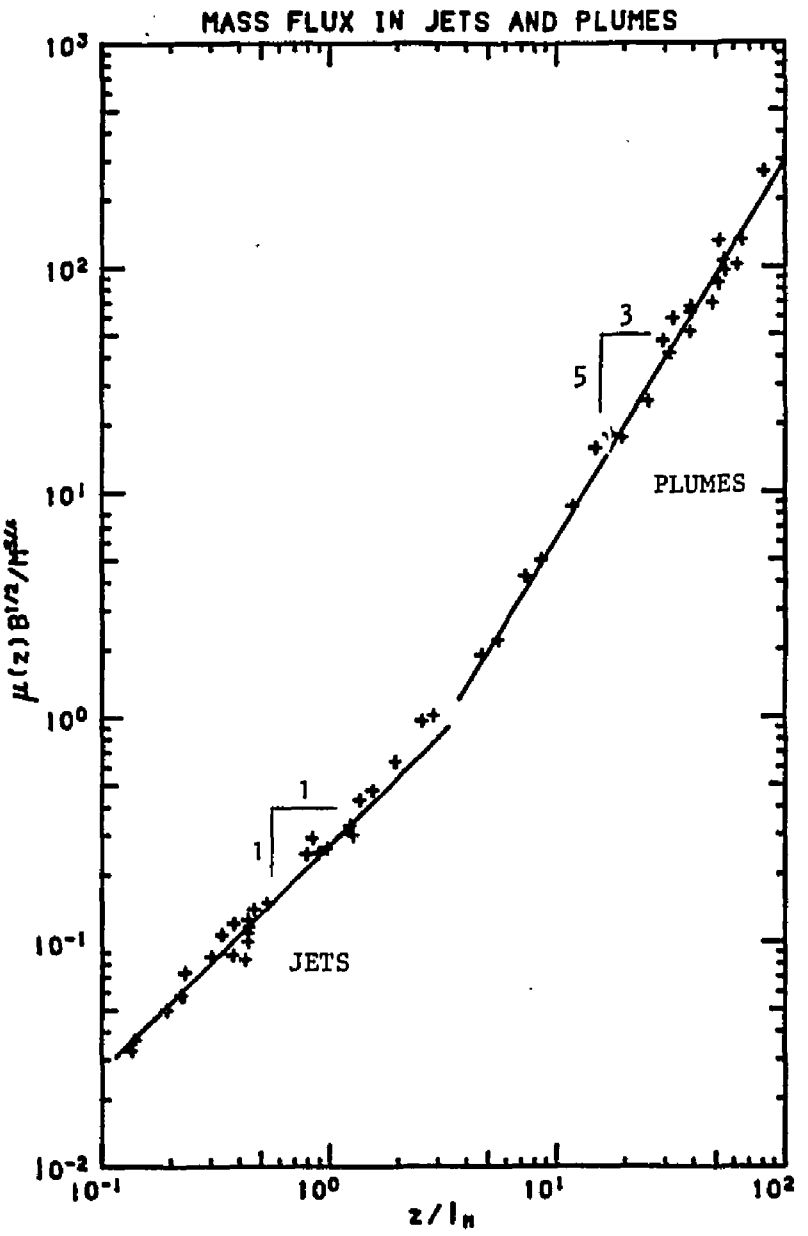


Figure 4.9.1. Volume flux in a turbulent buoyant jet plotted against non-dimensional distance $z/\ell_M$ from jet origin.

$z/l_M$ <1 in section 4.3.4 the normalized mean mass flux was found

$$\frac{\mu}{Q} = 0.284\ \frac{z}{D} \tag{4.9.2}$$

and is shown to be proportional to z (slope 1:1). For $z/l_M$ >5

$$\frac{\mu B^{1/2}}{M^{5/4}} = b_3' \left(\frac{z}{\ell_M}\right)^{5/3} \tag{4.9.3}$$

where $b_3'$ was estimated to be 0.140 from a least square fit to the data, and it is lower than 0.150 suggested by Fischer et al (1979).

The local mean momentum flux for a jet was calculated in section 4.3.4 and found

$$m(z)/M = 0.96. \tag{4.9.4}$$

In Figure 4.9.2 m(z)/M has been plotted as a constant (zero slope) versus $z/l_M$. For $z/l_M$>5 dimensional arguments lead to

$$\frac{m}{M} = b_2'\left(\frac{z}{\ell_M}\right)^{4/3} \tag{4.9.5}$$

The constant of proportionality $b_2'$ was calculated from a least square fit to the data for $z/l_M$ >5 and found

$$b_2' = 0.290$$

lower than the value 0.35 that Fischer et al. (1979) suggest.

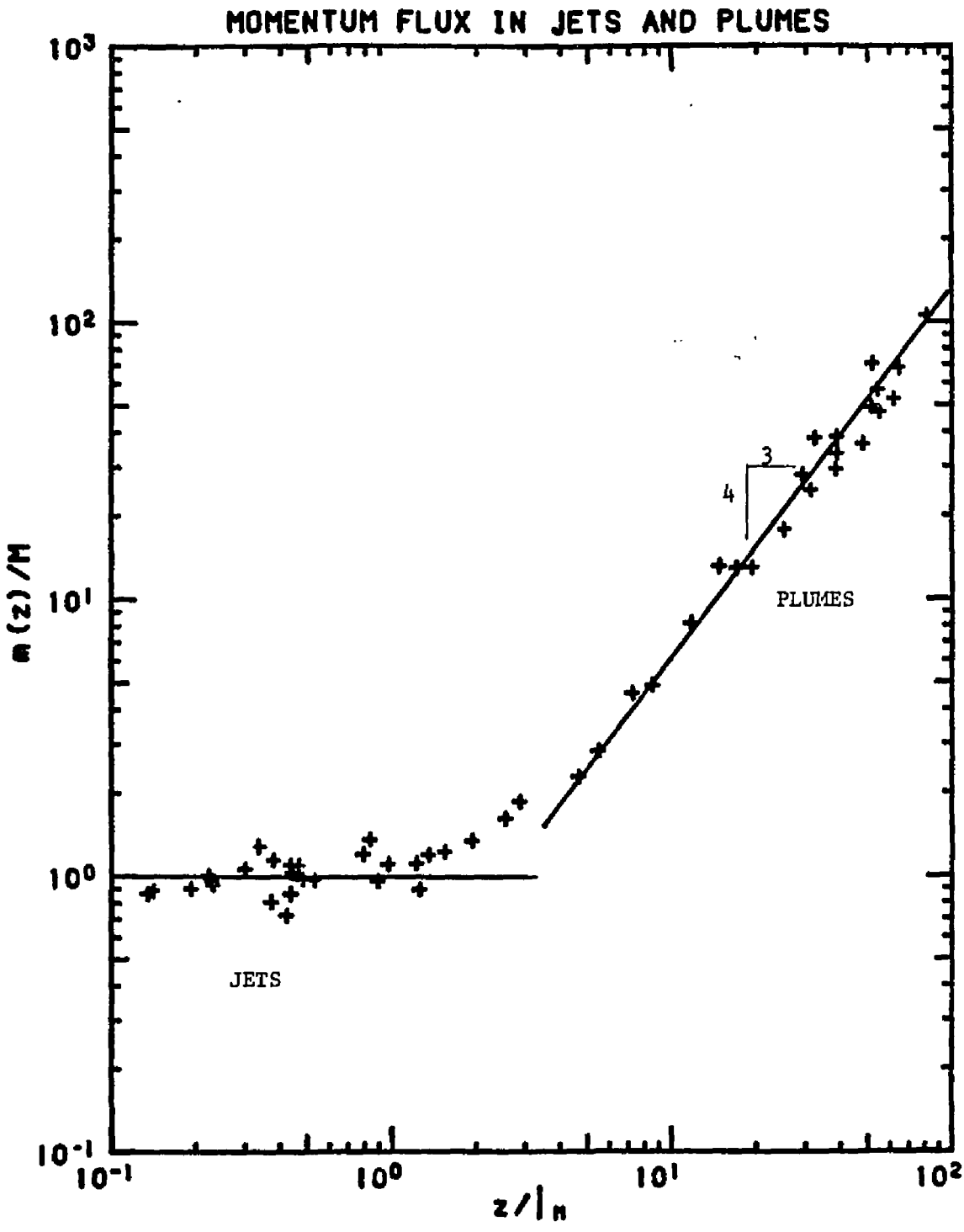


Figure 4.9.2. Momentum flux in a turbulent buoyant jet plotted against non-dimensional distance $z/\ell_M$ from jet origin.

It would be of importance to estimate the contribution of the turbulence to the momentum flux transported by the mean flow at some distance z from the jet origin. In Figure 4.9.3 the ratio $m_T(z)/m(z)$ has been plotted versus $z/l_M$ where

$$m_T(z) = \int_0^{b(z)} \overline{w'^2}\, 2\pi r dr.$$

It is shown clearly that the turbulent momentum flux is fairly constant with $z/l_M$ and approximately equal to about 15%m(z) close to the estimate 14% obtained in section 4.3.4 for the jet regime. This was expected because of the similarities in the mean velocity profiles and intensity of the turbulent axial velocity in both jets and plumes. This is a further evidence to the fact that the turbulent tracer transport should be of order of 10% to 20% discussed in section 4.7 of the present chapter.

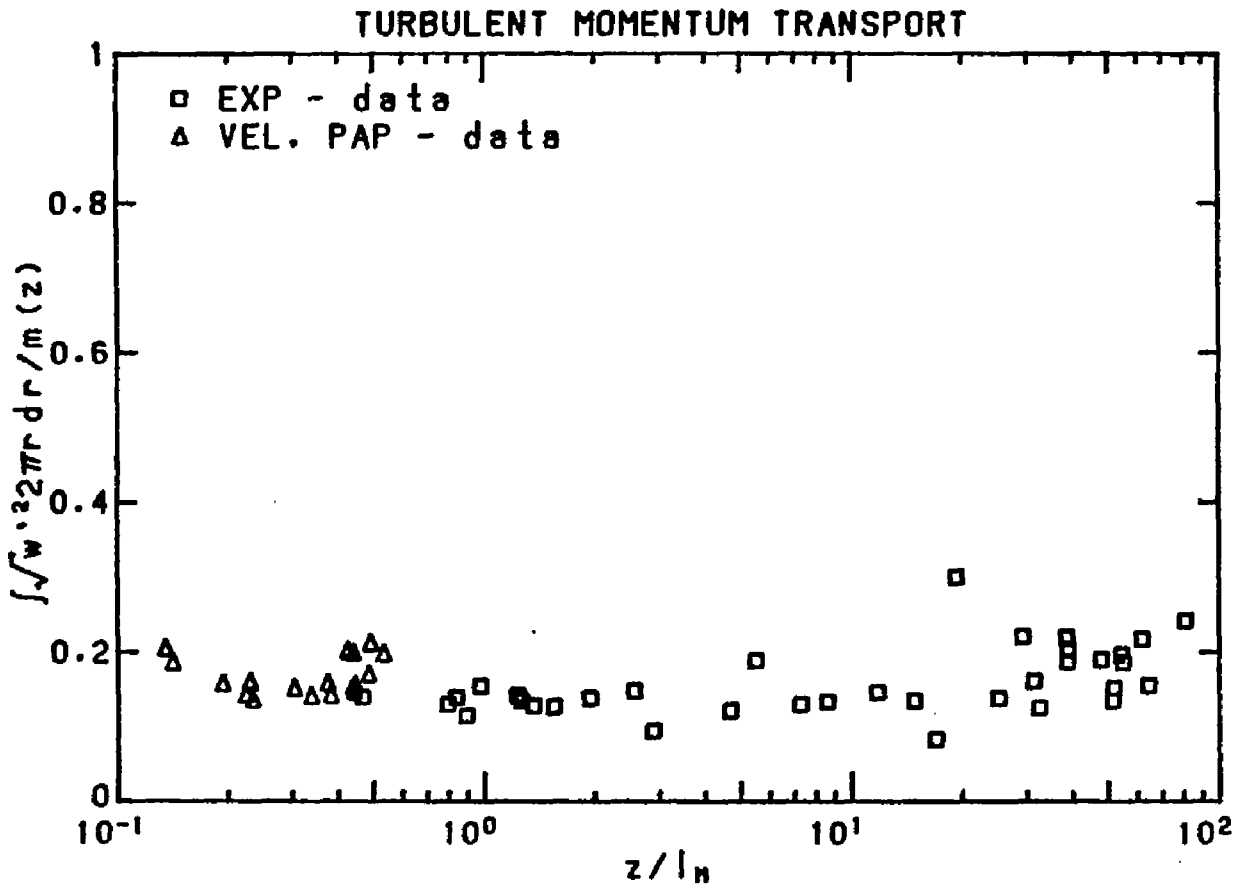


Figure 4.9.3. Turbulent momentum transport normalized with the local mean momentum transport, as a function of $z/\ell_M$.

# 5. SUMMARY, DISCUSSION, CONCLUSIONS

The present experimental work is an investigation of the growth laws, velocity and concentration decay laws, and turbulence properties of round vertical buoyant jets. All three flow regimes, a jet (momentum driven), a plume (buoyancy driven) and the transition from jets to plumes were investigated. The results obtained have been applied to a reevaluation of the basic assumptions used in analysis and have practical applications in problems of technical fluid mechanics. The measurement techniques developed can be usefully applied in other experiments that involve turbulent shear flows.

## 5.1 Instrumentation

A novel experimental measuring technique was introduced for the experimental task of this project. A two reference beam laser - Doppler velocimeter that allowed measurements of the longitudinal and radial velocity components was combined with a laser - induced fluorescence measuring device for simultaneous measurement of the concentration of a Rhodamine 6G dye. The advantages of the technique are: (i) The flow field was not disturbed as in probe - based techniques. (ii) Turbulent transport of tracer mass (Rhodamine 6G dye), and therefore the buoyancy flux of the motion could be obtained from direct simultaneous measurement of the velocity and concentration at the same point of the flow field and (iii) The instrument sensitivity allowed measurements at

many jet diameters downstream from the flow origin, thus in the region where the flow became self similar.

The only restriction that limited the measurements to 110 jet and 80 plume diameters downstream was the tank aspect ratio (tank width/jet diameter), which in the present experiment varied from 75 (plumes) to about 155 (jets). Thus for axial distances greater than 100 jet diameters the recirculation in the tank affected both velocimetry and concentration measurements. More specifically, nonlinearities in the jet growth would occur that affected the self similarity of the mean and turbulence transverse profiles of velocity and concentration. The initial jet concentrations of Rhodamine 6G dye used varied from 100 to 250 ppb in order to obtain mean concentrations many diameters downstream that would provide sufficiently accurate measurement of the concentration. The sensitivity in the fluorescence measurement was 0.1 ppb. The initial jet concentration of Rhodamine 6G dye did not affect the initial buoyancy input to the jet. This is the great advantage of the technique versus temperature or salt concentration measurements especially in the case of a momentum jet. Use of temperature or salinity for concentration measurements in jets applies two limitations (i) the concentration (temperature) cannot be measured accurately enough beyond 40 or 50 jet diameters due to the rate of decay of salt concentration or excess temperature with distance from the flow origin and (ii) the initial high buoyancy input to the jet resulted in plume formation at a few jet diameters downstream.

## 5.2 Jet growth and decay of the mean velocity and concentration

### 5.2.1 Width of a buoyant jet

Equations (4.4.11) and (4.6.5) showed clearly the non - linear behavior of the jet growth for both $b_w$ and $b_c$ if the jet is initially driven by both momentum and buoyancy. From equations (4.3.7) and (4.4.12), and (4.5.3) and (4.6.5a) it becomes clear that the spreading angle of a plume is smaller than that of a jet for both mean velocity and concentration. This is an indication that the buoyancy disperses transverse to the jet axis slower than the momentum. If at some point of the flow field of a plume a volume of fluid of high concentration and therefore buoyancy is existing, then the local buoyancy force acts as a driving mechanism which accelerates this local fluid volume. This mechanism explains the higher concentration fluctuations apparent in the plume regime.

For both jets and plumes the mean concentration profile appeared to be wider than the mean velocity profile, contrary to what George et al (1977) and Nakagome and Hirata (1976) have reported. Their results were obtained at only 12 and 16 diameters downstream where the flow was clearly not fully developed.

The ratio $\lambda=b_c/b_w$ has not been found to be constant in all jet, plume and transition regimes. From equations (4.3.7) and (4.5.3) $\lambda=1.275$ for a jet and from equations (4.4.12) and (4.6.5a) $\lambda=1.067$ for a plume. An average value of $\lambda=1.194$ has been derived from equations (4.4.11) and (4.6.5). In the following paragraph a plume definition will be introduced and its self similarity will be discussed.

5.2.2 Velocity and concentration decay in a buoyant jet

Figures 4.4.1 and 4.6.1 show the decay of the normalized mean and turbulent intensities decay for the velocity and concentration respectively along the axis of a buoyant jet versus the normalized distance from the jet origin $z/l_M$ . Equations (1.3.2b), (1.3.6b), (1.3.7b) and (1.3.10b) in Table 1.3.1 and these figures show clearly the jet - like or the plume - like behavior of a jet. More specifically, for a jet $\sqrt{M}/\overline{w}_c z$=constant and $SQ/z\sqrt{M}$=constant, $S=C_o/\overline{c}_c$ . Figures 4.4.1 and 4.6.1 show this for $z/l_M$ <1. The same figures for a plume show that $\sqrt{M}/\overline{w}_c z \sim (z/l_M)^{-2/3}$ and $SQ/z\sqrt{M} \sim (z/l_M)^{2/3}$ for $z/l_M$ >5. Therefore, regardless of the initial jet diameter, and for a known initial jet buoyancy length scale $l_M$ , one has that

if $z/l_M$ <1, jet - like flow

if $z/l_M$ >5, plume - like flow and

if 1<$z/l_M$ <5, transition from jets to plumes.

Jets with a slight initial buoyancy after 5 characteristic lengths $l_M$ therefore "forget" their origin and follow the plume laws as derived from dimensional arguments in Section 1.3.

5.2.3 Turbulence properties

The normalized rms values of w, u and c plotted versus $z/l_M$ follow the same decay laws as their corresponding mean values.This is shown clearly in Figures 4.4.1 and 4.6.1. The only difference between the mean and rms decay is the transition from jets to plumes is gradual for the mean values and abrupt for the rms values. The slope of the asymptotic power laws for $z/l_M$ <1 and $z/l_M$ >5 changes abruptly from 0 to -2/3 for the rms velocities around $z/l_M$ =3, and from 0 to 2/3 for the rms concentrations at about $z/l_M$ =8. This explains the fact that while

the normalized rms velocities do not vary from jets to plumes, the normalized rms concentration on the flow axis varies from 0.22 (jets) to 0.40 (plumes). By contrast the turbulence intensity of the velocity flow field is the same for jets and plumes. The normalized rms velocity profiles show a maximum longitudinal value of 0.23 and 0.15 for the radial velocity component at the jet axis. The rms normalized concentration profile in jets is quite different from plumes. In jets it is much wider than the profile of the rms axial velocity as shown in Figure 5.2.1. The centerline value is 0.22 and the maximum value 0.26 occurs at about r/z=0.10. In plumes the rms concentration profile is flat around the centerline with a maximum value of approximately 0.40, almost twice the jet centerline value of the rms concentration. Furthermore it is not much wider than the rms axial velocity profile as shown in Figure 5.2.2. From the above observations it is apparent that a passive contaminant is dispersed laterally much faster in momentum driven jets than in plumes. Also lateral spreading of the momentum flux is less than the spreading of the mean and rms concentration of a passive contaminant in momentum driven jets. In plumes the lateral spreading of the mean and turbulence intensities is very much the same for both velocities and concentrations but the relative intensity of the turbulent fluctuations of a passive contaminant is greater.

The self similarity in a jet can be observed in Figure 4.3.1 and was discussed in section 4.3.1 of chapter 4. The normalized turbulent shear stress profiles are not self similar in jets, as is shown in Figures 4.3.10 and 4.3.11. For $25<z/D<50$ the maximum value of the normalized shear stress varied from 0.003 to about 0.01. For $z/D>50$ it became constant with an average value of 0.013. For a plume for $z/l_M > 5$

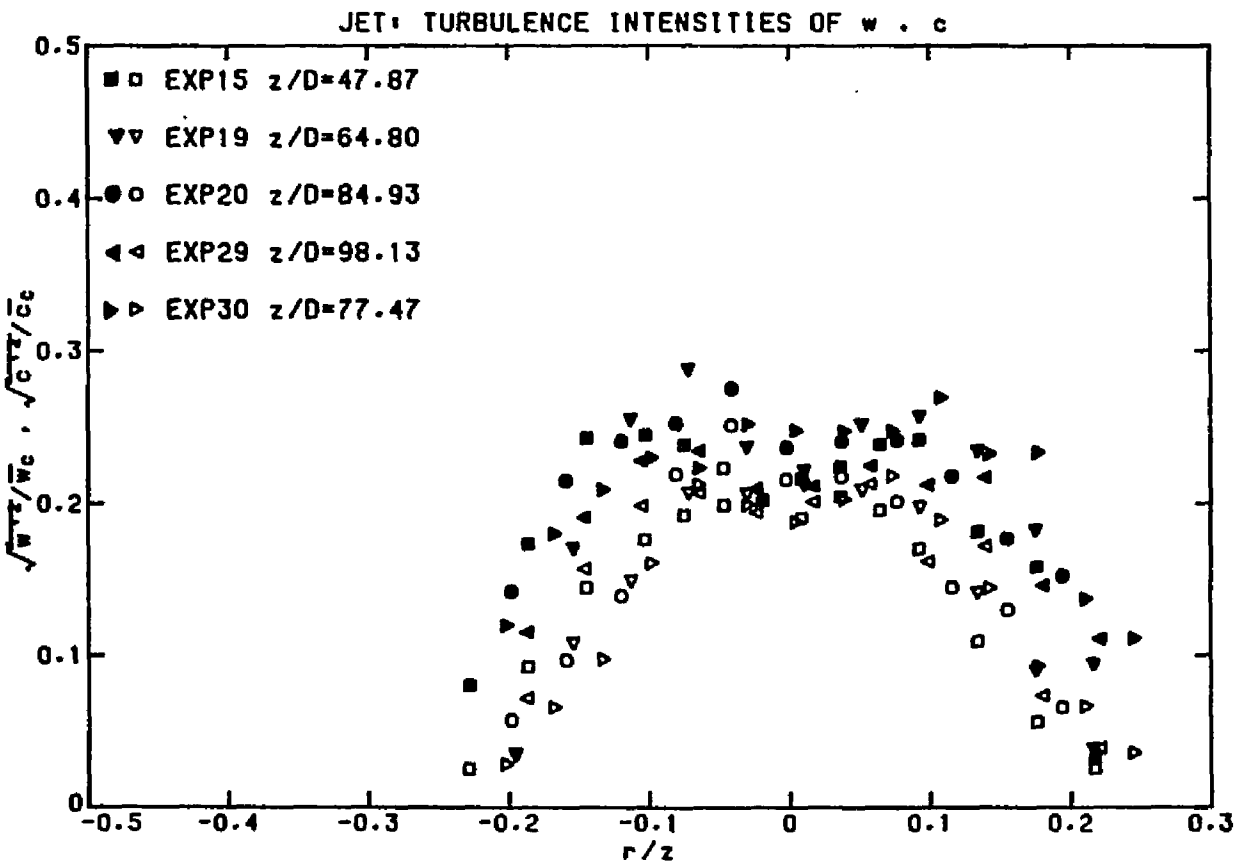


Figure 5.2.1. Profiles of the intensity of turbulent fluctuations across a turbulent jet.
(a) Closed symbols, concentration.
(b) Open symbols, axial velocity.

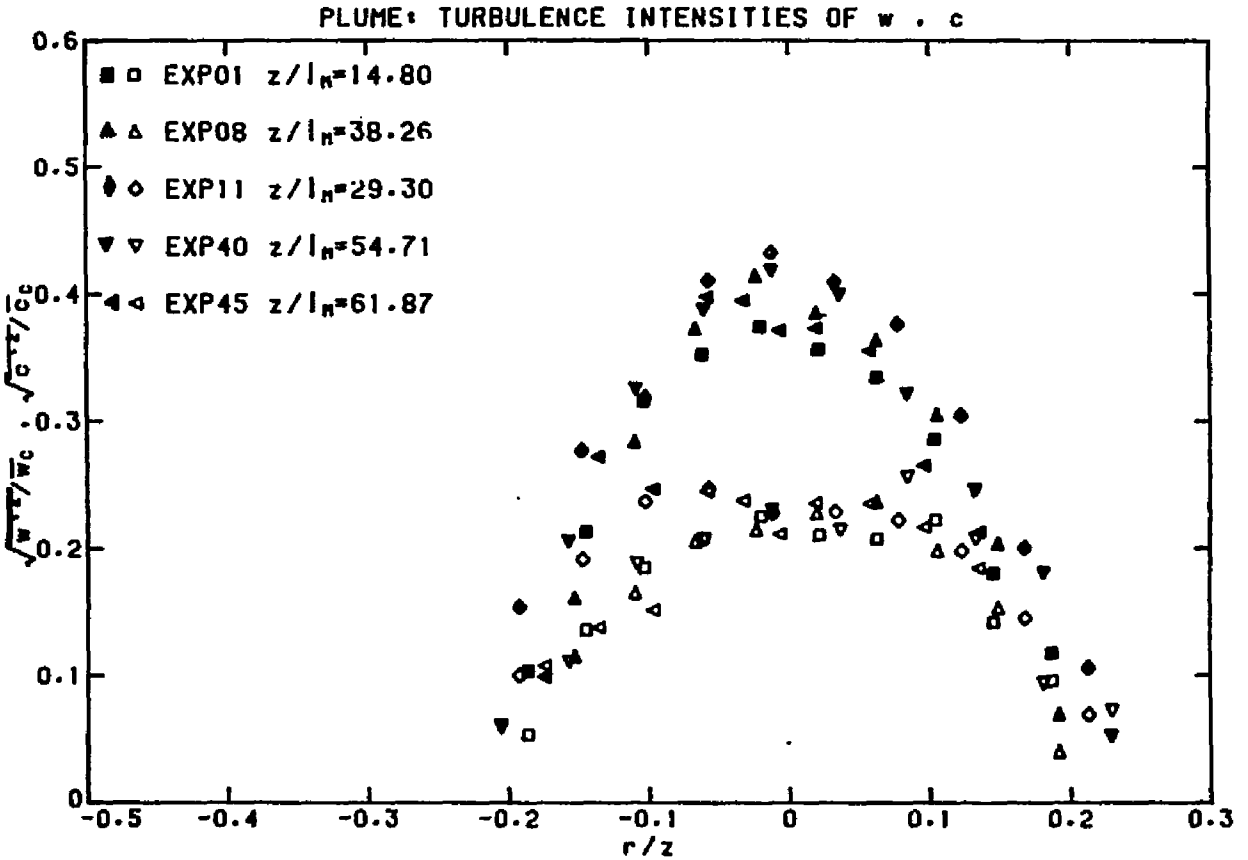


Figure 5.2.2. Profiles of the intensity of turbulent fluctuations across a turbulent plume.
(a) Closed symbols, concentration.
(b) Open symbols, axial velocity.

the normalized turbulence shear stress profile was self similar. This also proves that a plume can be assumed to become self similar after about 5 characteristic lengths $l_M$.

5.2.4 Turbulent flux of a tracer (or buoyancy)

It is shown clearly from Tables 1.4.1 and 1.4.2 that the jet parameters defined experimentally are found to be different by various investigators. This is true for the jet growth laws and mean and turbulence decay properties. Plume investigators have not reported consistent results concerning the plume growth and the decay of the mean and turbulence velocities and concentrations (see for example Rouse et al (1952), Nakagome and Hirata (1976) and George et al (1977)). Therefore an attempt to derive the contribution of the turbulence to the transport of a tracer by the jet

$$H_T = QC_o - \int_o^{b(z)} \overline{wc} 2\pi r dr$$

would probably lead to inaccurate estimates of the tracer transported by the jet turbulence for the case where w and c are chosen from different investigations with different experimental set - ups and initial jet conditions. In Tables 1.4.1 and 1.4.2 the reported mean values of velocity and concentration (temperature) along the jet axis are quite different for different experimental investigations. In the present investigation the fraction of the tracer transported by the jet turbulence was calculated as

$$H_T = \int_o^{b(z)} \overline{w'c'} 2\pi r dr$$

from the profile of $\overline{w'c'}$ which was measured directly. It was found to vary from 6% to 14% of the total (initial tracer transport) for a jet and from 15% to 20% for a plume. Kotsovinos (1975) reported much higher values for the 2-D plume (40%) and it is believed that the turbulent heat tranfer was overestimated. The longitudinal rms velocities measured by Kotsovinos (1975) were found to be much higher in the plume regime than those in a jet, something that was not observed in the present experiment. It is believed that the changes in the refractive index due to temperature fluctuations increased the noise level of the velocity signal resulting in higher turbulence velocities and therefore higher velocity - temperature correlations.

The turbulence transport term $\overline{w'c'}$ therefore cannot be neglected in the integration of the time averaged equations of motion and energy, especially in plumes where relatively high values were measured. In Section 4.3.4 it was also shown that neglecting the contribution of the axial turbulence intensities in the momentum flux equation underestimated by about 15% the momentum flux calculated from the mean velocity profile.

5.2.5 The mass and momentum balance in a buoyant jet

In Section 4.9.2 the constants to the equations (1.3.8a) and (1.3.9a) were estimated to be $b_2'=0.290$ and $b_3'=0.140$ respectively for the momentum and the mass transported by a plume. Substituting the equations (1.3.8a) and (1.3.9a) into the expressions for the plume Richardson number and the plume growth coefficient

$$R_p = \frac{\mu B^{1/2}}{m^{5/4}}, \quad c_p = \frac{\mu}{z m^{1/2}}$$

respectively one determines the relations $R_p = b_3 b_2^{-5/4}$ and $c_p = b_3/b_2^{1/2}$. Substituting $b_2$ and $b_3$ into these relations one finds that $R_p = 0.658$ and $c_p = 0.260$. The value $c_p = 0.260$ is in agreement with the measured average growth parameter $c_p = 0.271$ for jets, plumes and transition. The plume Richardson number is lower than the value 0.716 estimated in Section 4.8.1. It was mentioned before that the mean concentrations were overestimated for both, jets and plumes. Again using the results of the preliminary work by Papanicolaou and List (1983) from temperature measurements in plumes i.e. $SQ/z\sqrt{M} = 0.09$ instead of 0.07 one has that

$$R_p = (0.716) \left(\frac{0.07}{0.09}\right)^{\frac{1}{2}} = 0.631$$

a value that agrees with that above. Again dimensional arguments and Figure 4.8.1 show that the plume Richarson number takes a constant value for $z/l_M > 5$. Thus it is obvious that a buoyant jet becomes plume for $z/l_M > 5$ or when the local Richardson number takes a limiting value of about 0.630.

At this point some remarks have to be made about the definition of a plume. If the buoyancy length scale is chosen to be $l_M = D$, where D is the initial plume diameter, then the initial Richardson number $R_o$ of the plume becomes $R_o = 1$. Hence the local plume Richardson number has to decay continuously in the initial plume regime until the limiting value 0.63 is reached. High initial Richardson numbers ($R_o > 0.630$) could cause instability of the flow at the jet exit resulting in ambient fluid entrainment through the jet orifice that would adjust the initial Richardson number to its limiting value 0.630 by reducing the effective jet diameter (increasing the jet exit velocity). This flow pattern was

observed in the laboratory when a disturbance was introduced to a jet with initial Richardson number close to unity.

Finally the jet and plume entrainment coefficients were found to be 0.0545 and 0.0875 respectively. Their ratio $a_p/a_j = 1.635 \cong 5/3$ as mentioned in Section 1.2 of the introduction. All the results are summarized in Table 5.2.1.

## 5.3 Conclusions

The main conclusion from this investigation is that the nature of flows in jets and plumes is quite different because of the different nature of the forces which act upon the fluid. A jet is maintained by continuous input of momentum flux and a plume by continuous input of buoyancy flux at its origin. This difference explains why the decay of the mean and turbulence characteristics of the jet flow field is quite different in these two flow patterns. However the shape, growth and transverse profiles of the mean and turbulence parameters are quite similar for both jets and plumes.

The dimensional arguments made in section 1.3 of the present work were verified experimentally. It was shown that a jet becomes self-similar after certain initial diameters downstream as found in the past by Wygnanski and Fiedler (1969) and Birch et al. (1978). Velocity and concentration measurements were performed in the plume flow field up to about 80 characteristic plume diameters ($z/l_M$). A plume became self similar after it had reached a limiting constant value of the local Richardson number 0.630, or for $z/l_M > 5$. A rigorous definition of the plume regime was given. This was not based upon the initial plume diameter which is eventually lost by the plume, but upon a length scale defined by a ratio of the initial buoyancy and momentum input. It was

JET AND PLUME PARAMETERS

| Parameter | JETS | PLUMES |
|---|---|---|
| $\frac{z}{l_M}$ | <1 | >5 |
| $\frac{\sqrt{M}}{\bar{w}_c z}$ | 0.132 | $0.260(z/l_M)^{-2/3}$ |
| $\frac{\sqrt{\overline{w_c'^2}}}{\bar{w}_c}$ | 0.230 | 0.230 |
| $\frac{\sqrt{\overline{u_c'^2}}}{\bar{w}_c}$ | 0.150 | 0.150 |
| $\max \frac{\overline{w'u'}}{\bar{w}_c^2}$ | 0.015 | 0.016 |
| $b_w(z)$ | 0.109 z | 0.105 z |
| $\frac{S\,Q}{z\sqrt{M}}$ | measured 0.147 corrected 0.165 | measured $0.07\left(\frac{z}{l_M}\right)^{2/3}$ corrected $0.09\left(\frac{z}{l_M}\right)^{2/3}$ |
| $\frac{\sqrt{\overline{c_c'^2}}}{\bar{c}_c}$ | 0.220 | 0.400 |
| $b_c(z)$ | 0.139 z | 0.112 z |
| $\lambda = \frac{b_c}{b_w}$ | 1.275 | 1.067 |

Table 5.2.1. Summary of the measured jet and plume parameters in the present experimental investigation.

JET AND PLUME PARAMETERS (continued)

| Parameter | JETS | PLUMES |
|---|---|---|
| $\frac{\overline{w'c'}}{\bar{w}_c \bar{c}_c}$ | centerline 0.020; peak 0.024 | centerline 0.030-0.040; peak 0.040-0.050 |
| $\frac{\overline{u'c'}}{\bar{w}_c \bar{c}_c}$ | centerline 0.00; peak 0.010 | centerline 0.00; peak 0.015-0.025 |
| $\frac{\int \overline{w'c'} 2\pi r dr}{Q\ C_o}$ | 6% - 14%<br>use 7% | 15% - 20%<br>use 16% |
| $\frac{\mu(z)}{Q}$ | $0.284 \frac{z}{D}$ or $0.252 \frac{z}{l_Q}$ | $0.140 \frac{B^{1/3}}{Q} z^{5/3}$ |
| $\frac{m(z)}{M}$ | 0.960 | $0.290 \left(\frac{z}{l_M}\right)^{4/3}$ |
| $\frac{m_T(z)}{m(z)}$ | 0.150 | 0.150 |
| $c_j$ , $c_p$ | $c_j = 0.252$ | $c_p = 0.260$ |
| C | 0.271 | |
| R(z) | $0.286 \frac{z}{l_M}$ | measured 0.716; corrected 0.631 |
| $a_e$ | $a_j = 0.0545$ | $a_p = 0.0875$ |

Table 5.2.1 (continued).

also shown that for both jets and plumes the mean concentration profile was consistently wider than the mean velocity profile, and that the growth rates were slightly lower in the plume case.

Previous mathematical models describing turbulent plume motion have assumed a constant entrainment coefficient and have neglected the contribution of turbulence to the longitudinal transport of momentum and tracer in the averaged integrated equations of motion. The results of this investigation have shown that the entrainment coefficient for a plume is very close to 5/3 times as great as that for a jet, indicating that some allowance for jet-to-plume transition should be made in the description of buoyant jets. The measurements of turbulent fluxes of momentum and tracer indicate that an allowance in plumes of 10% for turbulent transport of momentum, and 20% for turbulent transport of tracer are reasonable. Future mathematical models of the evolution of mean transport in buoyant jets should therefore consider the longitudinal transport terms $\overline{w'c'}$ and $\overline{w'^2}$ in the equations of motion.

A table of recommended formulae for the asymptotic behavior of jets and plumes has been developed. These formulae, which describe the evolution of the dilution, velocity, mean concentration and relative root-mean square turbulence quantities, should be useful in practical applications of the results to engineering problems related to the design of wastewater and other disposal systems that depend upon jet and plume induced dilutions.

The experimental work performed has indicated that it is possible to measure turbulent fluxes of momentum and tracers using a technique combining laser-Doppler velocimetry with laser-induced fluorescence based concentration measurements. However, it is apparent that the

laser-induced fluorescence technique needs further refinement in that the system employed here clearly overestimated the mean concentration of fluorescing tracer. The cause of this error, which was corrected for in the presentation of the results, appears to lie in excess light collected by the receiving optics from scattering centers within the flow field other than at the focal point of the laser-Doppler beams. It seems likely also that this overestimation may have been contributed to by the adsorption of fluorescing dye onto the small organic scattering particles suspended in the flow and necessary for operation of the laser-Doppler system. Future investigators using these techniques should carefully evaluate the above sources of possible error.

# REFERENCES

Abbiss, J.B., Bradbury, L.J.S., and Wright, M.P. (1975). Measurements on an axisymmetric jet using a photon correlator. In Proc. of the LDA Symposium, Copenhagen, 319-335.

Abraham, G. (1960). Jet diffusion in liquid of greater density. Proc. ASCE, J. Hyd. Div., 86, 1-13.

Abraham, G. (1963). Jet diffusion in stagnant ambient fluid. Delft Hyd. Lab., Publication No. 29.

Abraham, G. (1965). Entrainment principle and its restrictions to solve problems of jets. J. Hyd. Res., 3(2), 1-23.

Abraham, G. (1967). Jet with negative buoyancy in homogeneous fluid. J. Hyd. Res., 5(4), 235-248.

Adrian, R.J. and Goldstein, R.J. (1971). Analysis of a laser Doppler anemometer. J. Physics, E: Sci. Instruments, 4, 505-511.

Albertson, M.L., Dai, Y.B., Jensen, R.A., and Rouse, H. (1950). Diffusion of submerged jets. Trans. ASCE, 115, 639-664.

Antonia, R.A., Prabhu, A., and Stephenson, S.E. (1975). Conditionally sampled measurements in a heated turbulent jet. J. Fluid Mech., 72, 455-480.

Antonia, R.A. and Prabhu, A. (1976). Reynolds shear stress and heat flux balance in a turbulent round jet. J. AIAA, 14(2), 221-228.

Antonia, R.A., Chambers, A.J., and Hussain, A.K.M.F. (1980). Errors in simultaneous measurements of temperature and velocity in the outer part of a heated jet. Phys. of Fluids, 23(5), 871-874.

Batchelor, G.K. (1954). Heat convection and buoyancy effects on fluids. Quart. J. Roy. Met. Soc., 80, 339-358.

Batchelor, G. (1970). An Introduction to Fluid Dynamics. Cambridge University Press.

Bates, C.J. (1977). Laser Doppler anemometry measurements in water flows. J. Physics, E: Sci. Instruments, 10, 669-675.

Becker, H.A., Hottel, H.C., and Williams, G.C. (1965). Concentration intermittency in jets. Tenth Symposium (Int.) on Combustion, The Comb. Institute, 1253-1263.

Becker, H.A., Hottel, H.C., and Williams, G.C. (1967). On the light-scattering technique for the study of turbulence and mixing. J. Fluid Mech., 30, 259-284.

Becker, H.A., Hottel, H.C., and Williams, G.C. (1967). The nozzle-fluid concetration field of the round turbulent free jet. J. Fluid Mech., 30, 285-303.

Bendat, J.S. and Piersol, A.G. (1971). Random Data: Analysis and Measurement Procedures. Wiley - Interscience, New York, London, Sydney, Toronto.

Bilger, R.W., Antonia, R.A., and Sreenivasan, K.R. (1976). Determination of intermittency from the probability density function of a passive scalar. Phys. of Fluids, 19(10), 1471-1474.

Birch, A.D., Brown, D.R., Dodson, M.G., and Thomas, J.R. (1978). The turbulent concentration field of a methane jet. J. Fluid Mech., 88,431-449.

Boguslawski, L. and Popiel, C.O. (1979). Flow structure of the free round turbulent jet in the initial region. J. Fluid Mech., 90(3), 531-539.

Brock, R.R. (1970). Power law solutions for vertical plumes. Proc.

ASCE, J. Hyd. Div., 96(9), 1803-1817.

Brooks, N.H. and Koh, R.C.Y. (1965). Discharge of Sewage Effluent from a Line Source into Stratified Ocean. XI Congr. Int. Assoc. Hydraul. Res., Paper No. 2.19.

Brooks, N.H. (1972). Dispersion in Hydrologic and Coastal Environments. W.M. Keck Laboratory of Hydraulics and Water Resources, Report No. KH-R-29, California Institute of Technology.

Bruun, H.H. (1977). A time-domain analysis of the large-scale flow structure in a circular jet: Part I - Moderate Reynolds number. J. Fluid Mech., 83, 641-671.

Bruun, H.H. (1979). A time-domain evaluation of the large-scale flow structure in a turbulent jet. Proc. Roy. Soc. London, A367, 193-218.

Cederwall, K. (1971). Buoyant slot jets into stagnant or flowing environments. Tech. Rept. KH-R-25, W.M. Keck Laboratory of Hydraulics and Water Resources, California Inst. of Technology, Pasadena, California.

Cederwall, K. (1975). Gross parameter solutions of jets and plumes. Proc. ASCE, J. Hyd. Div., 101(HY5), 489-509.

Chen, J.C. and Rodi, W. (1980). Vertical turbulent buoyant jets: A review of experimental data. Pergamon Press, Oxford.

Chevray, R. and Tutu N.K. (1978). Intermittency and preferential transport of heat in a round jet. J. Fluid Mech., 88, 133-160.

Cleeves, V. and Boelter, L.M.K. (1947). Isothermal and non-isothermal air-jet investigations. Chem. Eng. Progress, 43(3), 123-134.

Corrsin, S. (1943). Investigation of flow in an axially symmetric heated jet of air. NACA Wartime Rept. W-94.

Corrsin, S. and Uberoi, M.S. (1950). Further experiments on the flow and heat transfer in a heated turbulent air jet. NACA Rept. 998.

Corrsin, S. and Kistler, A.L. (1955). Free stream boundaries of turbulent flows. NACA Rept. 1244.

Crapper, P.F. (1977). Forced plume characteristics. Tellus, 29, 470-475.

Crow, S.C. and Champagne, F.H. (1971). Orderly structure in jet turbulence. J. Fluid Mech., 48, 547-591.

Davies, P.O.A.L., Fisher, M.J., and Barratt, M.J. (1962). The characteristics of the turbulence in the mixing region of a round jet. J. Fluid Mech., 15, 337-367.

Drain, L.E. (1980). The Laser Doppler Technique. John Wiley & Sons.

Drexhage, K.H. (1976). Structure and properties of laser dyes. In Topics in Appl. Physics, 1, Springer-Verlag, New York, Heidelberg, Berlin.

Durst, F., Melling, A., and Whitelaw, J.H. (1976). Principles and Practice of Laser-Doppler Anemometry. Academic Press, London.

Fan, L.N. (1967). Turbulent buoyant jets into stratified or flowing ambient fluids. Report No. KH-R-15, W.M. Keck Laboratory of Hydraulics and Water Resources, California Inst. of Technology, Pasadena, California.

Fan, L.N. and Brooks, N.H. (1969). Numerical solutions of turbulent buoyant jet problems. Report No. KH-R-18, W.M. Keck Laboratory of Hydraulics and Water Resources, California Inst. of Technology, Pasadena, California.

Fischer, H.B., List, E.J., Koh, R.C.Y., Imberger, J., and Brooks, N.H. (1979). Mixing in Inland and Coastal waters. Academic Press, New York.

Forstall, W. and Gaylord, E.W. (1955). Momentum and mass transfer in a submerged water jet. J. Appl. Mech., 22, 161-164.

Fox, D.G. (1970). Forced plume in a stratified fluid. J. Geophys. Res., 75, 6818-6835.

Gartrell, G.Jr. (1978). A signal processor for a laser-Doppler velocimeter. Tech. Memo. 78-5, W.M. Keck Laboratory of Hydraulics and Water Resources, California Inst. of Technology, Pasadena, California.

Gartrell, G.Jr. (1979). Studies on the mixing in a density-stratified shear flow. Report No. KH-R-39, W.M. Keck Laboratory of Hydraulics and Water Resources, California Inst. of Technology, Pasadena, California.

George, W.K., Alpert, R.L., and Tamanini, F. (1977). Turbulence measurements in an axi-symmetric buoyant plume. Int. J. Heat Mass Transfer, 20, 1145-1154.

Germeles, A.E. (1975). Forced plumes and mixing of liquids in tanks. J. Fluid Mech., 71, 601-623.

Gibson, M.M. (1963). Spectra of turbulence in a round jet. J. Fluid Mech., 15, 161-173.

Gibson, C.H. and Schwarz, W.H. (1963). Detection of conductivity fluctuations in a turbulent flow field. J. Fluid Mech., 16, 357-364.

Gibson, C.H. and Schwarz, W.H. (1963). The universal equilibrium spectra of turbulent velocity and scalar fields. J. Fluid Mech.,

16, 365-384.

Goldstein, R.J. and Andrian, R.J. (1971). Measurement of fluid velocity gradients using laser - Doppler techniques. Rev. Sci. Instruments, 42(9), 1317-1320.

Goodman, J., Abuaf, N., and Laufer, G. (1974). Investigation of the velocity field in a free convection plume using a laser - Doppler velocity measuring technique. Israel J. Technology, 12, 198-205.

Grandmaison, E.W., Rathgeber, D.E., and Becker, H.A. (1977). Some characteristics of concentration fluctuations in free turbulent jets. In Preprints, Symposium on Turbulent Shear Flows, Penn. State Univ., 15.21-15-29.

Hayashi, T. and Ito, M. (1974). Initial dilution of effluent discharging into stagnant sea water. Int. Disch. of Sewage from Sea Outfalls Symposium, 253-264.

Hill, B.J. (1972). Measurement of local entrainment rate in the initial region of axisymmetric turbulent air jets. J. Fluid Mech., 51, 773-779.

Hinze, J. (1959). Turbulence. McGraw-Hill Company.

Hinze, J.O. and van der Hegge Zijen, B.G. (1949). Transfer of heat and matter in the turbulent mixing zone of an axially symmetric jet. Appl. Sci. Res., A1, 435-461.

Hunt, J.R. (1978). Private communication (see Gartrell (1979)).

Hussain, A.K.M.F. and Zedan, M.F. (1978). Effects of the initial condition on the axisymmetric free shear layer: Effects of the initial momentum thickness. Phys. of Fluids, 21(7), 1100-1112.

Kiser, K.M. (1963). Material and momentum transport in axisymmetric turbulent jets of water. AIChe J., 9, 386-390.

Koh, R.C.Y. and Brooks, N.H. (1975). Fluid mechanics of waste-water disposal in the ocean. Ann. Rev. Fluid Mech., 7, 187-211.

Kotsovinos, N.E. (1975). A study of the entrainment and turbulence in a plane jet. Report No. KH-R-32, W.M. Keck Laboratory of Hydraulics and Water Resources, California Inst. of Technology, Pasadena, California.

Kotsovinos, N.E. (1976). A note on the spreading rate and virtual origin of a plane turbulent jet. J. Fluid Mech., 77, 305-311.

Kotsovinos, N.E. and List, E.J. (1976). Turbulent buoyant jets. In Proc. 1976 ICHMT Seminar on Turbulent Buoyant Convention, Hemisphere Publishing, 349-359.

Kotsovinos, N.E. and List, E.J. (1977). Plane turbulent buoyant jets: Part 1- Integral properties. J. Fluid Mech., 81, 25-44.

Kotsovinos, N.E. and List, E.J. (1977). Plane turbulent buoyant jets: Part 2- Turbulence structure. J. Fluid Mech., 81, 45-62.

Kotsovinos, N.E. (1978). Dilution in a vertical round buoyant jet. Proc. ASCE, J. Hyd. Div., 795-798.

Landau, L.D. and Lifshitz, E.M. (1975). Fluid Mechanics. Pergamon Press.

Lassiter, L.W. (1957). Turbulence in small air jets at exit velocities up to 705 feet per second. J. Appl. Mech., 24, 349-354.

Lau, J.C., Morris, P.J., and Fisher, M.J. (1979). Measurements in subsonic and supersonic free jets using a laser velocimeter. J. Fluid Mech., 93, 1-27.

Laufer, J. (1975). New trends in experimental turbulence research. Ann. Rev. Fluid Mech., 7, 307-326.

Launder, B.E. and Spalding, D.B. (1972). Mathematical Models of Turbulence. Academic Press, London and New York.

List, E.J. and Imberger, J. (1973). Turbulent entrainment in buoyant jets. Proc. ASCE, J. Hyd. Div., 99, 1461-1474.

List, E.J. and Imberger, J. (1975). Closure of discussion to: Turbulent entrainment in buoyant jets and plumes. Proc. ASCE, J. Hyd. Div., 101, 617-620.

List, E.J. (1982). Turbulent jets and plumes. Ann. Rev. Fluid Mech., 14, 189-212.

Lumley, J.L. (1971). Explanation of thermal plume growth rates. Phys. of Fluids, 14, 2537-2538.

Magrab, E.B. and Blomquist, D.S. (1971). Measurement of Time Varying Phenomena: Fundamentals and applications. Wiley Interscience, New York.

McDougall, T.J. (1979). On the elimination of the refractive index variations in turbulent density-stratified liquid flows. J. Fluid Mech., 93, 83-96.

Middleton, J.H. (1975). The asymptotic behaviour of a starting plume. J. Fluid Mech., 72, 753-771.

Miller, D.R. and Comings, E.W. (1957). Static pressure distribution in the free turbulent jet. J. Fluid Mech., 3, 1-16.

Mizushina, T., Ogino, F., Veda, H., and Komori, S. (1979). Application of laser-Doppler velocimetry to turbulence measurement in non-isothermal flow. Proc. Roy. Soc. London, A366, 63-79.

Morton, B.R., Taylor, G.I., and Turner, J.S. (1956). Turbulent gravitational convection from maintained and instantaneous sources. Proc. Roy. Soc. London, A234, 1-23.

Morton, B.R. (1957). Buoyant plumes in a moist atmosphere. J. Fluid Mech., 2, 127-144.

Morton, B.R. (1959). Forced plumes. J. Fluid Mech., 5, 151-163.

Morton, B.R. (1971). The choice of conservation equations for plume models. J. Geophys. Res., 76(30), 7409-7416.

Nakagome, H. and Mirata, M. (1976). The structure of turbulent diffusion in an axisymmetric thermal plume. Proc 1976 ICHMT Seminar on Turbulent Buoyant Convection, Hemisphere Publishing, 361-372.

Nakatani, N., Hanioka, N., Konishi, T., and Yamada, T. (1977). Optimization of the receiving optical system in the laser - Doppler velocimeter for reduction of the sampling volume. J. Physics, E: Sci. Instruments, 10, 846-847.

Ooms, G. and Wicks, M. (1975). Concentration fluctuations in a turbulent jet. Appl. Sci. Research, 30(5), 381-399.

Papanicolaou, P.N. and List, E.J. (1983). Statistical and spectral properties of a heated round turbulent buoyant jet. Proc. ASCE, Eng. Mech. Specialty Conference, Purdue University, West Lafayette, Indiana (See Appendix A).

Priestley, C.H.B. and Ball, F.K. (1955). Continuous convection from an isolated source of heat. Quart. J. Roy. Met. Soc., 81(348), 144-157.

Pryputniewicz, R.J. and Bowley, W.W. (1975). An experimental study of vertical buoyant jets discharged into water of finite depth. Trans. ASME, 97(2), 274-281.

Rajaratnam, N. (1976). Turbulent Jets. Elsevier Scientific Publishing Company.

Ramaprian, B.R. and Chandrasekhara, M.S. (1983). Study of vertical plane turbulent jets and plumes. IIHR Report No. 257, Iowa Inst. of Hydraulic Research.

Rao, V.K. and Brzustowski, T.A. (1969). Preliminary hot-wire measurements on free-convection zones over model fires. Comb. Sci. Tech., 1, 171-180.

Ribeiro, M.M. and Whitelaw, J.H. (1980). The structure of turbulent jets. Proc. Roy. Soc. London, A370, 281-301.

Ricou, F.P. and Spalding, D.B. (1960). Measurements of entrainment by axisymmetrical turbulent jets. J. Fluid Mech., 11, 21-32.

Rodi, W. (1980). Turbulence models and their applications in hydraulics: A state of the art review. Delft, The Netherlands, IAHR.

Rosenweig, R.E., Hottel, H.C., and Williams, G.C. (1961). Smoke scattered light measurement of turbulent concentration fluctuations. Chem. Eng. Sci., 15, 111-129.

Rosler, R.S. and Bankoff, S.G. (1963). Large scale turbulence characteristics of a submerged water jet. AIChe J., 9(5), 672-676.

Rouse, H., Yih, C.S., and Humphreys, H.W. (1952). Gravitational convection from a boundary source. Tellus, 4, 201-210.

Saffman, P.G. (1970). A model of inhomogeneous turbulent flow. Proc. Roy. Soc. London, A317, 417-433.

Schlichting, H. (1968). Boundary Layer Theory. McGraw-Hill, Sixth Edition.

Scorer, R.S. (1957). Experiments on convection of isolated masses of buoyant fluid. J. Fluid Mech., 2, 583-594.

Scorer, R.S. (1959). The behaviour of chimney plumes. Int. J. Air Pollution, 1, 198-220.

Sforza, P.M. and Mons, R.F. (1978). Mass, momentum and energy transport in turbulent free jets. Int. J. Heat Mass Transfer, 21, 371-384.

Shaughnessy, E.J. and Morton, J.B. (1977). Laser light-scattering measurements of particle concentration in a turbulent jet. J. Fluid Mech., 80, 129-148.

Sreenivasan, K.R., Antonia, R.A., and Britz, K. (1979). Local isotropy and large structures in a heated turbulent jet. J. Fluid Mech., 94, 745-775.

Stevenson, W.H. (1970). Optical frequency shifting by means of a rotating diffraction grating. Applied Optics, 9(3), 649-652.

Stevenson, W.H., Thompson, H.D., and Roesler, T.C. (1983). Direct measurement of laser velocimeter bias errors in a turbulent flow. J. AIAA, 20, 1720-1723.

Sunavala, P.D., Hulse, C., and Turing, M.W. (1957). Mixing and combustion in free and enclosed turbulent jet diffusion flumes. Combust. Flame, 1, 79-193.

Taylor, G.I. (1932). The transport of vorticity and heat through fluids in turbulent motion. Proc. Roy. Soc. London, A135, 685-702.

Taylor, G.I. (1958). Flow induced by jets. J. Aerosp. Sci., 25, 464-465.

Tennekes, H. and Lumley, J.L. (1972). A First Course in Turbulence. MIT Press.

Tollmien, W. (1926). Die Berechung Turbulenter Ausbreitungsvorgange.

ZAMM 6, 468-478, (NACA TM 1085,1945).

Townsend, A.A. (1966). The mechanism of entrainment in free turbulent flows. J. Fluid Mech., 26, 689-715.

Townsend, A.A. (1970). Entrainment and the structure of turbulent flow. J. Fluid Mech., 41, 13-46.

Townsend, A.A. (1976). The structure of turbulent shear flows. Cambridge Univ. Press, Second Edition.

Turner, J.S. (1962). The "starting plume" in neutral surroundings. J. Fluid Mech., 13, 356-368.

Turner, J.S. (1963). The motion of buoyant elements in turbulent surroundings. J. Fluid Mech., 16, 1-16.

Turner, J.S. (1966). Jets and plumes with negative or reversing buoyancy. J. Fluid Mech., 26, 779-792.

Turner, J.S. (1969). Buoyant plumes and thermals. Ann. Rev. Fluid Mech., 1, 29-44.

Turner, J.S. (1973). Buoyancy Effects of Fluids. Cambridge University Press.

Venkataramani, K.S., Tutu, N.K., and Chevray, R. (1975). Probability distributions in a round heated jet. Phys. of Fluids, 18(11), 1413-1420.

Watrasiewicz, B.M. and Rudd, M.J. (1976). Laser - Doppler Measurements. Butterworth, London.

White, D.A. (1967). Velocity measurements in axisymmetric jets of dilute polymer solutions. J. Fluid Mech., 28, 195-204.

Wilson, R.A.M. and Danckwerts, P.V. (1964). Studies in turbulent mixing II: A hot air jet. Chem. Eng. Sci., 19, 885-895.

Wygnanski, I. and Fiedler, H. (1969). Some measurements in the

self-preserving jet. J. Fluid Mech., 38, 577-612.

Wygnanski, I. and Gutmark, E. (1971). Lateral motion of the two-dimensional jet boundaries. Phys. of Fluids, 14(7), 1309-1311.

Yih, C.S. (1953). Free convection due to boundary sources. Proc. of the 1st Symposium of the Use of Models in Geoph. Fluid Dynamics, Fluid Models in Geophysics R.R. Long, ed.

Yih, C.S. (1977). Turbulent buoyant plumes. Phys. of Fluids, 20(8), 1234-1237.

Zeldovich, Y.B. (1937). Limiting laws for turbulent flows in free convection. Zh. Eksp. Teoret. Fiz., 7(12), 1463.

Zimin, V.D. and Frik, P.G. (1977). Averaged temperature fields in asymmetrical turbulent streams over localized heat sources. Izv. Akad. Nauk. SSSR, Mekhanika Zhidkosti Gaza, 2, 199-203.

# APPENDIX A

## STATISTICAL AND SPECTRAL PROPERTIES OF A HEATED ROUND TURBULENT BUOYANT JET

# STATISTICAL AND SPECTRAL PROPERTIES OF A HEATED ROUND TURBULENT BOUYANT JET

P. Papanicolaou and E.J. List*

Presented at the ASCE Engineering Mechanics Specialty Conference, Purdue University, West Lafayette, Indiana, 23-25 May 1983.

A round vertical heated water jet discharging into a body of water of uniform density is the subject of the present experimental work. Interest is centered on the description of a tracer (temperature) which is transported by the jet fluid, and in particular the jet growth laws, temperature decay laws and turbulent spectral properties. Temperatures were measured using fast response thermistor probes (characteristic time was found to be 0.014 seconds) up to 40 jet diameters downstream from the jet orifice. The Reynolds number at the exit of the jet varied from 3700 to 17000. The flow patterns examined were: (a) pure momentum jet, dirven by continuous addition of momentum at the source, (b) pure plume, where the flow was mainly driven by the buoyancy due to the density difference between the jet and ambient fluid, and (c) buoyant jet were the flow was in transition from jet to plume. These flows are characterized by the ratio of the axial distance from the jet orifice z to a length scale $l_M=M^{3/4}/B^{1/2}$ where M is the specific momentum flux of the jet and B the specific buoyancy flux.

The relationships of the mean, rms and maximum temperature to the dimensionless distance $z/l_M$ are shown in Figure 1. If $S=\Delta T_o/\Delta T_c$ is the mean dilution along the jet centerline then dimensional arguments lead

*W. M. Keck Laboratory of Hydraulics and Water Resources, California Institute of Technology, Pasadena, CA 91125.

to $SQ/(zM^{1/2})$ = constant with $z/l_M \ll 1$ (momentum dominant) or to $SQ/(z^{5/3}B^{1/3})$ = constant with $z/l_M \gg 1$ (buoyancy dominant). For $z/l_M \ll 1$ Figure 1 shows that for jet-like flow $SQ/(zM^{1/2})=0.165$, while for $z/l_M \gg 5$ (plume-like behavior) $SQ/(z^{5/3}B^{1/3})=0.090$. Fischer et al. [7] give the values 0.175 and 0.106, respectively. In the region $1<z/l_M<5$ there is a transition from momentum jets to plumes. Therefore knowledge of the initial B and M at the jet orifice enables one to predict how the flow pattern changes with z. From Figure 1 it can also be seen that the minimum and "rms" dilutions follow the same trend as the mean. For the pure jet case the mean temperature profile $\Delta T/\Delta T_c$ (Figure 2(a)) is found to be $\Delta T/\Delta T_c=\exp[-75(r/z)^2]$. The turbulent intensities (Figure 2(b)) $\sqrt{\overline{(\Delta T')^2}}/\Delta T_c$ have a value of 0.15 to 0.18 on the centerline and a peak value of 0.20 to 0.25 at $r/z=0.07$. These results are in agreement with those found by Antonia et al. [2] and [3], Becker et al. [4], Birch et al. [5], Chevray and Tutu [6] and Shaughnessy and Morton [12]. For the pure plume case (Figures 3(a) and 3(b)) $\Delta T/\Delta T_c=\exp[-80(r/z)^2]$ while the turbulent intensities have a maximum value of 0.40 at the centerline. These results agree with those given by Zimin and Frik [13] and George, Alpert and Tamanini [8]. The 1/e (0.37) widths are found to be 0.127 and 0.111 for jets and plumes respectively, results which agree with the averages given by Fischer et al. [7].

The probability density function (pdf) of temperature fluctuations for both jets and plumes were calculated and plotted versus $(T-T_a)/\Delta T_c$ for all radial positions r/z, as is shown in Figures 4(a) and 4(b). Exponential curves can be fitted in both cases for r/z=0.0 to 0.1. However, in the region $r/z>0.1$ the distributions become asymmetrical indicating a highly intermittent region. At the jet boundaries the pdf

approaches the form of a delta function. Typical power spectra estimates are shown in Figures 5(a) and 5(b), for r/z=0.00 and 0.05 respectively, at an axial distance z/D=53.33 and for $z/l_M$=1.52 (buoyant jet region). In both figures it is made clear that for frequencies 1 to 10 Hz the turbulence intensity decays following the -5/3 logarithmic law with the frequency, while for higher frequencies a -3 slope is apparent. Furthermore, the spectral power decays by two orders of magnitude in the region from 1 to 10 Hz. The similarity of the two spectra is a further indication that the intermittency has to be the same for $0.0<r/z<0.05$.

ACKNOWLEDGEMENT

The authors gratefully acknowledge the financial support of the National Science Foundation through Grant No. CEE-8117272.

REFERENCES

[1] Albertson, M.L., Dai, Y.B., Jensen, R.A., and Rouse, H. (1950). Diffusion of submerged jets. Trans. ASCE, 115, 639-664.

[2] Antonia, R.A., Prabhu, A., and Stephenson, S.E. (1975). Conditionally sampled measurements in a heated turbulent jet. J. Fluid Mech., 72, 455-480.

[3] Antonia, R.A., Chambers, A.J., and Hussain, A.K.M.F. (1980). Errors in simultaneous measurements of temperature and velocity in the outer region of a heated jet. Phys. Fluids, 23(5), 871-874.

[4] Becker, H.A., Hottel, H.C., Williams, G.C. (1967). The nozzle fluid concentration field of the round turbulent free jet. J. Fluid Mech., 30(2), 285-303.

[5] Birch, A.D., Brown, D.R., Dodson, M.G., Thomas, J.R. (1978). The turbulent concentration field of a methane jet. J. Fluid Mech., 88(3), 431-449.

[6] Chevray, R. and Tutu, N.K. (1978). Intermittency and preferential transport of heat in a round jet. J. Fluid Mech., 88(1), 133-160.

[7] Fischer, H.B., List, E.J., Koh, R.C.Y., Imberger, J., and Brooks, N.H. (1979). Mixing in Inland and Coastal Waters. Academic Press, New York.

[8] George, W.K., Alpert, R.L., and Tamanini, F. (1977). Turbulence measurements in an axi-symmetric buoyant plume. Int. J. Heat Mass Transfer, 20, 1145-1154.

[9] Hinze, J.O. and van der Hegge-Zijnen, B.G. (1949). Transfer of heat and matter in the turbulent mixing zone of an axially symmetric jet. Appl. Sci. Res., A1, 435-461.

[10] Kotsovinos, N.E. (1975). A study of the entrainment and turbulence in a plane jet. Report No. KH-R-32, California Institute of Technology, Pasadena, California.

[11] List, E.J. (1982). Turbulent jets and plumes. Ann. Rev. Fluid Mech., 14, 189-212.

[12] Shaughnessy, E.J. and Morton, J.B. (1977). Laser light-scattering measurements of particle concentration in a turbulent jet. J. Fluid Mech., 80(1), 129-148.

[13] Zimin, V.D. and Frik, P.G. (1977). Averaged temperature fields in asymmetrical turbulent streams over localized heat sources. Izv. Akad. Nauk. SSSR, Mekhanika Zhidkosti Gaza, 2, 199-203.

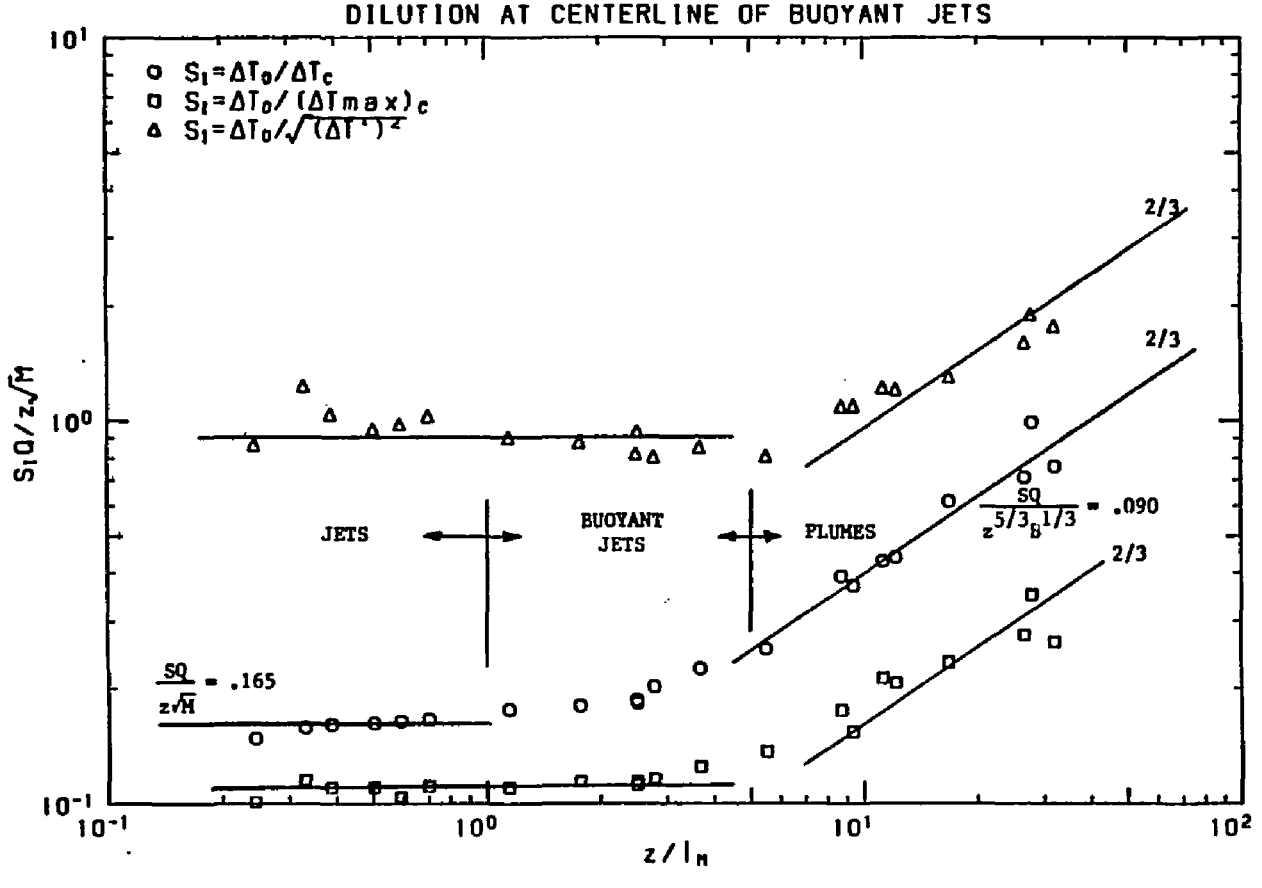


Figure 1. Mean, minimum and "rms" dilutions along the jet centerline.

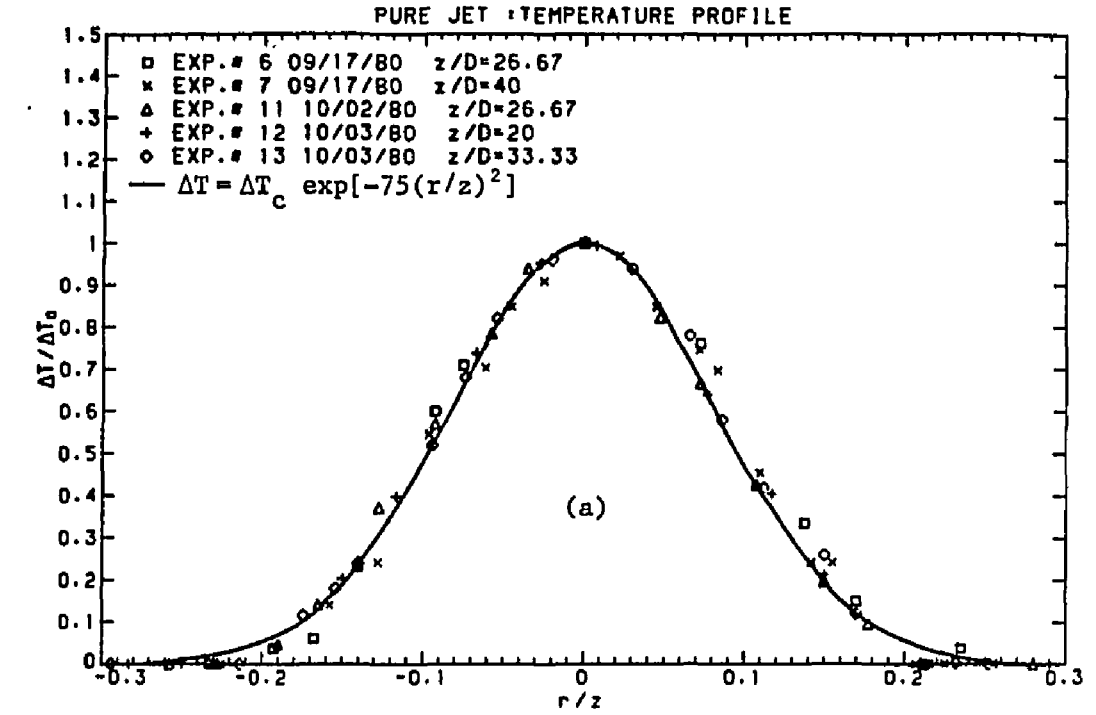


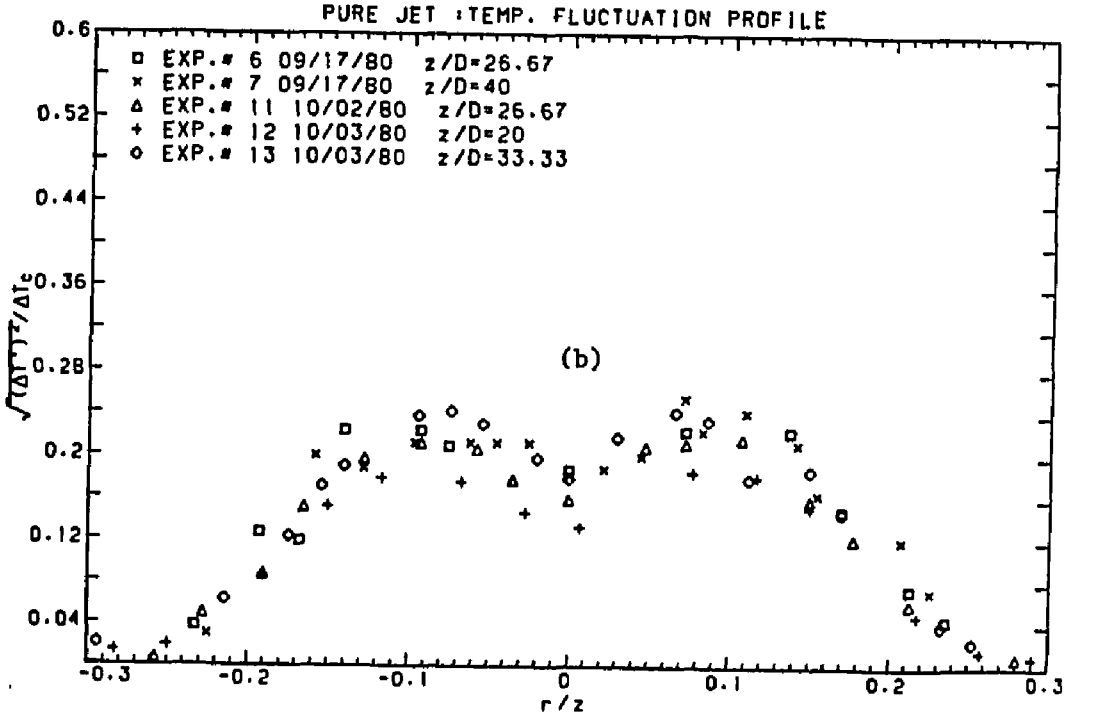


Figure 2. (a) Jet, mean temperature profile.
(b) Jet, turbulent intensities.

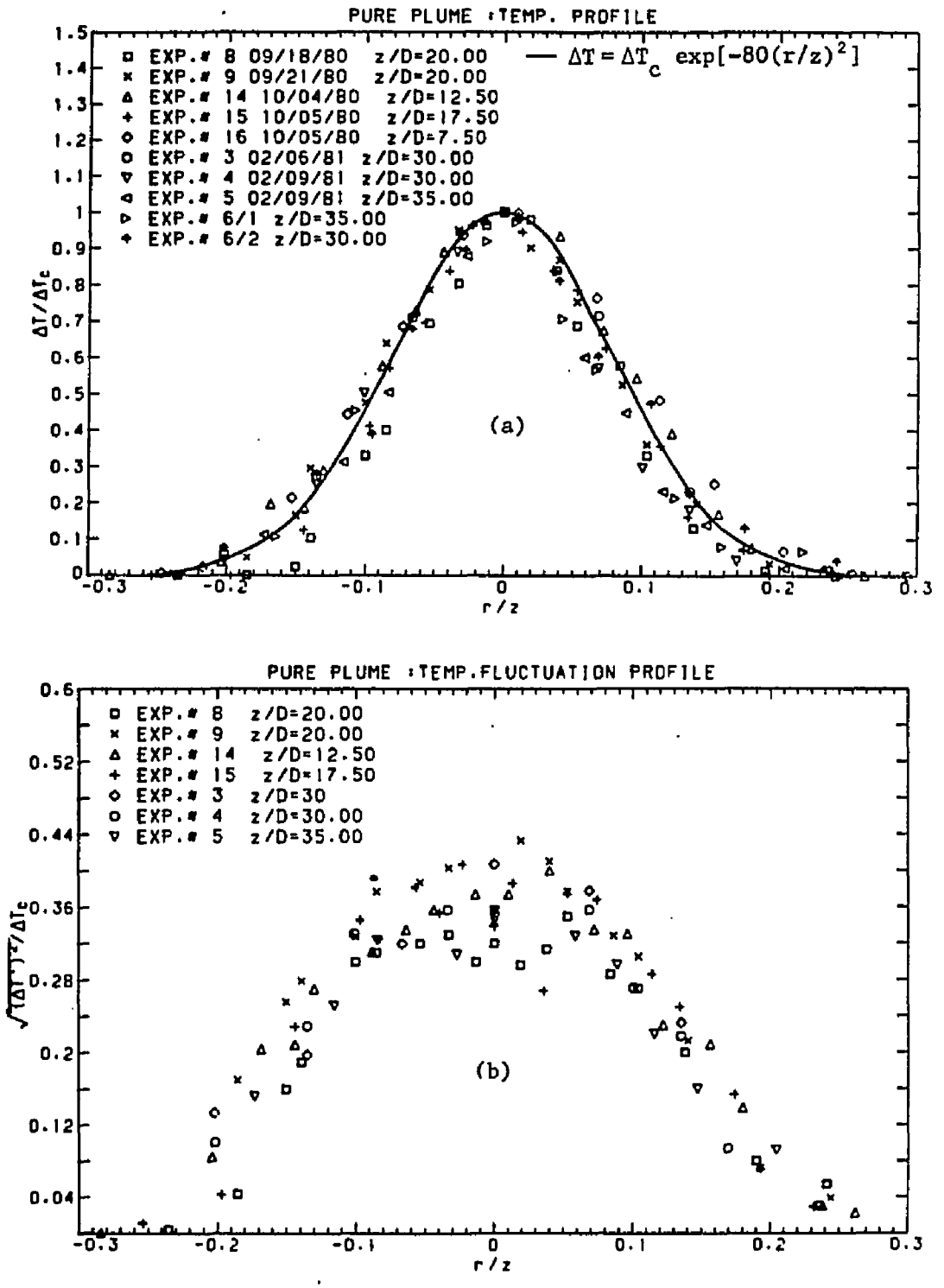


Figure 3. (a) Plume, mean temperature profile.
(b) Plume, turbulent intensities.

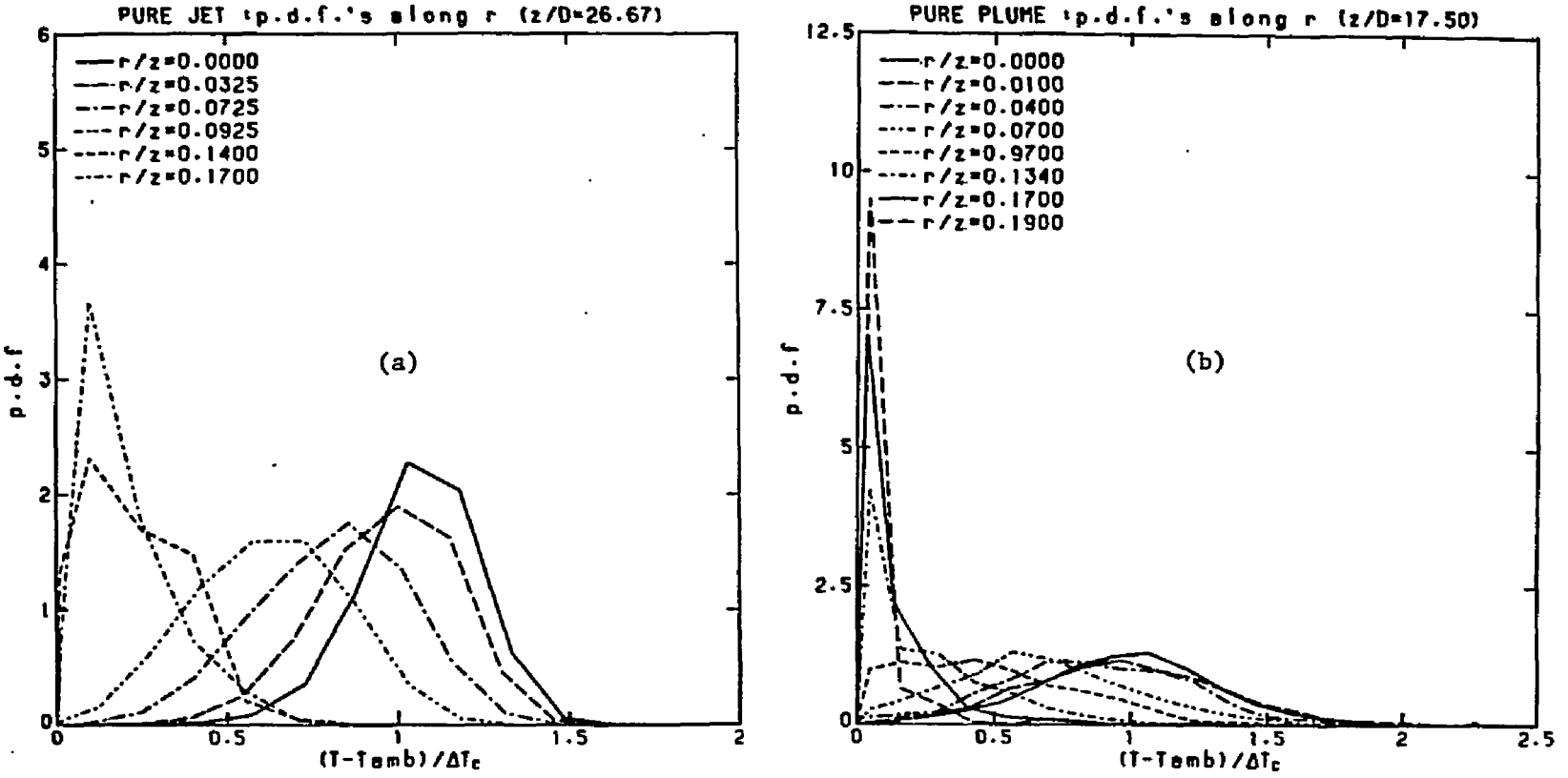


Figure 4. Probability density functions: (a) across a jet, (b) across a plume.

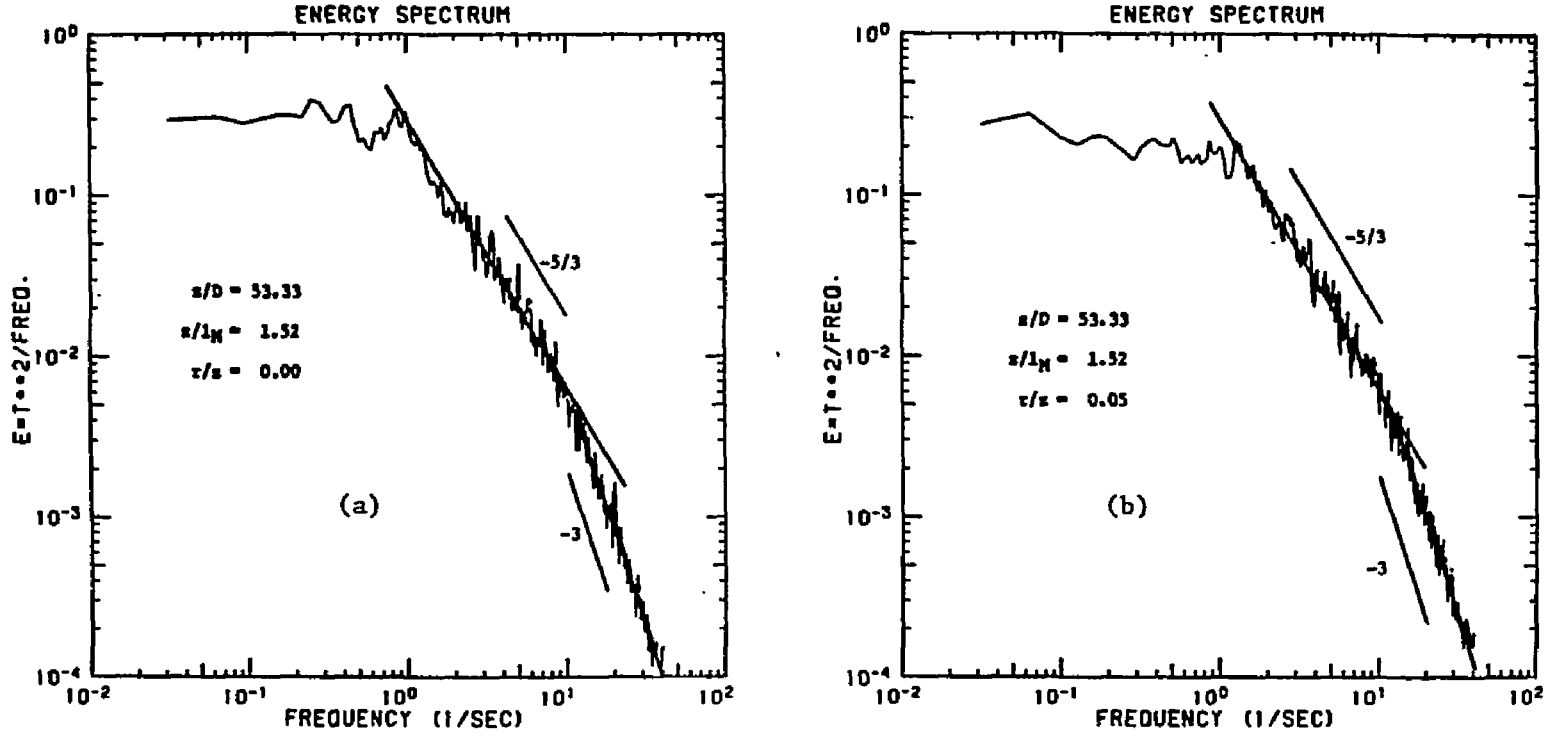


Figure 5. Power spectra of a buoyant jet 53 diameters downstream; (a) centerline, (b) r/z = 0.05.

# APPENDIX B

## DATA

The data tables and figures in this Appendix correspond to the experiments EXP series, VEL series and PAP series shown in tables 4.1.1, 4.1.2 and 4.1.3 of Chapter 4. All the data used for the non-dimensional profiles of the normalized time-averaged mean values, turbulence intensities and cross-correlations for velocities w and u and concentration c versus r/z, have also been plotted in dimensional form. They are shown in the same page with the data table of the corresponding experiment. The radial distance r has been calculated from the reference distance X as $r = X - \bar{X}$, where $\bar{X}$ corresponds to the jet centerline and has to be defined somehow. The description of the headings of the tabulated data is

X = relative reference location of the point of measurement (cm)

W = $\bar{w}$ (cm/sec)

WP = $\sqrt{\overline{w'^2}}$ (cm/sec)

UP = $\sqrt{\overline{u'^2}}$ (cm/sec)

WPUP = $\overline{w'u'}$ ($cm^2/sec^2$)

MAX W = max w (cm/sec)

MIN W = min w (cm/sec)

C = $\bar{c}$ (ppb)

CP = $\sqrt{\overline{c'^2}}$ (ppb)

WPCP = $\overline{w'c'}$ (ppb cm/sec)

UPCP = $\overline{u'c'}$ (ppb cm/sec)

The initial jet parameters for all the experiments, such as, W, z, D, $(\Delta\rho/\rho_a)_o g$ and $C_o$ are given in tables 4.1.1 and 4.1.3 of Chapter 4.

EXP01

| X | W | WP | UP | WPUP | C | CP | WPCP | UPCP |
|---|---|---|---|---|---|---|---|---|
| 70.000 | 0.335 | 0.278 | 0.355 | 0.003 | 0.558 | 0.659 | 0.034 | 0.059 |
| 72.000 | 1.190 | 0.705 | 0.439 | -0.063 | 1.711 | 1.353 | 0.461 | 0.188 |
| 74.000 | 2.520 | 0.960 | 0.566 | -0.152 | 3.364 | 2.007 | 1.049 | 0.388 |
| 76.000 | 3.539 | 1.079 | 0.703 | -0.221 | 4.770 | 2.239 | 1.190 | 0.472 |
| 78.000 | 4.444 | 1.170 | 0.795 | -0.023 | 5.814 | 2.379 | 1.509 | 0.107 |
| 80.000 | 5.171 | 1.091 | 0.741 | 0.086 | 6.370 | 2.264 | 1.159 | -0.132 |
| 82.000 | 4.225 | 1.076 | 0.720 | 0.190 | 5.165 | 2.125 | 0.991 | -0.443 |
| 84.000 | 2.487 | 1.153 | 0.639 | 0.261 | 2.838 | 1.817 | 0.990 | -0.436 |
| 86.000 | 1.048 | 0.736 | 0.533 | 0.166 | 1.212 | 1.148 | 0.379 | -0.259 |
| 88.000 | 0.461 | 0.497 | 0.385 | 0.013 | 0.605 | 0.748 | 0.196 | -0.090 |

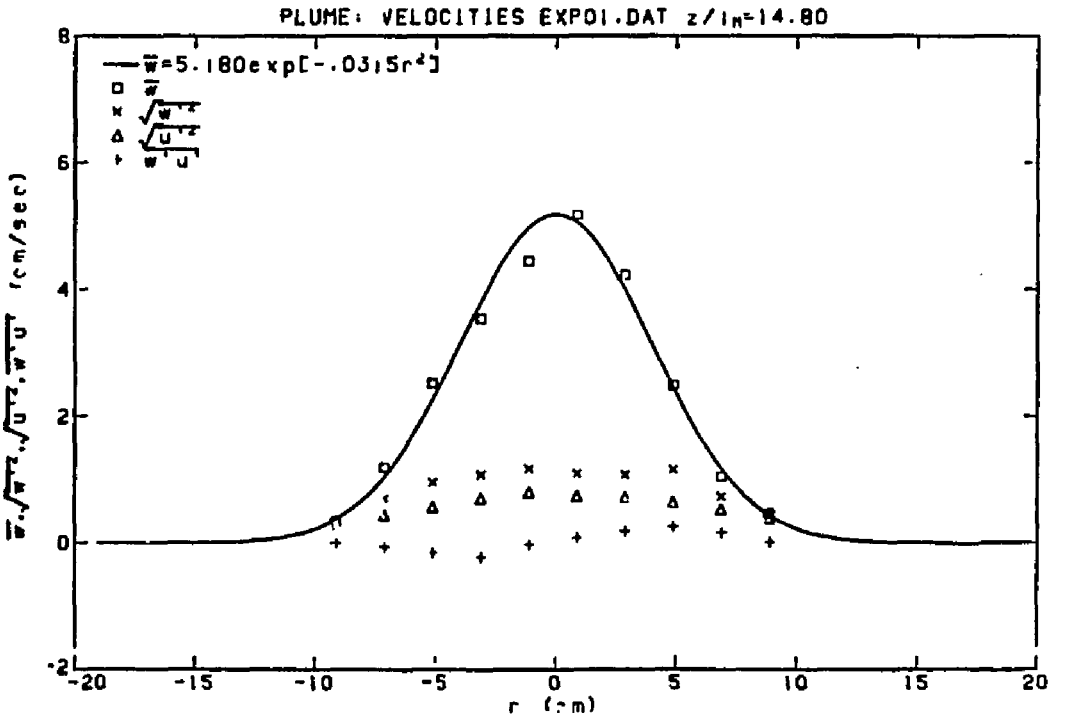

EXP01

| X | W | WP | UP | WPUP | C | CP | WPCP | UPCP |
|---|---|---|---|---|---|---|---|---|
| 70.000 | 0.335 | 0.278 | 0.355 | 0.003 | 0.558 | 0.659 | 0.034 | 0.059 |
| 72.000 | 1.190 | 0.705 | 0.439 | -0.063 | 1.711 | 1.353 | 0.461 | 0.188 |
| 74.000 | 2.520 | 0.960 | 0.566 | -0.152 | 3.364 | 2.007 | 1.049 | 0.388 |
| 76.000 | 3.539 | 1.079 | 0.703 | -0.221 | 4.770 | 2.239 | 1.190 | 0.472 |
| 78.000 | 4.444 | 1.170 | 0.795 | -0.023 | 5.814 | 2.379 | 1.509 | 0.107 |
| 80.000 | 5.171 | 1.091 | 0.741 | 0.086 | 6.370 | 2.264 | 1.159 | -0.132 |
| 82.000 | 4.225 | 1.076 | 0.720 | 0.190 | 5.165 | 2.125 | 0.991 | -0.443 |
| 84.000 | 2.487 | 1.153 | 0.639 | 0.261 | 2.838 | 1.817 | 0.990 | -0.436 |
| 86.000 | 1.048 | 0.736 | 0.533 | 0.166 | 1.212 | 1.148 | 0.379 | -0.259 |
| 88.000 | 0.461 | 0.497 | 0.385 | 0.013 | 0.605 | 0.748 | 0.196 | -0.090 |

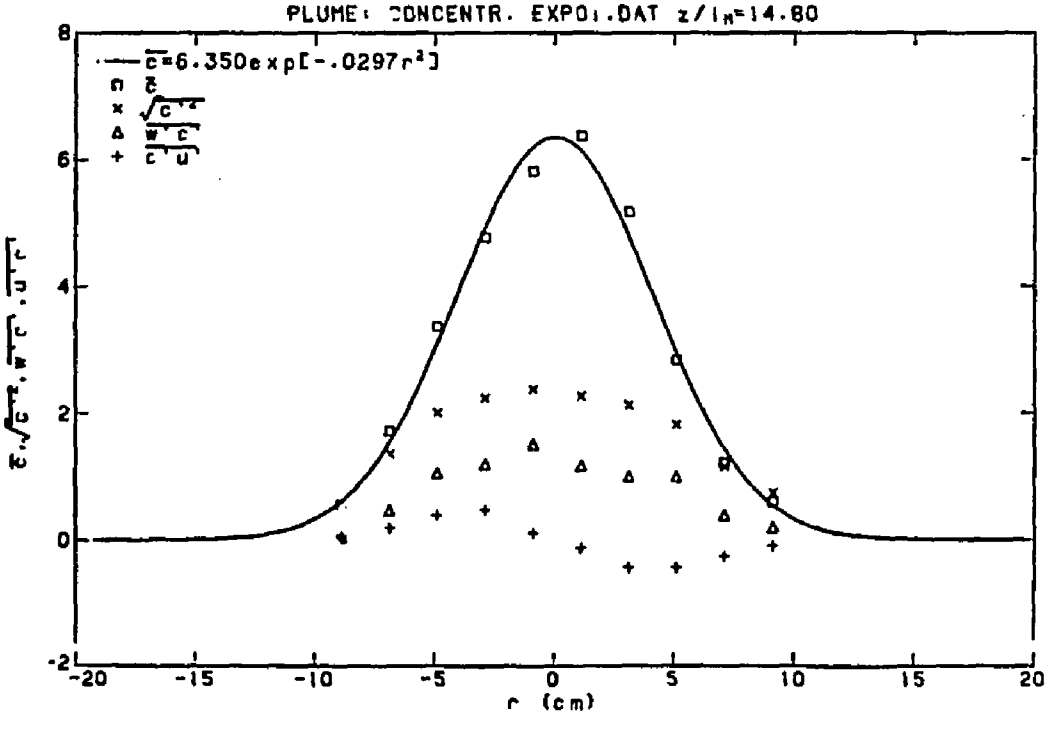

EXP05

| X | W | WP | UP | WPUP | C | CP | WPCP | UPCP |
|---|---|---|---|---|---|---|---|---|
| 72.000 | 0.429 | 0.351 | 0.289 | -0.007 | 1.429 | 1.180 | 0.171 | 0.054 |
| 74.000 | 0.907 | 0.676 | 0.421 | -0.082 | 2.224 | 1.723 | 0.394 | 0.228 |
| 76.000 | 2.300 | 1.145 | 0.550 | -0.188 | 4.268 | 2.638 | 1.688 | 0.530 |
| 78.000 | 4.692 | 0.989 | 0.635 | -0.058 | 7.498 | 2.697 | 1.115 | 0.232 |
| 80.000 | 4.497 | 1.069 | 0.651 | 0.098 | 6.892 | 2.636 | 1.350 | -0.270 |
| 82.000 | 3.066 | 1.043 | 0.593 | 0.172 | 4.565 | 2.392 | 1.176 | -0.543 |
| 84.000 | 1.226 | 0.865 | 0.549 | 0.142 | 1.942 | 2.046 | 1.043 | -0.478 |
| 86.000 | 0.187 | 0.269 | 0.279 | 0.006 | 0.494 | 0.942 | 0.110 | -0.069 |
| 88.000 | 0.059 | 0.149 | 0.149 | -0.002 | -0.049 | 0.121 | -0.004 | -0.006 |

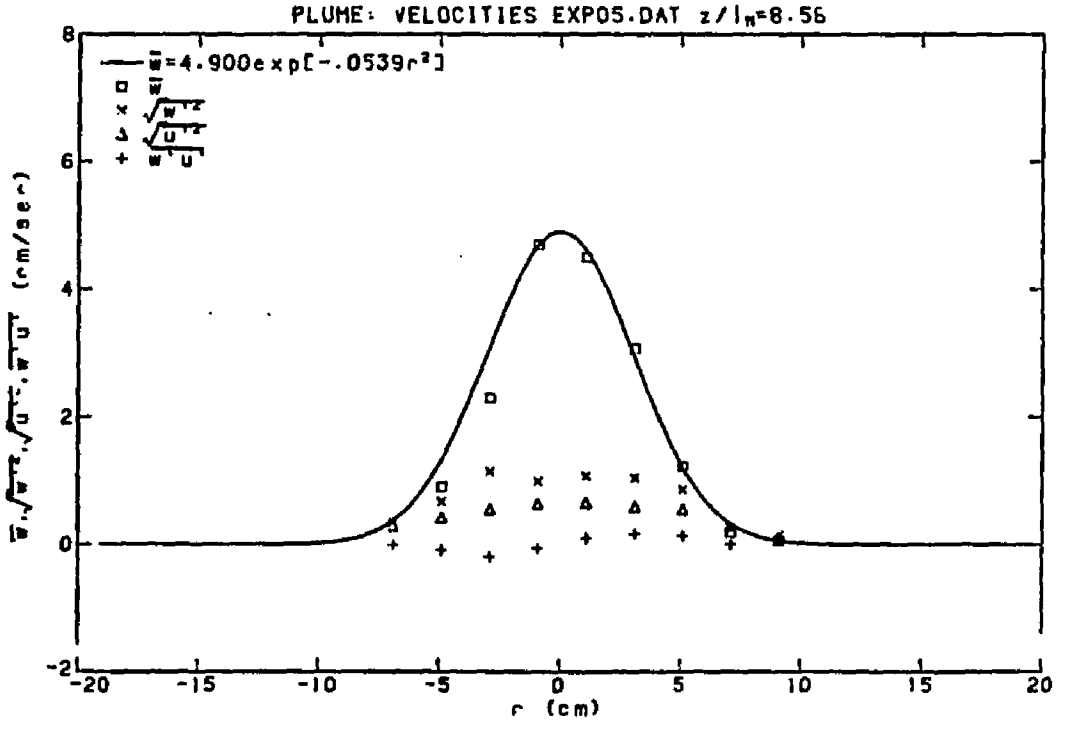

EXP05

| X | W | WP | UP | WPUP | C | CP | WPCP | UPCP |
|---|---|---|---|---|---|---|---|---|
| 72.000 | 0.429 | 0.351 | 0.289 | -0.007 | 1.429 | 1.180 | 0.171 | 0.054 |
| 74.000 | 0.907 | 0.676 | 0.421 | -0.082 | 2.224 | 1.723 | 0.394 | 0.228 |
| 76.000 | 2.300 | 1.145 | 0.550 | -0.188 | 4.268 | 2.638 | 1.688 | 0.530 |
| 78.000 | 4.692 | 0.989 | 0.635 | -0.058 | 7.498 | 2.697 | 1.115 | 0.232 |
| 80.000 | 4.497 | 1.069 | 0.651 | 0.098 | 6.892 | 2.636 | 1.350 | -0.270 |
| 82.000 | 3.066 | 1.043 | 0.593 | 0.172 | 4.565 | 2.392 | 1.176 | -0.543 |
| 84.000 | 1.226 | 0.865 | 0.549 | 0.142 | 1.942 | 2.046 | 1.043 | -0.478 |
| 86.000 | 0.187 | 0.269 | 0.279 | 0.006 | 0.494 | 0.942 | 0.110 | -0.069 |
| 88.000 | 0.059 | 0.149 | 0.149 | -0.002 | -0.049 | 0.121 | -0.004 | -0.006 |

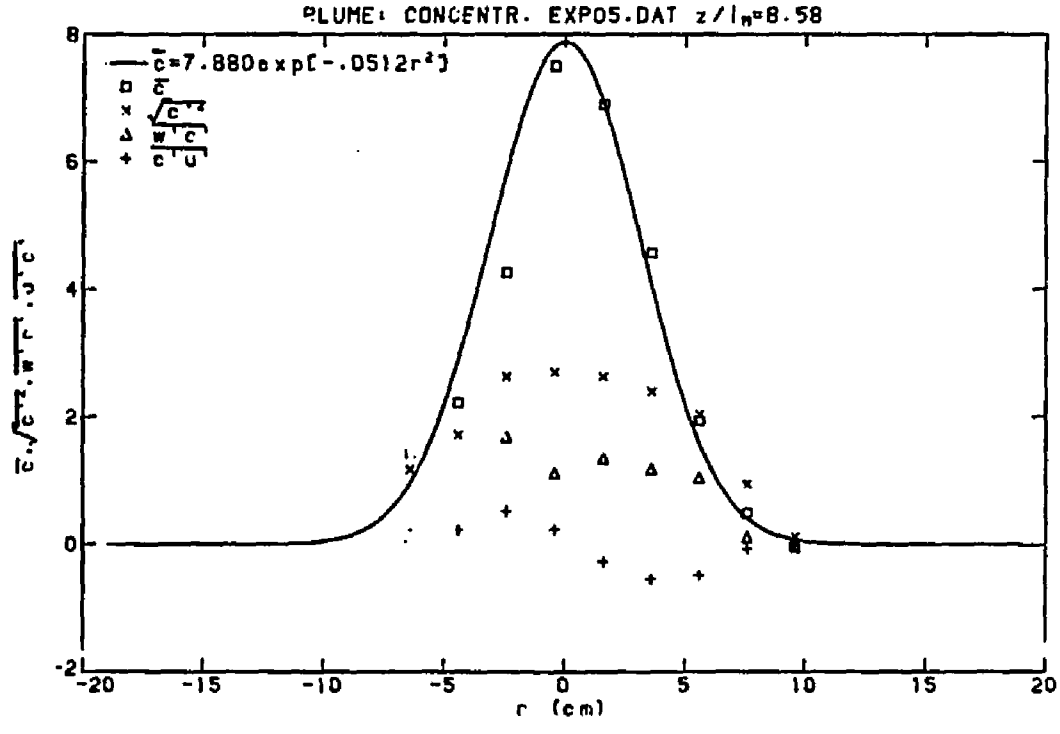

EXP08

| X | W | WP | UP | WPUP | C | CP | WPCP | UPCP |
|---|---|---|---|---|---|---|---|---|
| 70.000 | 0.560 | 0.519 | 0.333 | -0.054 | 0.658 | 0.564 | 0.155 | 0.048 |
| 72.500 | 1.529 | 0.743 | 0.423 | -0.071 | 1.373 | 0.993 | 0.332 | 0.119 |
| 75.000 | 3.073 | 0.926 | 0.614 | -0.184 | 2.592 | 1.303 | 0.644 | 0.322 |
| 77.500 | 4.419 | 0.967 | 0.643 | -0.080 | 3.774 | 1.447 | 0.727 | 0.139 |
| 80.000 | 4.117 | 1.025 | 0.616 | 0.155 | 3.392 | 1.346 | 0.649 | -0.180 |
| 82.500 | 2.841 | 1.066 | 0.587 | 0.258 | 2.521 | 1.271 | 0.779 | -0.306 |
| 85.000 | 2.170 | 0.892 | 0.635 | 0.250 | 1.657 | 1.066 | 0.528 | -0.283 |
| 87.500 | 0.810 | 0.690 | 0.434 | 0.123 | 0.729 | 0.713 | 0.265 | -0.133 |
| 90.000 | 0.077 | 0.180 | 0.191 | -0.002 | 0.295 | 0.243 | 0.000 | -0.004 |

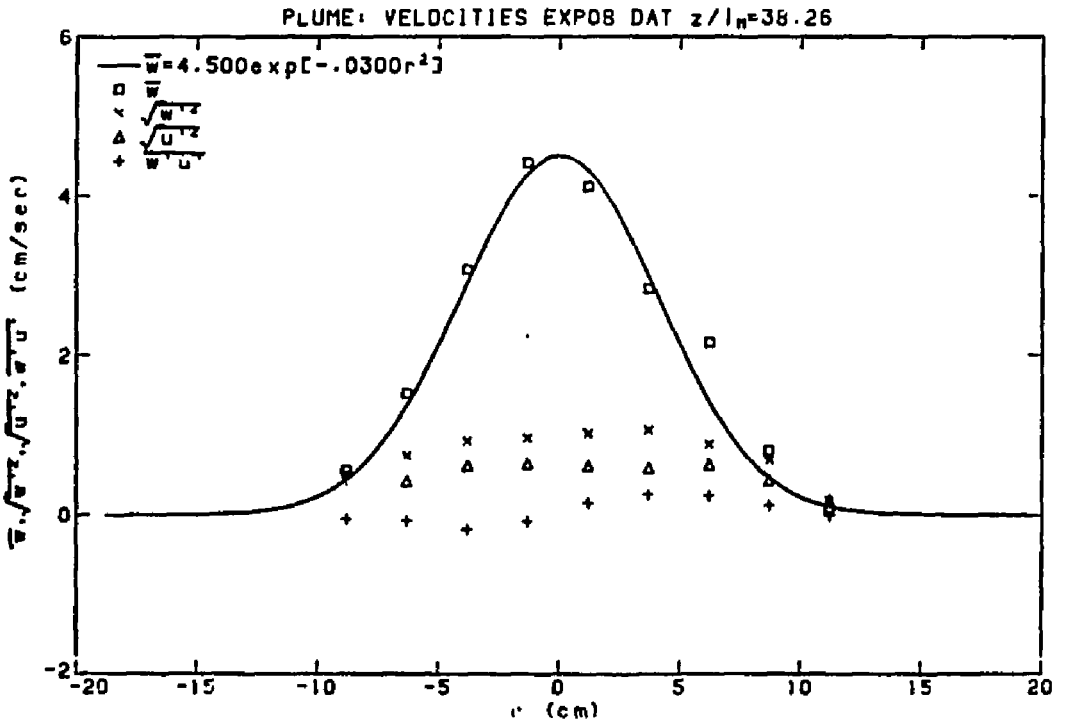

EXP08

| X | W | WP | UP | WPUP | C | CP | WPCP | UPCP |
|---|---|---|---|---|---|---|---|---|
| 70.000 | 0.560 | 0.519 | 0.333 | -0.054 | 0.658 | 0.564 | 0.155 | 0.048 |
| 72.500 | 1.529 | 0.743 | 0.423 | -0.071 | 1.373 | 0.993 | 0.332 | 0.119 |
| 75.000 | 3.073 | 0.926 | 0.614 | -0.184 | 2.592 | 1.303 | 0.644 | 0.322 |
| 77.500 | 4.419 | 0.967 | 0.643 | -0.080 | 3.774 | 1.447 | 0.727 | 0.139 |
| 80.000 | 4.117 | 1.025 | 0.616 | 0.155 | 3.392 | 1.346 | 0.649 | -0.180 |
| 82.500 | 2.841 | 1.066 | 0.587 | 0.258 | 2.521 | 1.271 | 0.779 | -0.306 |
| 85.000 | 2.170 | 0.892 | 0.635 | 0.250 | 1.657 | 1.066 | 0.528 | -0.283 |
| 87.500 | 0.810 | 0.690 | 0.434 | 0.123 | 0.729 | 0.713 | 0.265 | -0.133 |
| 90.000 | 0.077 | 0.180 | 0.191 | -0.002 | 0.295 | 0.243 | 0.000 | -0.004 |

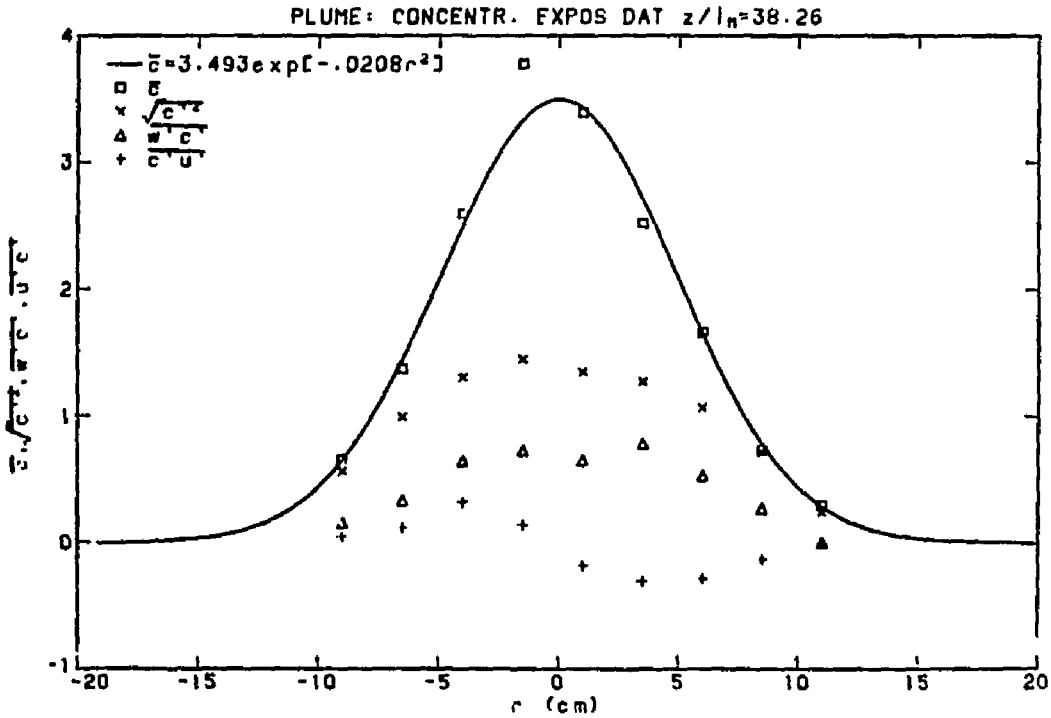

EXP09

| X | W | WP | UP | WPUP | C | CP | WPCP | UPCP |
|---|---|---|---|---|---|---|---|---|
| 70.000 | 1.203 | 0.818 | 0.460 | -0.110 | 1.177 | 0.997 | 0.328 | 0.153 |
| 72.500 | 2.299 | 1.108 | 0.635 | -0.254 | 2.257 | 1.497 | 0.906 | 0.388 |
| 75.000 | 3.749 | 1.234 | 0.713 | -0.178 | 3.582 | 1.932 | 1.241 | 0.388 |
| 77.500 | 5.885 | 1.210 | 0.868 | -0.149 | 5.888 | 2.114 | 1.345 | 0.379 |
| 80.000 | 5.322 | 1.475 | 0.824 | 0.319 | 5.490 | 2.222 | 1.890 | -0.470 |
| 82.500 | 4.367 | 1.454 | 0.832 | 0.445 | 4.484 | 2.122 | 1.622 | -0.651 |
| 85.000 | 2.093 | 1.099 | 0.602 | 0.241 | 2.116 | 1.528 | 0.949 | -0.407 |
| 87.500 | 1.006 | 0.833 | 0.519 | 0.136 | 1.149 | 1.085 | 0.441 | -0.211 |
| 90.000 | 0.034 | 0.275 | 0.286 | -0.008 | 0.420 | 0.400 | 0.003 | -0.007 |

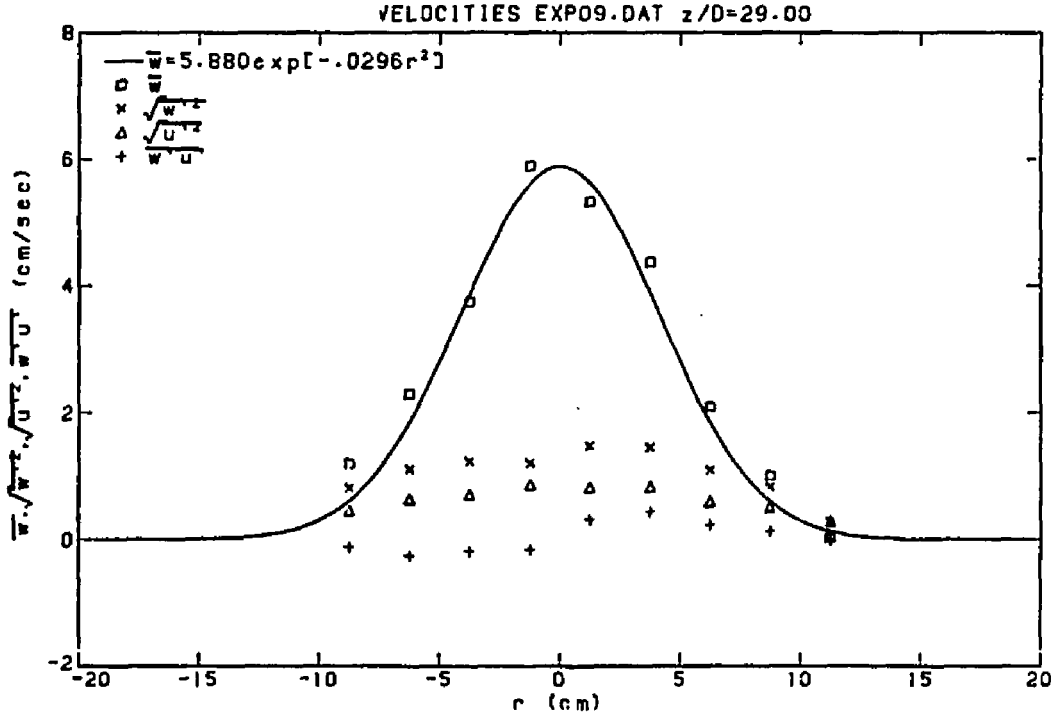

EXP09

| X | W | WP | UP | WPUP | C | CP | WPCP | UPCP |
|---|---|---|---|---|---|---|---|---|
| 70.000 | 1.203 | 0.818 | 0.460 | -0.110 | 1.177 | 0.997 | 0.328 | 0.153 |
| 72.500 | 2.299 | 1.108 | 0.635 | -0.254 | 2.257 | 1.497 | 0.906 | 0.388 |
| 75.000 | 3.749 | 1.234 | 0.713 | -0.178 | 3.582 | 1.932 | 1.241 | 0.388 |
| 77.500 | 5.885 | 1.210 | 0.868 | -0.149 | 5.888 | 2.114 | 1.345 | 0.379 |
| 80.000 | 5.322 | 1.475 | 0.824 | 0.319 | 5.490 | 2.222 | 1.890 | -0.470 |
| 82.500 | 4.367 | 1.454 | 0.832 | 0.445 | 4.484 | 2.122 | 1.622 | -0.651 |
| 85.000 | 2.093 | 1.099 | 0.602 | 0.241 | 2.116 | 1.528 | 0.949 | -0.407 |
| 87.500 | 1.006 | 0.833 | 0.519 | 0.136 | 1.149 | 1.085 | 0.441 | -0.211 |
| 90.000 | 0.034 | 0.275 | 0.286 | -0.008 | 0.420 | 0.400 | 0.003 | -0.007 |

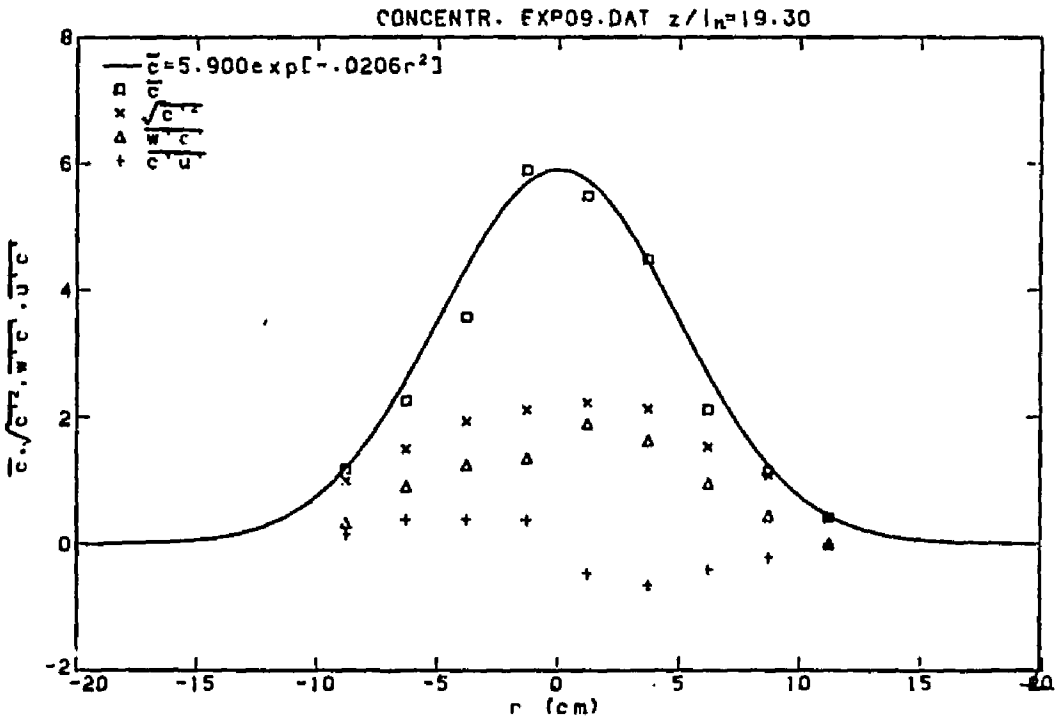

EXP10

| X | W | WP | UP | WPUP | C | CP | WPCP | UPCP |
|---|---|---|---|---|---|---|---|---|
| 71.000 | 0.583 | 0.156 | 0.193 | 0.003 | 0.043 | 0.322 | -0.014 | 0.003 |
| 73.000 | 0.496 | 0.486 | 0.354 | -0.019 | 0.413 | 0.781 | 0.217 | 0.055 |
| 75.000 | 1.644 | 0.827 | 0.504 | -0.096 | 1.616 | 1.341 | 0.598 | 0.236 |
| 77.000 | 2.772 | 1.025 | 0.610 | -0.132 | 2.710 | 1.739 | 0.987 | 0.240 |
| 79.000 | 4.715 | 1.036 | 0.731 | -0.052 | 4.709 | 1.918 | 1.053 | 0.135 |
| 81.000 | 4.251 | 1.099 | 0.734 | 0.095 | 4.136 | 1.775 | 1.069 | -0.212 |
| 83.000 | 2.974 | 1.151 | 0.658 | 0.296 | 2.723 | 1.749 | 1.100 | -0.394 |
| 85.000 | 1.525 | 0.868 | 0.503 | 0.178 | 1.060 | 1.208 | 0.619 | -0.284 |
| 87.000 | 0.412 | 0.588 | 0.398 | 0.090 | -0.064 | 0.848 | 0.258 | -0.148 |

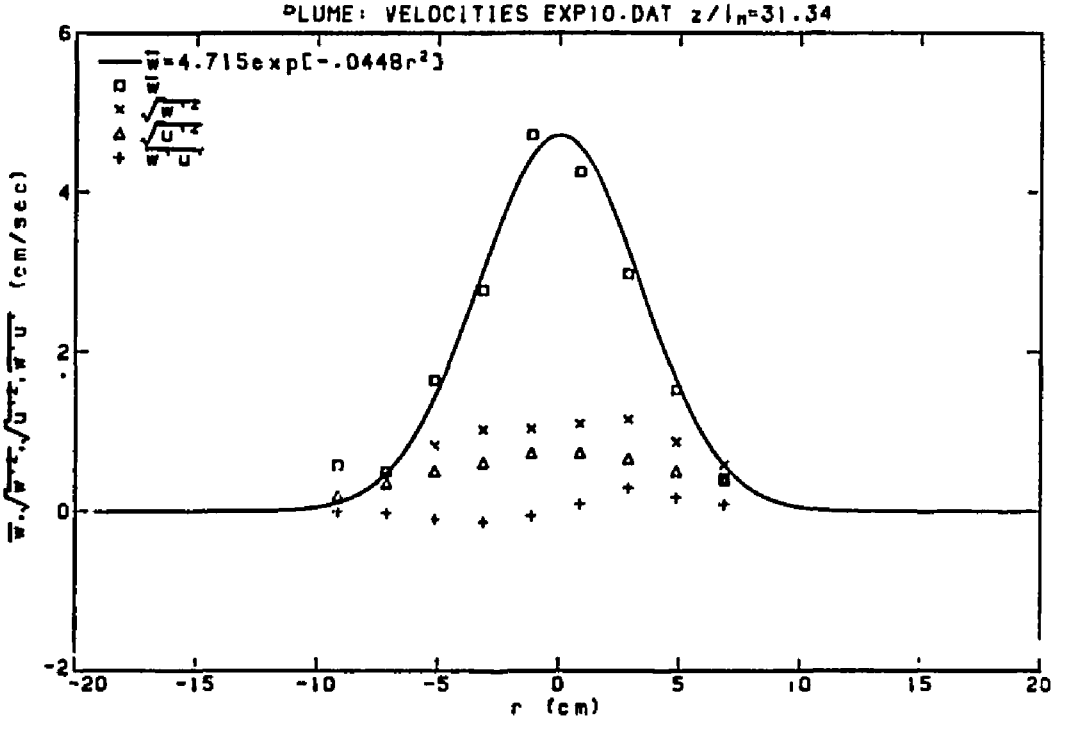

EXP11

| X | W | WP | UP | WPUP | C | CP | WPCP | UPCP |
|---|---|---|---|---|---|---|---|---|
| 71.000 | 0.353 | 0.471 | 0.349 | -0.020 | 0.572 | 0.719 | 0.200 | 0.053 |
| 73.000 | 1.190 | 0.900 | 0.434 | -0.133 | 1.221 | 1.294 | 0.670 | 0.214 |
| 75.000 | 2.114 | 1.115 | 0.532 | -0.214 | 1.994 | 1.489 | 0.684 | 0.304 |
| 77.000 | 3.541 | 1.162 | 0.617 | -0.128 | 3.663 | 1.918 | 1.088 | 0.284 |
| 79.000 | 4.589 | 1.071 | 0.654 | -0.050 | 4.672 | 2.019 | 1.105 | 0.171 |
| 81.000 | 4.373 | 1.077 | 0.669 | 0.148 | 4.148 | 1.913 | 0.994 | -0.255 |
| 83.000 | 3.245 | 1.046 | 0.666 | 0.253 | 2.901 | 1.759 | 1.009 | -0.445 |
| 85.000 | 1.987 | 0.930 | 0.542 | 0.220 | 1.616 | 1.422 | 0.627 | -0.302 |
| 87.000 | 0.859 | 0.683 | 0.422 | 0.095 | 0.584 | 0.937 | 0.347 | -0.207 |
| 89.000 | 0.212 | 0.327 | 0.264 | 0.019 | 0.111 | 0.495 | 0.046 | -0.037 |

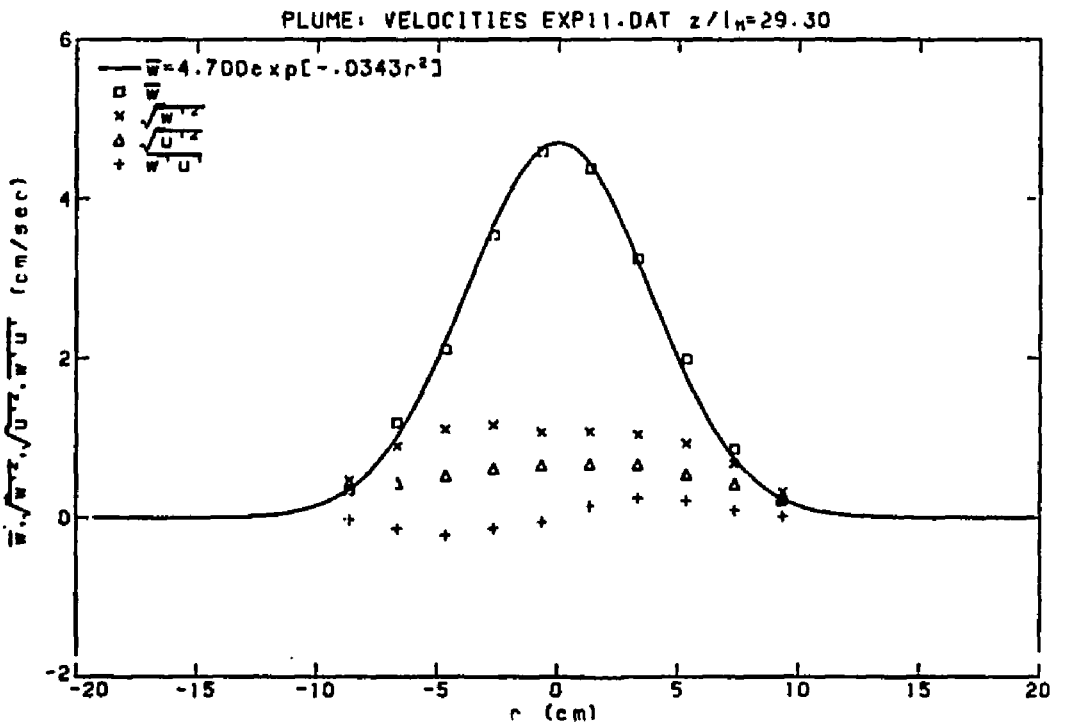

**EXP11**

| X | W | WP | UP | WPUP | C | CP | WPCP | UPCP |
|---|---|---|---|---|---|---|---|---|
| 71.000 | 0.353 | 0.471 | 0.349 | -0.020 | 0.572 | 0.719 | 0.200 | 0.053 |
| 73.000 | 1.190 | 0.900 | 0.434 | -0.133 | 1.221 | 1.294 | 0.670 | 0.214 |
| 75.000 | 2.114 | 1.115 | 0.532 | -0.214 | 1.994 | 1.489 | 0.684 | 0.304 |
| 77.000 | 3.541 | 1.162 | 0.617 | -0.128 | 3.663 | 1.918 | 1.088 | 0.284 |
| 79.000 | 4.589 | 1.071 | 0.654 | -0.050 | 4.672 | 2.019 | 1.105 | 0.171 |
| 81.000 | 4.373 | 1.077 | 0.669 | 0.148 | 4.148 | 1.913 | 0.994 | -0.255 |
| 83.000 | 3.245 | 1.046 | 0.666 | 0.253 | 2.901 | 1.759 | 1.009 | -0.445 |
| 85.000 | 1.987 | 0.930 | 0.542 | 0.220 | 1.616 | 1.422 | 0.627 | -0.302 |
| 87.000 | 0.859 | 0.683 | 0.422 | 0.095 | 0.584 | 0.937 | 0.347 | -0.207 |
| 89.000 | 0.212 | 0.327 | 0.264 | 0.019 | 0.111 | 0.495 | 0.046 | -0.037 |

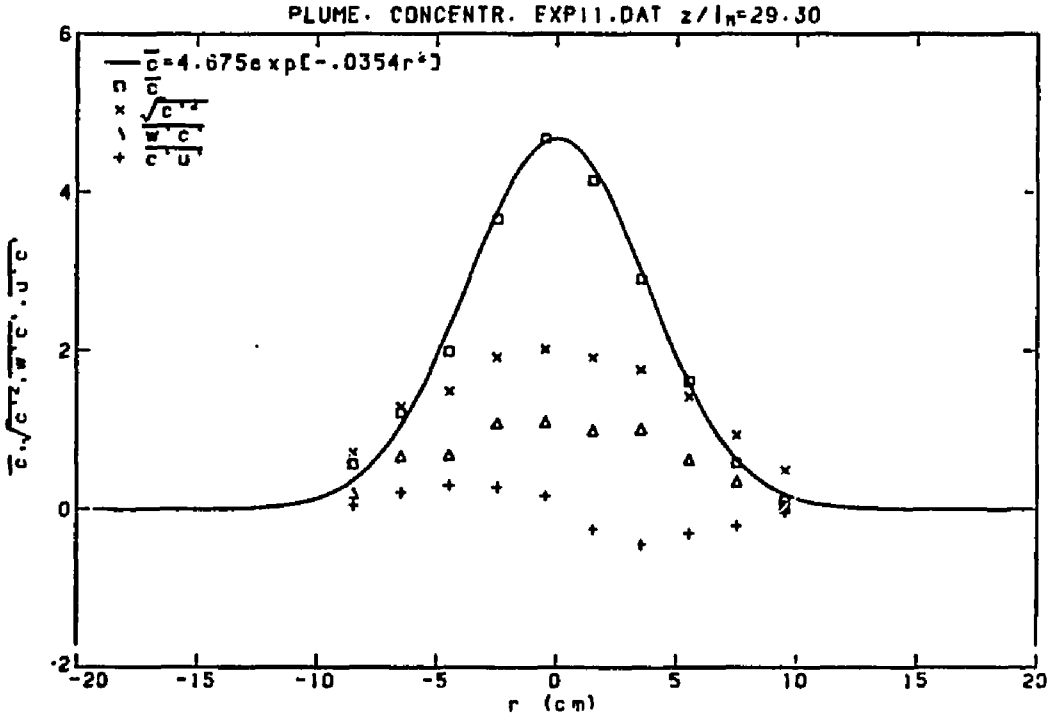

**EXP12**

| X | W | WP | UP | WPUP | C | CP | WPCP | UPCP |
|---|---|---|---|---|---|---|---|---|
| 64.000 | 0.364 | 0.416 | 0.406 | -0.018 | 0.132 | 0.349 | 0.079 | 0.035 |
| 68.000 | 0.802 | 0.895 | 0.477 | -0.106 | 0.302 | 0.381 | 0.215 | 0.053 |
| 71.000 | 2.657 | 1.351 | 0.645 | -0.460 | 0.831 | 0.656 | 0.519 | 0.201 |
| 74.000 | 3.616 | 1.409 | 0.713 | -0.363 | 1.292 | 0.731 | 0.661 | 0.196 |
| 77.000 | 5.016 | 1.320 | 0.779 | -0.136 | 1.817 | 0.734 | 0.601 | 0.113 |
| 80.000 | 4.978 | 1.295 | 0.829 | 0.115 | 1.847 | 0.736 | 0.574 | -0.054 |
| 83.500 | 4.009 | 1.175 | 0.824 | 0.392 | 1.633 | 0.621 | 0.370 | -0.205 |
| 87.000 | 3.092 | 1.231 | 0.745 | 0.327 | 1.311 | 0.596 | 0.366 | -0.167 |
| 90.500 | 1.219 | 0.783 | 0.473 | 0.160 | 0.823 | 0.357 | 0.172 | -0.095 |
| 94.000 | 0.200 | 0.422 | 0.313 | 0.025 | 0.635 | 0.166 | 0.027 | -0.011 |

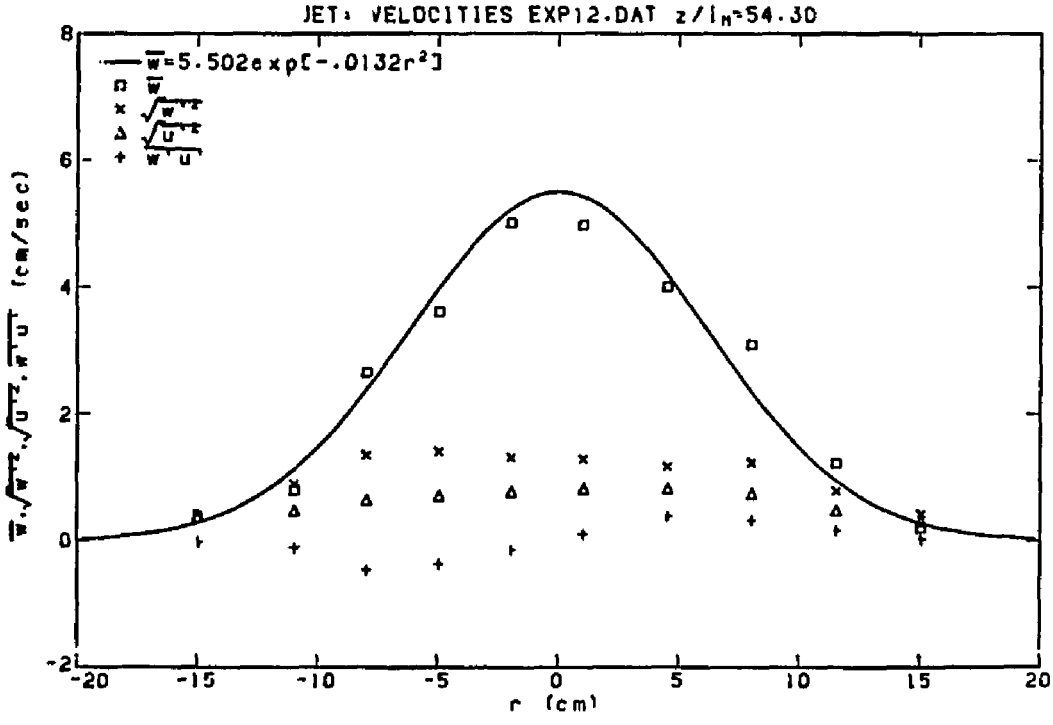

EXP12

| X | W | WP | UP | WPUP | C | CP | WPCP | UPCP |
|---|---|---|---|---|---|---|---|---|
| 64.000 | 0.364 | 0.416 | 0.406 | -0.018 | 0.132 | 0.349 | 0.079 | 0.035 |
| 68.000 | 0.802 | 0.895 | 0.477 | -0.106 | 0.302 | 0.381 | 0.215 | 0.053 |
| 71.000 | 2.657 | 1.351 | 0.645 | -0.460 | 0.831 | 0.656 | 0.519 | 0.201 |
| 74.000 | 3.616 | 1.409 | 0.713 | -0.363 | 1.292 | 0.731 | 0.661 | 0.196 |
| 77.000 | 5.016 | 1.320 | 0.779 | -0.136 | 1.817 | 0.734 | 0.601 | 0.113 |
| 80.000 | 4.978 | 1.295 | 0.829 | 0.115 | 1.847 | 0.736 | 0.574 | -0.054 |
| 83.500 | 4.009 | 1.175 | 0.824 | 0.392 | 1.633 | 0.621 | 0.370 | -0.205 |
| 87.000 | 3.092 | 1.231 | 0.745 | 0.327 | 1.311 | 0.596 | 0.366 | -0.167 |
| 90.500 | 1.219 | 0.783 | 0.473 | 0.160 | 0.823 | 0.357 | 0.172 | -0.095 |
| 94.000 | 0.200 | 0.422 | 0.313 | 0.025 | 0.635 | 0.166 | 0.027 | -0.011 |

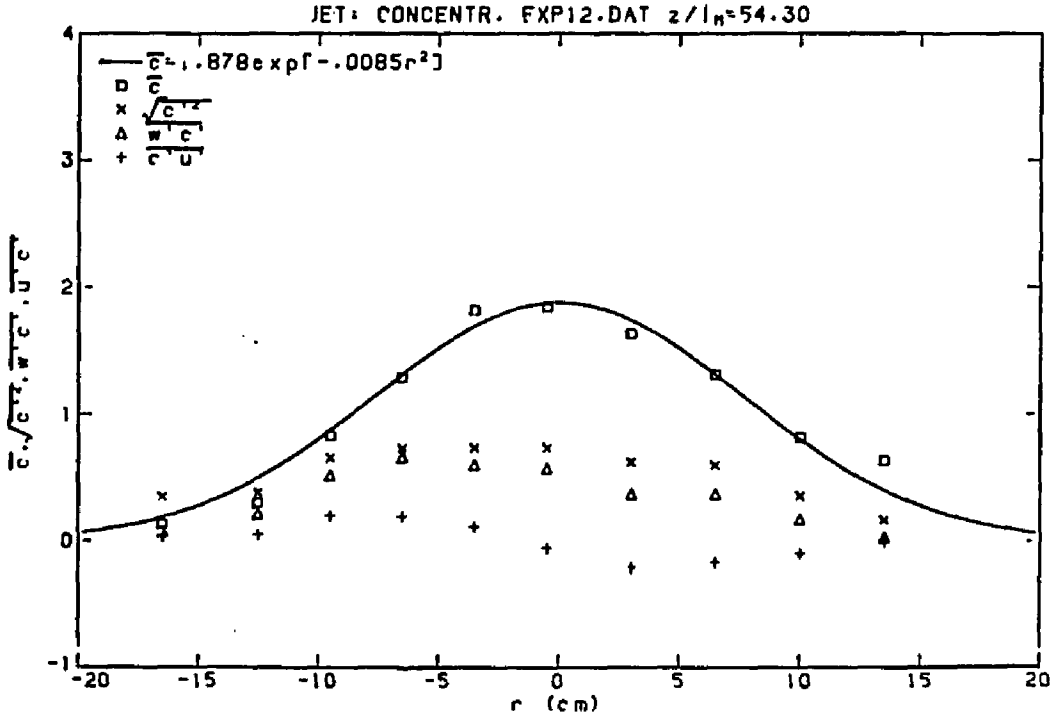

**EXP15**

| X | W | WP | UP | WPUP | C | CP | WPCP | UPCP |
|---|---|---|---|---|---|---|---|---|
| 72.000 | 0.060 | 0.178 | 0.240 | 0.001 | 0.599 | 0.920 | -0.021 | 0.014 |
| 73.500 | 0.621 | 0.656 | 0.458 | -0.073 | 2.013 | 1.994 | 0.710 | 0.216 |
| 75.000 | 1.459 | 1.028 | 0.687 | -0.230 | 4.074 | 2.792 | 1.560 | 0.687 |
| 76.500 | 3.097 | 1.253 | 0.754 | -0.142 | 6.951 | 2.814 | 1.350 | 0.617 |
| 77.500 | 4.453 | 1.368 | 0.915 | -0.199 | 8.873 | 2.743 | 1.522 | 0.650 |
| 78.500 | 5.843 | 1.414 | 1.023 | -0.214 | 10.621 | 2.567 | 1.461 | 0.546 |
| 79.500 | 6.917 | 1.436 | 1.014 | -0.063 | 12.022 | 2.325 | 1.371 | 0.279 |
| 80.500 | 6.450 | 1.354 | 0.990 | 0.108 | 11.242 | 2.491 | 1.358 | -0.251 |
| 81.500 | 5.280 | 1.456 | 0.959 | 0.339 | 10.275 | 2.577 | 1.711 | -0.671 |
| 82.500 | 4.035 | 1.391 | 0.905 | 0.296 | 8.758 | 2.744 | 1.841 | -0.788 |
| 83.500 | 2.632 | 1.210 | 0.840 | 0.292 | 6.563 | 2.781 | 1.545 | -0.732 |
| 85.000 | 1.072 | 0.777 | 0.530 | 0.048 | 3.971 | 2.087 | 0.585 | -0.238 |
| 86.500 | 0.283 | 0.398 | 0.404 | 0.033 | 2.172 | 1.820 | 0.258 | -0.198 |
| 88.000 | -0.039 | 0.181 | 0.235 | -0.004 | 1.129 | 0.363 | -0.010 | 0.002 |

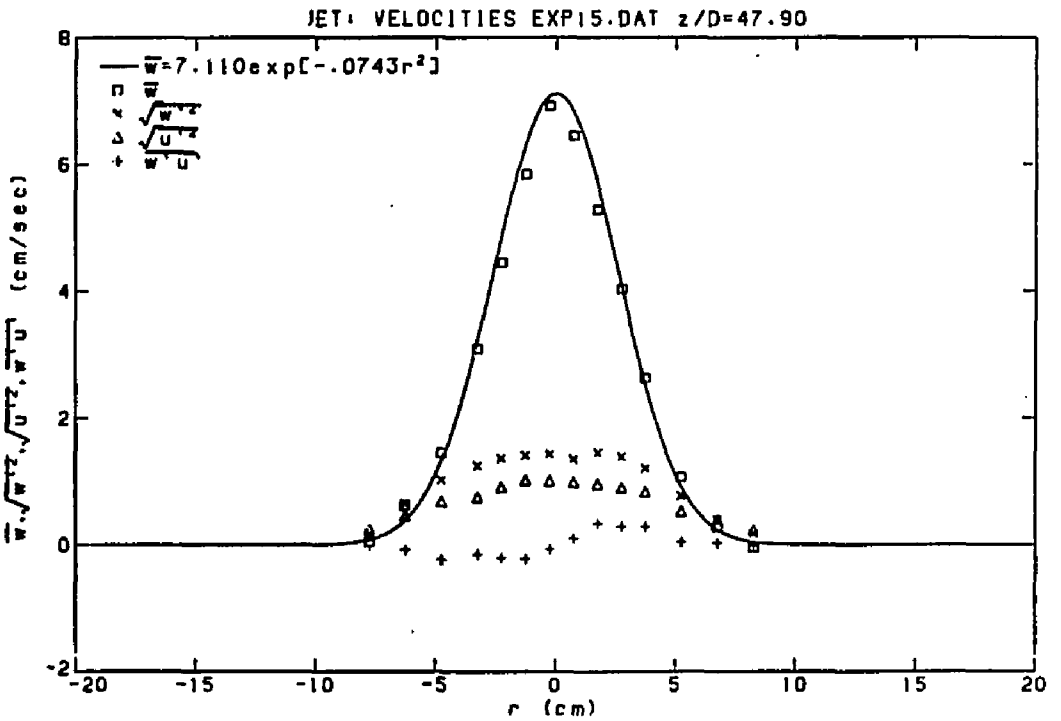

**EXP15**

| X | W | WP | UP | WPUP | C | CP | WPCP | UPCP |
|---|---|---|---|---|---|---|---|---|
| 72.000 | 0.060 | 0.178 | 0.240 | 0.001 | 0.599 | 0.920 | -0.021 | 0.014 |
| 73.500 | 0.621 | 0.656 | 0.458 | -0.073 | 2.013 | 1.994 | 0.710 | 0.216 |
| 75.000 | 1.459 | 1.028 | 0.687 | -0.230 | 4.074 | 2.792 | 1.560 | 0.687 |
| 76.500 | 3.097 | 1.253 | 0.754 | -0.142 | 6.951 | 2.814 | 1.350 | 0.617 |
| 77.500 | 4.453 | 1.368 | 0.915 | -0.199 | 8.873 | 2.743 | 1.522 | 0.650 |
| 78.500 | 5.843 | 1.414 | 1.023 | -0.214 | 10.621 | 2.567 | 1.461 | 0.546 |
| 79.500 | 6.917 | 1.436 | 1.014 | -0.063 | 12.022 | 2.325 | 1.371 | 0.279 |
| 80.500 | 6.450 | 1.354 | 0.990 | 0.108 | 11.242 | 2.491 | 1.358 | -0.251 |
| 81.500 | 5.280 | 1.456 | 0.959 | 0.339 | 10.275 | 2.577 | 1.711 | -0.671 |
| 82.500 | 4.035 | 1.391 | 0.905 | 0.296 | 8.758 | 2.744 | 1.841 | -0.788 |
| 83.500 | 2.632 | 1.210 | 0.840 | 0.292 | 6.563 | 2.781 | 1.545 | -0.732 |
| 85.000 | 1.072 | 0.777 | 0.530 | 0.048 | 3.971 | 2.087 | 0.585 | -0.238 |
| 86.500 | 0.283 | 0.398 | 0.404 | 0.033 | 2.172 | 1.820 | 0.258 | -0.198 |
| 88.000 | -0.039 | 0.181 | 0.235 | -0.004 | 1.129 | 0.363 | -0.010 | 0.002 |

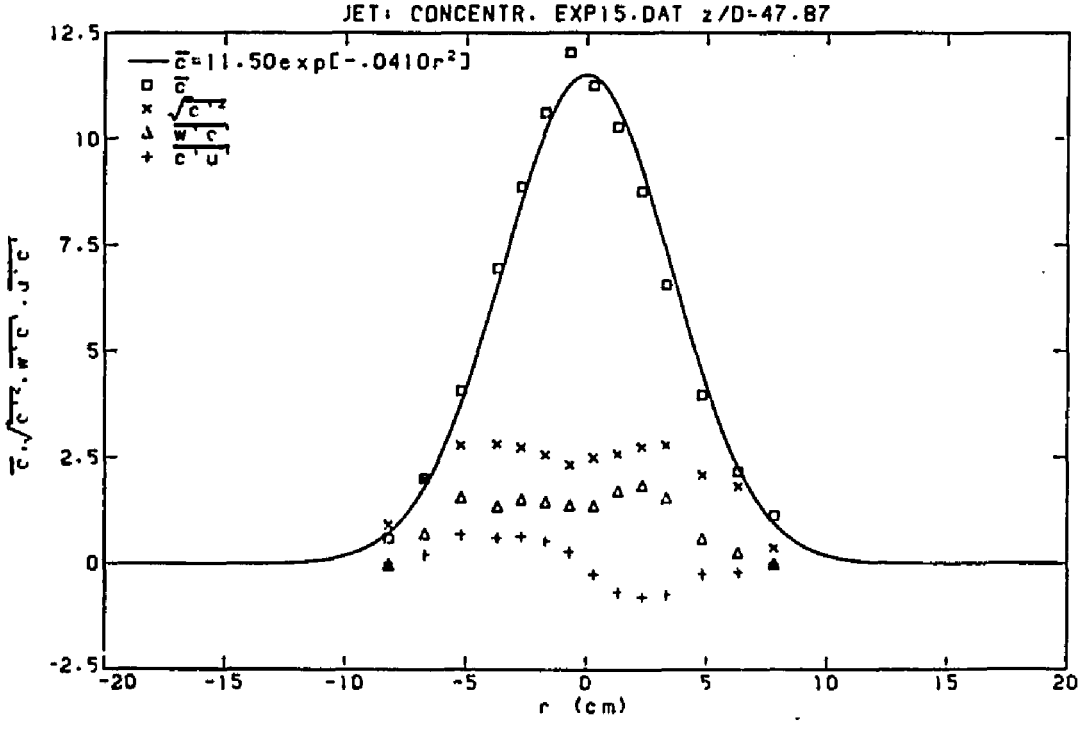

EXP16

| X | W | WP | UP | WPUP | C | CP | WPCP | UPCP |
|---|---|---|---|---|---|---|---|---|
| 68.000 | 0.073 | 0.131 | 0.192 | -0.000 | 0.229 | 0.090 | -0.001 | -0.000 |
| 70.000 | 0.206 | 0.341 | 0.342 | -0.005 | 1.370 | 1.348 | 0.055 | 0.044 |
| 72.000 | 0.877 | 0.671 | 0.469 | -0.062 | 2.279 | 1.720 | 0.618 | 0.247 |
| 74.000 | 2.178 | 1.048 | 0.658 | -0.200 | 4.697 | 2.128 | 1.082 | 0.535 |
| 76.000 | 3.555 | 1.095 | 0.775 | -0.208 | 6.237 | 1.992 | 1.061 | 0.531 |
| 80.000 | 5.545 | 1.207 | 0.914 | 0.144 | 8.131 | 1.889 | 1.188 | -0.122 |
| 82.000 | 4.454 | 1.239 | 0.864 | 0.236 | 6.815 | 1.817 | 1.021 | -0.342 |
| 84.000 | 3.010 | 1.109 | 0.753 | 0.253 | 5.282 | 2.060 | 1.138 | -0.537 |
| 86.000 | 1.470 | 0.924 | 0.659 | 0.243 | 3.083 | 2.000 | 1.087 | -0.561 |
| 88.000 | 0.837 | 0.630 | 0.528 | 0.097 | 1.884 | 1.620 | 0.483 | -0.198 |
| 90.000 | 0.065 | 0.289 | 0.271 | 0.024 | 0.756 | 0.704 | 0.039 | -0.061 |
| 92.000 | -0.044 | 0.151 | 0.264 | -0.004 | 0.624 | 0.408 | -0.019 | -0.009 |

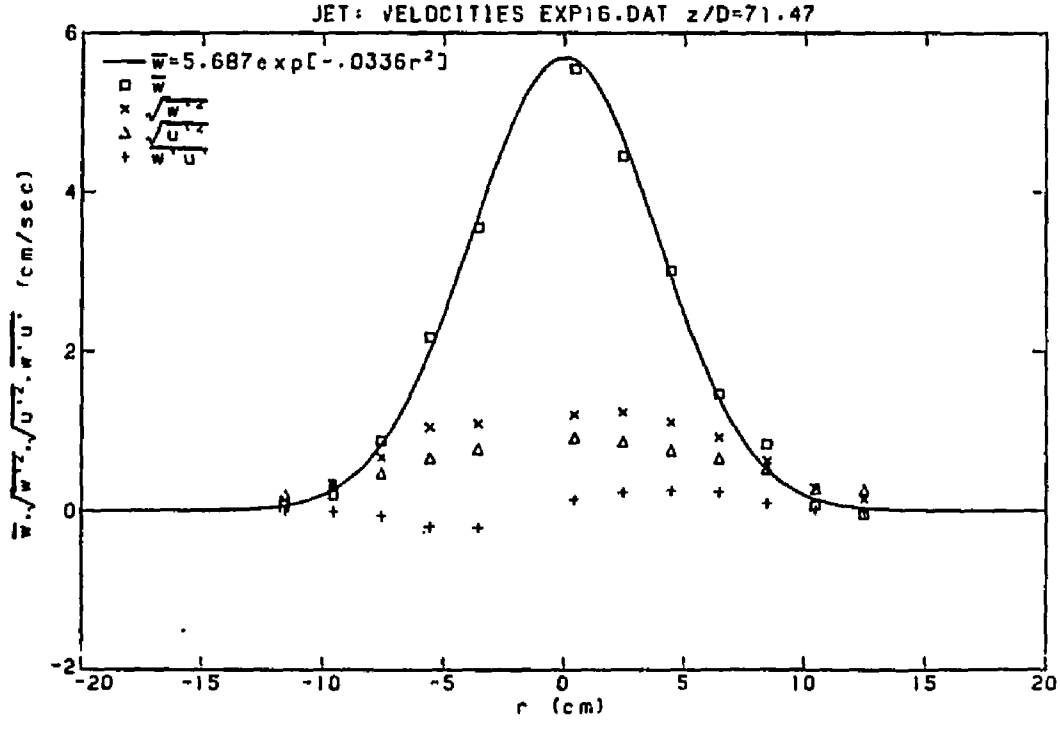

**EXP16**

| X | W | WP | UP | WPUP | C | CP | WPCP | UPCP |
|---|---|---|---|---|---|---|---|---|
| 68.000 | 0.073 | 0.131 | 0.192 | -0.000 | 0.229 | 0.090 | -0.001 | -0.000 |
| 70.000 | 0.206 | 0.341 | 0.342 | -0.005 | 1.370 | 1.348 | 0.055 | 0.044 |
| 72.000 | 0.877 | 0.671 | 0.469 | -0.062 | 2.279 | 1.720 | 0.618 | 0.247 |
| 74.000 | 2.178 | 1.048 | 0.658 | -0.200 | 4.697 | 2.128 | 1.082 | 0.535 |
| 76.000 | 3.555 | 1.095 | 0.775 | -0.208 | 6.237 | 1.992 | 1.061 | 0.531 |
| 80.000 | 5.545 | 1.207 | 0.914 | 0.144 | 8.131 | 1.889 | 1.188 | -0.122 |
| 82.000 | 4.454 | 1.239 | 0.864 | 0.236 | 6.815 | 1.817 | 1.021 | -0.342 |
| 84.000 | 3.010 | 1.109 | 0.753 | 0.253 | 5.282 | 2.060 | 1.138 | -0.537 |
| 86.000 | 1.470 | 0.924 | 0.659 | 0.243 | 3.083 | 2.000 | 1.087 | -0.561 |
| 88.000 | 0.837 | 0.630 | 0.528 | 0.097 | 1.884 | 1.620 | 0.483 | -0.198 |
| 90.000 | 0.065 | 0.289 | 0.271 | 0.024 | 0.756 | 0.704 | 0.039 | -0.061 |
| 92.000 | -0.044 | 0.151 | 0.264 | -0.004 | 0.624 | 0.408 | -0.019 | -0.009 |

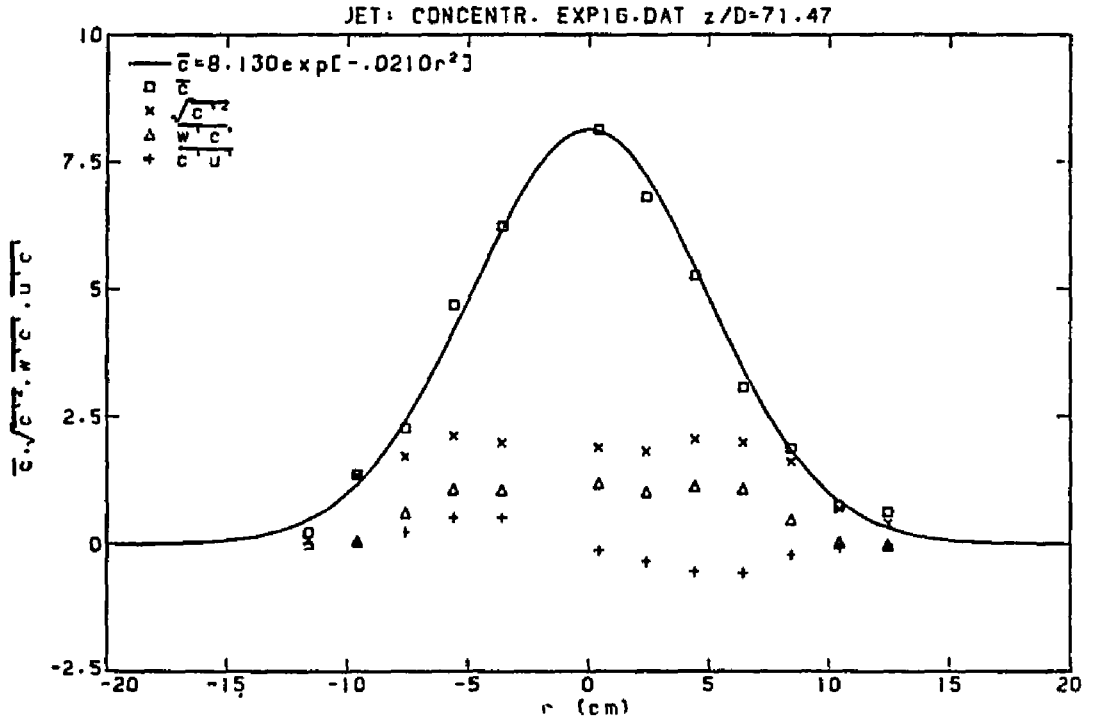

EXP17

| X | W | WP | UP | WPUP | C | CP | WPCP | UPCP |
|---|---|---|---|---|---|---|---|---|
| 74.000 | 0.205 | 0.135 | 0.161 | -0.005 | 0.987 | 0.910 | 0.035 | 0.025 |
| 75.000 | 0.310 | 0.259 | 0.239 | -0.003 | 1.602 | 1.350 | 0.141 | 0.075 |
| 76.000 | 0.890 | 0.570 | 0.454 | -0.040 | 4.574 | 3.126 | 0.810 | 0.313 |
| 77.000 | 2.227 | 1.066 | 0.641 | -0.102 | 8.205 | 3.696 | 2.358 | 0.571 |
| 78.000 | 4.282 | 1.142 | 0.841 | -0.116 | 12.804 | 3.726 | 1.913 | 0.758 |
| 79.000 | 6.058 | 1.286 | 0.947 | -0.058 | 15.958 | 3.280 | 2.016 | 0.394 |
| 80.000 | 6.509 | 1.276 | 1.003 | 0.101 | 16.643 | 3.271 | 2.029 | -0.137 |
| 81.000 | 5.611 | 1.334 | 0.962 | 0.269 | 15.540 | 3.582 | 2.522 | -0.813 |
| 82.000 | 3.899 | 1.193 | 0.878 | 0.208 | 12.364 | 3.897 | 2.233 | -0.949 |
| 83.000 | 1.794 | 1.007 | 0.672 | 0.148 | 7.316 | 3.558 | 1.732 | -0.639 |
| 84.000 | 0.481 | 0.499 | 0.414 | 0.037 | 3.042 | 2.566 | 0.637 | -0.325 |
| 85.000 | 0.149 | 0.195 | 0.248 | 0.004 | 1.194 | 1.793 | 0.031 | -0.079 |
| 86.000 | -0.029 | 0.115 | 0.177 | -0.001 | 0.319 | 0.811 | -0.009 | -0.032 |

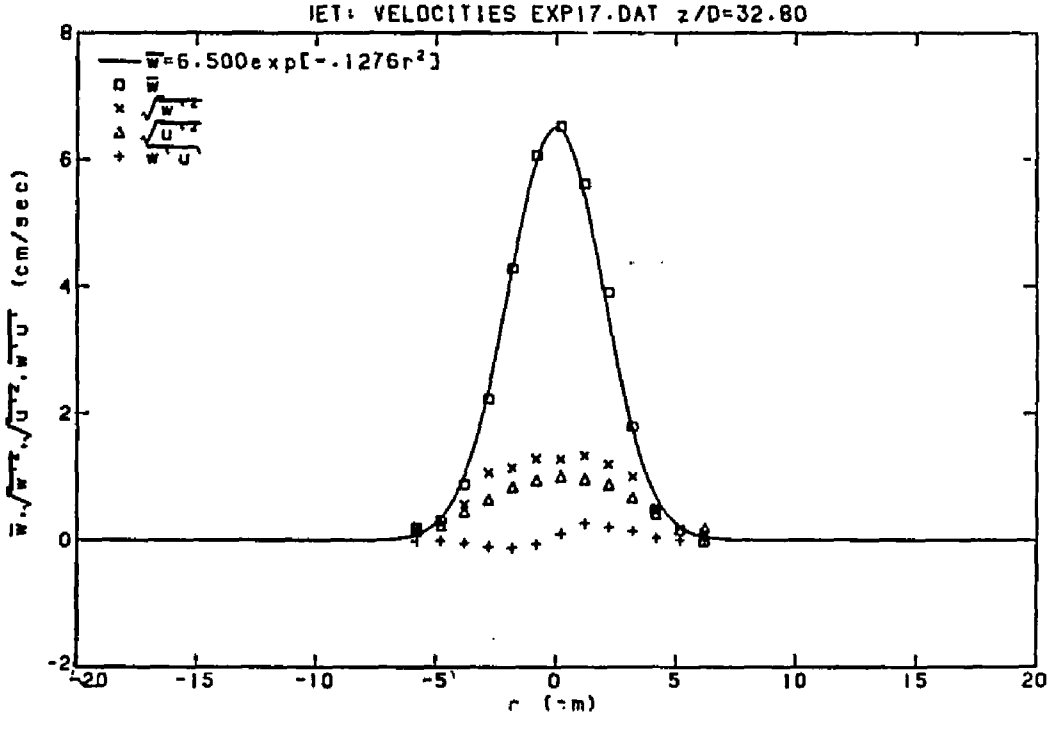

EXP17

| X | W | WP | UP | WPUP | C | CP | WPCP | UPCP |
|---|---|---|---|---|---|---|---|---|
| 74.000 | 0.205 | 0.135 | 0.161 | -0.005 | 0.987 | 0.910 | 0.035 | 0.025 |
| 75.000 | 0.310 | 0.259 | 0.239 | -0.003 | 1.602 | 1.350 | 0.141 | 0.075 |
| 76.000 | 0.890 | 0.570 | 0.454 | -0.040 | 4.574 | 3.126 | 0.810 | 0.313 |
| 77.000 | 2.227 | 1.066 | 0.641 | -0.102 | 8.205 | 3.696 | 2.358 | 0.571 |
| 78.000 | 4.282 | 1.142 | 0.841 | -0.116 | 12.804 | 3.726 | 1.913 | 0.758 |
| 79.000 | 6.058 | 1.286 | 0.947 | -0.058 | 15.958 | 3.280 | 2.016 | 0.394 |
| 80.000 | 6.509 | 1.276 | 1.003 | 0.101 | 16.643 | 3.271 | 2.029 | -0.137 |
| 81.000 | 5.611 | 1.334 | 0.962 | 0.269 | 15.540 | 3.582 | 2.522 | -0.813 |
| 82.000 | 3.899 | 1.193 | 0.878 | 0.208 | 12.364 | 3.897 | 2.233 | -0.949 |
| 83.000 | 1.794 | 1.007 | 0.672 | 0.148 | 7.316 | 3.558 | 1.732 | -0.639 |
| 84.000 | 0.481 | 0.499 | 0.414 | 0.037 | 3.042 | 2.566 | 0.637 | -0.325 |
| 85.000 | 0.149 | 0.195 | 0.248 | 0.004 | 1.194 | 1.793 | 0.031 | -0.079 |
| 86.000 | -0.029 | 0.115 | 0.177 | -0.001 | 0.319 | 0.811 | -0.009 | -0.032 |

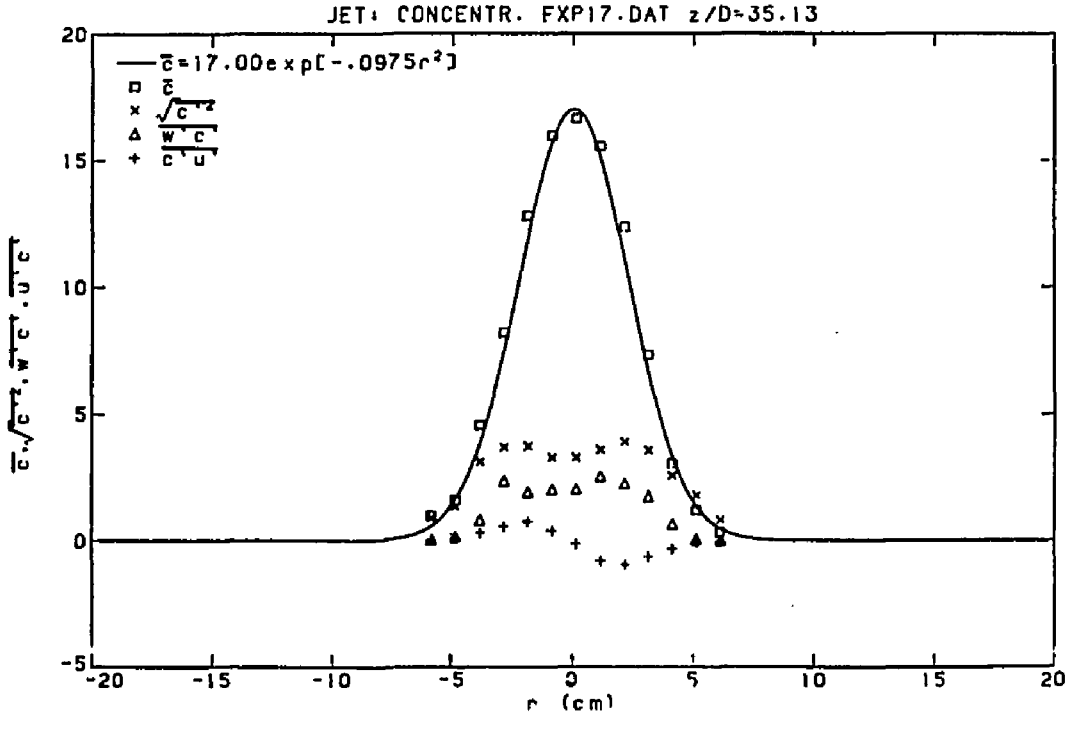

EXP18

| X | W | WP | UP | WPUP | C | CP | WPCP | UPCP |
|---|---|---|---|---|---|---|---|---|
| 70.000 | 0.170 | 0.099 | 0.182 | -0.001 | 0.018 | 0.157 | -0.004 | -0.002 |
| 71.500 | 0.367 | 0.294 | 0.245 | -0.014 | 1.032 | 1.426 | 0.294 | 0.106 |
| 73.000 | 1.703 | 0.562 | 0.430 | -0.065 | 4.290 | 1.987 | 0.545 | 0.285 |
| 75.000 | 2.105 | 0.639 | 0.462 | -0.057 | 4.915 | 2.100 | 0.671 | 0.304 |
| 77.000 | 2.562 | 0.705 | 0.528 | -0.097 | 5.988 | 2.168 | 0.762 | 0.351 |
| 78.500 | 3.200 | 0.750 | 0.569 | -0.053 | 7.310 | 1.956 | 0.625 | 0.251 |
| 80.000 | 3.661 | 0.778 | 0.567 | -0.050 | 7.539 | 1.898 | 0.745 | 0.100 |
| 82.000 | 3.358 | 0.676 | 0.576 | 0.072 | 7.233 | 1.870 | 0.446 | -0.166 |
| 84.000 | 1.914 | 0.633 | 0.491 | 0.077 | 4.598 | 1.916 | 0.508 | -0.303 |
| 86.000 | 0.852 | 0.566 | 0.413 | 0.063 | 2.182 | 1.990 | 0.678 | -0.301 |

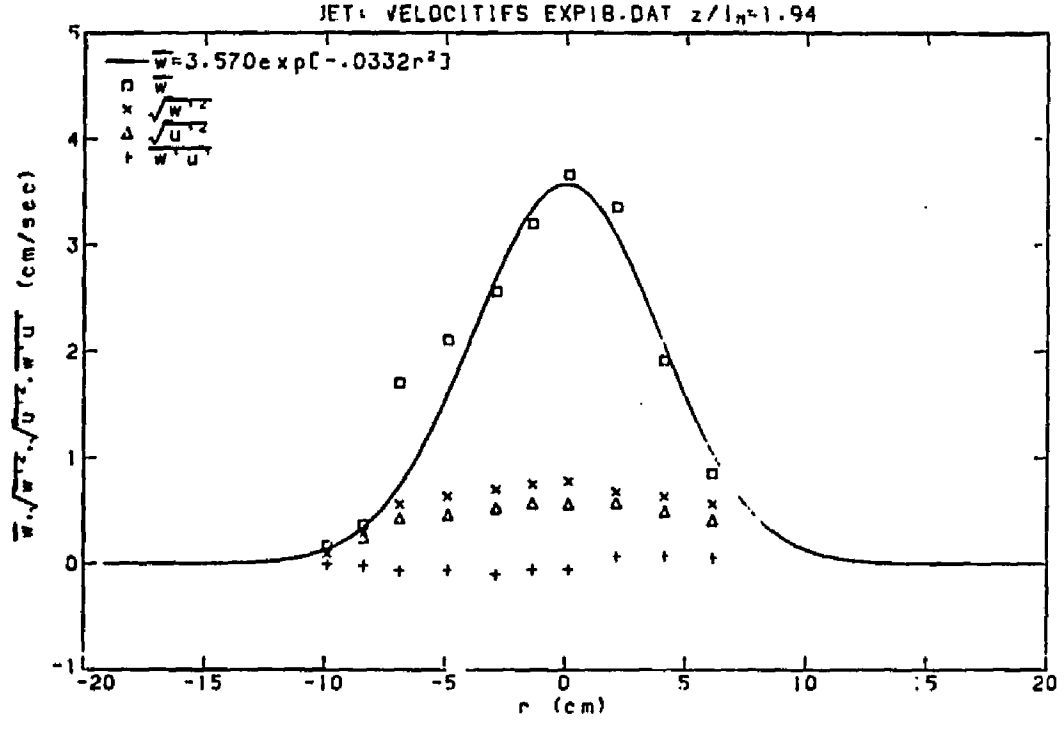

**EXP18**

| X | W | WP | UP | WPUP | C | CP | WPCP | UPCP |
|---|---|---|---|---|---|---|---|---|
| 70.000 | 0.170 | 0.099 | 0.182 | -0.001 | 0.018 | 0.157 | -0.004 | -0.002 |
| 71.500 | 0.367 | 0.294 | 0.245 | -0.014 | 1.032 | 1.426 | 0.294 | 0.106 |
| 73.000 | 1.703 | 0.562 | 0.430 | -0.065 | 4.290 | 1.987 | 0.545 | 0.285 |
| 75.000 | 2.105 | 0.639 | 0.462 | -0.057 | 4.915 | 2.100 | 0.671 | 0.304 |
| 77.000 | 2.562 | 0.705 | 0.528 | -0.097 | 5.988 | 2.168 | 0.762 | 0.351 |
| 78.500 | 3.200 | 0.750 | 0.569 | -0.053 | 7.310 | 1.956 | 0.625 | 0.251 |
| 80.000 | 3.661 | 0.778 | 0.567 | -0.050 | 7.539 | 1.898 | 0.745 | 0.100 |
| 82.000 | 3.358 | 0.676 | 0.576 | 0.072 | 7.233 | 1.870 | 0.446 | -0.166 |
| 84.000 | 1.914 | 0.633 | 0.491 | 0.077 | 4.598 | 1.916 | 0.508 | -0.303 |
| 86.000 | 0.852 | 0.566 | 0.413 | 0.063 | 2.182 | 1.990 | 0.678 | -0.301 |

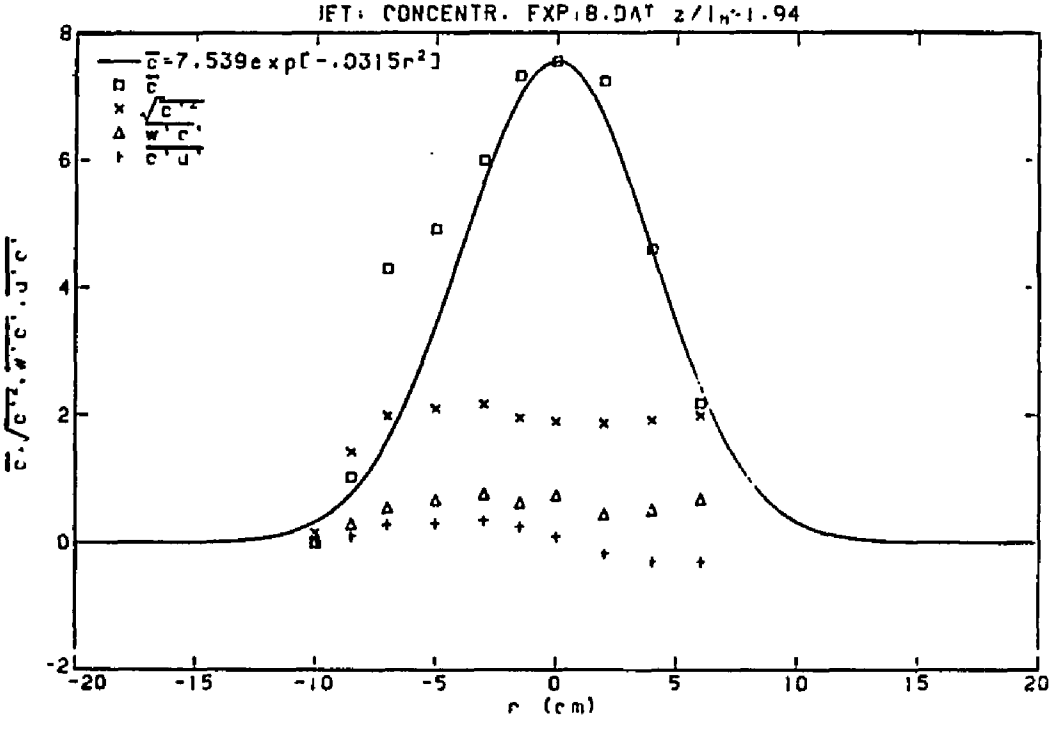

EXP19

| X | W | WP | UP | WPUP | C | CP | WPCP | UPCP |
|---|---|---|---|---|---|---|---|---|
| 70.000 | 0.108 | 0.118 | 0.155 | -0.001 | 0.356 | 0.345 | -0.006 | 0.007 |
| 72.000 | 0.400 | 0.374 | 0.242 | -0.022 | 2.304 | 1.699 | 0.254 | 0.070 |
| 74.000 | 1.024 | 0.517 | 0.383 | -0.067 | 4.593 | 2.545 | 0.523 | 0.320 |
| 76.000 | 2.233 | 0.718 | 0.486 | -0.071 | 7.142 | 2.872 | 0.996 | 0.426 |
| 78.000 | 3.164 | 0.715 | 0.535 | -0.053 | 9.202 | 2.362 | 0.711 | 0.324 |
| 80.000 | 3.475 | 0.736 | 0.532 | 0.014 | 9.717 | 2.209 | 0.705 | -0.036 |
| 82.000 | 2.908 | 0.724 | 0.510 | 0.080 | 8.239 | 2.509 | 0.690 | -0.268 |
| 84.000 | 1.569 | 0.685 | 0.470 | 0.105 | 5.472 | 2.562 | 0.788 | -0.481 |
| 86.000 | 0.747 | 0.490 | 0.358 | 0.049 | 2.864 | 2.338 | 0.455 | -0.223 |
| 88.000 | 0.331 | 0.311 | 0.307 | -0.007 | 1.601 | 1.818 | 0.172 | -0.109 |
| 90.000 | 0.082 | 0.131 | 0.205 | -0.003 | 0.237 | 0.935 | -0.002 | -0.005 |

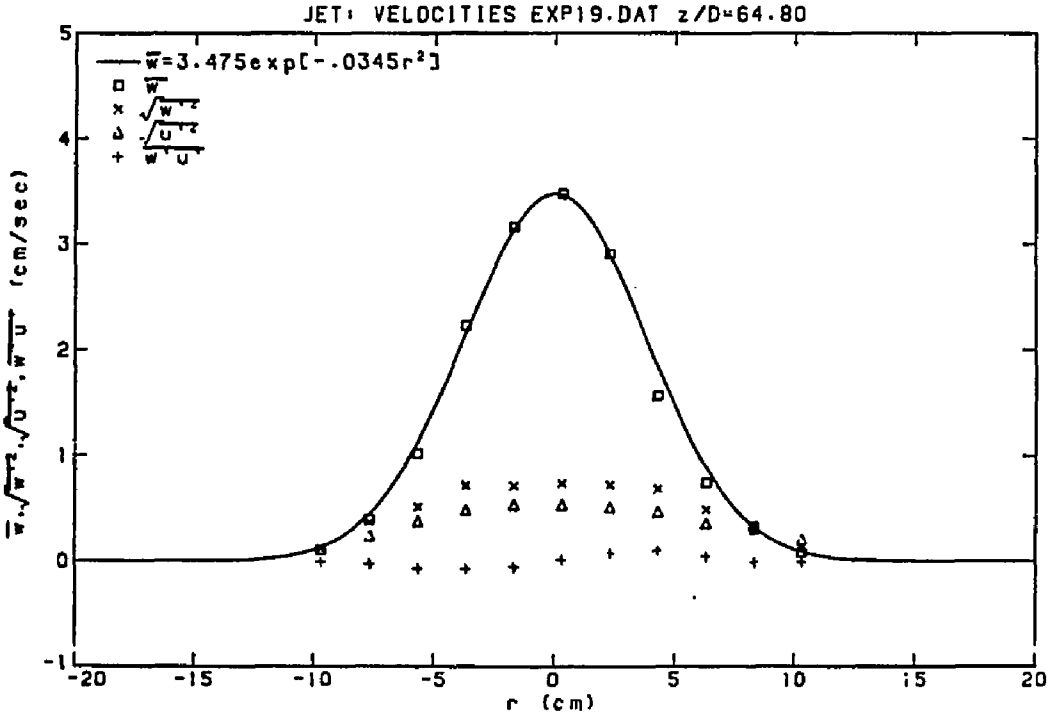

EXP19

| X | W | WP | UP | WPUP | C | CP | WPCP | UPCP |
|---|---|---|---|---|---|---|---|---|
| 70.000 | 0.108 | 0.118 | 0.155 | -0.001 | 0.356 | 0.345 | -0.006 | 0.007 |
| 72.000 | 0.400 | 0.374 | 0.242 | -0.022 | 2.304 | 1.699 | 0.254 | 0.070 |
| 74.000 | 1.024 | 0.517 | 0.383 | -0.067 | 4.593 | 2.545 | 0.523 | 0.320 |
| 76.000 | 2.233 | 0.718 | 0.486 | -0.071 | 7.142 | 2.872 | 0.996 | 0.426 |
| 78.000 | 3.164 | 0.715 | 0.535 | -0.053 | 9.202 | 2.362 | 0.711 | 0.324 |
| 80.000 | 3.475 | 0.736 | 0.532 | 0.014 | 9.717 | 2.209 | 0.705 | -0.036 |
| 82.000 | 2.908 | 0.724 | 0.510 | 0.080 | 8.239 | 2.509 | 0.690 | -0.268 |
| 84.000 | 1.569 | 0.685 | 0.470 | 0.105 | 5.472 | 2.562 | 0.788 | -0.481 |
| 86.000 | 0.747 | 0.490 | 0.358 | 0.049 | 2.864 | 2.338 | 0.455 | -0.223 |
| 88.000 | 0.331 | 0.311 | 0.307 | -0.007 | 1.601 | 1.818 | 0.172 | -0.109 |
| 90.000 | 0.082 | 0.131 | 0.205 | -0.003 | 0.237 | 0.935 | -0.002 | -0.005 |

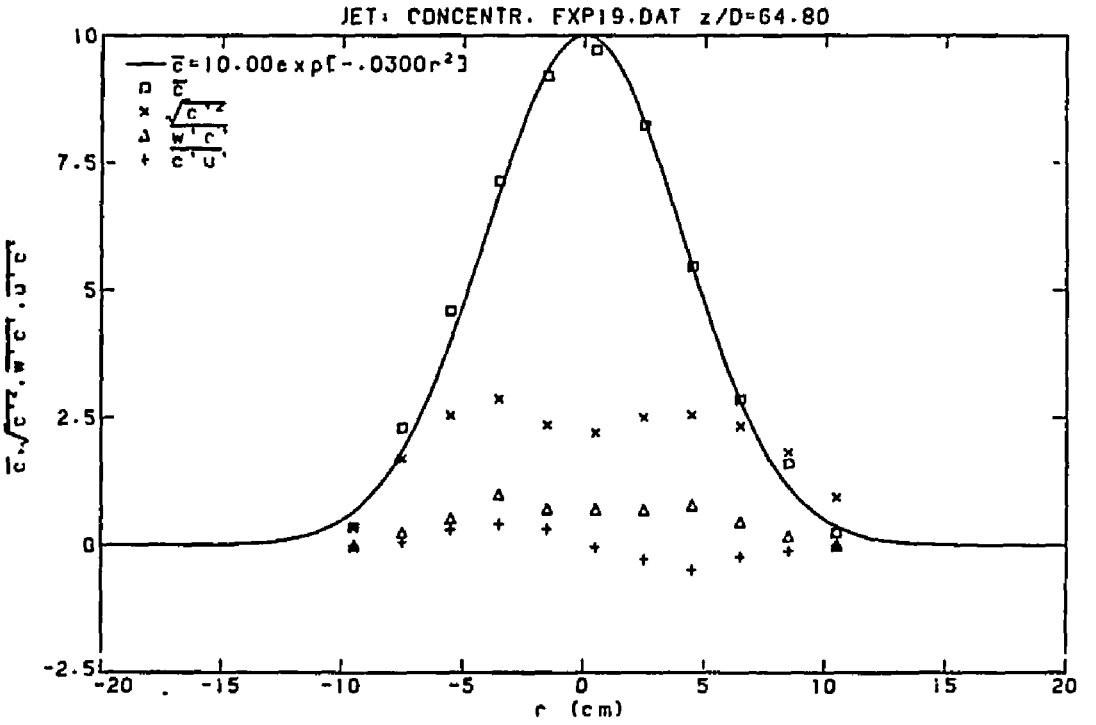

EXP20

| X | W | WP | UP | WPUP | C | CP | WPCP | UPCP |
|---|---|---|---|---|---|---|---|---|
| 67.500 | 0.195 | 0.213 | 0.222 | -0.005 | 0.625 | 0.974 | 0.079 | 0.059 |
| 70.000 | 0.462 | 0.361 | 0.315 | -0.016 | 1.724 | 1.472 | 0.184 | 0.115 |
| 72.500 | 0.995 | 0.520 | 0.442 | -0.066 | 2.744 | 1.649 | 0.394 | 0.235 |
| 75.000 | 2.455 | 0.817 | 0.502 | -0.088 | 5.234 | 1.728 | 0.603 | 0.239 |
| 77.500 | 3.182 | 0.936 | 0.572 | -0.156 | 5.748 | 1.885 | 0.886 | 0.376 |
| 80.000 | 3.728 | 0.882 | 0.628 | 0.008 | 6.753 | 1.477 | 0.506 | 0.072 |
| 82.500 | 3.264 | 0.811 | 0.573 | 0.086 | 6.281 | 1.647 | 0.558 | -0.254 |
| 85.000 | 2.103 | 0.750 | 0.557 | 0.171 | 4.296 | 1.652 | 0.372 | -0.298 |
| 87.500 | 1.445 | 0.540 | 0.445 | 0.073 | 3.449 | 1.493 | 0.322 | -0.173 |
| 90.000 | 0.597 | 0.484 | 0.380 | 0.070 | 1.791 | 1.210 | 0.217 | -0.130 |
| 92.500 | 0.243 | 0.245 | 0.319 | -0.013 | 0.702 | 1.042 | 0.124 | -0.032 |

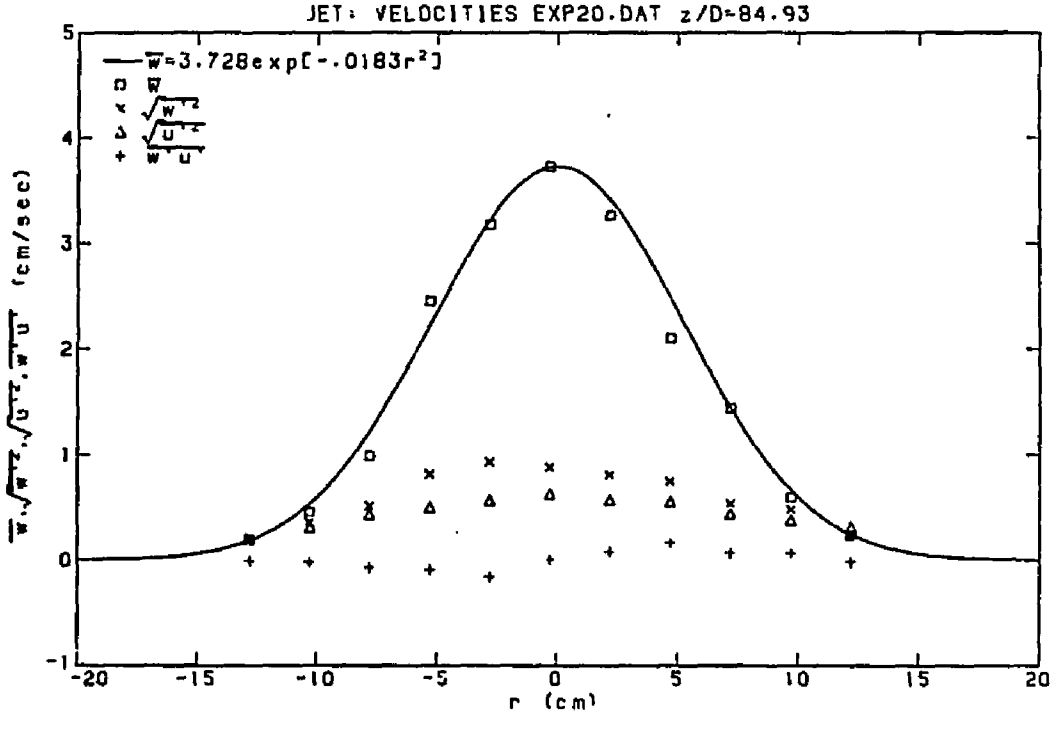

EXP20

| X | W | WP | UP | WPUP | C | CP | WPCP | UPCP |
|---|---|---|---|---|---|---|---|---|
| 67.500 | 0.195 | 0.213 | 0.222 | -0.005 | 0.625 | 0.974 | 0.079 | 0.059 |
| 70.000 | 0.462 | 0.361 | 0.315 | -0.016 | 1.724 | 1.472 | 0.184 | 0.115 |
| 72.500 | 0.995 | 0.520 | 0.442 | -0.066 | 2.744 | 1.649 | 0.394 | 0.235 |
| 75.000 | 2.455 | 0.817 | 0.502 | -0.088 | 5.234 | 1.728 | 0.603 | 0.239 |
| 77.500 | 3.182 | 0.936 | 0.572 | -0.156 | 5.748 | 1.885 | 0.886 | 0.376 |
| 80.000 | 3.728 | 0.882 | 0.628 | 0.008 | 6.753 | 1.477 | 0.506 | 0.072 |
| 82.500 | 3.264 | 0.811 | 0.573 | 0.086 | 6.281 | 1.647 | 0.558 | -0.254 |
| 85.000 | 2.103 | 0.750 | 0.557 | 0.171 | 4.296 | 1.652 | 0.372 | -0.298 |
| 87.500 | 1.445 | 0.540 | 0.445 | 0.073 | 3.449 | 1.493 | 0.322 | -0.173 |
| 90.000 | 0.597 | 0.484 | 0.380 | 0.070 | 1.791 | 1.210 | 0.217 | -0.130 |
| 92.500 | 0.243 | 0.245 | 0.319 | -0.013 | 0.702 | 1.042 | 0.124 | -0.032 |

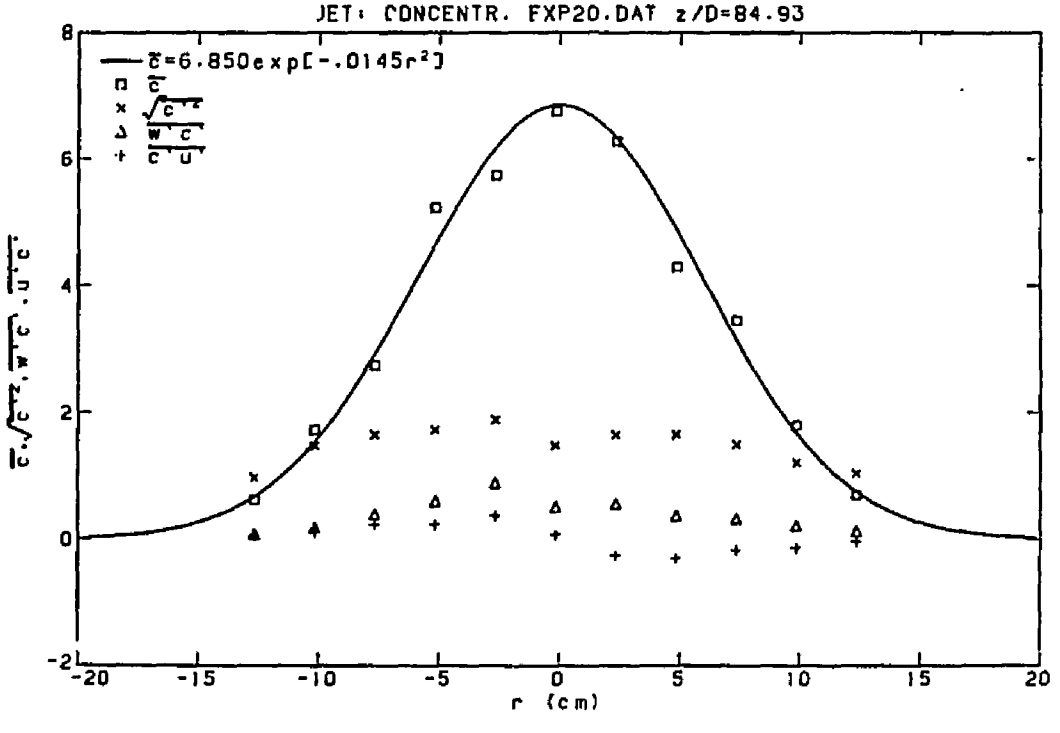

**EXP21**

| X | W | WP | UP | WPUP | C | CP | WPCP | UPCP |
|---|---|---|---|---|---|---|---|---|
| 71.500 | 0.610 | 0.483 | 0.333 | -0.044 | 2.905 | 2.355 | 0.636 | 0.259 |
| 73.000 | 1.087 | 0.603 | 0.407 | -0.073 | 4.590 | 2.638 | 0.670 | 0.333 |
| 74.500 | 2.018 | 0.691 | 0.479 | -0.112 | 6.990 | 2.523 | 0.772 | 0.395 |
| 76.000 | 2.608 | 0.710 | 0.553 | -0.078 | 7.832 | 2.773 | 0.962 | 0.512 |
| 77.500 | 3.194 | 0.825 | 0.606 | -0.068 | 8.450 | 2.591 | 1.057 | 0.368 |
| 79.000 | 4.012 | 0.834 | 0.638 | 0.039 | 9.569 | 2.352 | 0.858 | 0.000 |
| 80.500 | 3.322 | 0.925 | 0.581 | 0.094 | 8.285 | 2.741 | 1.117 | -0.338 |
| 82.000 | 2.164 | 0.929 | 0.585 | 0.156 | 6.109 | 2.710 | 1.281 | -0.588 |
| 83.500 | 1.200 | 0.839 | 0.521 | 0.133 | 4.286 | 2.751 | 1.135 | -0.501 |
| 85.000 | 0.364 | 0.411 | 0.277 | 0.023 | 1.320 | 1.841 | 0.406 | -0.107 |
| 86.500 | 0.019 | 0.179 | 0.259 | -0.004 | 0.537 | 0.696 | -0.031 | -0.028 |

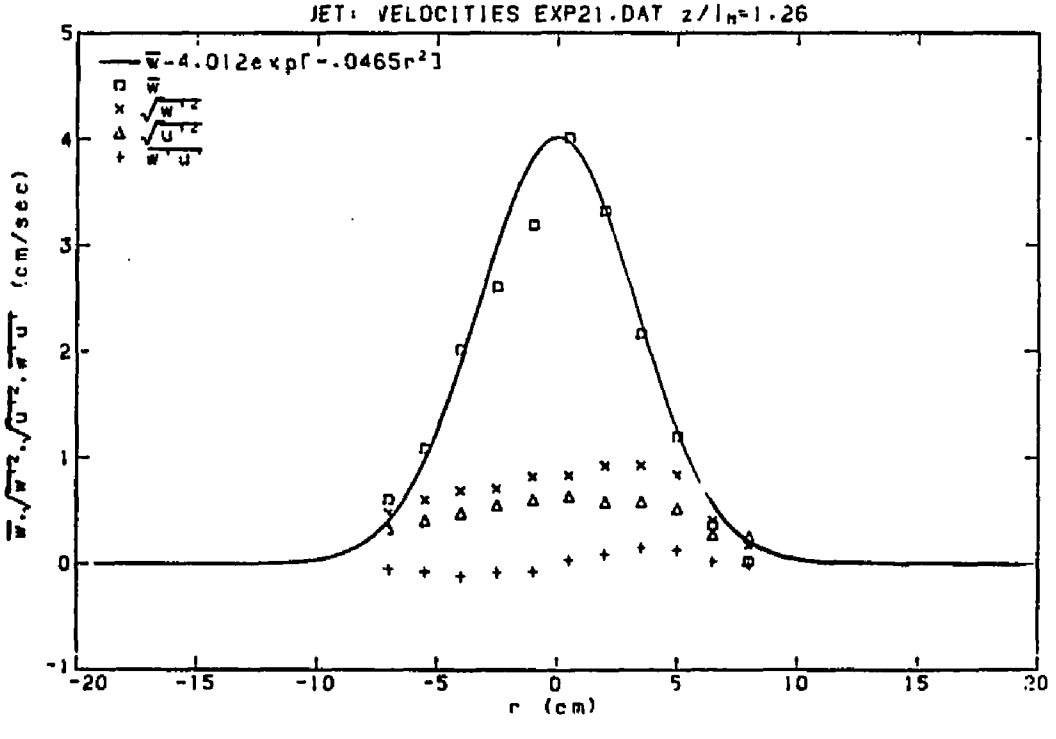

**EXP21**

| X | W | WP | UP | WPUP | C | CP | WPCP | UPCP |
|---|---|---|---|---|---|---|---|---|
| 71.500 | 0.610 | 0.483 | 0.333 | -0.044 | 2.905 | 2.355 | 0.636 | 0.259 |
| 73.000 | 1.087 | 0.603 | 0.407 | -0.073 | 4.590 | 2.638 | 0.670 | 0.333 |
| 74.500 | 2.018 | 0.691 | 0.479 | -0.112 | 6.990 | 2.523 | 0.772 | 0.395 |
| 76.000 | 2.608 | 0.710 | 0.553 | -0.078 | 7.832 | 2.773 | 0.962 | 0.512 |
| 77.500 | 3.194 | 0.825 | 0.606 | -0.068 | 8.450 | 2.591 | 1.057 | 0.368 |
| 79.000 | 4.012 | 0.834 | 0.638 | 0.039 | 9.569 | 2.352 | 0.858 | 0.000 |
| 80.500 | 3.322 | 0.925 | 0.581 | 0.094 | 8.285 | 2.741 | 1.117 | -0.338 |
| 82.000 | 2.164 | 0.929 | 0.585 | 0.156 | 6.109 | 2.710 | 1.281 | -0.588 |
| 83.500 | 1.200 | 0.839 | 0.521 | 0.133 | 4.286 | 2.751 | 1.135 | -0.501 |
| 85.000 | 0.364 | 0.411 | 0.277 | 0.023 | 1.320 | 1.841 | 0.406 | -0.107 |
| 86.500 | 0.019 | 0.179 | 0.259 | -0.004 | 0.537 | 0.696 | -0.031 | -0.028 |

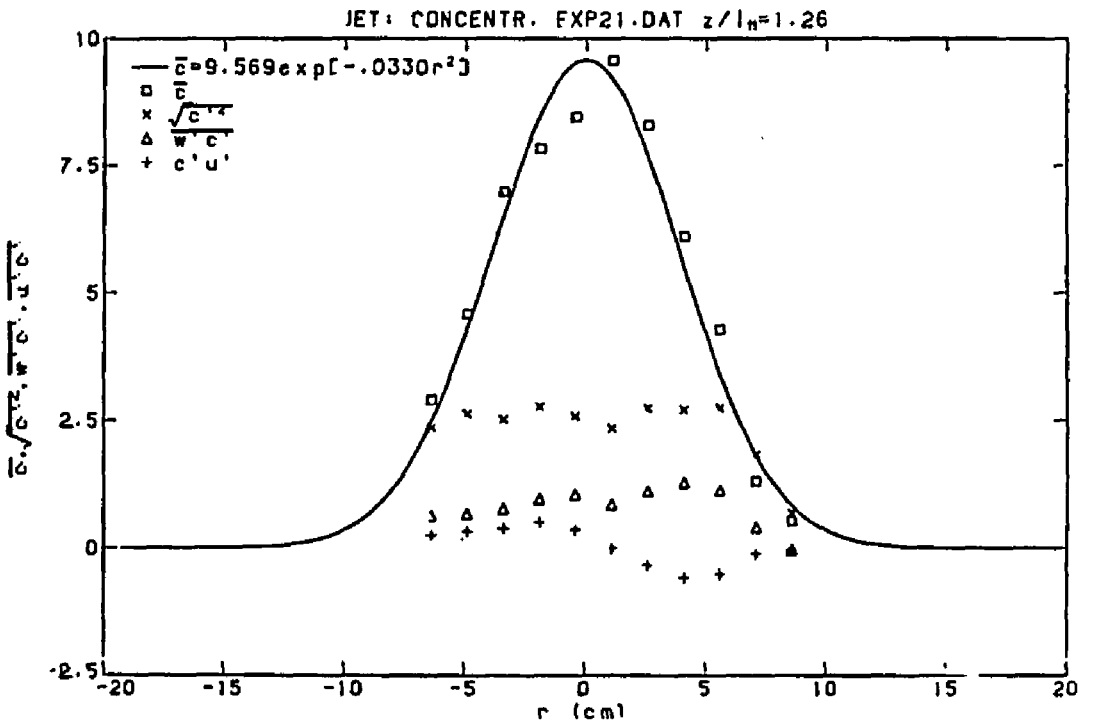

EXP23

| X | W | WP | UP | WPUP | C | CP | WPCP | UPCP |
|---|---|---|---|---|---|---|---|---|
| 67.500 | 0.092 | 0.114 | 0.182 | -0.002 | 0.255 | 0.081 | -0.000 | 0.000 |
| 70.000 | 0.474 | 0.513 | 0.351 | -0.030 | 0.577 | 0.620 | 0.203 | 0.073 |
| 72.000 | 1.211 | 0.743 | 0.518 | -0.111 | 1.521 | 1.110 | 0.492 | 0.212 |
| 74.000 | 1.627 | 1.003 | 0.557 | -0.113 | 2.090 | 1.420 | 0.841 | 0.261 |
| 76.000 | 3.358 | 1.058 | 0.667 | -0.244 | 3.738 | 1.683 | 1.058 | 0.419 |
| 78.000 | 4.542 | 1.009 | 0.697 | -0.109 | 4.793 | 1.693 | 0.957 | 0.269 |
| 80.000 | 5.023 | 1.048 | 0.734 | 0.048 | 5.250 | 1.595 | 0.879 | -0.067 |
| 82.000 | 4.450 | 1.014 | 0.721 | 0.182 | 4.512 | 1.492 | 0.789 | -0.296 |
| 84.000 | 3.116 | 1.007 | 0.690 | 0.222 | 3.292 | 1.434 | 0.722 | -0.380 |
| 86.000 | 1.733 | 0.945 | 0.599 | 0.248 | 1.776 | 1.214 | 0.703 | -0.301 |
| 88.000 | 1.048 | 0.771 | 0.521 | 0.157 | 1.189 | 0.965 | 0.418 | -0.191 |
| 90.000 | 0.059 | 0.281 | 0.302 | 0.016 | 0.422 | 0.475 | 0.046 | -0.044 |

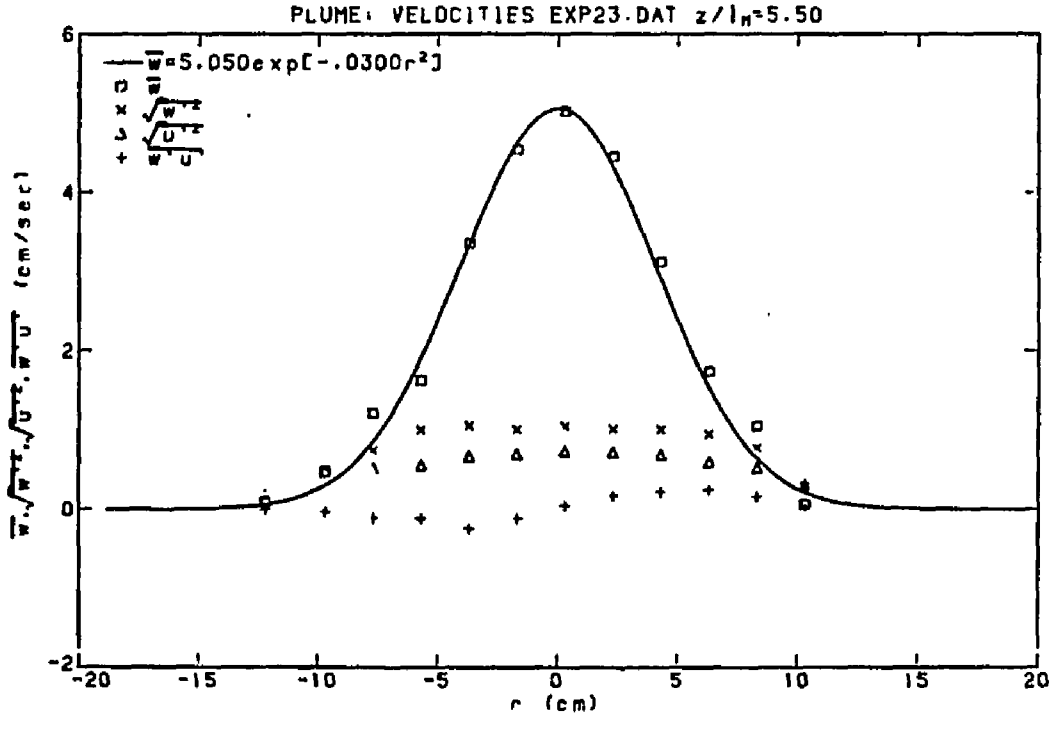

EXP23

| X | W | WP | UP | WPUP | C | CP | WPCP | UPCP |
|---|---|---|---|---|---|---|---|---|
| 67.500 | 0.092 | 0.114 | 0.182 | -0.002 | 0.255 | 0.081 | -0.000 | 0.000 |
| 70.000 | 0.474 | 0.513 | 0.351 | -0.030 | 0.577 | 0.620 | 0.203 | 0.073 |
| 72.000 | 1.211 | 0.743 | 0.518 | -0.111 | 1.521 | 1.110 | 0.492 | 0.212 |
| 74.000 | 1.627 | 1.003 | 0.557 | -0.113 | 2.090 | 1.420 | 0.841 | 0.261 |
| 76.000 | 3.358 | 1.058 | 0.667 | -0.244 | 3.738 | 1.683 | 1.058 | 0.419 |
| 78.000 | 4.542 | 1.009 | 0.697 | -0.109 | 4.793 | 1.693 | 0.957 | 0.269 |
| 80.000 | 5.023 | 1.048 | 0.734 | 0.048 | 5.250 | 1.595 | 0.879 | -0.067 |
| 82.000 | 4.450 | 1.014 | 0.721 | 0.182 | 4.512 | 1.492 | 0.789 | -0.296 |
| 84.000 | 3.116 | 1.007 | 0.690 | 0.222 | 3.292 | 1.434 | 0.722 | -0.380 |
| 86.000 | 1.733 | 0.945 | 0.599 | 0.248 | 1.776 | 1.214 | 0.703 | -0.301 |
| 88.000 | 1.048 | 0.771 | 0.521 | 0.157 | 1.189 | 0.965 | 0.418 | -0.191 |
| 90.000 | 0.059 | 0.281 | 0.302 | 0.016 | 0.422 | 0.475 | 0.046 | -0.044 |

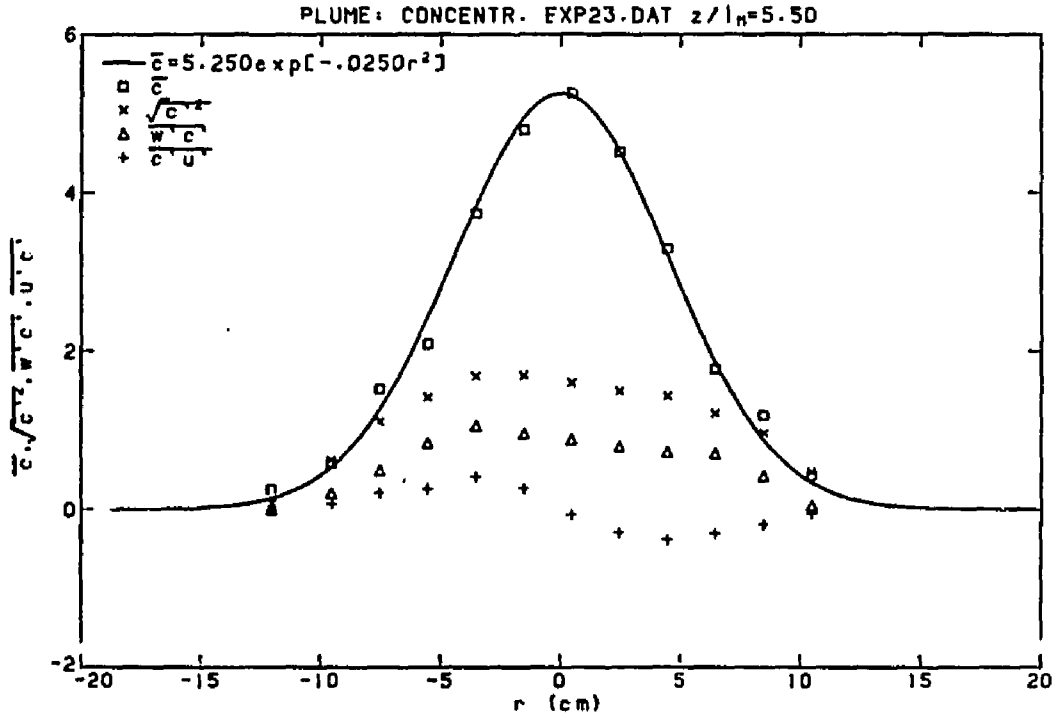

EXP25

| X | W | WP | UP | WPUP | C | CP | WPCP | UPCP |
|---|---|---|---|---|---|---|---|---|
| 69.000 | 0.471 | 0.287 | 0.267 | -0.020 | 0.730 | 0.573 | 0.067 | 0.037 |
| 70.500 | 0.945 | 0.337 | 0.282 | -0.013 | 1.213 | 0.981 | 0.112 | 0.022 |
| 72.100 | 1.626 | 0.621 | 0.477 | -0.092 | 2.392 | 1.614 | 0.502 | 0.197 |
| 73.500 | 1.765 | 0.665 | 0.480 | -0.043 | 2.520 | 1.865 | 0.636 | 0.224 |
| 75.000 | 3.058 | 0.841 | 0.567 | -0.081 | 4.662 | 2.228 | 0.980 | 0.268 |
| 76.500 | 3.933 | 0.833 | 0.635 | -0.010 | 5.706 | 2.227 | 0.868 | 0.162 |
| 78.000 | 4.002 | 0.868 | 0.648 | 0.092 | 6.030 | 2.181 | 0.838 | -0.120 |
| 79.500 | 3.229 | 1.054 | 0.625 | 0.147 | 4.948 | 2.275 | 1.253 | -0.325 |
| 81.000 | 1.679 | 0.795 | 0.550 | 0.146 | 2.926 | 1.855 | 0.777 | -0.331 |
| 82.500 | 0.860 | 0.628 | 0.410 | 0.067 | 1.688 | 1.333 | 0.459 | -0.138 |
| 84.000 | 0.840 | 0.522 | 0.392 | 0.064 | 1.419 | 1.161 | 0.279 | -0.161 |
| 85.500 | 0.728 | 0.347 | 0.354 | 0.038 | 0.909 | 0.672 | 0.091 | -0.072 |
| 87.000 | 0.141 | 0.155 | 0.182 | 0.001 | 0.258 | 0.340 | 0.012 | -0.010 |

EXP28

| X | W | WP | UP | WPUP | C | CP | WPCP | UPCP |
|---|---|---|---|---|---|---|---|---|
| 72.000 | 0.663 | 0.361 | 0.338 | -0.023 | 2.700 | 1.885 | 0.210 | 0.122 |
| 70.000 | 0.174 | 0.156 | 0.207 | -0.003 | 0.359 | 0.431 | -0.004 | 0.006 |
| 74.000 | 1.877 | 0.770 | 0.528 | -0.070 | 5.588 | 2.570 | 0.772 | 0.349 |
| 76.000 | 3.942 | 1.175 | 0.795 | -0.200 | 9.639 | 2.889 | 1.643 | 0.808 |
| 79.000 | 5.302 | 1.324 | 0.825 | 0.150 | 11.422 | 2.611 | 1.676 | -0.303 |
| 80.500 | 4.430 | 1.180 | 0.788 | 0.187 | 9.823 | 2.613 | 1.301 | -0.525 |
| 82.000 | 2.545 | 1.003 | 0.621 | 0.140 | 6.928 | 2.626 | 1.043 | -0.408 |
| 83.500 | 0.935 | 0.637 | 0.437 | 0.079 | 3.757 | 2.170 | 0.602 | -0.259 |
| 85.000 | 0.150 | 0.291 | 0.288 | 0.006 | 1.292 | 1.722 | 0.109 | -0.047 |
| 86.500 | 0.031 | 0.128 | 0.198 | -0.001 | 0.052 | 0.210 | -0.005 | -0.005 |

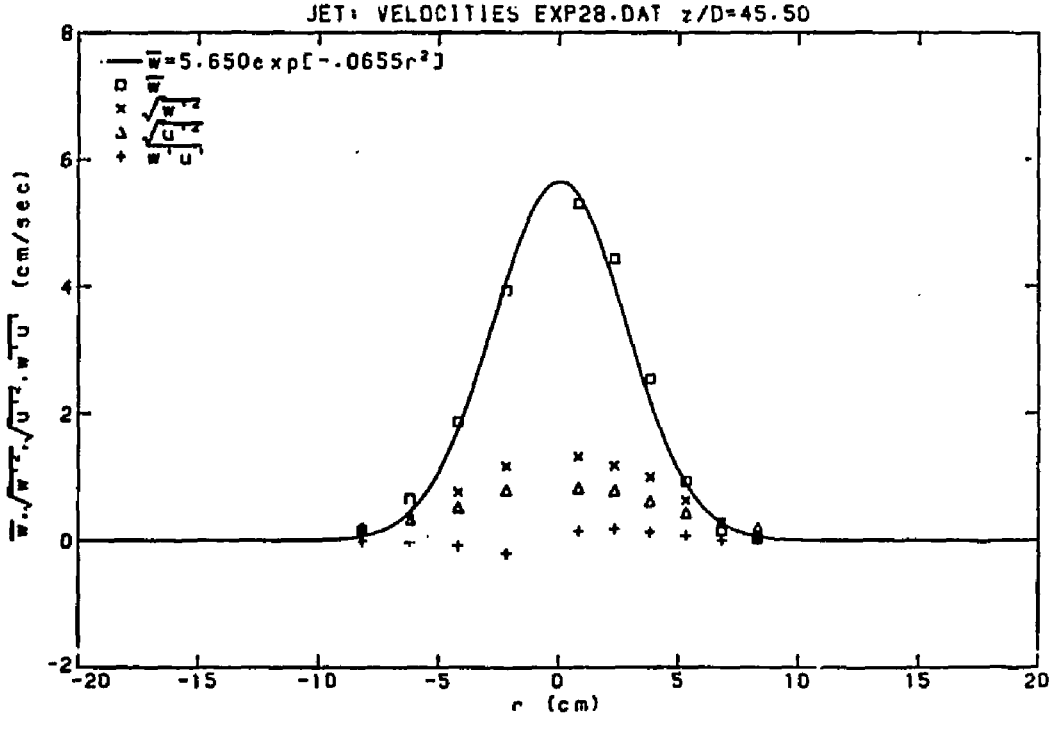

**EXP28**

| X | W | WP | UP | WPUP | C | CP | WPCP | UPCP |
|---|---|---|---|---|---|---|---|---|
| 72.000 | 0.663 | 0.361 | 0.338 | -0.023 | 2.700 | 1.885 | 0.210 | 0.122 |
| 70.000 | 0.174 | 0.156 | 0.207 | -0.003 | 0.359 | 0.431 | -0.004 | 0.006 |
| 74.000 | 1.877 | 0.770 | 0.528 | -0.070 | 5.588 | 2.570 | 0.772 | 0.349 |
| 76.000 | 3.942 | 1.175 | 0.795 | -0.200 | 9.639 | 2.889 | 1.643 | 0.808 |
| 79.000 | 5.302 | 1.324 | 0.825 | 0.150 | 11.422 | 2.611 | 1.676 | -0.303 |
| 80.500 | 4.430 | 1.180 | 0.788 | 0.187 | 9.823 | 2.613 | 1.301 | -0.525 |
| 82.000 | 2.545 | 1.003 | 0.621 | 0.140 | 6.928 | 2.626 | 1.043 | -0.408 |
| 83.500 | 0.935 | 0.637 | 0.437 | 0.079 | 3.757 | 2.170 | 0.602 | -0.259 |
| 85.000 | 0.150 | 0.291 | 0.288 | 0.006 | 1.292 | 1.722 | 0.109 | -0.047 |
| 86.500 | 0.031 | 0.128 | 0.198 | -0.001 | 0.052 | 0.210 | -0.005 | -0.005 |

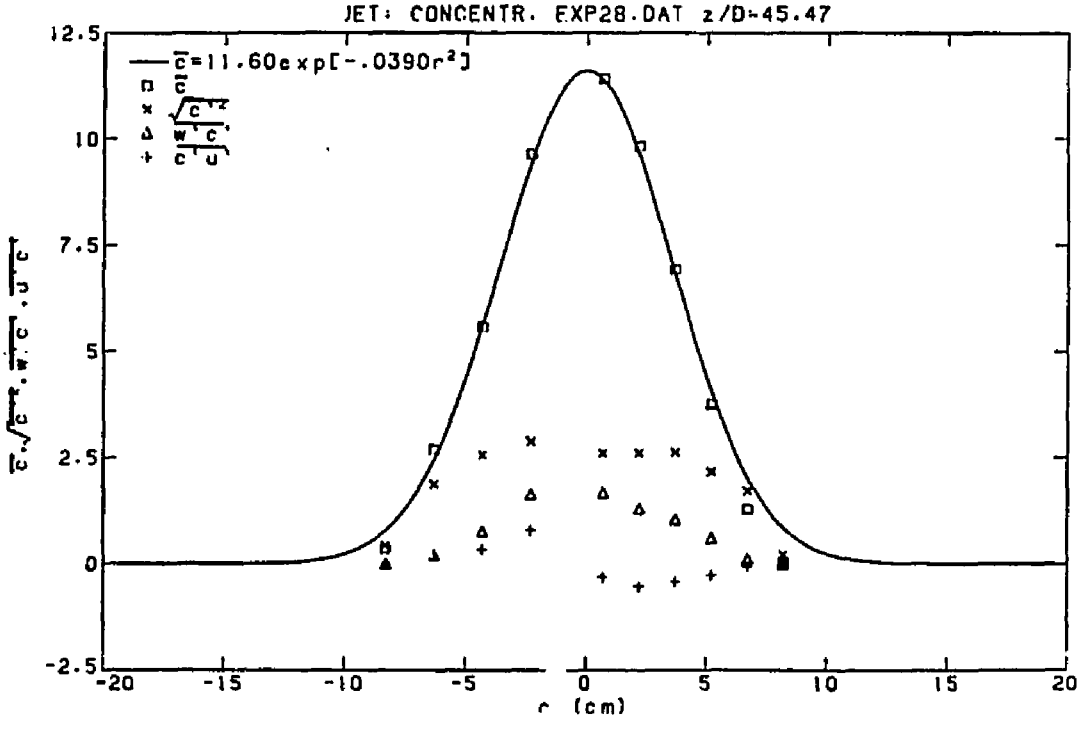

EXP29

| X | W | WP | UP | WPUP | C | CP | WPCP | UPCP |
|---|---|---|---|---|---|---|---|---|
| 64.000 | 0.439 | 0.240 | 0.300 | -0.014 | 1.388 | 0.842 | 0.095 | 0.084 |
| 67.000 | 0.705 | 0.526 | 0.349 | -0.077 | 2.791 | 1.395 | 0.436 | 0.183 |
| 70.000 | 1.745 | 0.665 | 0.447 | -0.140 | 4.744 | 1.667 | 0.512 | 0.294 |
| 73.000 | 2.685 | 0.693 | 0.515 | -0.090 | 6.463 | 1.713 | 0.585 | 0.300 |
| 76.000 | 3.302 | 0.702 | 0.554 | -0.035 | 7.183 | 1.419 | 0.408 | 0.064 |
| 79.000 | 3.108 | 0.708 | 0.598 | 0.134 | 6.686 | 1.471 | 0.483 | -0.244 |
| 82.000 | 2.426 | 0.753 | 0.530 | 0.124 | 5.813 | 1.557 | 0.492 | -0.297 |
| 85.000 | 1.453 | 0.542 | 0.411 | 0.069 | 4.238 | 1.552 | 0.437 | -0.233 |
| 88.000 | 1.001 | 0.576 | 0.422 | 0.107 | 3.236 | 1.589 | 0.451 | -0.311 |
| 91.000 | 0.332 | 0.246 | 0.229 | 0.015 | 2.103 | 1.068 | -0.018 | 0.004 |
| 94.000 | 0.178 | 0.130 | 0.203 | -0.005 | 0.682 | 0.810 | 0.019 | 0.005 |

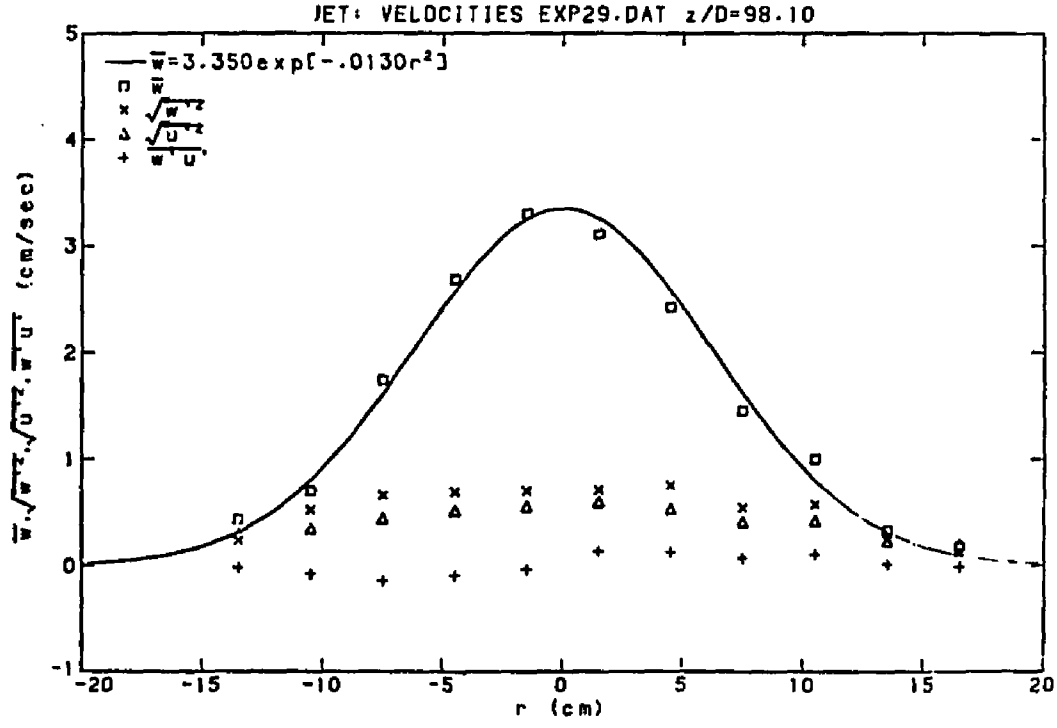

EXP29

| X | W | WP | UP | WPUP | C | CP | WPCP | UPCP |
|---|---|---|---|---|---|---|---|---|
| 64.000 | 0.439 | 0.240 | 0.300 | -0.014 | 1.388 | 0.842 | 0.095 | 0.084 |
| 67.000 | 0.705 | 0.526 | 0.349 | -0.077 | 2.791 | 1.395 | 0.436 | 0.183 |
| 70.000 | 1.745 | 0.665 | 0.447 | -0.140 | 4.744 | 1.667 | 0.512 | 0.294 |
| 73.000 | 2.685 | 0.693 | 0.515 | -0.090 | 6.463 | 1.713 | 0.585 | 0.300 |
| 76.000 | 3.302 | 0.702 | 0.554 | -0.035 | 7.183 | 1.419 | 0.408 | 0.064 |
| 79.000 | 3.108 | 0.708 | 0.598 | 0.134 | 6.686 | 1.471 | 0.483 | -0.244 |
| 82.000 | 2.426 | 0.753 | 0.530 | 0.124 | 5.813 | 1.557 | 0.492 | -0.297 |
| 85.000 | 1.453 | 0.542 | 0.411 | 0.069 | 4.238 | 1.552 | 0.437 | -0.233 |
| 88.000 | 1.001 | 0.576 | 0.422 | 0.107 | 3.236 | 1.589 | 0.451 | -0.311 |
| 91.000 | 0.332 | 0.246 | 0.229 | 0.015 | 2.103 | 1.068 | -0.018 | 0.004 |
| 94.000 | 0.178 | 0.130 | 0.203 | -0.005 | 0.682 | 0.810 | 0.019 | 0.005 |

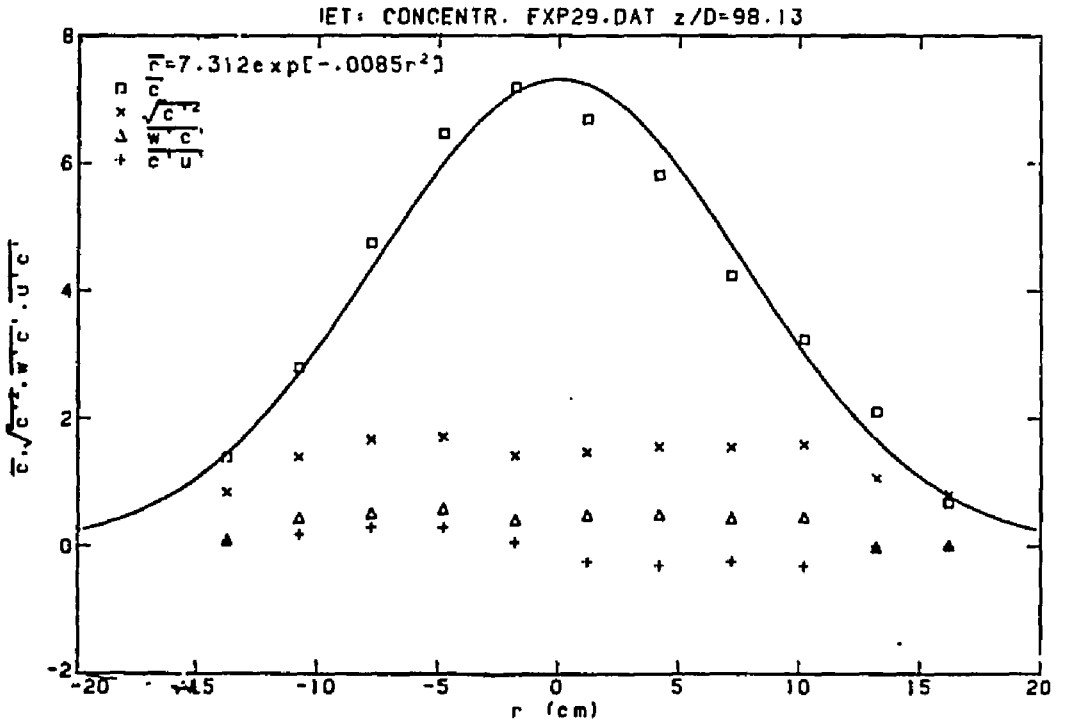

EXP30

| X | W | WP | UP | WPUP | C | CP | WPCP | UPCP |
|---|---|---|---|---|---|---|---|---|
| 66.000 | 0.084 | 0.100 | 0.163 | -0.001 | 1.030 | 0.863 | -0.032 | -0.002 |
| 68.000 | 0.136 | 0.230 | 0.239 | -0.000 | 1.426 | 1.297 | 0.077 | 0.096 |
| 70.000 | 0.587 | 0.342 | 0.288 | -0.013 | 3.985 | 1.507 | 0.180 | 0.030 |
| 72.000 | 1.112 | 0.563 | 0.429 | -0.078 | 5.122 | 1.656 | 0.402 | 0.271 |
| 74.000 | 1.932 | 0.744 | 0.495 | -0.096 | 6.564 | 1.607 | 0.448 | 0.249 |
| 76.000 | 2.881 | 0.697 | 0.554 | -0.060 | 7.646 | 1.812 | 0.619 | 0.243 |
| 78.000 | 3.507 | 0.658 | 0.553 | -0.016 | 8.177 | 1.783 | 0.537 | 0.044 |
| 80.000 | 3.274 | 0.710 | 0.556 | 0.090 | 7.519 | 1.780 | 0.552 | -0.199 |
| 82.000 | 2.545 | 0.764 | 0.552 | 0.150 | 6.173 | 1.782 | 0.593 | -0.374 |
| 84.000 | 1.755 | 0.663 | 0.516 | 0.115 | 4.417 | 1.939 | 0.642 | -0.386 |
| 86.000 | 1.037 | 0.506 | 0.401 | 0.071 | 2.664 | 1.675 | 0.434 | -0.202 |
| 88.000 | 0.429 | 0.325 | 0.279 | 0.041 | 1.487 | 1.681 | 0.203 | -0.121 |
| 90.000 | 0.241 | 0.233 | 0.213 | 0.018 | 1.090 | 0.989 | 0.084 | -0.024 |
| 92.000 | 0.059 | 0.126 | 0.145 | 0.001 | 1.178 | 0.801 | -0.013 | -0.020 |

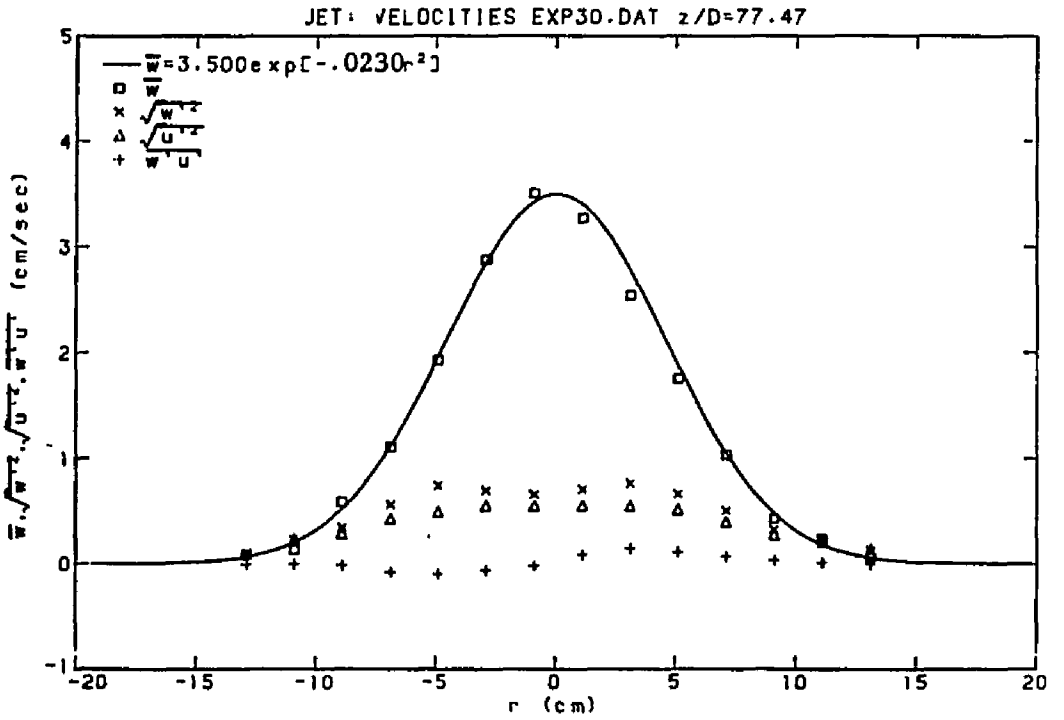

EXP30

| X | W | WP | UP | WPUP | C | CP | WPCP | UPCP |
|---|---|---|---|---|---|---|---|---|
| 66.000 | 0.084 | 0.100 | 0.163 | -0.001 | 1.030 | 0.863 | -0.032 | -0.002 |
| 68.000 | 0.136 | 0.230 | 0.239 | -0.000 | 1.426 | 1.297 | 0.077 | 0.096 |
| 70.000 | 0.587 | 0.342 | 0.288 | -0.013 | 3.985 | 1.507 | 0.180 | 0.030 |
| 72.000 | 1.112 | 0.563 | 0.429 | -0.078 | 5.122 | 1.656 | 0.402 | 0.271 |
| 74.000 | 1.932 | 0.744 | 0.495 | -0.096 | 6.564 | 1.607 | 0.448 | 0.249 |
| 76.000 | 2.881 | 0.697 | 0.554 | -0.060 | 7.646 | 1.812 | 0.619 | 0.243 |
| 78.000 | 3.507 | 0.658 | 0.553 | -0.016 | 8.177 | 1.783 | 0.537 | 0.044 |
| 80.000 | 3.274 | 0.710 | 0.556 | 0.090 | 7.519 | 1.780 | 0.552 | -0.199 |
| 82.000 | 2.545 | 0.764 | 0.552 | 0.150 | 6.173 | 1.782 | 0.593 | -0.374 |
| 84.000 | 1.755 | 0.663 | 0.516 | 0.115 | 4.417 | 1.939 | 0.642 | -0.386 |
| 86.000 | 1.037 | 0.506 | 0.401 | 0.071 | 2.664 | 1.675 | 0.434 | -0.202 |
| 88.000 | 0.429 | 0.325 | 0.279 | 0.041 | 1.487 | 1.681 | 0.203 | -0.121 |
| 90.000 | 0.241 | 0.233 | 0.213 | 0.018 | 1.090 | 0.989 | 0.084 | -0.024 |
| 92.000 | 0.059 | 0.126 | 0.145 | 0.001 | 1.178 | 0.801 | -0.013 | -0.020 |

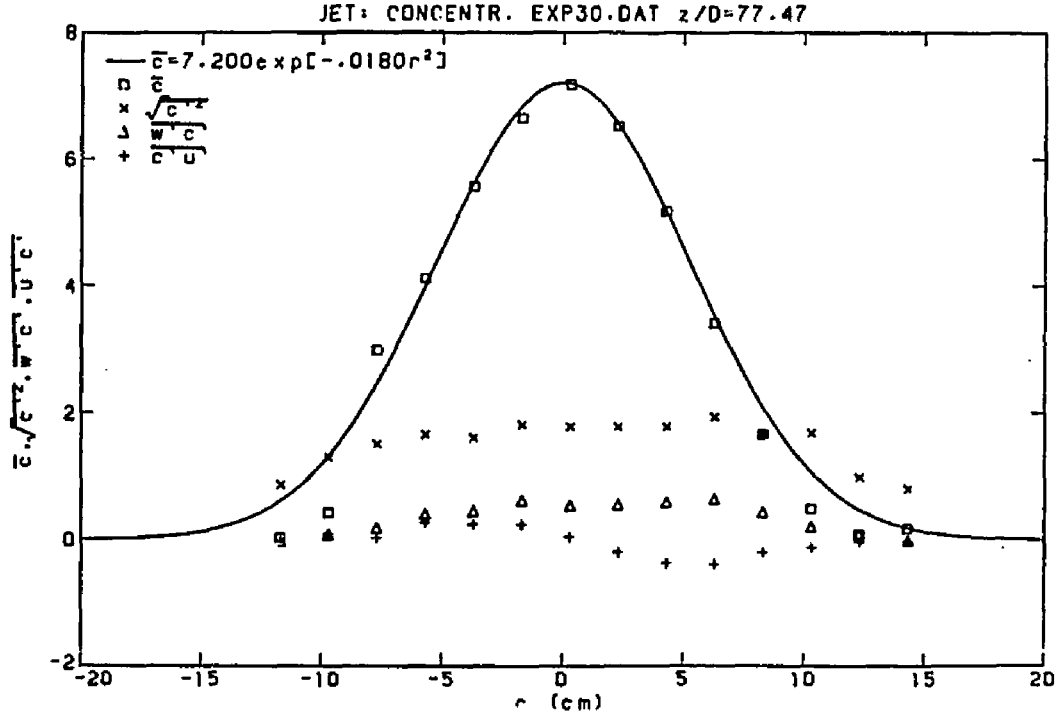

EXP31

| X | W | WP | UP | WPUP | C | CP | WPCP | UPCP |
|---|---|---|---|---|---|---|---|---|
| 68.000 | 0.661 | 0.469 | 0.441 | -0.047 | 0.684 | 0.774 | 0.200 | 0.091 |
| 70.000 | 0.921 | 0.600 | 0.381 | -0.059 | 0.797 | 0.743 | 0.238 | 0.092 |
| 72.000 | 1.722 | 0.828 | 0.494 | -0.127 | 1.597 | 1.141 | 0.506 | 0.145 |
| 74.000 | 2.913 | 0.971 | 0.569 | -0.194 | 2.783 | 1.518 | 0.826 | 0.322 |
| 76.000 | 3.629 | 0.980 | 0.627 | -0.148 | 3.222 | 1.433 | 0.737 | 0.247 |
| 78.000 | 3.998 | 0.806 | 0.635 | -0.021 | 3.124 | 1.382 | 0.546 | -0.002 |
| 80.000 | 3.534 | 0.848 | 0.563 | 0.132 | 2.790 | 1.311 | 0.512 | -0.154 |
| 82.000 | 2.753 | 0.824 | 0.540 | 0.173 | 1.933 | 1.080 | 0.418 | -0.202 |
| 84.000 | 1.643 | 0.727 | 0.488 | 0.134 | 0.970 | 0.830 | 0.326 | -0.121 |
| 86.000 | 1.342 | 0.702 | 0.443 | 0.115 | 0.671 | 0.639 | 0.222 | -0.100 |
| 88.000 | 0.647 | 0.481 | 0.359 | 0.039 | 0.414 | 0.475 | 0.061 | -0.034 |

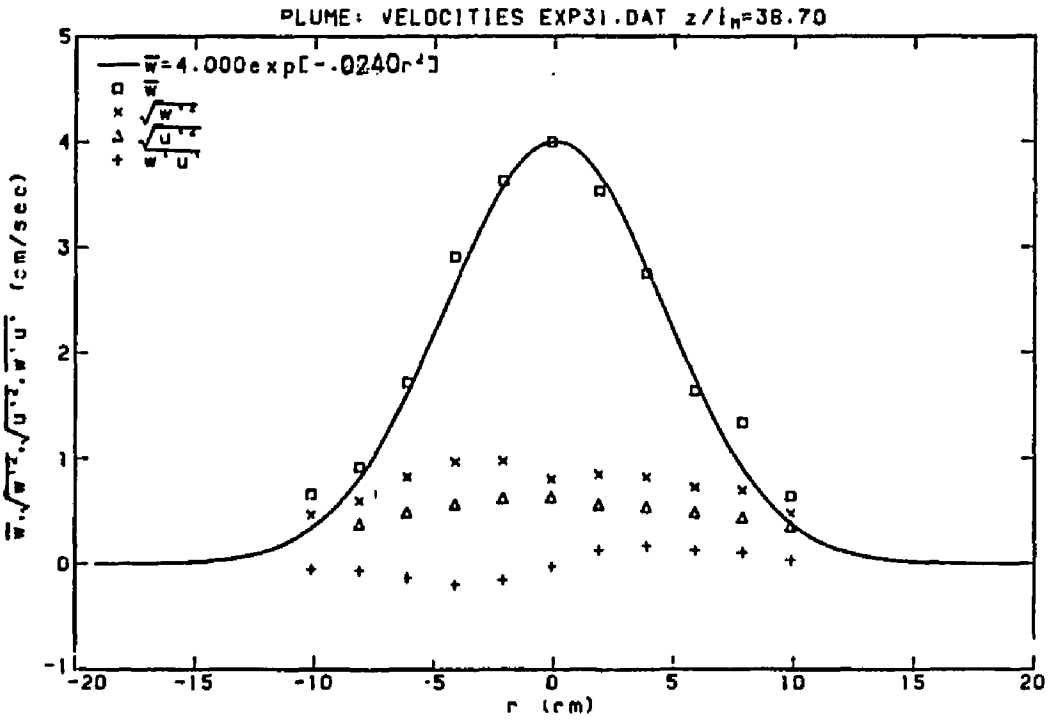

EXP31

| X | W | WP | UP | WPUP | C | CP | WPCP | UPCP |
|---|---|---|---|---|---|---|---|---|
| 68.000 | 0.661 | 0.469 | 0.441 | -0.047 | 0.684 | 0.774 | 0.200 | 0.091 |
| 70.000 | 0.921 | 0.600 | 0.381 | -0.059 | 0.797 | 0.743 | 0.238 | 0.092 |
| 72.000 | 1.722 | 0.828 | 0.494 | -0.127 | 1.597 | 1.141 | 0.506 | 0.145 |
| 74.000 | 2.913 | 0.971 | 0.569 | -0.194 | 2.783 | 1.518 | 0.826 | 0.322 |
| 76.000 | 3.629 | 0.980 | 0.627 | -0.148 | 3.222 | 1.433 | 0.737 | 0.247 |
| 78.000 | 3.998 | 0.806 | 0.635 | -0.021 | 3.124 | 1.382 | 0.546 | -0.002 |
| 80.000 | 3.534 | 0.848 | 0.563 | 0.132 | 2.790 | 1.311 | 0.512 | -0.154 |
| 82.000 | 2.753 | 0.824 | 0.540 | 0.173 | 1.933 | 1.080 | 0.418 | -0.202 |
| 84.000 | 1.643 | 0.727 | 0.488 | 0.134 | 0.970 | 0.830 | 0.326 | -0.121 |
| 86.000 | 1.342 | 0.702 | 0.443 | 0.115 | 0.671 | 0.639 | 0.222 | -0.100 |
| 88.000 | 0.647 | 0.481 | 0.359 | 0.039 | 0.414 | 0.475 | 0.061 | -0.034 |

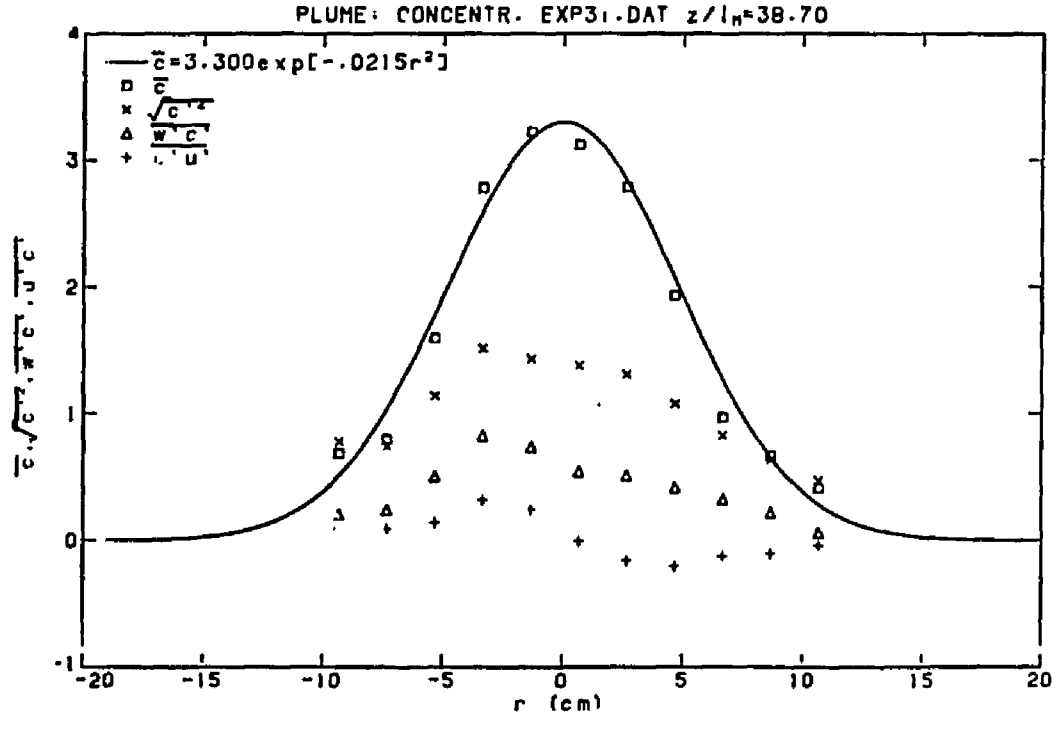

EXP33

| X | W | WP | UP | WPUP | C | CP | WPCP | UPCP |
|---|---|---|---|---|---|---|---|---|
| 70.000 | 0.188 | 0.157 | 0.222 | 0.007 | 0.436 | 0.326 | -0.011 | 0.014 |
| 72.000 | 0.750 | 0.692 | 0.423 | -0.060 | 1.295 | 1.355 | 0.505 | 0.190 |
| 74.000 | 2.399 | 1.138 | 0.660 | -0.119 | 3.991 | 2.408 | 1.343 | 0.493 |
| 76.000 | 4.757 | 1.331 | 0.821 | -0.255 | 7.428 | 3.053 | 2.348 | 0.797 |
| 78.000 | 6.356 | 1.209 | 0.967 | 0.002 | 9.531 | 3.051 | 1.860 | 0.286 |
| 80.000 | 5.863 | 1.236 | 0.887 | 0.165 | 8.884 | 3.121 | 2.093 | -0.561 |
| 82.000 | 3.305 | 1.163 | 0.804 | 0.297 | 5.212 | 2.556 | 1.513 | -0.709 |
| 84.000 | 1.326 | 0.977 | 0.618 | 0.190 | 2.427 | 1.936 | 1.210 | -0.487 |
| 86.000 | 0.292 | 0.298 | 0.316 | -0.001 | 0.859 | 0.958 | 0.032 | -0.067 |
| 88.000 | 0.142 | 0.100 | 0.121 | 0.000 | 0.383 | 0.157 | -0.004 | -0.001 |

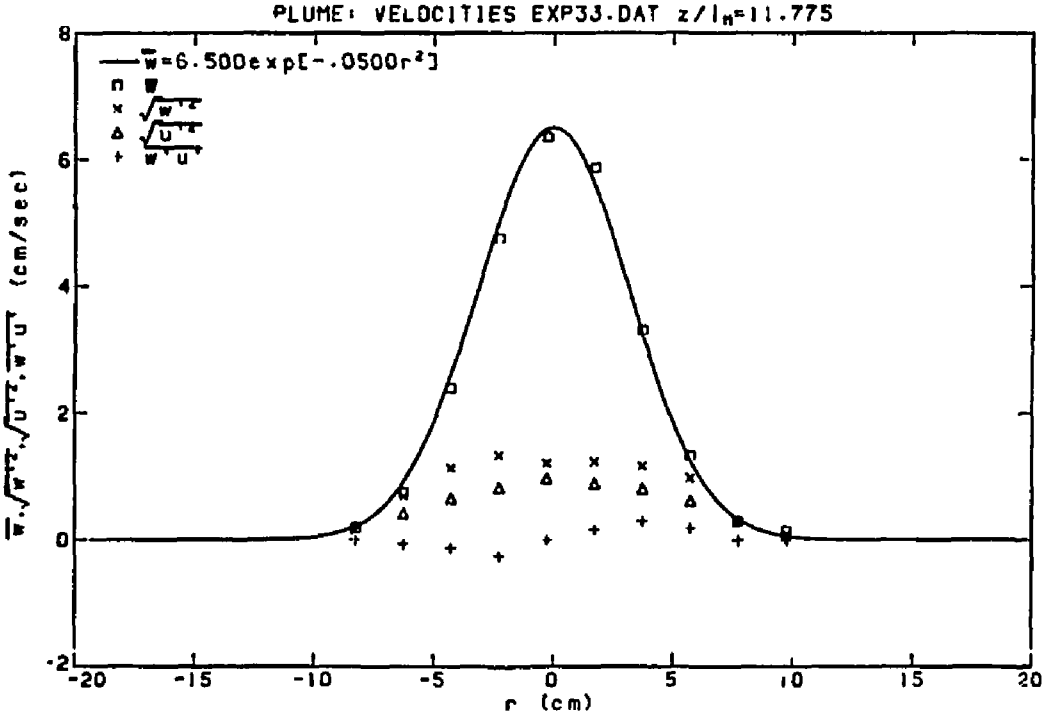

## EXP33

| X | W | WP | UP | WPUP | C | CP | WPCP | UPCP |
|---|---|---|---|---|---|---|---|---|
| 70.000 | 0.188 | 0.157 | 0.222 | 0.007 | 0.436 | 0.326 | -0.011 | 0.014 |
| 72.000 | 0.750 | 0.692 | 0.423 | -0.060 | 1.295 | 1.355 | 0.505 | 0.190 |
| 74.000 | 2.399 | 1.138 | 0.660 | -0.119 | 3.991 | 2.408 | 1.343 | 0.493 |
| 76.000 | 4.757 | 1.331 | 0.821 | -0.255 | 7.428 | 3.053 | 2.348 | 0.797 |
| 78.000 | 6.356 | 1.209 | 0.967 | 0.002 | 9.531 | 3.051 | 1.860 | 0.286 |
| 80.000 | 5.863 | 1.236 | 0.887 | 0.165 | 8.884 | 3.121 | 2.093 | -0.561 |
| 82.000 | 3.305 | 1.163 | 0.804 | 0.297 | 5.212 | 2.556 | 1.513 | -0.709 |
| 84.000 | 1.326 | 0.977 | 0.618 | 0.190 | 2.427 | 1.936 | 1.210 | -0.487 |
| 86.000 | 0.292 | 0.298 | 0.316 | -0.001 | 0.859 | 0.958 | 0.032 | -0.067 |
| 88.000 | 0.142 | 0.100 | 0.121 | 0.000 | 0.383 | 0.157 | -0.004 | -0.001 |

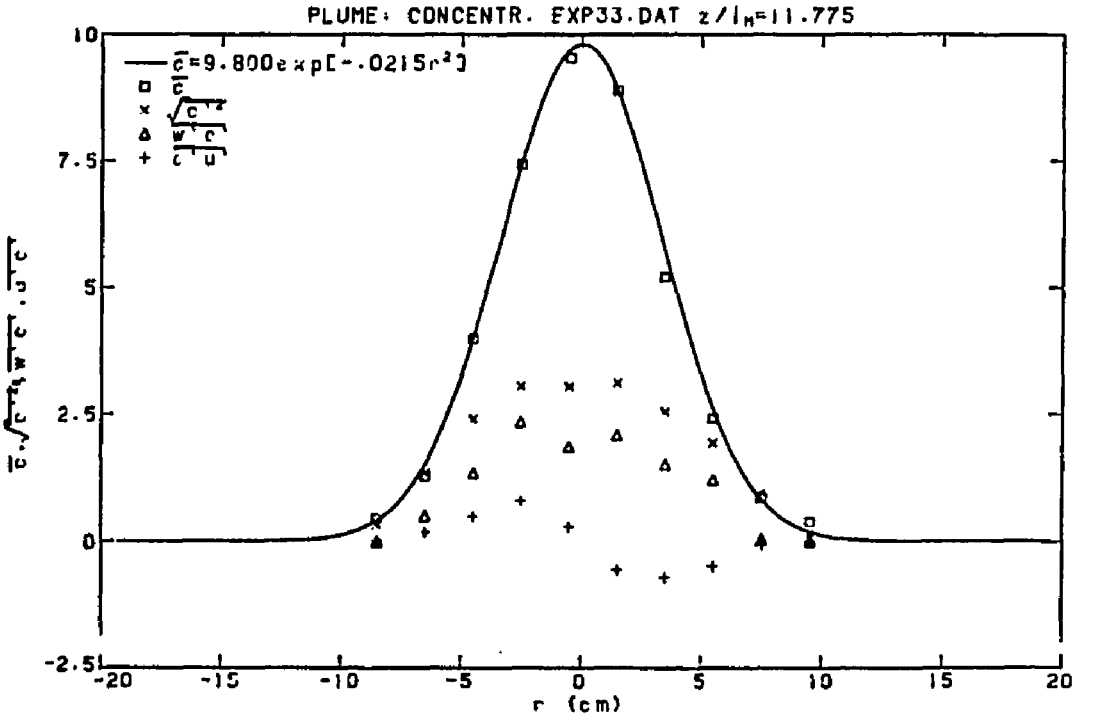

EXP34

| X | W | WP | UP | WPUP | C | CP | WPCP | UPCP |
|---|---|---|---|---|---|---|---|---|
| 66.000 | 0.217 | 0.322 | 0.235 | -0.012 | -0.166 | 0.344 | 0.060 | 0.023 |
| 69.000 | 0.825 | 0.534 | 0.401 | -0.057 | 0.399 | 0.715 | 0.174 | 0.117 |
| 72.000 | 2.301 | 0.833 | 0.609 | -0.162 | 1.394 | 1.080 | 0.426 | 0.286 |
| 75.000 | 3.482 | 1.097 | 0.652 | -0.118 | 2.724 | 1.257 | 0.743 | 0.252 |
| 77.000 | 4.685 | 0.947 | 0.737 | -0.138 | 3.672 | 1.384 | 0.692 | 0.208 |
| 79.000 | 4.632 | 1.027 | 0.743 | 0.066 | 3.769 | 1.384 | 0.732 | -0.078 |
| 81.000 | 3.940 | 1.017 | 0.829 | 0.269 | 2.911 | 1.384 | 0.792 | -0.325 |
| 83.000 | 3.274 | 1.053 | 0.650 | 0.277 | 2.607 | 1.243 | 0.750 | -0.287 |
| 85.000 | 2.525 | 1.045 | 0.656 | 0.305 | 1.979 | 1.085 | 0.667 | -0.289 |
| 87.000 | 1.430 | 0.834 | 0.578 | 0.185 | 1.254 | 0.812 | 0.373 | -0.178 |
| 89.000 | 0.368 | 0.242 | 0.284 | -0.004 | 0.547 | 0.432 | 0.018 | -0.026 |
| 91.000 | 0.107 | 0.152 | 0.224 | 0.001 | 0.377 | 0.226 | 0.003 | -0.008 |

EXP35

| X | W | WP | UP | WPUP | C | CP | WPCP | UPCP |
|---|---|---|---|---|---|---|---|---|
| 72.000 | 0.227 | 0.177 | 0.223 | 0.005 | 0.417 | 0.617 | 0.028 | 0.028 |
| 73.000 | 0.512 | 0.355 | 0.313 | -0.010 | 0.869 | 1.190 | 0.230 | 0.050 |
| 74.000 | 0.883 | 0.555 | 0.431 | -0.023 | 1.545 | 1.589 | 0.348 | 0.140 |
| 75.000 | 1.420 | 0.748 | 0.540 | -0.027 | 2.533 | 2.174 | 0.782 | 0.324 |
| 76.000 | 3.210 | 1.019 | 0.658 | -0.167 | 5.465 | 3.066 | 1.745 | 0.545 |
| 77.000 | 4.381 | 1.123 | 0.728 | -0.157 | 7.689 | 3.606 | 2.030 | 0.609 |
| 78.000 | 4.692 | 1.136 | 0.728 | -0.085 | 8.193 | 3.681 | 2.301 | 0.518 |
| 79.000 | 4.919 | 1.086 | 0.745 | 0.163 | 8.779 | 3.416 | 1.822 | -0.327 |
| 80.000 | 4.242 | 1.286 | 0.870 | 0.209 | 7.533 | 3.613 | 2.696 | -0.542 |
| 81.500 | 2.660 | 1.046 | 0.706 | 0.171 | 4.947 | 2.999 | 1.634 | -0.519 |
| 83.000 | 0.698 | 0.635 | 0.487 | 0.076 | 1.814 | 1.914 | 0.542 | -0.222 |
| 84.500 | 0.253 | 0.301 | 0.298 | 0.001 | 0.578 | 0.764 | 0.009 | -0.020 |
| 86.000 | 0.055 | 0.139 | 0.198 | -0.001 | 0.084 | 0.178 | -0.008 | -0.006 |

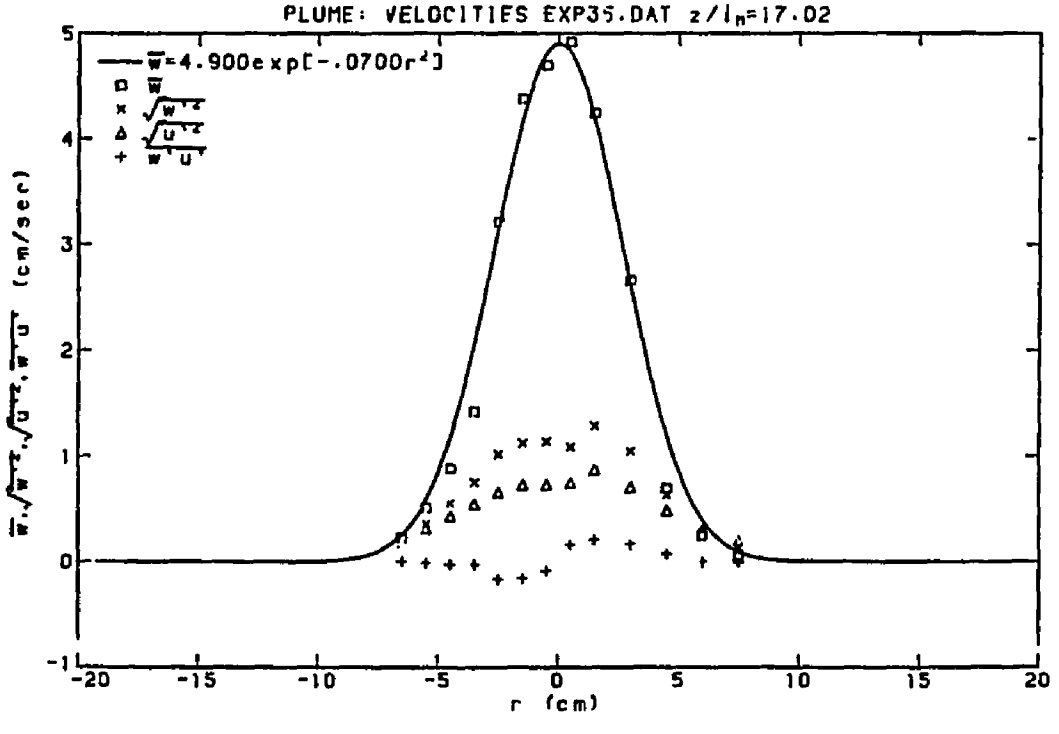

EXP35

| X | W | WP | UP | WPUP | C | CP | WPCP | UPCP |
|---|---|---|---|---|---|---|---|---|
| 72.000 | 0.227 | 0.177 | 0.223 | 0.005 | 0.417 | 0.617 | 0.028 | 0.028 |
| 73.000 | 0.512 | 0.355 | 0.313 | -0.010 | 0.869 | 1.190 | 0.230 | 0.050 |
| 74.000 | 0.883 | 0.555 | 0.431 | -0.023 | 1.545 | 1.589 | 0.348 | 0.140 |
| 75.000 | 1.420 | 0.748 | 0.540 | -0.027 | 2.533 | 2.174 | 0.782 | 0.324 |
| 76.000 | 3.210 | 1.019 | 0.658 | -0.167 | 5.465 | 3.066 | 1.745 | 0.545 |
| 77.000 | 4.381 | 1.123 | 0.728 | -0.157 | 7.689 | 3.606 | 2.030 | 0.609 |
| 78.000 | 4.692 | 1.136 | 0.728 | -0.085 | 8.193 | 3.681 | 2.301 | 0.518 |
| 79.000 | 4.919 | 1.086 | 0.745 | 0.163 | 8.779 | 3.416 | 1.822 | -0.327 |
| 80.000 | 4.242 | 1.286 | 0.870 | 0.209 | 7.533 | 3.613 | 2.696 | -0.542 |
| 81.500 | 2.660 | 1.046 | 0.706 | 0.171 | 4.947 | 2.999 | 1.634 | -0.519 |
| 83.000 | 0.698 | 0.635 | 0.487 | 0.076 | 1.814 | 1.914 | 0.542 | -0.222 |
| 84.500 | 0.253 | 0.301 | 0.298 | 0.001 | 0.578 | 0.764 | 0.009 | -0.020 |
| 86.000 | 0.055 | 0.139 | 0.198 | -0.001 | 0.084 | 0.178 | -0.008 | -0.006 |

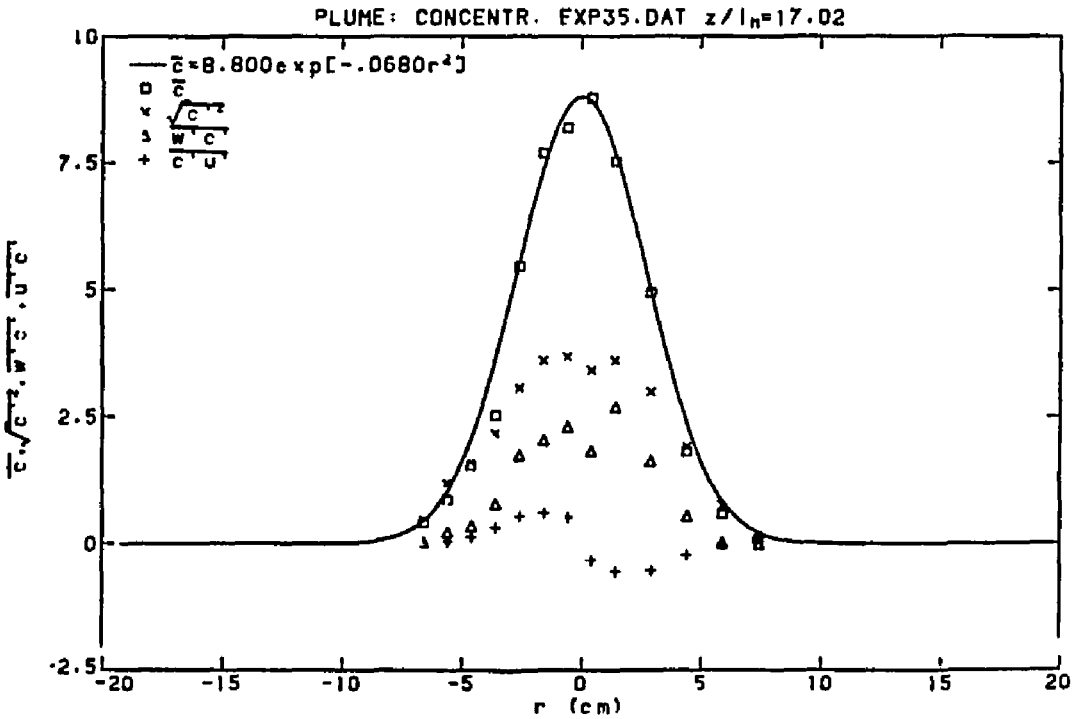

EXP36

| X | W | WP | UP | WPUP | C | CP | WPCP | UPCP |
|---|---|---|---|---|---|---|---|---|
| 70.000 | 0.396 | 0.106 | 0.172 | -0.001 | 0.282 | 0.473 | 0.009 | 0.016 |
| 71.500 | 0.353 | 0.132 | 0.191 | -0.002 | 0.646 | 1.065 | 0.062 | 0.032 |
| 73.000 | 0.655 | 0.458 | 0.359 | -0.016 | 2.299 | 2.436 | 0.447 | 0.284 |
| 74.500 | 1.823 | 0.684 | 0.556 | -0.083 | 5.790 | 3.563 | 1.392 | 0.643 |
| 76.000 | 2.992 | 0.832 | 0.599 | -0.075 | 9.895 | 4.533 | 1.628 | 0.707 |
| 77.500 | 4.387 | 0.904 | 0.685 | -0.052 | 13.816 | 4.542 | 1.822 | 0.547 |
| 79.000 | 4.377 | 1.022 | 0.683 | 0.098 | 13.889 | 5.058 | 2.723 | -0.422 |
| 80.500 | 3.101 | 0.816 | 0.616 | 0.096 | 10.593 | 4.505 | 1.609 | -0.618 |
| 82.000 | 1.143 | 0.811 | 0.504 | 0.128 | 4.494 | 3.845 | 1.696 | -0.662 |
| 83.500 | 0.256 | 0.295 | 0.288 | 0.010 | 1.411 | 2.003 | 0.175 | -0.121 |
| 85.000 | 0.138 | 0.113 | 0.156 | -0.001 | 0.317 | 0.167 | -0.003 | -0.003 |
| 78.500 | 4.456 | 0.972 | 0.668 | 0.082 | 15.521 | 4.920 | 2.445 | -0.293 |

EXP37

| X | W | WP | UP | WPUP | C | CP | WPCP | UPCP |
|---|---|---|---|---|---|---|---|---|
| 71.000 | 0.214 | 0.096 | 0.130 | -0.001 | 0.171 | 0.139 | -0.002 | -0.001 |
| 72.500 | 0.331 | 0.191 | 0.185 | -0.000 | 0.453 | 0.571 | 0.055 | 0.012 |
| 74.000 | 0.826 | 0.337 | 0.345 | 0.001 | 1.500 | 1.591 | 0.201 | -0.027 |
| 75.500 | 2.147 | 0.883 | 0.555 | -0.126 | 3.943 | 3.018 | 1.689 | 0.564 |
| 77.000 | 4.035 | 0.967 | 0.700 | -0.097 | 8.230 | 3.284 | 1.604 | 0.602 |
| 78.500 | 5.205 | 0.918 | 0.716 | 0.001 | 10.412 | 3.096 | 1.457 | 0.091 |
| 80.000 | 4.218 | 1.006 | 0.719 | 0.180 | 8.855 | 3.464 | 1.962 | -0.598 |
| 81.500 | 2.302 | 0.949 | 0.619 | 0.182 | 4.724 | 3.359 | 1.774 | -0.634 |
| 83.000 | 1.120 | 0.685 | 0.465 | 0.120 | 1.910 | 2.486 | 0.875 | -0.364 |
| 84.500 | 0.507 | 0.335 | 0.335 | 0.005 | 0.800 | 1.207 | 0.141 | -0.112 |
| 86.000 | 0.313 | 0.106 | 0.184 | -0.004 | 0.200 | 0.269 | -0.012 | -0.020 |

EXP38

| X | W | WP | UP | WPUP | C | CP | WPCP | UPCP |
|---|---|---|---|---|---|---|---|---|
| 70.000 | 0.523 | 0.502 | 0.353 | -0.081 | 1.060 | 1.508 | 0.538 | 0.274 |
| 72.000 | 0.852 | 0.497 | 0.393 | -0.044 | 1.952 | 1.842 | 0.443 | 0.190 |
| 74.000 | 2.697 | 0.900 | 0.636 | -0.110 | 5.642 | 2.621 | 1.168 | 0.583 |
| 75.500 | 2.984 | 0.966 | 0.655 | -0.129 | 5.884 | 2.718 | 1.447 | 0.511 |
| 77.000 | 4.520 | 0.955 | 0.705 | -0.066 | 8.486 | 2.464 | 1.066 | 0.179 |
| 78.500 | 4.548 | 0.937 | 0.700 | 0.138 | 8.485 | 2.355 | 1.050 | -0.308 |
| 80.000 | 3.774 | 1.042 | 0.699 | 0.213 | 7.189 | 2.696 | 1.641 | -0.600 |
| 81.500 | 2.164 | 0.938 | 0.626 | 0.196 | 4.463 | 2.729 | 1.448 | -0.737 |
| 83.000 | 0.891 | 0.630 | 0.409 | 0.053 | 2.383 | 1.787 | 0.650 | -0.204 |
| 84.500 | 0.515 | 0.440 | 0.342 | 0.053 | 1.427 | 1.413 | 0.365 | -0.148 |
| 86.000 | 0.073 | 0.244 | 0.226 | 0.013 | 0.389 | 0.691 | 0.058 | -0.032 |

EXP39

| X | W | WP | UP | WPUP | C | CP | WPCP | UPCP |
|---|---|---|---|---|---|---|---|---|
| 65.500 | 0.339 | 0.492 | 0.344 | 0.012 | -0.203 | 0.792 | 0.052 | 0.028 |
| 69.000 | 1.048 | 0.702 | 0.490 | -0.078 | 0.554 | 0.827 | 0.257 | 0.117 |
| 72.000 | 2.463 | 0.879 | 0.561 | -0.171 | 1.859 | 1.392 | 0.760 | 0.346 |
| 75.000 | 3.458 | 1.063 | 0.657 | -0.143 | 2.773 | 1.611 | 0.991 | 0.325 |
| 78.000 | 4.155 | 1.137 | 0.724 | -0.117 | 3.301 | 1.680 | 1.192 | 0.177 |
| 81.000 | 3.575 | 1.046 | 0.632 | 0.043 | 2.733 | 1.533 | 0.787 | -0.073 |
| 84.000 | 2.588 | 1.050 | 0.635 | 0.211 | 1.884 | 1.133 | 0.658 | -0.235 |
| 87.000 | 1.211 | 0.818 | 0.498 | 0.129 | 1.096 | 0.866 | 0.240 | -0.127 |
| 90.000 | 0.519 | 0.625 | 0.447 | 0.049 | 0.649 | 0.417 | 0.206 | -0.044 |
| 93.000 | 0.083 | 0.257 | 0.228 | -0.004 | 0.323 | 0.078 | -0.000 | -0.004 |

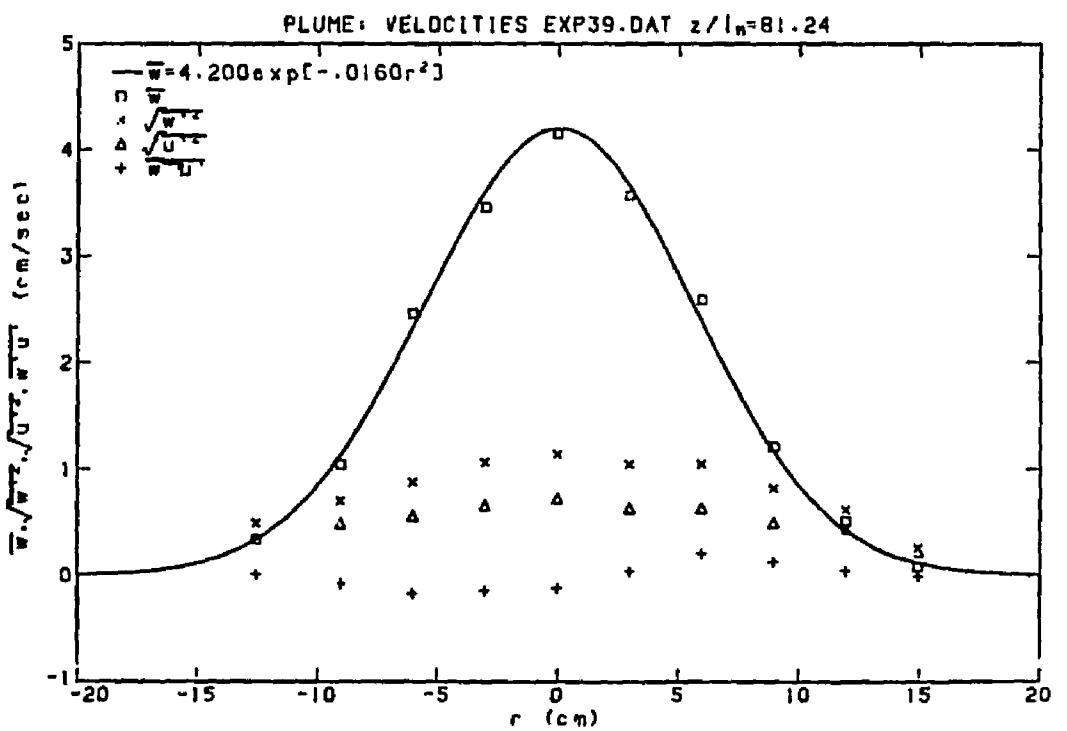

EXP39

| X | W | WP | UP | WPUP | C | CP | WPCP | UPCP |
|---|---|---|---|---|---|---|---|---|
| 65.500 | 0.339 | 0.492 | 0.344 | 0.012 | -0.203 | 0.792 | 0.052 | 0.028 |
| 69.000 | 1.048 | 0.702 | 0.490 | -0.078 | 0.554 | 0.827 | 0.257 | 0.117 |
| 72.000 | 2.463 | 0.879 | 0.561 | -0.171 | 1.859 | 1.392 | 0.760 | 0.346 |
| 75.000 | 3.458 | 1.063 | 0.657 | -0.143 | 2.773 | 1.611 | 0.991 | 0.325 |
| 78.000 | 4.155 | 1.137 | 0.724 | -0.117 | 3.301 | 1.680 | 1.192 | 0.177 |
| 81.000 | 3.575 | 1.046 | 0.632 | 0.043 | 2.733 | 1.533 | 0.787 | -0.073 |
| 84.000 | 2.588 | 1.050 | 0.635 | 0.211 | 1.884 | 1.133 | 0.658 | -0.235 |
| 87.000 | 1.211 | 0.818 | 0.498 | 0.129 | 1.096 | 0.866 | 0.240 | -0.127 |
| 90.000 | 0.519 | 0.625 | 0.447 | 0.049 | 0.649 | 0.417 | 0.206 | -0.044 |
| 93.000 | 0.083 | 0.257 | 0.228 | -0.004 | 0.323 | 0.078 | -0.000 | -0.004 |

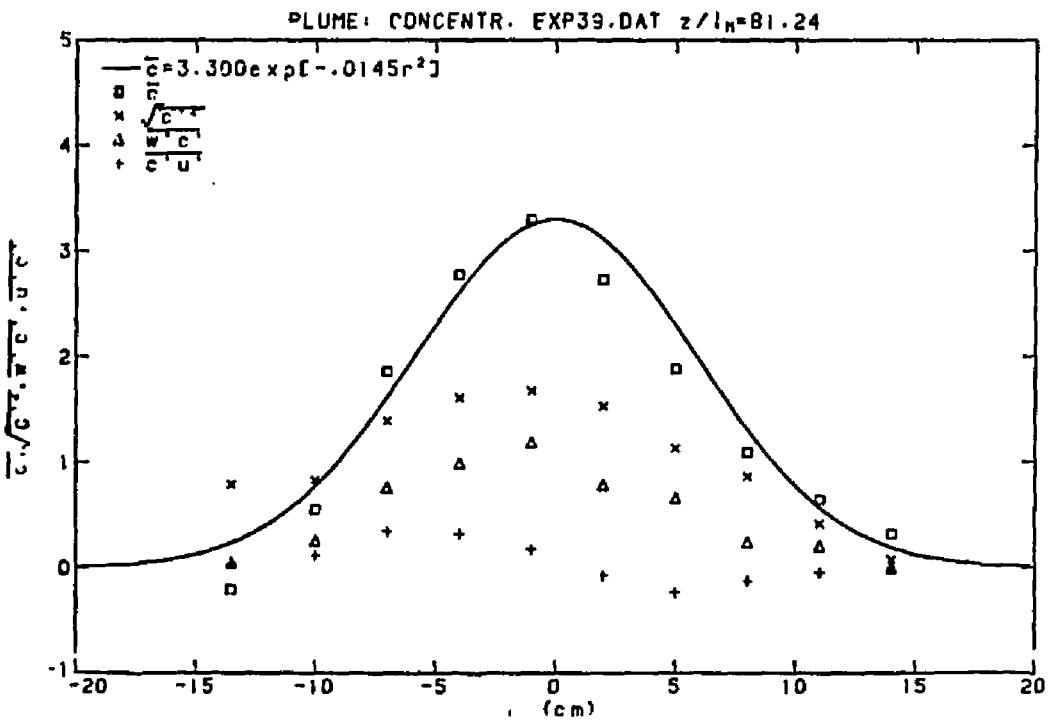

EXP40

| X | W | WP | UP | WPUP | C | CP | WPCP | UPCP |
|---|---|---|---|---|---|---|---|---|
| 66.000 | 0.016 | 0.308 | 0.289 | -0.011 | 0.312 | 0.287 | 0.016 | 0.006 |
| 69.000 | 0.610 | 0.577 | 0.421 | -0.050 | 0.957 | 0.967 | 0.280 | 0.118 |
| 72.000 | 2.183 | 0.979 | 0.598 | -0.127 | 2.340 | 1.528 | 0.730 | 0.319 |
| 75.000 | 3.758 | 1.077 | 0.696 | -0.075 | 3.655 | 1.822 | 0.897 | 0.279 |
| 78.000 | 4.851 | 1.197 | 0.787 | -0.022 | 4.581 | 1.965 | 1.346 | 0.007 |
| 81.000 | 4.487 | 1.116 | 0.780 | 0.042 | 4.318 | 1.877 | 1.009 | -0.150 |
| 84.000 | 2.251 | 1.333 | 0.676 | 0.331 | 2.452 | 1.511 | 1.257 | -0.409 |
| 87.000 | 1.446 | 1.077 | 0.580 | 0.232 | 1.802 | 1.155 | 0.712 | -0.314 |
| 90.000 | 0.330 | 0.489 | 0.436 | 0.041 | 1.083 | 0.850 | 0.070 | -0.131 |
| 93.000 | 0.133 | 0.376 | 0.258 | 0.050 | 0.597 | 0.245 | 0.048 | -0.029 |

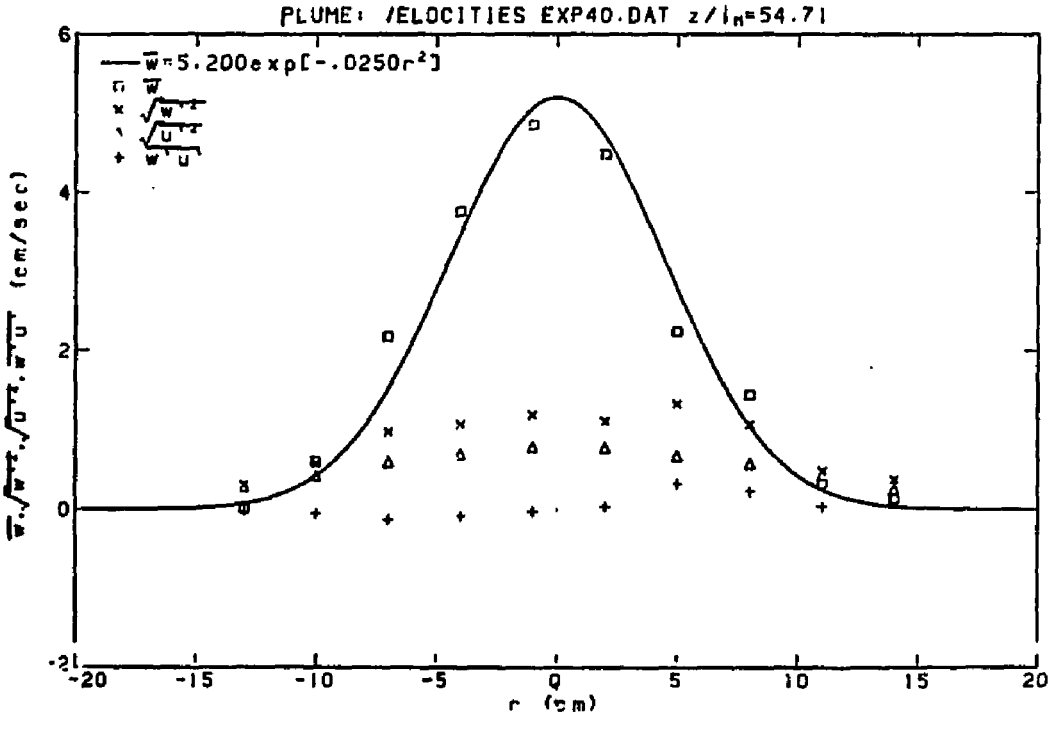

EXP40

| X | W | WP | UP | WPUP | C | CP | WPCP | UPCP |
|---|---|---|---|---|---|---|---|---|
| 66.000 | 0.016 | 0.308 | 0.289 | -0.011 | 0.312 | 0.287 | 0.016 | 0.006 |
| 69.000 | 0.610 | 0.577 | 0.421 | -0.050 | 0.957 | 0.967 | 0.280 | 0.118 |
| 72.000 | 2.183 | 0.979 | 0.598 | -0.127 | 2.340 | 1.528 | 0.730 | 0.319 |
| 75.000 | 3.758 | 1.077 | 0.696 | -0.075 | 3.655 | 1.822 | 0.897 | 0.279 |
| 78.000 | 4.851 | 1.197 | 0.787 | -0.022 | 4.581 | 1.965 | 1.346 | 0.007 |
| 81.000 | 4.487 | 1.116 | 0.780 | 0.042 | 4.318 | 1.877 | 1.009 | -0.150 |
| 84.000 | 2.251 | 1.333 | 0.676 | 0.331 | 2.452 | 1.511 | 1.257 | -0.409 |
| 87.000 | 1.446 | 1.077 | 0.580 | 0.232 | 1.802 | 1.155 | 0.712 | -0.314 |
| 90.000 | 0.330 | 0.489 | 0.436 | 0.041 | 1.083 | 0.850 | 0.070 | -0.131 |
| 93.000 | 0.133 | 0.376 | 0.258 | 0.050 | 0.597 | 0.245 | 0.048 | -0.029 |

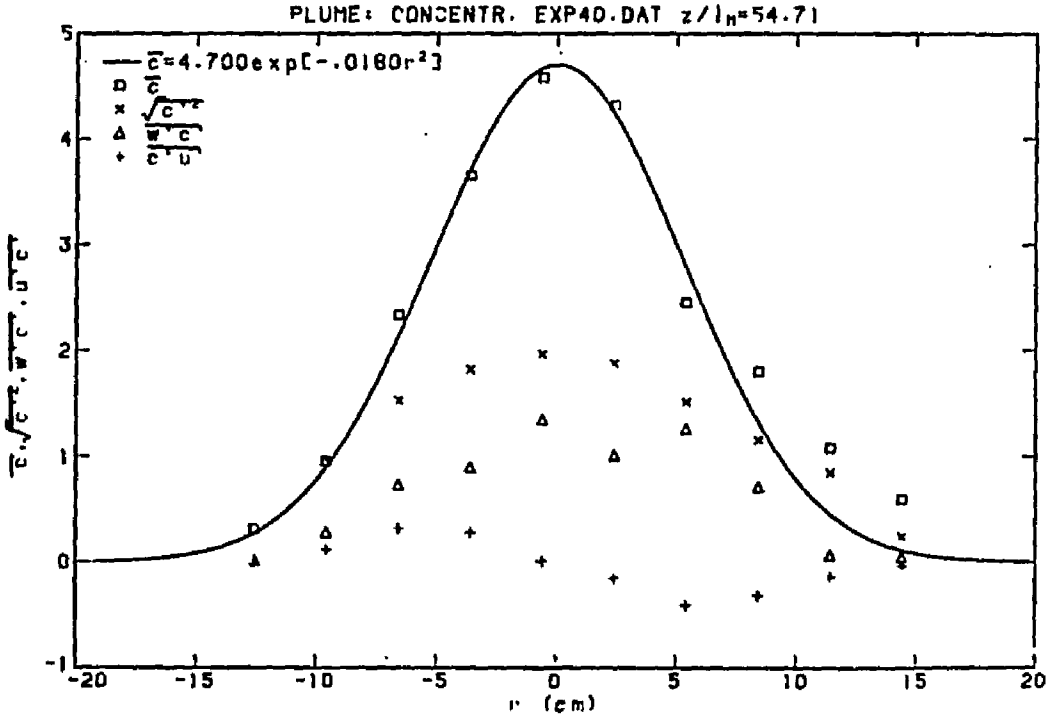

EXP41

| X | W | WP | UP | WPUP | C | CP | WPCP | UPCP |
|---|---|---|---|---|---|---|---|---|
| 60.000 | 0.111 | 0.178 | 0.191 | 0.003 | 0.033 | 0.081 | -0.004 | 0.001 |
| 64.000 | 0.385 | 0.394 | 0.350 | -0.035 | 0.343 | 0.593 | 0.116 | 0.043 |
| 68.000 | 0.969 | 0.687 | 0.472 | -0.043 | 0.764 | 0.888 | 0.259 | 0.154 |
| 72.000 | 2.896 | 1.103 | 0.667 | -0.289 | 1.776 | 1.200 | 0.830 | 0.306 |
| 75.000 | 3.684 | 0.965 | 0.638 | -0.108 | 3.072 | 1.135 | 0.559 | 0.210 |
| 78.000 | 4.723 | 0.921 | 0.757 | 0.001 | 3.953 | 1.238 | 0.546 | 0.039 |
| 81.000 | 4.114 | 0.987 | 0.629 | 0.152 | 3.756 | 1.144 | 0.626 | -0.150 |
| 85.000 | 2.685 | 0.848 | 0.597 | 0.155 | 2.880 | 0.921 | 0.372 | -0.178 |
| 89.000 | 1.437 | 0.721 | 0.553 | 0.209 | 2.112 | 0.681 | 0.252 | -0.194 |
| 93.000 | 0.318 | 0.355 | 0.328 | 0.029 | 1.597 | 0.311 | 0.028 | -0.048 |

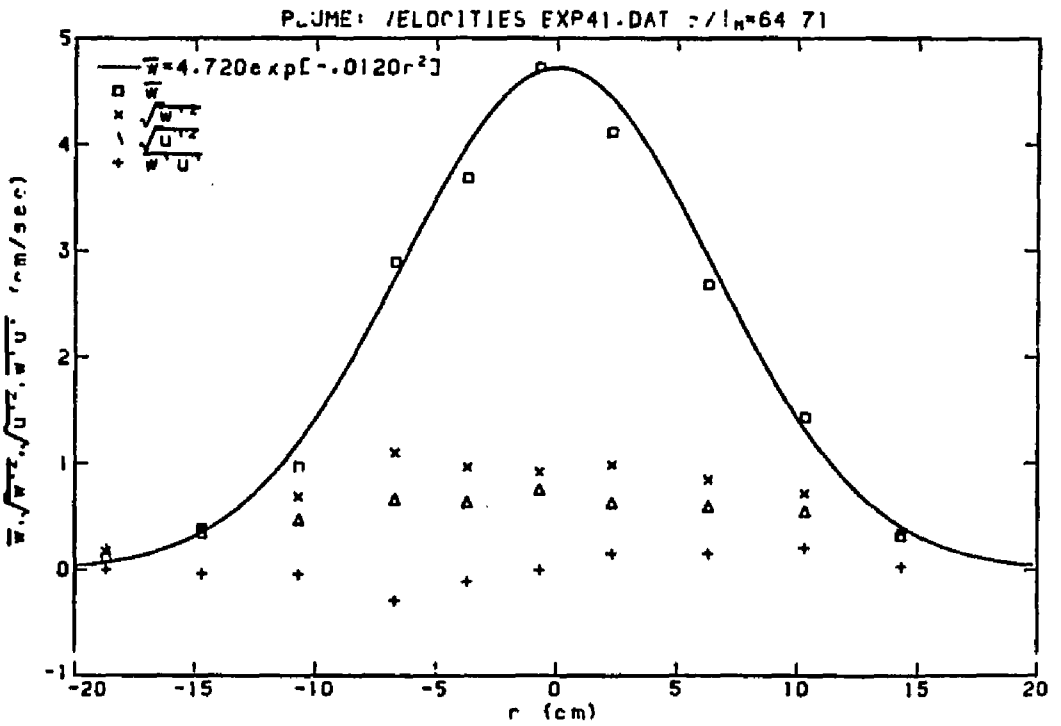

EXP42

| X | W | WP | UP | WPUP | C | CP | WPCP | UPCP |
|---|---|---|---|---|---|---|---|---|
| 64.000 | 0.159 | 0.158 | 0.214 | 0.002 | -0.034 | 0.123 | -0.006 | 0.005 |
| 68.000 | 0.826 | 0.698 | 0.406 | -0.040 | 0.763 | 1.058 | 0.337 | 0.114 |
| 72.000 | 2.634 | 1.078 | 0.715 | -0.372 | 2.587 | 1.812 | 1.220 | 0.564 |
| 75.000 | 4.197 | 1.015 | 0.632 | -0.048 | 4.610 | 1.982 | 1.029 | 0.260 |
| 78.000 | 4.776 | 1.123 | 0.779 | -0.047 | 4.989 | 2.057 | 1.253 | 0.118 |
| 81.000 | 4.390 | 1.283 | 0.690 | 0.262 | 4.333 | 1.975 | 1.487 | -0.339 |
| 84.000 | 2.793 | 1.204 | 0.653 | 0.363 | 3.038 | 1.838 | 1.334 | -0.547 |
| 87.000 | 1.682 | 0.857 | 0.555 | 0.162 | 2.006 | 1.211 | 0.469 | -0.296 |
| 90.000 | 0.848 | 0.600 | 0.432 | 0.034 | 1.318 | 0.810 | 0.165 | -0.115 |
| 93.000 | 0.223 | 0.342 | 0.288 | 0.023 | 0.895 | 0.306 | 0.034 | -0.021 |

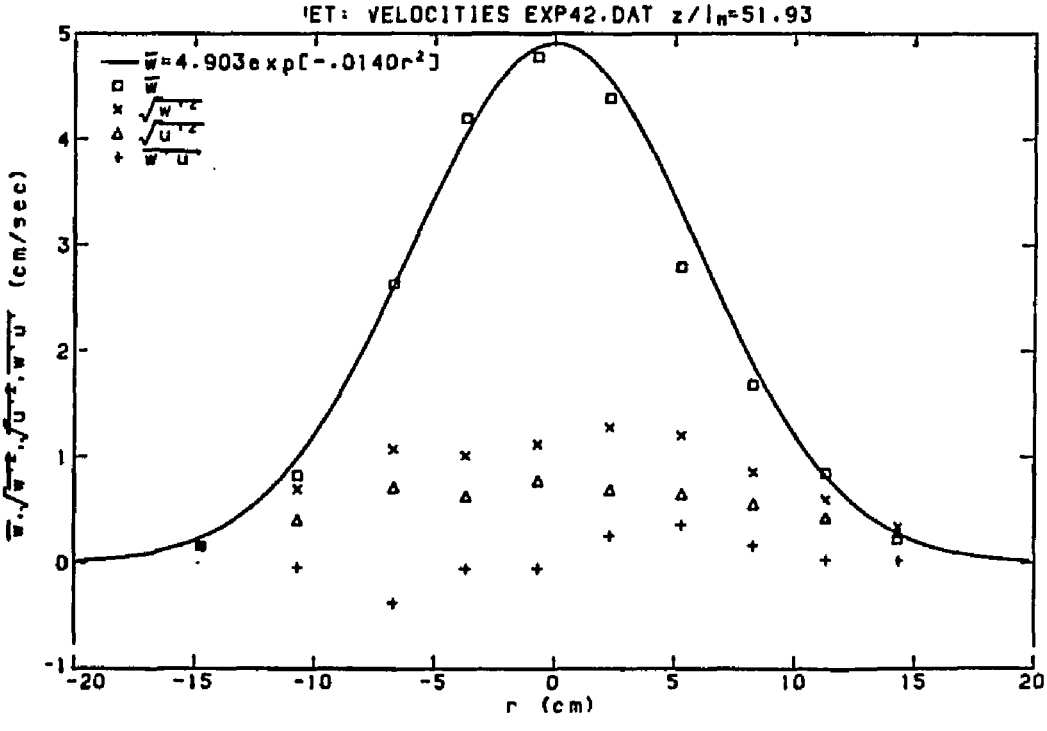

EXP43

| X | W | WP | UP | WPUP | C | CP | WPCP | UPCP |
|---|---|---|---|---|---|---|---|---|
| 67.000 | 0.233 | 0.158 | 0.218 | 0.004 | 0.107 | 0.190 | -0.008 | 0.008 |
| 70.000 | 0.755 | 0.898 | 0.487 | -0.133 | 1.079 | 1.507 | 0.919 | 0.304 |
| 73.000 | 2.335 | 1.077 | 0.681 | -0.211 | 3.044 | 2.158 | 1.139 | 0.502 |
| 76.000 | 4.741 | 1.213 | 0.876 | -0.134 | 6.191 | 2.722 | 1.760 | 0.367 |
| 78.000 | 4.874 | 1.072 | 0.790 | 0.013 | 5.997 | 2.624 | 1.467 | -0.041 |
| 80.000 | 4.513 | 1.267 | 0.841 | 0.260 | 5.555 | 2.767 | 2.039 | -0.646 |
| 83.000 | 2.872 | 1.278 | 0.724 | 0.470 | 3.124 | 2.166 | 1.732 | -0.628 |
| 86.000 | 0.938 | 0.861 | 0.576 | 0.201 | 1.175 | 1.544 | 0.737 | -0.361 |
| 89.000 | 0.284 | 0.428 | 0.378 | 0.042 | 0.478 | 0.700 | 0.134 | -0.087 |

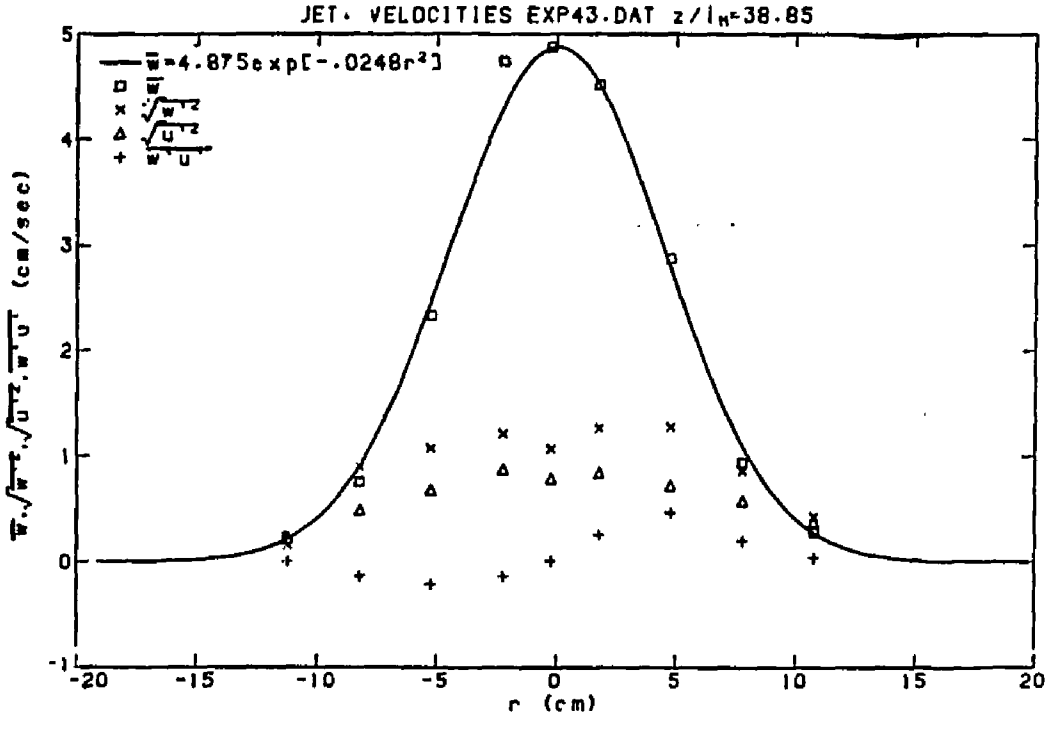

EXP44

| X | W | WP | UP | WPUP | C | CP | WPCP | UPCP |
|---|---|---|---|---|---|---|---|---|
| 65.000 | 0.283 | 0.318 | 0.327 | 0.008 | -0.634 | 0.713 | 0.122 | 0.038 |
| 68.000 | 1.238 | 0.774 | 0.449 | -0.098 | 0.070 | 1.029 | 0.344 | 0.177 |
| 71.000 | 2.132 | 0.848 | 0.507 | -0.119 | 0.866 | 1.259 | 0.619 | 0.206 |
| 74.000 | 3.575 | 1.336 | 0.679 | -0.318 | 2.426 | 1.789 | 1.409 | 0.467 |
| 76.000 | 4.664 | 1.076 | 0.716 | -0.091 | 3.561 | 1.714 | 0.925 | 0.127 |
| 78.000 | 5.005 | 1.121 | 0.711 | -0.056 | 3.671 | 1.792 | 1.126 | 0.083 |
| 80.000 | 4.703 | 1.029 | 0.755 | 0.179 | 3.355 | 1.715 | 0.873 | -0.272 |
| 83.000 | 3.732 | 0.985 | 0.752 | 0.203 | 2.454 | 1.571 | 0.814 | -0.451 |
| 86.000 | 1.726 | 0.963 | 0.552 | 0.215 | 1.089 | 1.211 | 0.650 | -0.295 |
| 89.000 | 0.317 | 0.452 | 0.366 | 0.022 | 0.056 | 0.544 | 0.043 | -0.042 |

EXP45

| X | W | WP | UP | WPUP | C | CP | WPCP | UPCP |
|---|---|---|---|---|---|---|---|---|
| 65.000 | 0.519 | 0.571 | 0.351 | -0.051 | 0.196 | 0.292 | 0.094 | 0.030 |
| 68.000 | 0.852 | 0.731 | 0.437 | -0.084 | 0.493 | 0.803 | 0.323 | 0.139 |
| 71.000 | 1.950 | 0.804 | 0.611 | -0.154 | 0.908 | 0.728 | 0.181 | 0.132 |
| 74.000 | 3.391 | 1.299 | 0.753 | -0.423 | 1.957 | 1.174 | 0.902 | 0.415 |
| 76.000 | 4.479 | 1.261 | 0.738 | -0.238 | 2.499 | 1.165 | 0.780 | 0.231 |
| 78.000 | 5.258 | 1.122 | 0.766 | 0.061 | 2.884 | 1.096 | 0.533 | 0.028 |
| 80.000 | 5.150 | 1.251 | 0.760 | 0.173 | 2.827 | 1.101 | 0.692 | -0.180 |
| 83.000 | 3.661 | 1.248 | 0.758 | 0.435 | 1.933 | 1.048 | 0.784 | -0.362 |
| 86.000 | 2.149 | 1.150 | 0.688 | 0.417 | 1.239 | 0.783 | 0.483 | -0.290 |
| 89.000 | 1.146 | 0.979 | 0.632 | 0.341 | 0.860 | 0.628 | 0.411 | -0.212 |

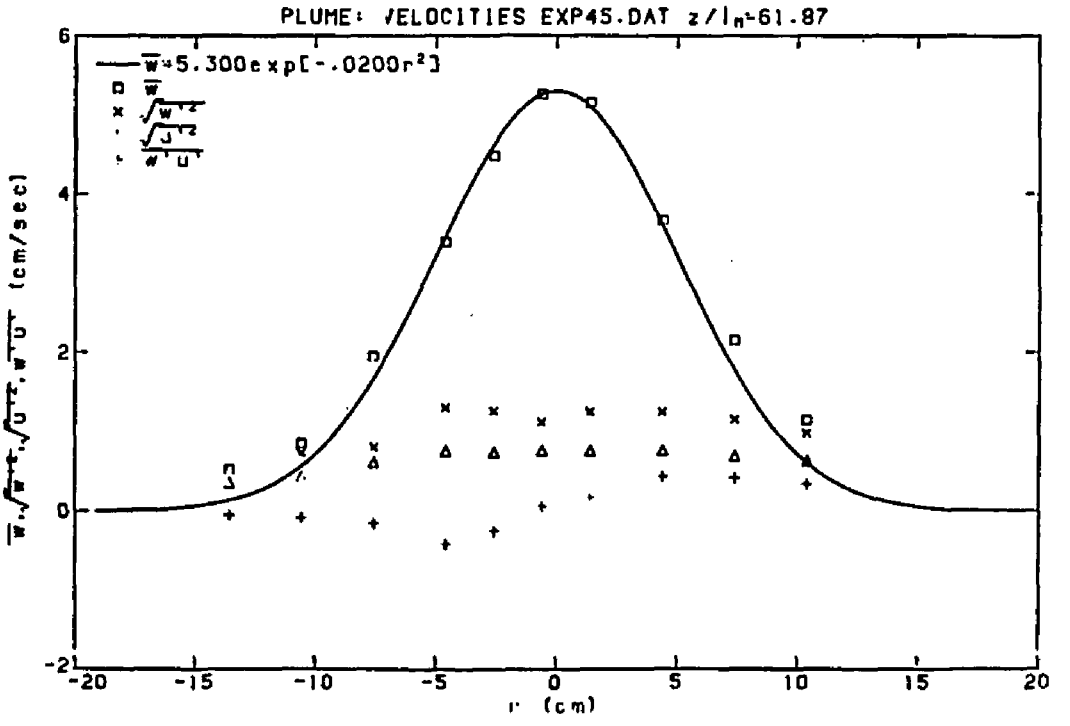

EXP45

| X | W | WP | UP | WPUP | C | CP | WPCP | UPCP |
|---|---|---|---|---|---|---|---|---|
| 65.000 | 0.519 | 0.571 | 0.351 | -0.051 | 0.196 | 0.292 | 0.094 | 0.030 |
| 68.000 | 0.852 | 0.731 | 0.437 | -0.084 | 0.493 | 0.803 | 0.323 | 0.139 |
| 71.000 | 1.950 | 0.804 | 0.611 | -0.154 | 0.908 | 0.728 | 0.181 | 0.132 |
| 74.000 | 3.391 | 1.299 | 0.753 | -0.423 | 1.957 | 1.174 | 0.902 | 0.415 |
| 76.000 | 4.479 | 1.261 | 0.738 | -0.238 | 2.499 | 1.165 | 0.780 | 0.231 |
| 78.000 | 5.258 | 1.122 | 0.766 | 0.061 | 2.884 | 1.096 | 0.533 | 0.028 |
| 80.000 | 5.150 | 1.251 | 0.760 | 0.173 | 2.827 | 1.101 | 0.692 | -0.180 |
| 83.000 | 3.661 | 1.248 | 0.758 | 0.435 | 1.933 | 1.048 | 0.784 | -0.362 |
| 86.000 | 2.149 | 1.150 | 0.688 | 0.417 | 1.239 | 0.783 | 0.483 | -0.290 |
| 89.000 | 1.146 | 0.979 | 0.632 | 0.341 | 0.860 | 0.628 | 0.411 | -0.212 |

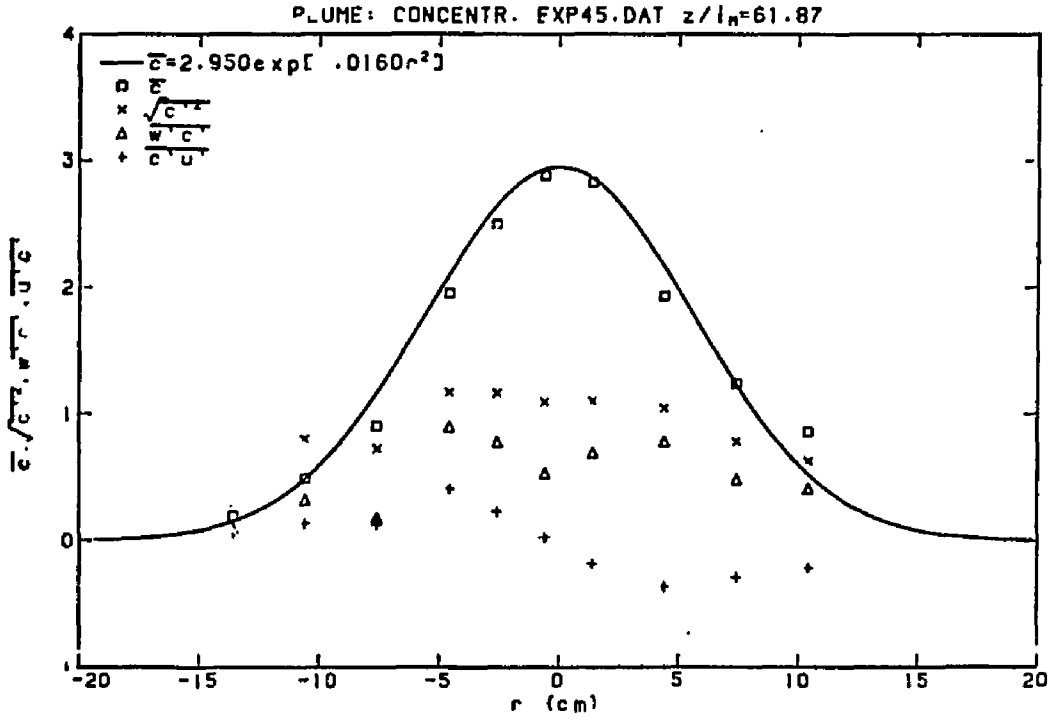

EXP46

| X | W | WP | UP | WPUP | C | CP | WPCP | UPCP |
|---|---|---|---|---|---|---|---|---|
| 70.000 | 0.212 | 0.207 | 0.230 | -0.005 | 0.483 | 0.211 | -0.017 | 0.010 |
| 71.500 | 1.570 | 0.923 | 0.564 | -0.124 | 2.343 | 2.057 | 0.617 | 0.370 |
| 73.000 | 2.995 | 1.167 | 0.693 | -0.301 | 4.204 | 2.611 | 1.389 | 0.718 |
| 74.500 | 4.135 | 1.260 | 0.724 | -0.259 | 6.083 | 3.145 | 1.785 | 0.655 |
| 76.000 | 5.708 | 1.285 | 0.848 | -0.219 | 8.315 | 3.370 | 2.315 | 0.599 |
| 77.500 | 6.172 | 1.243 | 0.912 | -0.034 | 9.346 | 3.596 | 2.119 | 0.319 |
| 78.500 | 6.249 | 1.304 | 0.943 | 0.092 | 9.303 | 3.464 | 2.089 | -0.255 |
| 79.500 | 5.752 | 1.375 | 0.946 | 0.257 | 8.483 | 3.611 | 2.486 | -0.538 |
| 81.000 | 4.699 | 1.330 | 0.815 | 0.287 | 7.075 | 3.268 | 2.113 | -0.747 |
| 82.500 | 2.667 | 1.349 | 0.740 | 0.340 | 4.152 | 2.901 | 1.995 | -0.877 |
| 84.000 | 0.606 | 0.736 | 0.491 | 0.093 | 1.677 | 1.757 | 0.368 | -0.315 |
| 85.500 | 0.402 | 0.617 | 0.375 | 0.049 | 0.866 | 1.429 | 0.435 | -0.156 |
| 87.000 | 0.105 | 0.207 | 0.193 | -0.000 | 0.191 | 0.142 | -0.009 | -0.002 |

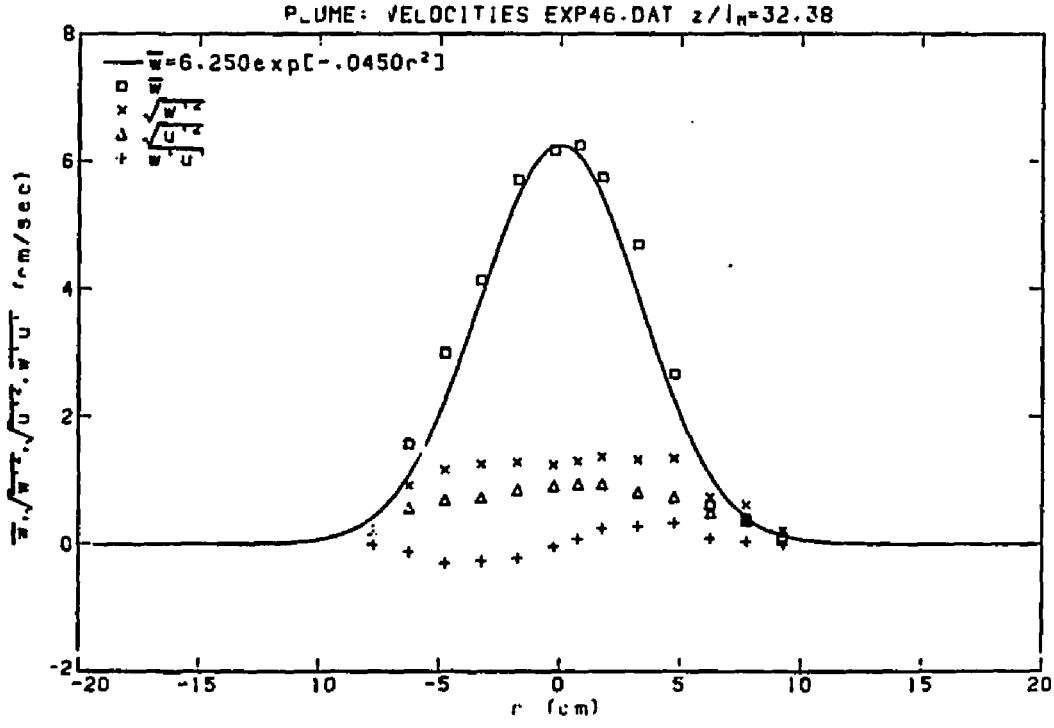

**EXP46**

| X | W | WP | UP | WPUP | C | CP | WPCP | UPCP |
|---|---|---|---|---|---|---|---|---|
| 70.000 | 0.212 | 0.207 | 0.230 | -0.005 | 0.483 | 0.211 | -0.017 | 0.010 |
| 71.500 | 1.570 | 0.923 | 0.564 | -0.124 | 2.343 | 2.057 | 0.617 | 0.370 |
| 73.000 | 2.995 | 1.167 | 0.693 | -0.301 | 4.204 | 2.611 | 1.389 | 0.718 |
| 74.500 | 4.135 | 1.260 | 0.724 | -0.259 | 6.083 | 3.145 | 1.785 | 0.655 |
| 76.000 | 5.708 | 1.285 | 0.848 | -0.219 | 8.315 | 3.370 | 2.315 | 0.599 |
| 77.500 | 6.172 | 1.243 | 0.912 | -0.034 | 9.346 | 3.596 | 2.119 | 0.319 |
| 78.500 | 6.249 | 1.304 | 0.943 | 0.092 | 9.303 | 3.464 | 2.089 | -0.255 |
| 79.500 | 5.752 | 1.375 | 0.946 | 0.257 | 8.483 | 3.611 | 2.486 | -0.538 |
| 81.000 | 4.699 | 1.330 | 0.815 | 0.287 | 7.075 | 3.268 | 2.113 | -0.747 |
| 82.500 | 2.667 | 1.349 | 0.740 | 0.340 | 4.152 | 2.901 | 1.995 | -0.877 |
| 84.000 | 0.606 | 0.736 | 0.491 | 0.093 | 1.677 | 1.757 | 0.368 | -0.315 |
| 85.500 | 0.402 | 0.617 | 0.375 | 0.049 | 0.866 | 1.429 | 0.435 | -0.156 |
| 87.000 | 0.105 | 0.207 | 0.193 | -0.000 | 0.191 | 0.142 | -0.009 | -0.002 |

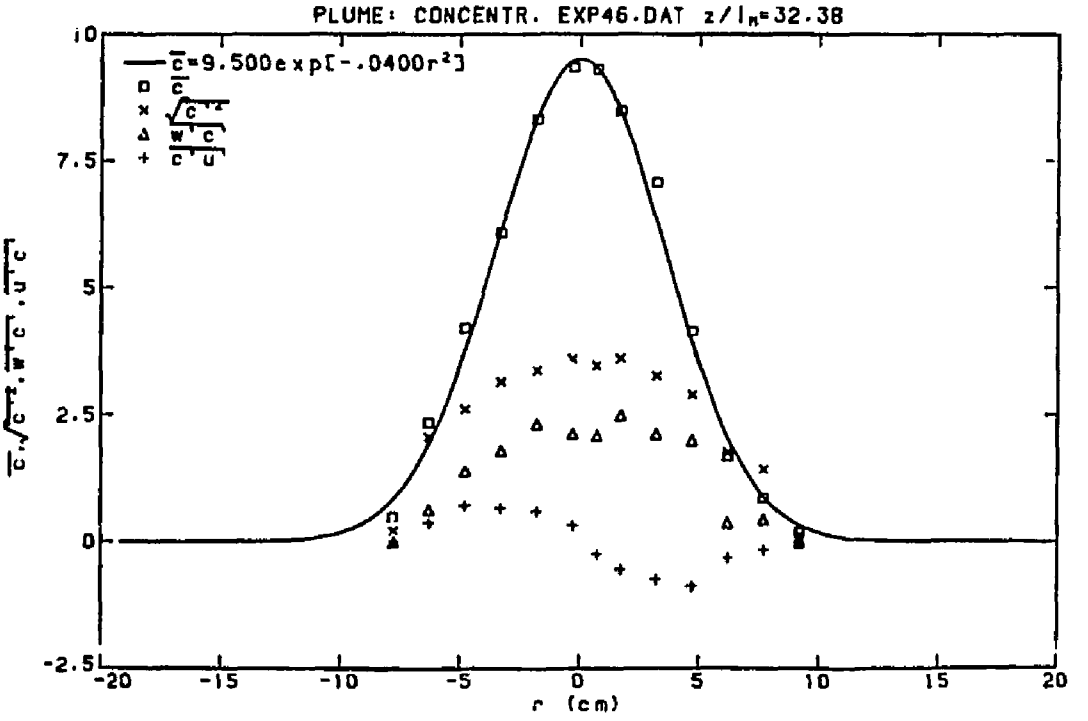

**EXP47**

| X | W | WP | UP | WPUP | C | CP | WPCP | UPCP |
|---|---|---|---|---|---|---|---|---|
| 66.000 | 0.099 | 0.324 | 0.316 | -0.024 | 0.019 | 0.300 | -0.025 | -0.021 |
| 68.000 | 0.052 | 0.264 | 0.311 | 0.019 | 0.071 | 0.532 | 0.009 | 0.056 |
| 70.000 | 1.166 | 0.912 | 0.516 | -0.124 | 0.864 | 1.137 | 0.651 | 0.241 |
| 72.000 | 2.411 | 1.233 | 0.623 | -0.215 | 1.893 | 1.449 | 1.036 | 0.336 |
| 74.000 | 3.597 | 1.233 | 0.770 | -0.276 | 3.041 | 1.875 | 1.224 | 0.580 |
| 76.000 | 4.951 | 1.305 | 0.810 | -0.123 | 4.529 | 2.043 | 1.440 | 0.319 |
| 78.000 | 5.334 | 1.274 | 0.868 | 0.221 | 4.589 | 2.012 | 1.191 | -0.167 |
| 80.000 | 5.021 | 1.247 | 0.773 | 0.133 | 4.375 | 1.939 | 1.114 | -0.190 |
| 82.000 | 3.041 | 1.510 | 0.765 | 0.391 | 2.608 | 1.742 | 1.103 | -0.480 |
| 84.000 | 1.664 | 1.061 | 0.648 | 0.328 | 0.972 | 1.255 | 0.776 | -0.349 |
| 86.000 | 0.712 | 0.893 | 0.590 | 0.138 | 0.528 | 1.056 | 0.337 | -0.232 |
| 88.000 | 0.449 | 0.466 | 0.452 | 0.045 | 0.043 | 0.832 | 0.135 | -0.061 |
| 90.000 | 0.004 | 0.345 | 0.217 | -0.009 | -0.346 | 0.102 | -0.002 | -0.002 |

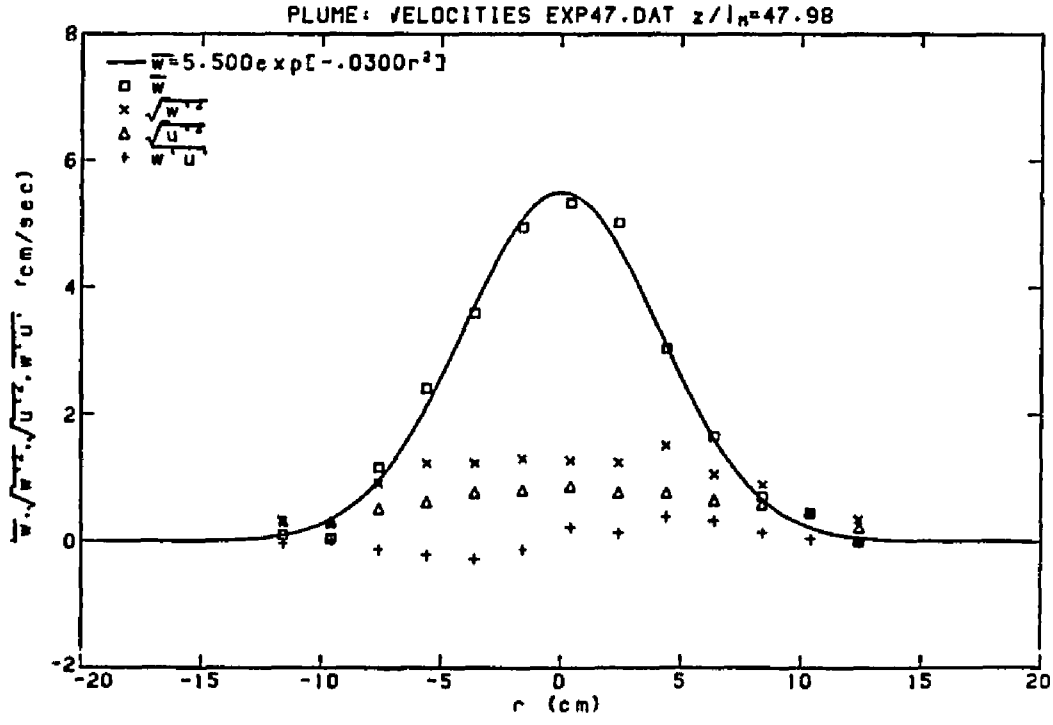

EXP47

| X | W | WP | UP | WPUP | C | CP | WPCP | UPCP |
|---|---|---|---|---|---|---|---|---|
| 66.000 | 0.099 | 0.324 | 0.316 | -0.024 | 0.019 | 0.300 | -0.025 | -0.021 |
| 68.000 | 0.052 | 0.264 | 0.311 | 0.019 | 0.071 | 0.532 | 0.009 | 0.056 |
| 70.000 | 1.166 | 0.912 | 0.516 | -0.124 | 0.864 | 1.137 | 0.651 | 0.241 |
| 72.000 | 2.411 | 1.233 | 0.623 | -0.215 | 1.893 | 1.449 | 1.036 | 0.336 |
| 74.000 | 3.597 | 1.233 | 0.770 | -0.276 | 3.041 | 1.875 | 1.224 | 0.580 |
| 76.000 | 4.951 | 1.305 | 0.810 | -0.123 | 4.529 | 2.043 | 1.440 | 0.319 |
| 78.000 | 5.334 | 1.274 | 0.868 | 0.221 | 4.589 | 2.012 | 1.191 | -0.167 |
| 80.000 | 5.021 | 1.247 | 0.773 | 0.133 | 4.375 | 1.939 | 1.114 | -0.190 |
| 82.000 | 3.041 | 1.510 | 0.765 | 0.391 | 2.608 | 1.742 | 1.103 | -0.480 |
| 84.000 | 1.664 | 1.061 | 0.648 | 0.328 | 0.972 | 1.255 | 0.776 | -0.349 |
| 86.000 | 0.712 | 0.893 | 0.590 | 0.138 | 0.528 | 1.056 | 0.337 | -0.232 |
| 88.000 | 0.449 | 0.466 | 0.452 | 0.045 | 0.043 | 0.832 | 0.135 | -0.061 |
| 90.000 | 0.004 | 0.345 | 0.217 | -0.009 | -0.346 | 0.102 | -0.002 | -0.002 |

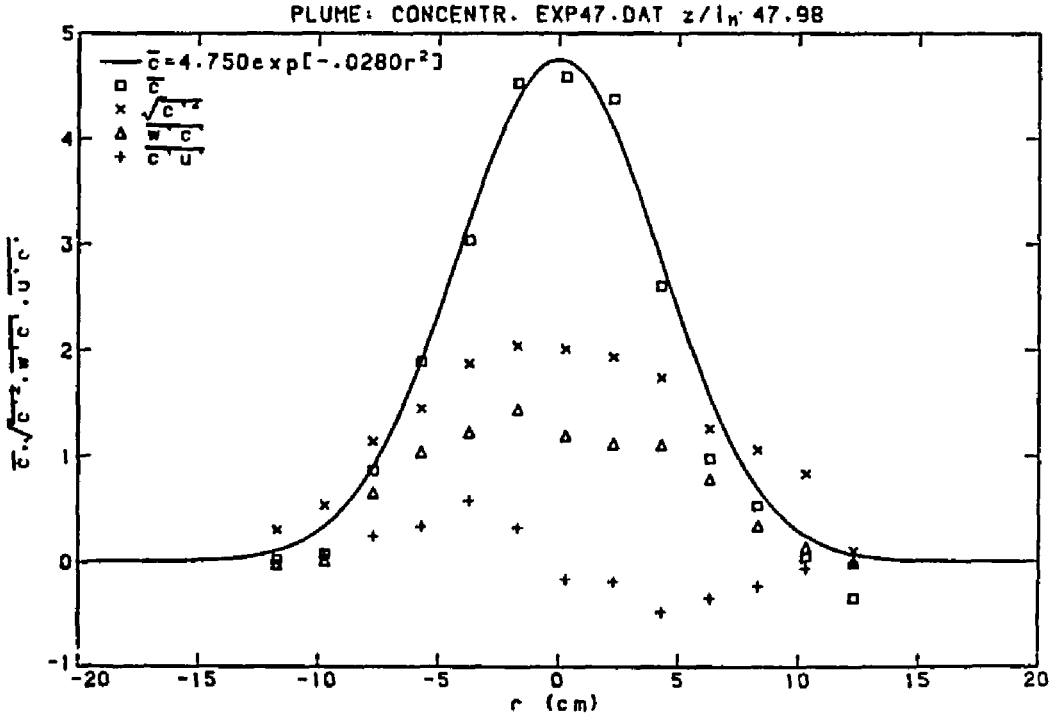

VELO5

| X | W | MAX W | MIN W | WP | UP | WPUP |
|---|---|---|---|---|---|---|
| 66.000 | 0.255 | 3.267 | -0.669 | 0.449 | 0.514 | 0.108 |
| 67.500 | 0.477 | 2.973 | -0.851 | 0.511 | 0.456 | 0.066 |
| 69.000 | 0.396 | 3.139 | -0.629 | 0.430 | 0.385 | 0.024 |
| 70.500 | 1.074 | 5.936 | -0.408 | 0.840 | 0.557 | 0.177 |
| 72.000 | 2.204 | 6.090 | -0.669 | 1.211 | 0.716 | 0.386 |
| 73.500 | 3.037 | 7.165 | 0.287 | 1.272 | 0.753 | 0.285 |
| 75.000 | 3.975 | 8.550 | 0.248 | 1.409 | 0.783 | 0.252 |
| 76.500 | 5.036 | 9.967 | 0.680 | 1.367 | 0.791 | 0.195 |
| 77.500 | 5.405 | 10.245 | 1.261 | 1.368 | 0.931 | 0.120 |
| 78.500 | 5.433 | 10.399 | 0.874 | 1.517 | 0.929 | -0.126 |
| 79.500 | 5.809 | 11.397 | 0.268 | 1.388 | 0.885 | -0.113 |
| 80.500 | 4.996 | 9.859 | 1.241 | 1.254 | 0.860 | -0.257 |
| 81.500 | 4.431 | 8.710 | 0.189 | 1.517 | 0.787 | -0.180 |
| 82.500 | 4.108 | 8.646 | 0.543 | 1.315 | 0.802 | -0.312 |
| 83.500 | 3.207 | 7.904 | -0.188 | 1.435 | 0.789 | -0.386 |
| 84.500 | 3.477 | 8.051 | 0.425 | 1.158 | 0.781 | -0.156 |
| 85.500 | 2.999 | 7.231 | -0.009 | 1.204 | 0.751 | -0.088 |
| 86.500 | 2.133 | 6.090 | -0.148 | 1.109 | 0.724 | -0.020 |
| 87.500 | 1.478 | 5.696 | -0.408 | 0.984 | 0.547 | -0.173 |
| 88.500 | 1.305 | 4.153 | -0.168 | 0.822 | 0.576 | -0.149 |

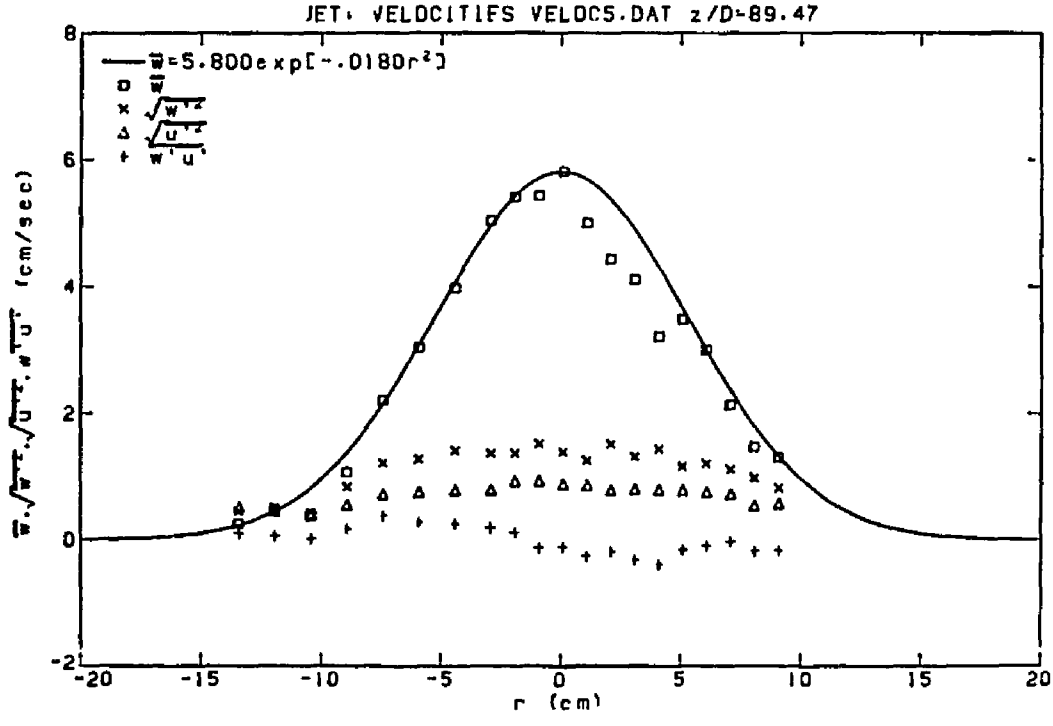

VEL07

| X | W | MAX W | MIN W | WP | UP | WPUP |
|---|---|---|---|---|---|---|
| 70.000 | 0.588 | 4.638 | -1.329 | 0.559 | 0.449 | 0.061 |
| 71.550 | 0.863 | 3.557 | -0.819 | 0.557 | 0.500 | 0.066 |
| 73.000 | 2.077 | 6.310 | -0.576 | 1.084 | 0.652 | 0.254 |
| 74.500 | 3.651 | 8.996 | -0.134 | 1.456 | 0.889 | 0.421 |
| 76.000 | 5.225 | 10.497 | 0.796 | 1.548 | 0.978 | 0.393 |
| 77.500 | 6.434 | 12.122 | 0.344 | 1.649 | 1.007 | 0.317 |
| 78.500 | 6.990 | 13.981 | 1.820 | 1.708 | 1.069 | 0.324 |
| 79.500 | 6.901 | 12.562 | 1.340 | 1.569 | 0.984 | -0.017 |
| 80.500 | 6.507 | 12.078 | 1.533 | 1.471 | 1.011 | -0.043 |
| 81.500 | 5.617 | 11.046 | 1.301 | 1.573 | 0.951 | -0.365 |
| 83.000 | 4.040 | 12.308 | 0.218 | 1.433 | 0.895 | -0.393 |
| 84.600 | 2.697 | 7.832 | -0.299 | 1.414 | 0.728 | -0.436 |
| 86.000 | 1.444 | 6.099 | -0.923 | 0.946 | 0.612 | -0.161 |
| 87.500 | 0.709 | 3.568 | -0.842 | 0.572 | 0.464 | -0.050 |
| 89.000 | 0.413 | 3.331 | -1.065 | 0.384 | 0.366 | -0.029 |

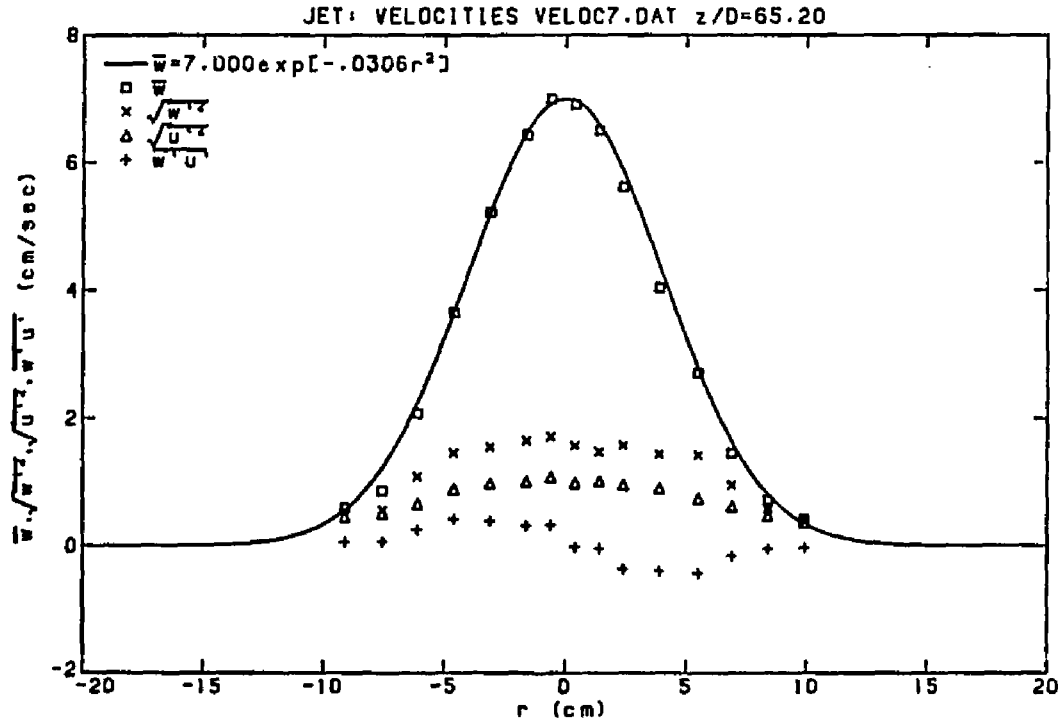

VEL10

| X | W | MAX W | MIN W | WP | UP | WPUP |
|---|---|---|---|---|---|---|
| 66.000 | 0.008 | 3.422 | -0.882 | 0.219 | 0.304 | -0.007 |
| 68.000 | 0.224 | 10.116 | -0.741 | 0.349 | 0.386 | 0.027 |
| 70.000 | 1.054 | 8.351 | -0.499 | 0.971 | 0.567 | 0.208 |
| 72.000 | 1.442 | 11.911 | -0.741 | 0.902 | 0.645 | 0.184 |
| 74.000 | 2.723 | 11.316 | 0.178 | 1.369 | 0.776 | 0.489 |
| 76.000 | 4.600 | 12.352 | 0.767 | 1.383 | 0.878 | 0.466 |
| 77.550 | 5.489 | 11.734 | 0.611 | 1.493 | 0.996 | 0.352 |
| 79.000 | 5.627 | 10.131 | 1.058 | 1.385 | 0.967 | -0.158 |
| 80.000 | 5.912 | 12.293 | 1.135 | 1.487 | 0.934 | -0.093 |
| 81.000 | 5.143 | 10.193 | 0.942 | 1.375 | 0.931 | -0.131 |
| 82.500 | 4.671 | 13.133 | 0.158 | 1.454 | 0.905 | -0.189 |
| 84.000 | 3.989 | 8.431 | -0.219 | 1.500 | 0.835 | -0.365 |
| 85.550 | 2.285 | 7.718 | -0.060 | 1.162 | 0.717 | -0.240 |
| 87.000 | 1.410 | 6.573 | -0.379 | 0.868 | 0.566 | -0.165 |
| 88.500 | 1.137 | 4.677 | -0.459 | 0.791 | 0.527 | -0.150 |
| 90.000 | 0.744 | 3.983 | -0.079 | 0.469 | 0.454 | -0.038 |
| 91.500 | 0.367 | 3.349 | -0.379 | 0.205 | 0.305 | 0.002 |
| 95.000 | 0.411 | 1.251 | -0.199 | 0.194 | 0.337 | -0.008 |

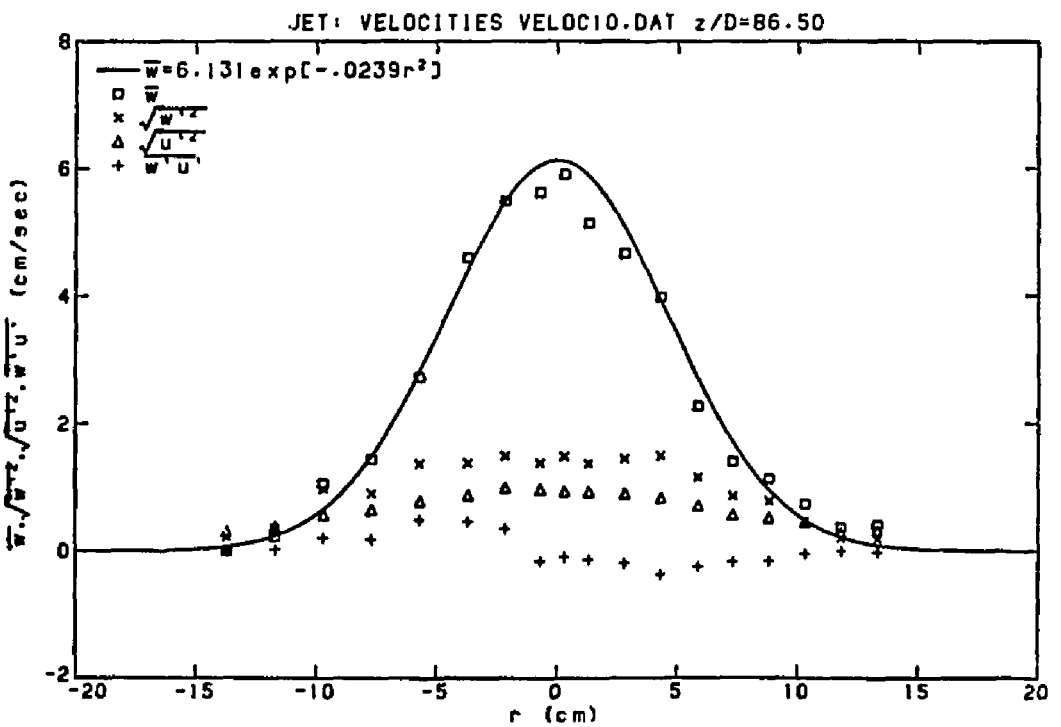

VEL11

| X | W | MAX W | MIN W | WP | UP | WPUP |
|---|---|---|---|---|---|---|
| 64.000 | 0.333 | 3.631 | -0.388 | 0.599 | 0.478 | 0.155 |
| 66.000 | 0.779 | 3.776 | -0.609 | 0.593 | 0.488 | 0.125 |
| 68.000 | 0.850 | 4.028 | -0.548 | 0.655 | 0.558 | 0.077 |
| 70.000 | 1.431 | 6.496 | -0.268 | 1.203 | 0.661 | 0.376 |
| 72.000 | 2.915 | 7.676 | 0.169 | 1.196 | 0.793 | 0.417 |
| 74.000 | 3.756 | 9.044 | 0.189 | 1.506 | 0.870 | 0.569 |
| 77.500 | 5.366 | 12.430 | 1.087 | 1.513 | 0.977 | 0.300 |
| 79.000 | 5.612 | 12.226 | 1.068 | 1.487 | 0.963 | 0.102 |
| 80.500 | 5.100 | 10.475 | 0.894 | 1.453 | 0.913 | -0.128 |
| 82.000 | 5.062 | 10.490 | 0.189 | 1.400 | 0.943 | -0.217 |
| 83.500 | 3.907 | 9.375 | 0.248 | 1.511 | 0.932 | -0.595 |
| 85.000 | 2.946 | 7.807 | -0.208 | 1.401 | 0.775 | -0.233 |
| 86.500 | 1.514 | 5.299 | -0.288 | 1.161 | 0.640 | -0.227 |
| 88.000 | 0.834 | 3.377 | -1.299 | 0.713 | 0.576 | -0.106 |
| 89.500 | 1.187 | 4.615 | -1.319 | 0.850 | 0.588 | -0.170 |
| 91.500 | 0.738 | 4.491 | -0.750 | 0.839 | 0.619 | -0.231 |
| 93.500 | 0.327 | 2.267 | -0.649 | 0.382 | 0.391 | -0.008 |

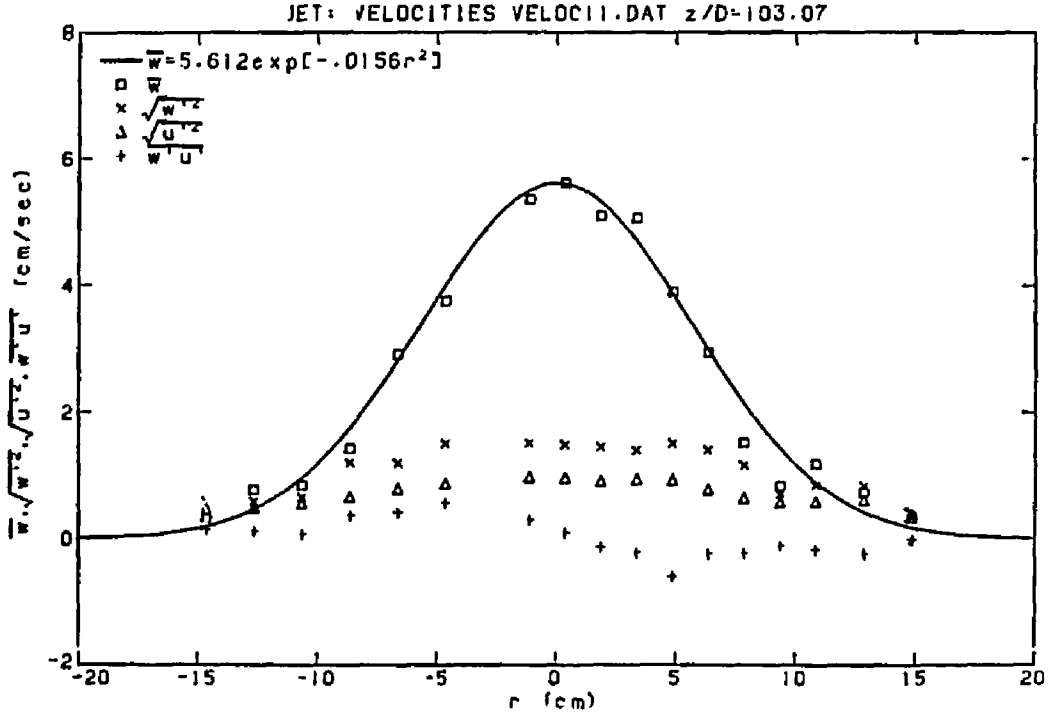

VEL13

| X | W | MAX W | MIN W | WP | UP | WPUP |
|---|---|---|---|---|---|---|
| 72.000 | -0.170 | 0.762 | -1.520 | 0.242 | 0.251 | 0.008 |
| 73.000 | 0.341 | 4.673 | -1.233 | 0.576 | 0.462 | 0.057 |
| 74.000 | 0.895 | 4.655 | -0.705 | 0.731 | 0.552 | 0.080 |
| 75.000 | 2.544 | 10.265 | -0.263 | 1.305 | 0.783 | 0.341 |
| 76.000 | 3.613 | 9.474 | -0.024 | 1.420 | 0.934 | 0.455 |
| 77.000 | 5.111 | 11.431 | 0.371 | 1.807 | 0.966 | 0.593 |
| 78.000 | 6.340 | 12.725 | 1.188 | 1.863 | 1.092 | 0.609 |
| 79.000 | 7.948 | 15.033 | 2.812 | 1.758 | 1.157 | 0.402 |
| 80.000 | 7.859 | 14.218 | 2.719 | 1.820 | 1.176 | -0.222 |
| 81.000 | 6.727 | 12.667 | 1.553 | 1.728 | 1.085 | -0.286 |
| 82.000 | 4.783 | 11.877 | 0.606 | 1.636 | 0.958 | -0.501 |
| 83.000 | 3.274 | 8.699 | -0.988 | 1.239 | 0.824 | -0.290 |
| 84.000 | 2.143 | 6.636 | -0.928 | 1.109 | 0.705 | -0.211 |
| 85.000 | 1.265 | 4.954 | -0.685 | 0.779 | 0.621 | -0.072 |
| 86.000 | 0.602 | 3.198 | -0.604 | 0.443 | 0.390 | -0.020 |
| 87.000 | 0.369 | 2.103 | -0.725 | 0.259 | 0.314 | -0.012 |

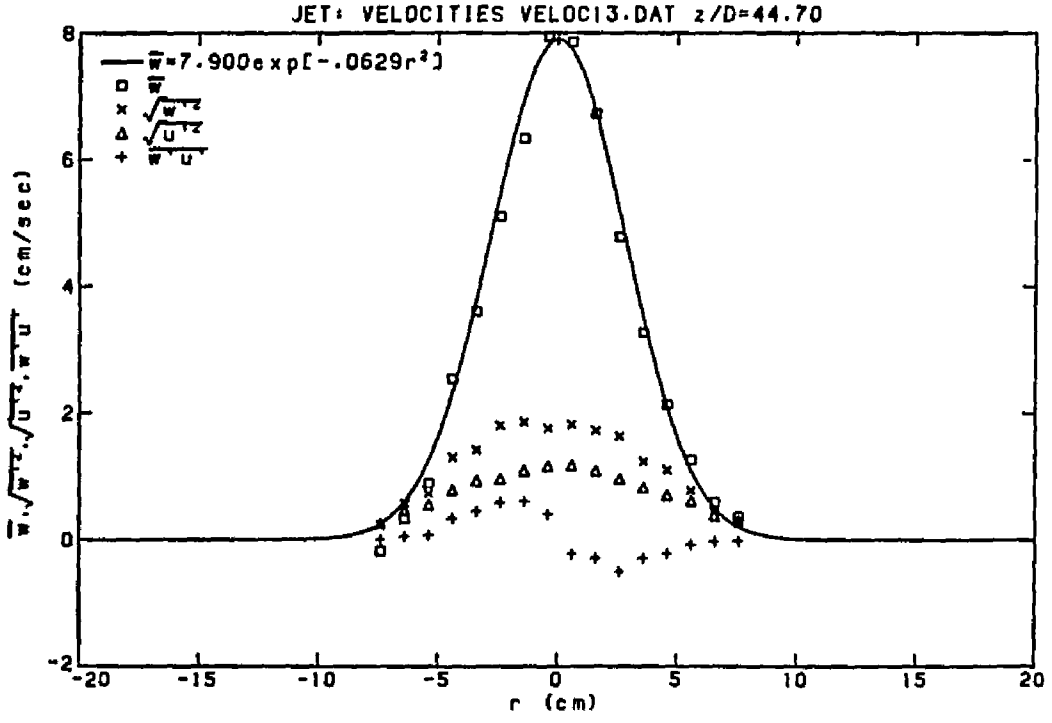

VEL15

| X | W | MAX W | MIN W | WP | UP | WPUP |
|---|---|---|---|---|---|---|
| 70.000 | 1.062 | 5.299 | -0.629 | 0.712 | 0.570 | 0.134 |
| 73.000 | 2.923 | 9.563 | 0.189 | 1.445 | 0.895 | 0.663 |
| 74.500 | 4.310 | 9.407 | -0.288 | 1.465 | 1.021 | 0.602 |
| 76.000 | 5.538 | 10.840 | 0.699 | 1.549 | 1.049 | 0.530 |
| 77.500 | 6.606 | 11.990 | 1.852 | 1.636 | 1.158 | 0.550 |
| 78.500 | 7.220 | 12.474 | 2.733 | 1.599 | 1.155 | 0.372 |
| 79.500 | 7.186 | 12.269 | 2.004 | 1.621 | 1.159 | -0.038 |
| 80.500 | 7.018 | 12.459 | 2.267 | 1.662 | 1.210 | -0.095 |
| 82.000 | 6.101 | 12.138 | 1.068 | 1.774 | 1.051 | -0.351 |
| 83.500 | 4.937 | 9.921 | 0.699 | 1.585 | 1.117 | -0.450 |
| 85.000 | 3.464 | 8.822 | 0.601 | 1.506 | 0.906 | -0.542 |
| 88.000 | 1.295 | 5.524 | -0.548 | 0.939 | 0.629 | -0.190 |
| 91.000 | 0.409 | 3.631 | -0.831 | 0.317 | 0.397 | -0.009 |
| 92.500 | 0.258 | 0.932 | -0.609 | 0.214 | 0.322 | -0.001 |

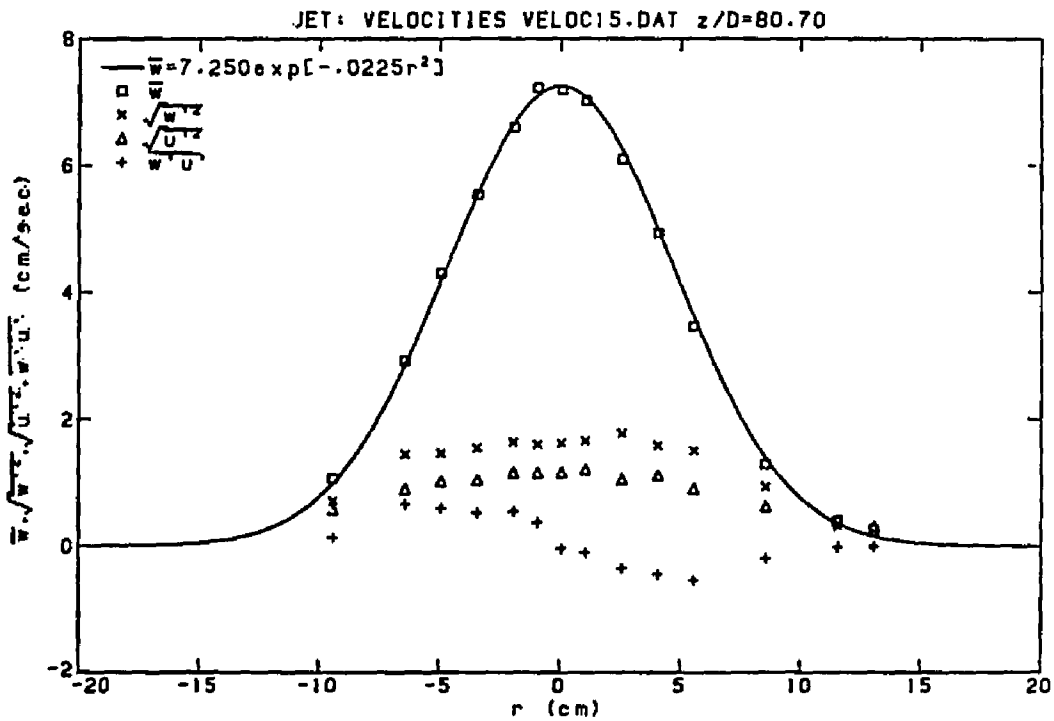

VEL17

| X | W | MAX W | MIN W | WP | UP | WPUP |
|---|---|---|---|---|---|---|
| 63.000 | 0.378 | 0.889 | -0.643 | 0.206 | 0.375 | 0.005 |
| 65.000 | 0.255 | 2.135 | -0.935 | 0.283 | 0.391 | 0.020 |
| 67.000 | 1.402 | 5.215 | -0.498 | 0.843 | 0.591 | 0.165 |
| 69.000 | 2.356 | 7.721 | -0.003 | 1.111 | 0.703 | 0.287 |
| 72.000 | 3.518 | 9.016 | 0.017 | 1.415 | 0.983 | 0.661 |
| 73.500 | 4.419 | 9.607 | 0.506 | 1.571 | 1.012 | 0.589 |
| 75.000 | 5.868 | 11.126 | 1.645 | 1.556 | 1.108 | 0.451 |
| 76.500 | 6.391 | 11.323 | 0.809 | 1.818 | 1.228 | 0.354 |
| 78.000 | 6.642 | 12.874 | 2.329 | 1.582 | 1.226 | 0.217 |
| 79.500 | 6.429 | 13.746 | 1.428 | 1.768 | 1.141 | 0.008 |
| 81.000 | 6.648 | 11.489 | 2.425 | 1.585 | 1.067 | -0.402 |
| 83.000 | 5.398 | 10.375 | 1.269 | 1.569 | 1.090 | -0.450 |
| 85.000 | 4.029 | 9.464 | 0.486 | 1.527 | 0.963 | -0.603 |
| 87.000 | 3.056 | 7.905 | 0.283 | 1.240 | 0.881 | -0.447 |
| 89.000 | 2.209 | 7.115 | -0.003 | 1.242 | 0.802 | -0.336 |
| 91.000 | 1.058 | 4.819 | -1.270 | 0.813 | 0.737 | -0.180 |
| 93.000 | 0.995 | 4.674 | -1.777 | 0.883 | 0.638 | -0.128 |
| 95.000 | 0.107 | 1.685 | -0.809 | 0.273 | 0.433 | -0.031 |

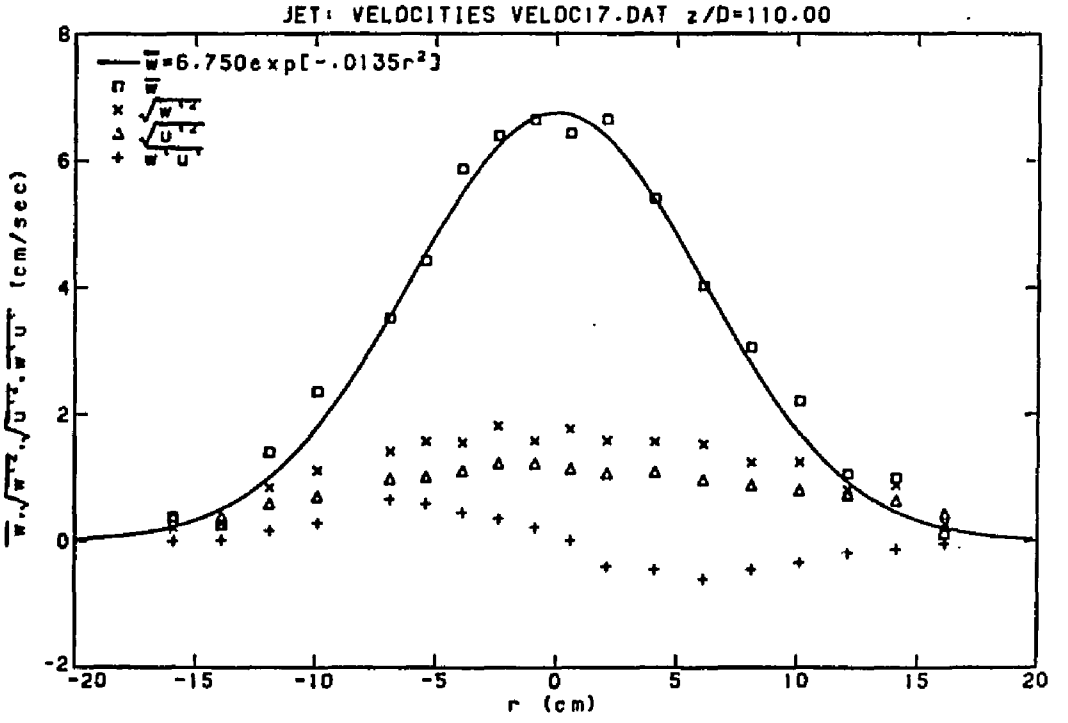

VEL19

| X | W | MAX W | MIN W | WP | UP | WPUP |
|---|---|---|---|---|---|---|
| 68.000 | 0.105 | 1.355 | -1.305 | 0.314 | 0.509 | 0.008 |
| 70.000 | 1.148 | 4.624 | -0.990 | 0.897 | 0.676 | 0.206 |
| 72.000 | 2.426 | 7.186 | -0.470 | 1.366 | 0.864 | 0.456 |
| 74.000 | 3.804 | 9.783 | -0.078 | 1.605 | 1.043 | 0.724 |
| 76.000 | 5.288 | 12.012 | 0.695 | 1.819 | 1.201 | 0.930 |
| 77.500 | 6.891 | 13.020 | 1.355 | 1.735 | 1.146 | 0.316 |
| 78.550 | 7.427 | 14.196 | 2.043 | 1.660 | 1.208 | 0.148 |
| 79.500 | 7.053 | 12.556 | 1.375 | 1.810 | 1.159 | 0.089 |
| 80.500 | 7.179 | 13.477 | 2.968 | 1.590 | 1.158 | -0.150 |
| 82.000 | 6.291 | 12.160 | 0.634 | 1.789 | 1.153 | -0.267 |
| 83.500 | 4.502 | 11.234 | 0.167 | 1.726 | 1.058 | -0.675 |
| 85.000 | 3.574 | 8.987 | -0.719 | 1.290 | 0.933 | -0.346 |
| 86.500 | 2.713 | 7.957 | -0.823 | 1.499 | 0.937 | -0.670 |
| 88.000 | 1.986 | 7.423 | -0.470 | 1.304 | 0.837 | -0.466 |
| 89.500 | 0.889 | 5.415 | -0.740 | 0.762 | 0.608 | 0.009 |

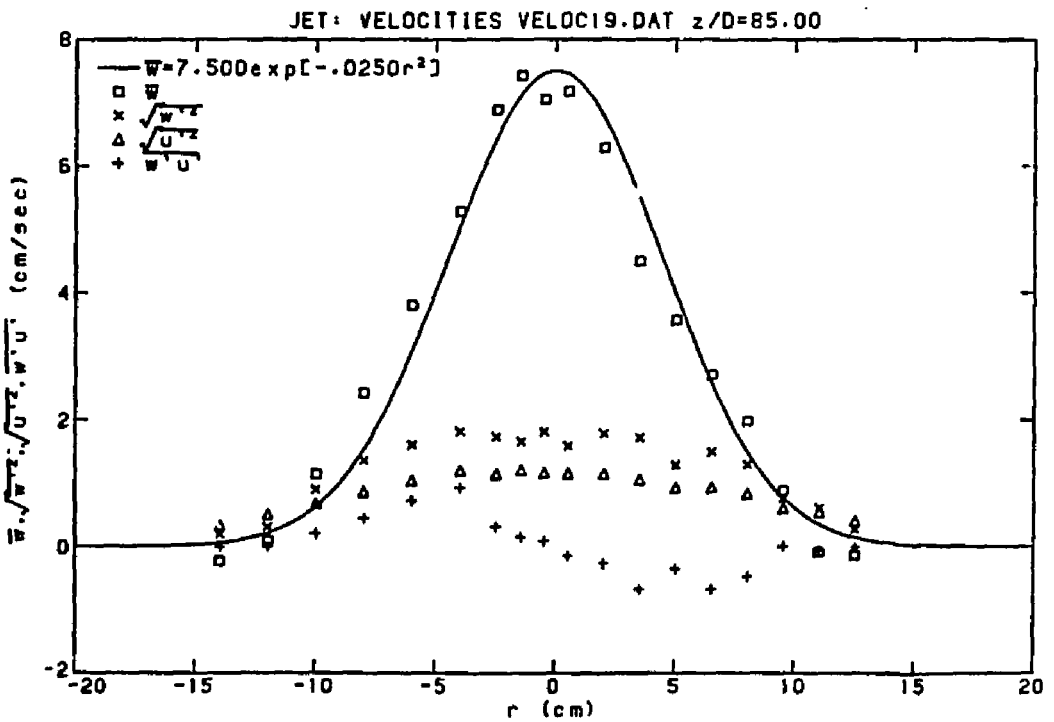

VEL21

| X | W | MAX W | MIN W | WP | UP | WPUP |
|---|---|---|---|---|---|---|
| 70.000 | -0.033 | 0.813 | -0.896 | 0.157 | 0.209 | -0.000 |
| 71.000 | 0.188 | 2.263 | -0.875 | 0.328 | 0.355 | 0.005 |
| 72.000 | 0.833 | 4.865 | -0.664 | 0.717 | 0.513 | 0.067 |
| 73.000 | 1.349 | 5.777 | -1.621 | 1.000 | 0.620 | 0.203 |
| 74.000 | 2.309 | 7.208 | -0.327 | 1.309 | 0.681 | 0.171 |
| 75.000 | 3.068 | 8.467 | -0.411 | 1.400 | 0.802 | 0.284 |
| 76.000 | 3.656 | 9.505 | 0.485 | 1.417 | 0.826 | 0.411 |
| 77.000 | 5.223 | 11.109 | 0.443 | 1.558 | 0.856 | 0.310 |
| 78.000 | 6.690 | 11.785 | 2.045 | 1.571 | 0.916 | 0.234 |
| 79.000 | 6.981 | 12.644 | 2.736 | 1.553 | 1.032 | 0.218 |
| 80.000 | 7.307 | 12.435 | 1.504 | 1.631 | 0.970 | 0.054 |
| 81.000 | 5.949 | 11.294 | 1.504 | 1.573 | 0.901 | -0.104 |
| 82.000 | 4.812 | 10.812 | -0.097 | 1.589 | 0.890 | -0.279 |
| 83.000 | 3.650 | 9.828 | -0.685 | 1.455 | 0.758 | -0.225 |
| 84.000 | 2.064 | 7.570 | -0.685 | 1.388 | 0.751 | -0.270 |
| 85.000 | 1.676 | 6.350 | -0.369 | 0.995 | 0.543 | -0.038 |
| 86.000 | 1.265 | 5.633 | -0.706 | 0.834 | 0.569 | -0.042 |
| 87.000 | 0.575 | 2.989 | -0.706 | 0.513 | 0.446 | -0.046 |
| 88.000 | 0.519 | 2.814 | -1.343 | 0.510 | 0.414 | -0.023 |
| 89.000 | 0.178 | 0.875 | -0.769 | 0.156 | 0.273 | 0.002 |

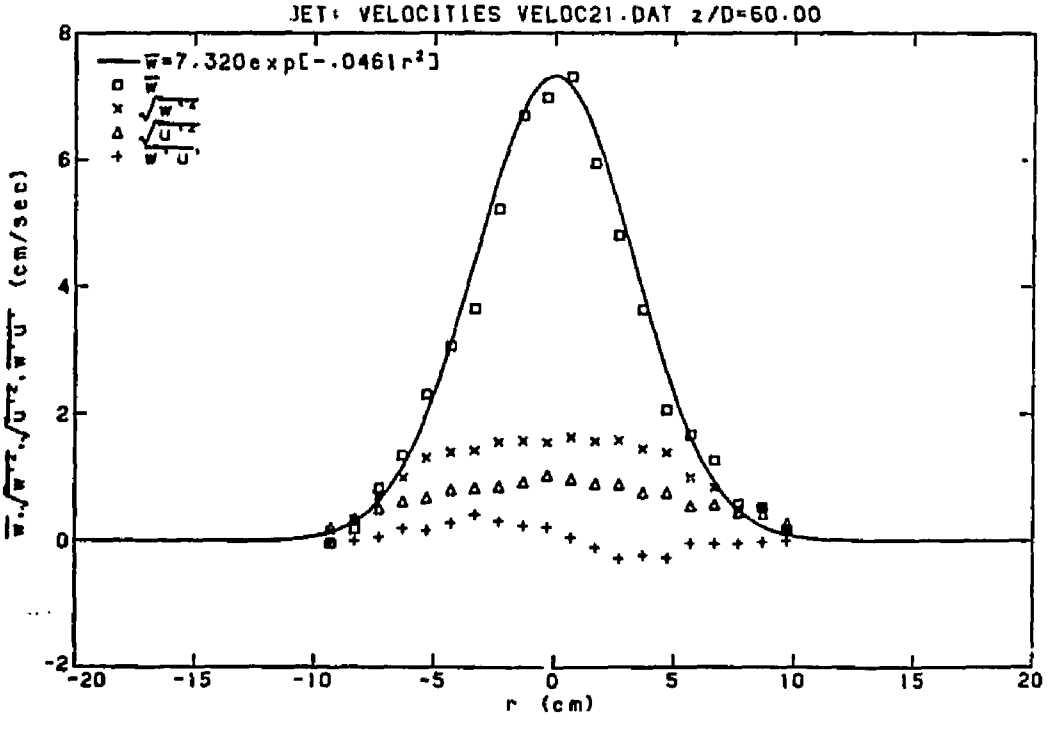

VEL23

| X | W | MAX W | MIN W | WP | UP | WPUP |
|---|---|---|---|---|---|---|
| 74.500 | 0.319 | 3.444 | -0.987 | 0.547 | 0.430 | 0.040 |
| 75.500 | 1.300 | 6.517 | -0.565 | 0.844 | 0.513 | 0.032 |
| 76.500 | 2.535 | 7.901 | -0.670 | 1.331 | 0.662 | 0.115 |
| 77.500 | 4.439 | 10.296 | 0.312 | 1.522 | 0.751 | 0.125 |
| 78.500 | 6.266 | 11.205 | 1.011 | 1.682 | 0.814 | 0.104 |
| 79.500 | 7.099 | 12.853 | 2.512 | 1.597 | 0.843 | 0.054 |
| 80.500 | 6.021 | 12.317 | 0.745 | 1.729 | 0.822 | -0.055 |
| 81.500 | 4.000 | 10.423 | 0.312 | 1.489 | 0.716 | -0.004 |
| 82.500 | 2.222 | 7.354 | -0.987 | 1.173 | 0.565 | -0.003 |
| 83.500 | 1.042 | 4.615 | -0.670 | 0.797 | 0.433 | -0.022 |
| 84.500 | 0.288 | 2.630 | -0.945 | 0.417 | 0.328 | -0.006 |
| 85.500 | 0.061 | 1.898 | -0.839 | 0.199 | 0.219 | -0.006 |

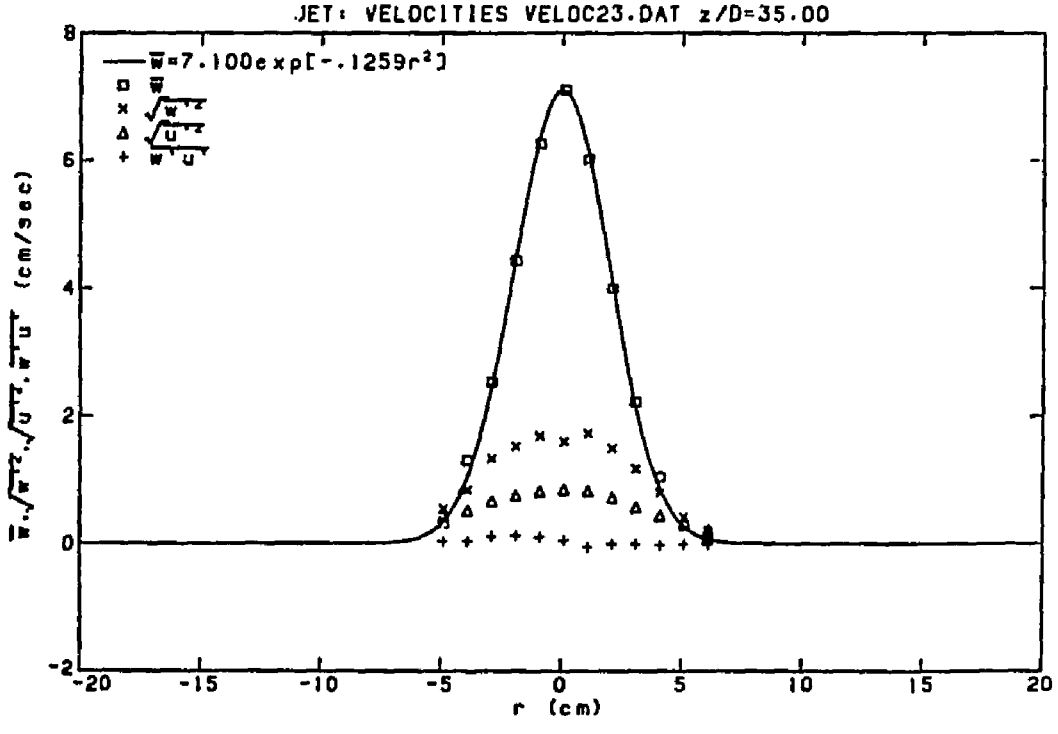

PAP12

| X | W | MAX W | MIN W | WP | UP | WPUP |
|---|---|---|---|---|---|---|
| 68.000 | 0.097 | 1.507 | -1.237 | 0.117 | 0.181 | -0.001 |
| 70.000 | 0.020 | 1.338 | -1.466 | 0.136 | 0.187 | -0.001 |
| 72.000 | 0.629 | 4.796 | -1.104 | 0.740 | 0.359 | 0.058 |
| 74.000 | 1.859 | 6.911 | -0.556 | 1.175 | 0.703 | 0.393 |
| 76.000 | 3.761 | 8.210 | -0.686 | 1.475 | 0.779 | 0.395 |
| 78.000 | 5.991 | 11.122 | 2.154 | 1.478 | 0.892 | 0.357 |
| 79.000 | 6.143 | 11.131 | 1.259 | 1.492 | 0.905 | 0.010 |
| 80.000 | 5.945 | 11.131 | 1.574 | 1.507 | 0.930 | 0.094 |
| 82.000 | 4.241 | 8.610 | 0.251 | 1.532 | 0.795 | -0.226 |
| 84.000 | 1.998 | 6.639 | -0.889 | 1.010 | 0.614 | -0.128 |
| 86.000 | 0.736 | 3.949 | -0.734 | 0.683 | 0.427 | -0.028 |
| 88.000 | 0.172 | 2.032 | -1.491 | 0.424 | 0.254 | -0.039 |
| 90.000 | 0.006 | 1.462 | -1.345 | 0.111 | 0.107 | 0.001 |

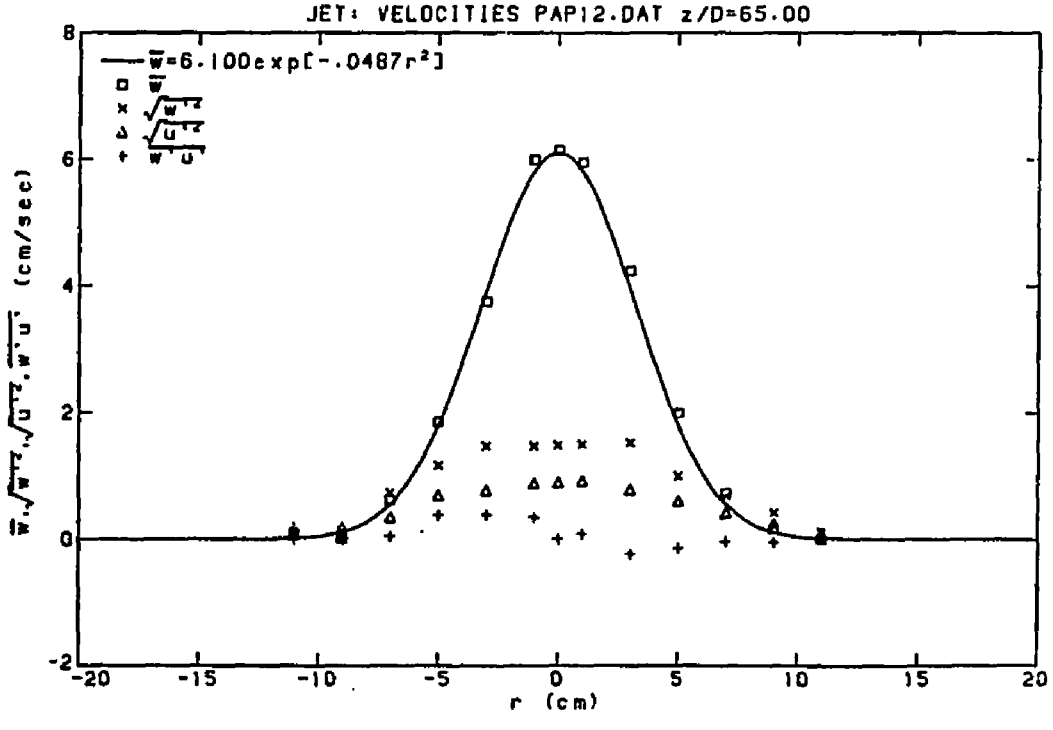

PAP13

| X | W | MAX W | MIN W | WP | UP | WPUP |
|---|---|---|---|---|---|---|
| 66.000 | 0.194 | 2.618 | -2.153 | 0.363 | 0.338 | 0.020 |
| 68.000 | 0.576 | 3.207 | -1.710 | 0.581 | 0.589 | 0.070 |
| 70.000 | 0.713 | 5.577 | -0.663 | 0.877 | 0.573 | 0.170 |
| 72.000 | 2.752 | 8.590 | -1.032 | 1.490 | 0.945 | 0.657 |
| 74.000 | 3.748 | 9.198 | -0.028 | 1.602 | 0.980 | 0.618 |
| 76.000 | 6.453 | 13.124 | 1.776 | 1.842 | 1.288 | 0.793 |
| 78.000 | 7.330 | 15.739 | 0.735 | 1.956 | 1.313 | 0.415 |
| 79.000 | 7.838 | 13.932 | 1.977 | 1.718 | 1.115 | 0.181 |
| 81.000 | 6.822 | 12.904 | 1.798 | 1.802 | 1.229 | -0.244 |
| 83.000 | 5.662 | 12.166 | 0.390 | 2.028 | 1.077 | -0.562 |
| 85.000 | 4.022 | 10.427 | 0.286 | 1.671 | 1.056 | -0.437 |
| 87.000 | 2.477 | 9.015 | -0.734 | 1.657 | 1.112 | -0.927 |
| 89.000 | 0.627 | 5.865 | -1.588 | 0.910 | 0.658 | -0.093 |

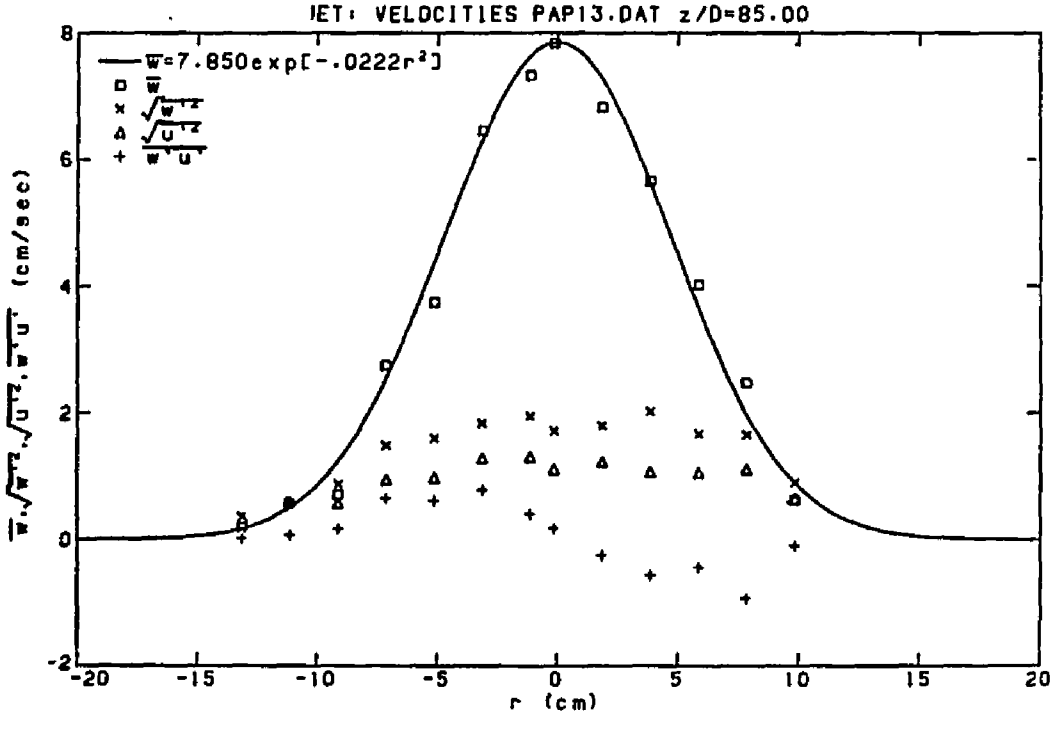

PAP16

| X | W | MAX W | MIN W | WP | UP | WPUP |
|---|---|---|---|---|---|---|
| 75.000 | 0.266 | 2.810 | -2.229 | 0.313 | 0.219 | 0.006 |
| 76.000 | 0.904 | 4.373 | -2.229 | 0.592 | 0.401 | 0.032 |
| 77.000 | 2.617 | 9.870 | -1.286 | 1.308 | 0.766 | 0.194 |
| 78.000 | 5.146 | 13.179 | 1.000 | 1.581 | 0.950 | 0.099 |
| 79.000 | 6.872 | 12.637 | 1.185 | 1.762 | 1.021 | 0.108 |
| 80.000 | 6.115 | 12.228 | 0.938 | 1.711 | 0.928 | -0.087 |
| 81.000 | 3.223 | 8.582 | -1.450 | 1.355 | 0.782 | -0.061 |
| 82.000 | 1.328 | 5.480 | -2.062 | 0.910 | 0.489 | -0.037 |
| 83.000 | 0.595 | 3.801 | -1.863 | 0.508 | 0.350 | -0.014 |

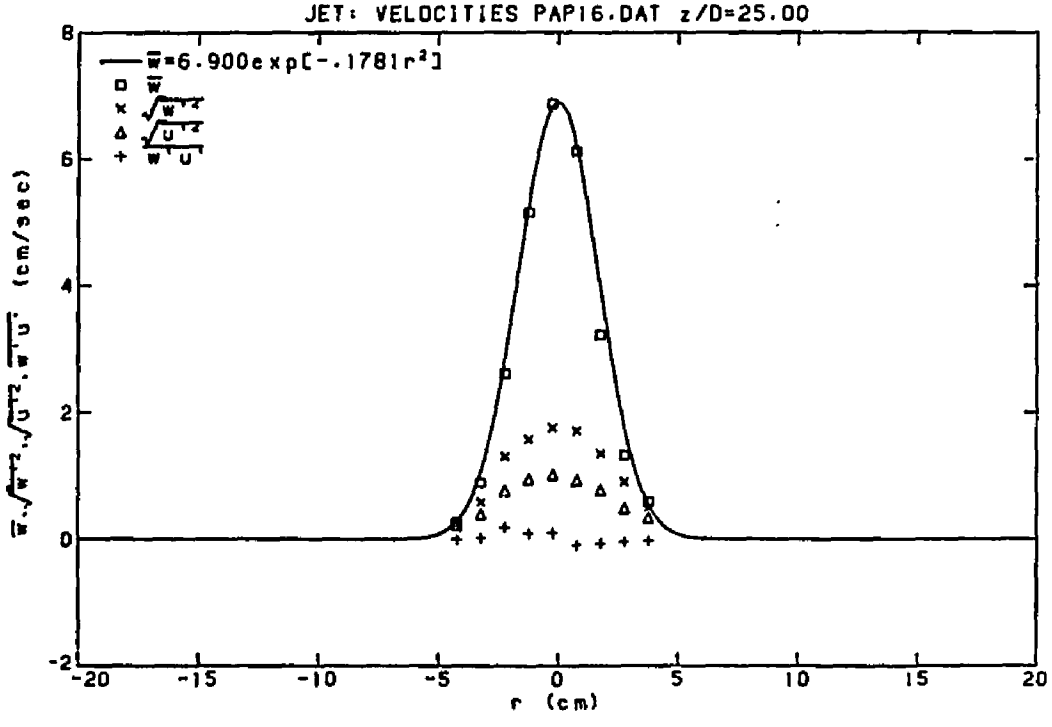

PAP17

| X | W | MAX W | MIN W | WP | UP | WPUP |
|---|---|---|---|---|---|---|
| 87.000 | 0.271 | 1.885 | -1.863 | 0.249 | 0.242 | 0.004 |
| 85.000 | 0.993 | 6.301 | -1.631 | 0.899 | 0.552 | -0.083 |
| 83.000 | 3.883 | 12.110 | -1.270 | 2.040 | 1.039 | -0.489 |
| 81.000 | 6.828 | 13.873 | 0.814 | 2.105 | 1.345 | -0.662 |
| 80.000 | 8.382 | 16.108 | 1.399 | 2.123 | 1.373 | -0.118 |
| 79.000 | 8.535 | 15.062 | 1.445 | 2.351 | 1.437 | 0.370 |
| 78.000 | 8.061 | 14.908 | 0.876 | 2.191 | 1.369 | 0.670 |
| 77.000 | 6.316 | 13.179 | 0.472 | 2.123 | 1.264 | 0.780 |
| 76.000 | 4.178 | 10.230 | -0.670 | 1.876 | 1.275 | 0.717 |
| 74.500 | 1.461 | 6.463 | -2.633 | 1.192 | 0.789 | 0.229 |
| 73.000 | 0.687 | 5.507 | -2.229 | 0.686 | 0.443 | 0.086 |
| 71.500 | 0.233 | 2.261 | -2.414 | 0.277 | 0.335 | -0.011 |
| 70.000 | 0.249 | 2.618 | -2.448 | 0.214 | 0.137 | 0.000 |

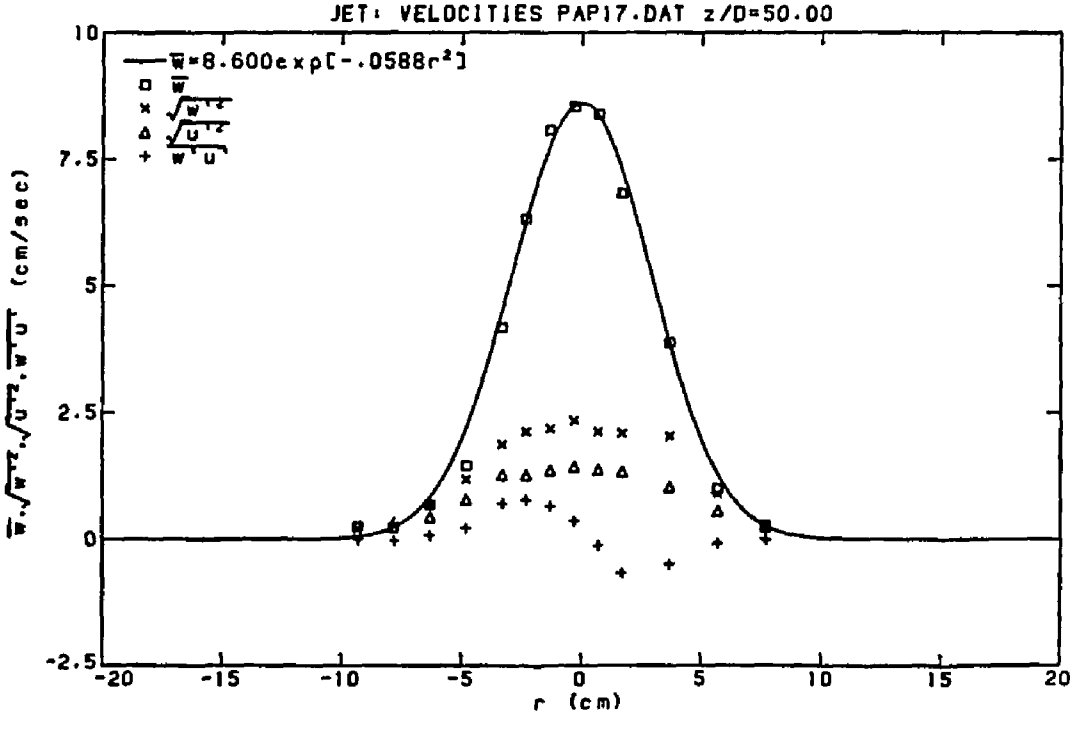

PAP20

| X | W | MAX W | MIN W | WP | UP | WPUP |
|---|---|---|---|---|---|---|
| 71.000 | 3.096 | 10.519 | -1.294 | 1.795 | 1.153 | 0.943 |
| 74.000 | 6.088 | 13.568 | -0.228 | 2.230 | 1.439 | 1.165 |
| 77.000 | 8.707 | 16.112 | 1.532 | 2.244 | 1.535 | 0.669 |
| 79.000 | 8.666 | 16.477 | 2.059 | 2.133 | 1.527 | 0.160 |
| 81.000 | 8.477 | 15.383 | 1.200 | 2.223 | 1.455 | -0.194 |
| 84.000 | 5.573 | 12.524 | -1.124 | 2.006 | 1.390 | -0.552 |
| 87.000 | 3.107 | 10.050 | -0.787 | 1.729 | 0.931 | -0.380 |
| 90.000 | 2.048 | 7.326 | -1.949 | 1.399 | 0.860 | -0.442 |
| 93.000 | 0.530 | 3.519 | -2.154 | 0.531 | 0.567 | 0.065 |
| 96.000 | 0.323 | 2.747 | -2.202 | 0.286 | 0.230 | -0.001 |

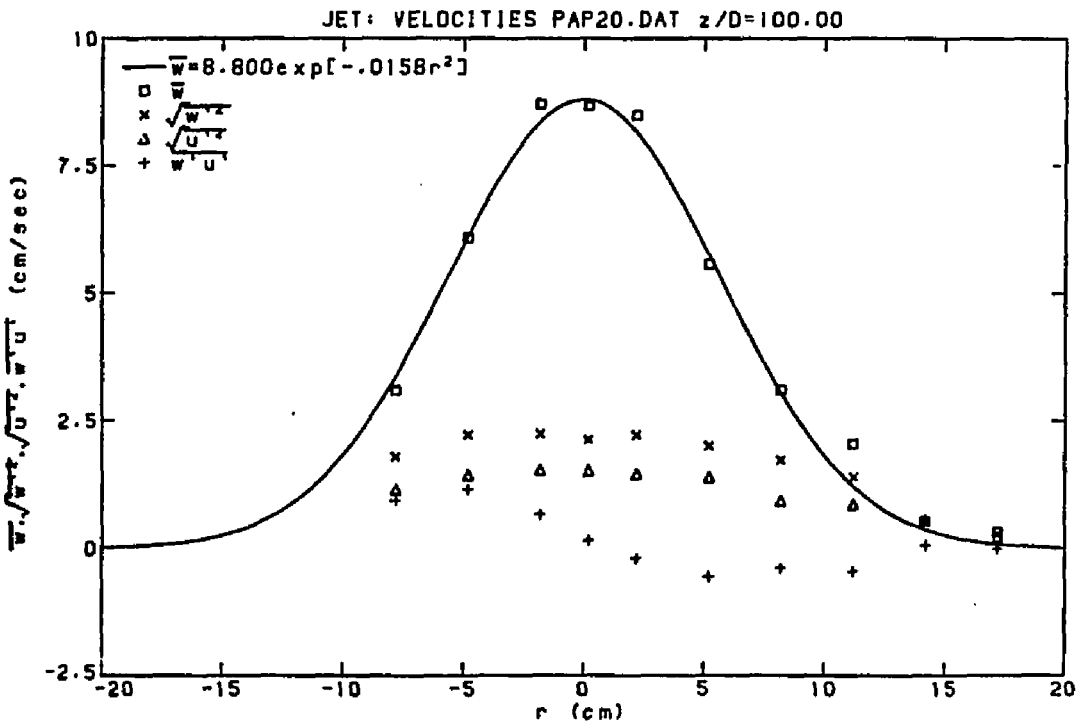

PAP21

| X | W | MAX W | MIN W | WP | UP | WPUP |
|---|---|---|---|---|---|---|
| 68.000 | 0.308 | 3.245 | -2.377 | 0.361 | 0.236 | 0.002 |
| 71.000 | 1.260 | 7.713 | -2.393 | 1.071 | 0.780 | 0.242 |
| 74.000 | 3.388 | 11.704 | -0.742 | 1.727 | 1.055 | 0.426 |
| 77.000 | 7.120 | 13.590 | -1.464 | 2.086 | 1.328 | 0.662 |
| 79.000 | 8.170 | 16.618 | 2.579 | 1.913 | 1.421 | -0.036 |
| 81.000 | 6.886 | 14.000 | -0.393 | 2.088 | 1.380 | -0.281 |
| 83.000 | 4.363 | 11.986 | -2.617 | 1.857 | 1.041 | -0.487 |
| 86.000 | 1.388 | 7.113 | -2.940 | 1.309 | 0.682 | -0.183 |
| 89.000 | 0.751 | 6.197 | -2.778 | 0.705 | 0.418 | -0.081 |

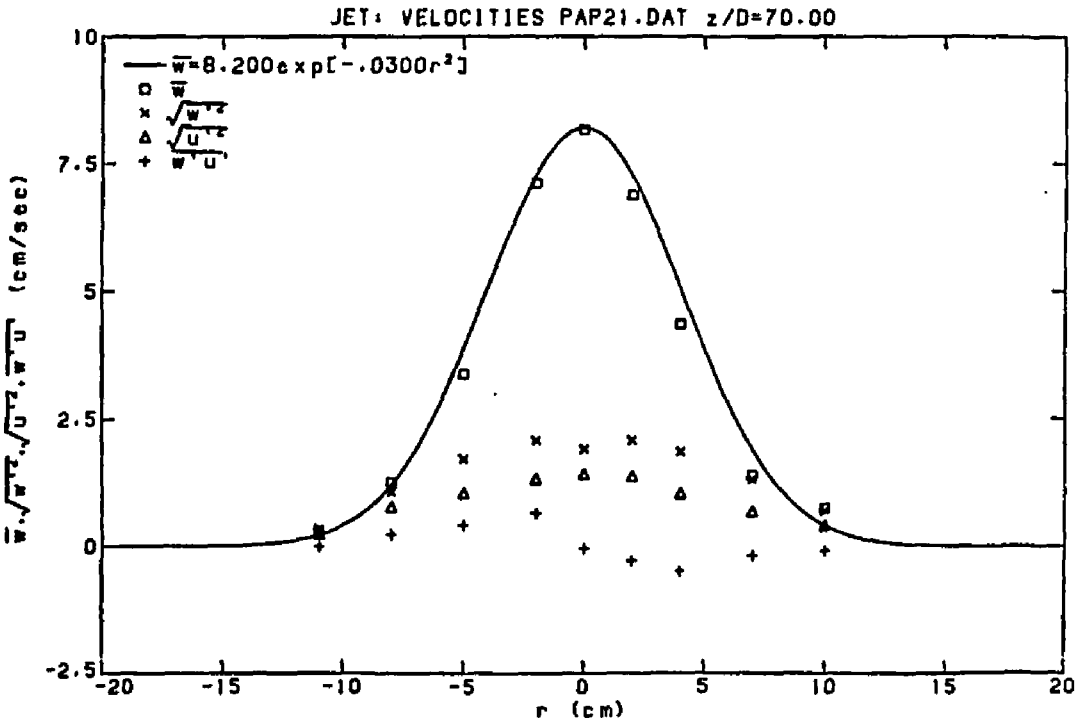

PAP30

| X | W | MAX W | MIN W | WP | UP | WPUP |
|---|---|---|---|---|---|---|
| 66.000 | 0.181 | 1.164 | -2.030 | 0.333 | 0.421 | 0.000 |
| 69.000 | 1.773 | 7.766 | -0.894 | 1.161 | 0.785 | 0.257 |
| 72.000 | 4.567 | 14.682 | -1.324 | 1.979 | 1.290 | 0.850 |
| 75.000 | 8.372 | 17.239 | 2.001 | 2.387 | 1.585 | 1.183 |
| 77.000 | 10.320 | 21.210 | 2.580 | 2.549 | 1.616 | 1.040 |
| 79.000 | 10.498 | 18.621 | 3.596 | 2.517 | 1.581 | -0.125 |
| 81.000 | 9.565 | 18.944 | 2.429 | 2.734 | 1.483 | -0.896 |
| 84.000 | 5.620 | 14.816 | 0.723 | 2.276 | 1.440 | -1.103 |
| 87.000 | 2.816 | 10.463 | -0.467 | 1.577 | 0.970 | -0.568 |
| 90.000 | 1.112 | 6.359 | -1.726 | 1.081 | 0.790 | -0.216 |

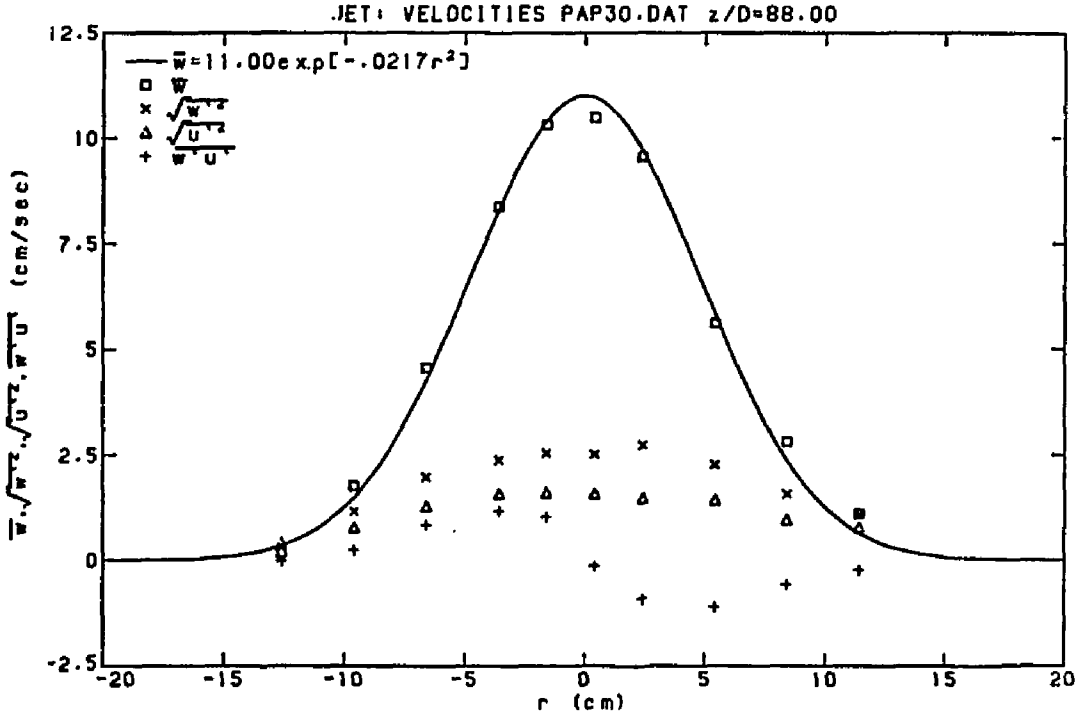

PAP32

| X | W | MAX W | MIN W | WP | UP | WPUP |
|---|---|---|---|---|---|---|
| 71.000 | 0.057 | 2.639 | -4.867 | 0.378 | 0.414 | -0.001 |
| 73.000 | 1.225 | 7.840 | -3.057 | 1.312 | 0.910 | 0.414 |
| 75.000 | 4.229 | 12.725 | -1.257 | 1.940 | 1.219 | 0.762 |
| 77.000 | 7.988 | 14.605 | 1.132 | 2.175 | 1.546 | 0.795 |
| 78.000 | 9.745 | 17.520 | 2.759 | 2.169 | 1.572 | 0.572 |
| 79.000 | 9.944 | 17.228 | 3.297 | 2.232 | 1.593 | 0.032 |
| 80.500 | 7.881 | 17.186 | 0.880 | 2.511 | 1.431 | -0.708 |
| 82.500 | 4.314 | 12.086 | -0.174 | 1.972 | 1.217 | -0.664 |
| 84.500 | 1.329 | 6.327 | -1.190 | 1.064 | 0.715 | -0.153 |
| 86.500 | 0.300 | 4.178 | -1.058 | 0.426 | 0.401 | -0.000 |

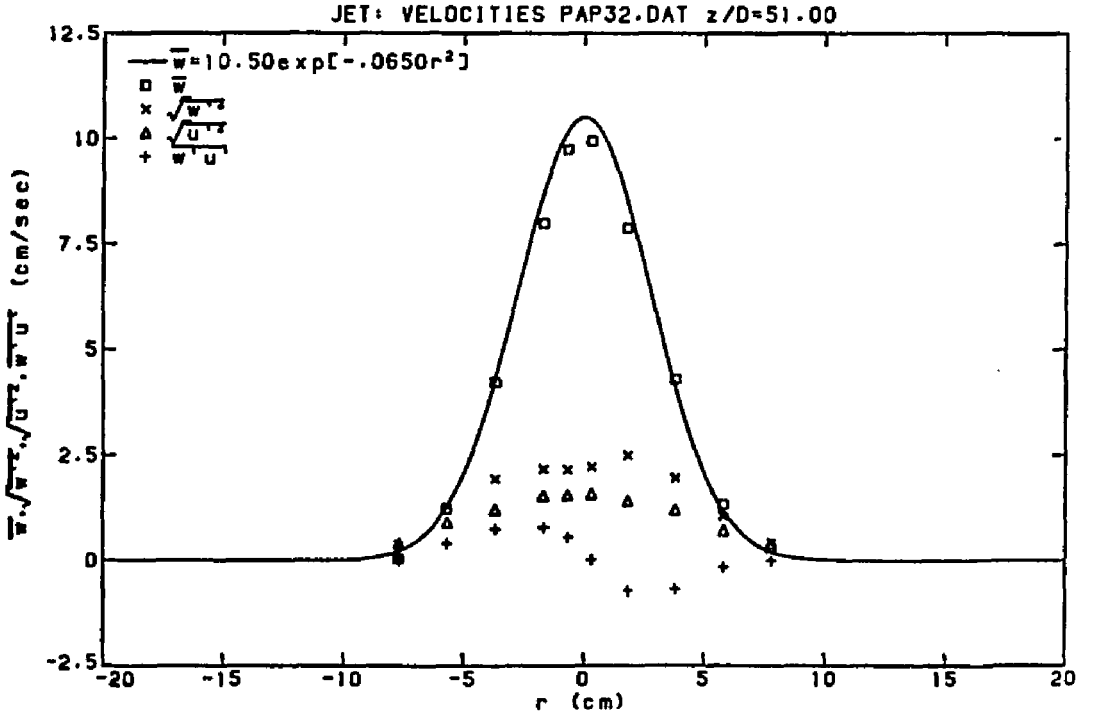

PAP32

| X | W | MAX W | MIN W | WP | UP | WPUP |
|---|---|---|---|---|---|---|
| 71.000 | 0.057 | 2.639 | -4.867 | 0.378 | 0.414 | -0.001 |
| 73.000 | 1.225 | 7.840 | -3.057 | 1.312 | 0.910 | 0.414 |
| 75.000 | 4.229 | 12.725 | -1.257 | 1.940 | 1.219 | 0.762 |
| 77.000 | 7.988 | 14.605 | 1.132 | 2.175 | 1.546 | 0.795 |
| 78.000 | 9.745 | 17.520 | 2.759 | 2.169 | 1.572 | 0.572 |
| 79.000 | 9.944 | 17.228 | 3.297 | 2.232 | 1.593 | 0.032 |
| 80.500 | 7.881 | 17.186 | 0.880 | 2.511 | 1.431 | -0.708 |
| 82.500 | 4.314 | 12.086 | -0.174 | 1.972 | 1.217 | -0.664 |
| 84.500 | 1.329 | 6.327 | -1.190 | 1.064 | 0.715 | -0.153 |
| 86.500 | 0.300 | 4.178 | -1.058 | 0.426 | 0.401 | -0.000 |